

2016-08-02

# Distribution and Source of Carbonate-Rich Intervals within the Vaca Muerta-Quintuco Mixed System, Neuquén Basin, Argentina.

Leticia Rodriguez Blanco

*University of Miami*, [leticiarblanco@yahoo.com](mailto:leticiarblanco@yahoo.com)

Follow this and additional works at: [https://scholarlyrepository.miami.edu/oa\\_theses](https://scholarlyrepository.miami.edu/oa_theses)

---

## Recommended Citation

Rodriguez Blanco, Leticia, "Distribution and Source of Carbonate-Rich Intervals within the Vaca Muerta-Quintuco Mixed System, Neuquén Basin, Argentina." (2016). *Open Access Theses*. 622.

[https://scholarlyrepository.miami.edu/oa\\_theses/622](https://scholarlyrepository.miami.edu/oa_theses/622)

This Embargoed is brought to you for free and open access by the Electronic Theses and Dissertations at Scholarly Repository. It has been accepted for inclusion in Open Access Theses by an authorized administrator of Scholarly Repository. For more information, please contact [repository.library@miami.edu](mailto:repository.library@miami.edu).

UNIVERSITY OF MIAMI

DISTRIBUTION AND SOURCE OF CARBONATE-RICH INTERVALS WITHIN  
THE VACA MUERTA-QUINTUCO MIXED SYSTEM, NEUQUÉN BASIN,  
ARGENTINA

By

Leticia Rodríguez Blanco

A THESIS

Submitted to the Faculty  
of the University of Miami  
in partial fulfillment of the requirements for  
the degree of Master of Science

Coral Gables, Florida

August 2016

©2016  
Leticia Rodríguez Blanco  
All Rights Reserved

UNIVERSITY OF MIAMI

A thesis submitted in partial fulfillment of  
the requirements for the degree of  
Master of Science

DISTRIBUTION AND SOURCE OF CARBONATE-RICH INTERVALS WITHIN  
THE VACA MUERTA-QUINTUCO MIXED SYSTEM, NEUQUÉN BASIN,  
ARGENTINA

Leticia Rodríguez Blanco

Approved:

---

Gregor P. Eberli, Ph.D.  
Professor of Marine Geosciences

---

Peter K. Swart, Ph.D.  
Lewis Weeks Professor of  
Marine Geosciences

---

Jose Luis Massaferro, Ph.D.  
Carbonate Specialist  
YPF S.A., Buenos Aires, Argentina

---

Guillermo Prado, Ph.D.  
Dean of the Graduate School

RODRÍGUEZ BLANCO, LETICIA

(M.S., Marine Geology and Geophysics)

Distribution and Source of  
Carbonate-Rich Intervals within  
the Vaca Muerta-Quintuco Mixed System,  
Neuquén Basin, Argentina.

(August 2016)

Abstract of a thesis at the University of Miami.

Thesis supervised by Professor Gregor P. Eberli

No. of pages in text. (145)

The Late Jurassic – Early Cretaceous slope and basin sediments of the Neuquén Basin, Argentina, consist mostly of siliciclastic mudstones of the Vaca Muerta Formation. However, carbonate-rich intervals of unknown origin occur at different stratigraphic levels within the Formation. This study aims to determine if these intervals were sourced from adjacent carbonate-rich shelves during sea level highstands. Logs and samples through sections from the southern slope and the basin center provide the information in regards of facies variability and stratal architecture that are placed within a biostratigraphic and sequence-stratigraphic framework. The thickest carbonate-rich interval (up to 70m) is known as the Los Catutos Member. Correlation of sections in the Sierra de la Vaca Muerta reveal a wedge-shape geometry with slump scars and channels in the southern and thicker portion, indicating a slope setting. Cycles within the Los Catutos carbonate-rich interval show an upward increase in carbonate content and skeletal debris. Northward, in the thinner part of the wedge, bed thickness, carbonate and skeletal content decrease indicating a southern origin. The time-equivalent Picún Leufú carbonate platform located further south is the identified as the source of the Los Catutos carbonates that are interpreted to be its periplatform apron. The geochemical evidence of the proximal-distal trend in the  $\delta^{13}\text{C}$  signature supports this interpretation. Three younger carbonate-rich intervals in a basinal

section in the Puerta Curaco (PC) area have very similar facies as the distal portion of the Los Catutos interval. They are, however, younger than the Picun Leufú platform in the south and are probably sourced from a different direction. No coeval carbonate platforms are exposed in outcrops but time-equivalent shallow-water carbonates are present in cores from the eastern shelf of the Neuquén Basin. The four studied carbonate-rich intervals occur in the regressive portion of sequences and, thus, indicate production and export of carbonates during sea level highstands.

## ACKNOWLEDGEMENTS

I am deeply grateful to all the people that, through their support and assistance, contributed to this project: my advisor, Gregor Eberli, for the gentle guidance and fruitful discussions, and for teaching me so much and not only about carbonates; the members of the thesis committee, Peter Swart and Jose Luis Massafarro, for the technical discussions and suggestions that helped me to improve this manuscript; CSL Vaca Muerta and SIL teams, for the shared field and lab work, with a special mention to Ralf Weger, for working side by side in all the technical steps of this project, and for always being there to encourage, give the necessary criticism and solve so many things when needed; professors, staff and students in MGS, for the friendly environment created daily through many gestures and for the enriching experiences shared; my family and friends, for their loving support along these two years, and for being a constant source of motivation; Fulbright and CSL sponsors, for the financial support.

## TABLE OF CONTENTS

	Page
LIST OF FIGURES .....	vi
LIST OF TABLES .....	viii
Chapter 1: Introduction .....	1
Rationale .....	1
Working hypothesis and objectives .....	3
The Neuquén Basin.....	5
Study interval .....	6
Chapter 2: Data set .....	10
Picún Leufú – Sierra de la Vaca Muerta.....	10
Puerta Curaco – Yesera del Tromen.....	14
Chapter 3: Methods .....	16
Data collection .....	16
Lithofacies analysis .....	16
Sequence stratigraphic analysis .....	17
Biostratigraphy.....	17
Geochemical analysis .....	17
X-ray powder diffraction (XRD) .....	17
Carbonate content .....	18
Organic content .....	18
$\delta^{13}\text{C}$ and $\delta^{18}\text{O}$ isotopes .....	18
Chapter 4: Results .....	20
Lithofacies analysis.....	21
Geochemistry .....	26
Stratigraphic distribution .....	34
Los Catutos Member (mid-late Tithonian) in Sierra de la Vaca Muerta .....	36
MDC section .....	36
VM23 section .....	49
Lateral variations within the Los Catutos interval.....	54
The younger carbonate-rich intervals in Puerta Curaco .....	60
PC reference section .....	60
First carbonate-rich interval.....	64
Second carbonate-rich interval .....	67
Third carbonate-rich interval .....	67
The mid-late Tithonian in PC .....	72



Sequence stratigraphy .....	75
Cycles and cycles sets .....	75
Sequences in Sierra de la Vaca Muerta .....	87
Sequences in Puerta Curaco.....	89
Correlations .....	93
Chapter 5: Discussion and implications .....	96
Facies and chemical partitioning in the carbonate-rich intervals .....	96
Lateral variability of the carbonate-rich intervals.....	97
The source issue .....	99
The platform sources .....	101
Carbon isotope ratios .....	105
Implications for hydrocarbon exploration and production .....	112
Chapter 6: Conclusions .....	114
WORKS CITED .....	117
APPENDICES .....	124
Appendix A: Complete data set of MDC and PC sections .....	124
Appendix B: Carbon isotope data from Picún Leufú .....	141
Appendix C: GR correlation .....	142
Appendix D: Nitrogen isotope data of mid-late Tithonian intervals .....	143

## LIST OF FIGURES

Figure 1.1: The Vaca Muerta Formation of the Neuquén Basin .....	1
Figure 1.2: The Los Catutos problem .....	2
Figure 1.3: Lithostratigraphic units .....	8
Figure 2.1: Studied outcrop locations .....	11
Figure 2.2: Picún Leufú-Sierra de la Vaca Muerta outcrops .....	13
Figure 2.3: Puerta Curaco outcrops .....	15
Figure 4.1: Lithofacies in outcrops .....	23
Figure 4.2: Microfacies .....	24
Figure 4.3: General statistics of the chemical proxies measured .....	33
Figure 4.4: %CO <sub>3</sub> plotted versus %TOC and $\delta^{13}C$ in for the analyzed intervals .....	34
Figure 4.5: Section legend .....	35
Figure 4.6: Ammonite zones .....	37
Figure 4.7: MDC section .....	39
Figure 4.8: Los Catutos Member in MDC .....	41
Figure 4.9: Outcrop facies of Los Catutos in MDC .....	42
Figure 4.10: Microfacies of Los Catutos in MDC .....	43
Figure 4.11: Moved strata in los Catutos in MDC .....	44
Figure 4.12: Geochemical variations within Los Catutos in MDC .....	45
Figure 4.13: Data analysis of Los Catutos in MDC .....	46
Figure 4.14: Data analysis of Unit II in MDC .....	47
Figure 4.15: %CO <sub>3</sub> plotted vs %TOC and $\delta^{13}C$ in for Los Catutos in MDC .....	47
Figure 4.16: Los Catutos Member in VM23 .....	50
Figure 4.17: Outcrop facies of Los Catutos in VM23 .....	51
Figure 4.18: Microfacies of Los Catutos in VM23 .....	51
Figure 4.19: Geochemical variations within Los Catutos in VM23 .....	52
Figure 4.20: Data analysis of Los Catutos in VM23 .....	52
Figure 4.21: %CO <sub>3</sub> plotted vs %TOC and $\delta^{13}C$ in for Los Catutos in VM23 .....	53
Figure 4.22: Lateral lithological variations within Los Catutos (MDC-VM23) .....	55
Figure 4.23: Tracing Los Catutos on satellite image .....	57
Figure 4.24: Lateral geochemical variations within Los Catutos (MDC-VM23) .....	58
Figure 4.25: Geochemical comparison of Units III and IV (MDC-VM23) .....	59
Figure 4.26: PC reference section .....	61
Figure 4.27: Ages of the lower part of the succession in PC .....	63
Figure 4.28: Lithology of the 1st carbonate-rich interval in PC .....	65
Figure 4.29: Geochemistry of the 1st carbonate-rich interval in PC .....	66
Figure 4.30: Lithology of the 2nd carbonate-rich interval in PC .....	68
Figure 4.31: Geochemistry of the 2nd carbonate-rich interval in PC .....	69
Figure 4.32: Lithology of the 3rd carbonate-rich interval in PC .....	70
Figure 4.33: Geochemistry of the 3rd carbonate-rich interval in PC .....	71
Figure 4.34: Lithology of the mid-late Tithonian interval in PC .....	73
Figure 4.35: Geochemistry of the mid-late Tithonian interval in PC .....	74
Figure 4.36: Cycles of Los Catutos in MDC .....	76

Figure 4.37: Geochemical signature of cycles -Los Catutos, MDC .....	77
Figure 4.38: Cycles of Los Catutos in VM23 .....	78
Figure 4.39: Geochemical signature of cycles -Los Catutos, VM23 .....	79
Figure 4.40: Cycles of the 1st carbonate-rich interval in PC .....	80
Figure 4.41: Geochemical signature of cycles -1st carbonate-rich interval, PC.....	81
Figure 4.42: Cycles of the 2nd carbonate-rich interval in PC.....	82
Figure 4.43: Geochemical signature of cycles -2nd carbonate interval, PC.....	83
Figure 4.44: Cycles of the 3rd carbonate-rich interval in PC .....	84
Figure 4.45: Geochemical signature of cycles -3rd carbonate interval, PC.....	85
Figure 4.46: Cycles of the mid-late Tithonian interval in PC.....	86
Figure 4.47: Geochemical signature of cycles - mid-late Tithonian, PC.....	86
Figure 4.48: Cycles and sequences in MDC section.....	88
Figure 4.49: Cycles and sequences in PC section.....	90
Figure 4.50: Los Catutos clinoform .....	94
Figure 4.51: Isotope stratigraphy .....	95
Figure 5.1: %CO <sub>3</sub> plotted vs %TOC and δ <sup>13</sup> C <sub>in</sub> for the carbonate-rich intervals .....	97
Figure 5.2: Proximal-distal variations in cycles of the studied intervals .....	98
Figure 5.3: Periplatform deposits.....	100
Figure 5.4: Composite section from Picún Leufú Anticline .....	102
Figure 5.5: Proposed origin of the carbonate-rich intervals .....	104
Figure 5.6: Proximal-distal isotope trend.....	106
Figure 5.7: Model of stratified waters.....	108
Figure 5.8: δ <sup>13</sup> C variations within the Tithonian-Valanginian succession in PC .....	111

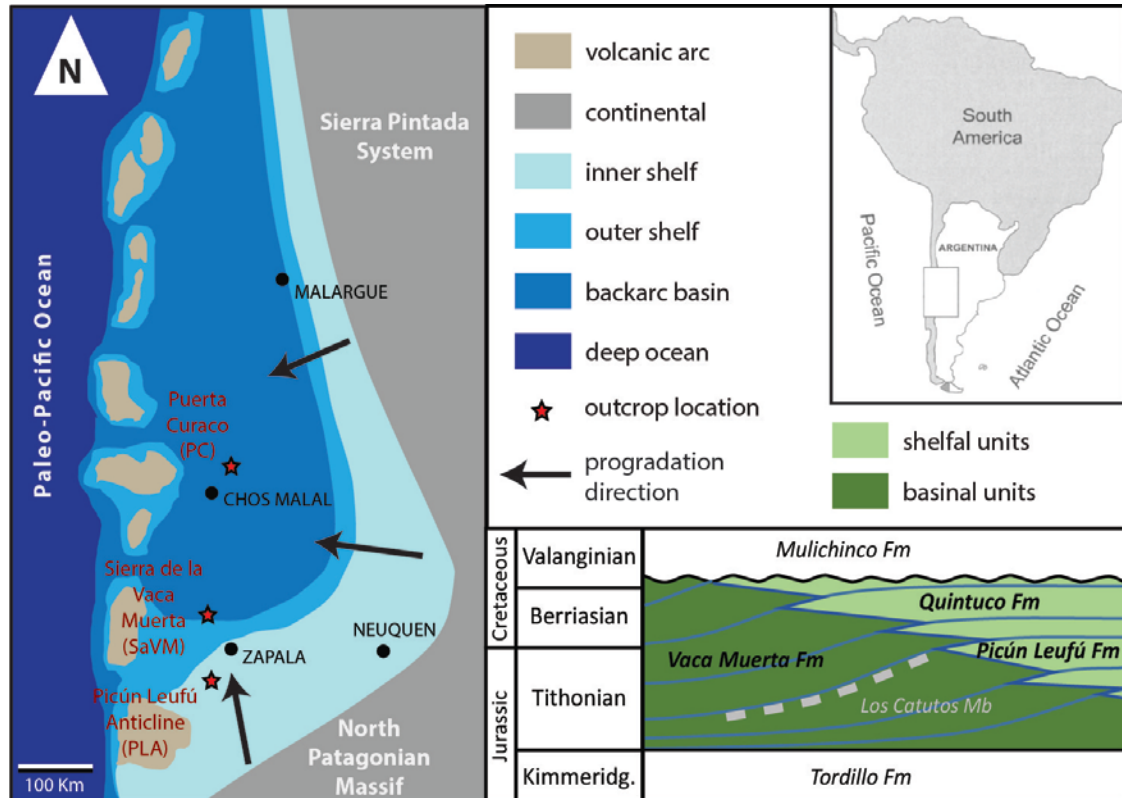
## LIST OF TABLES

Table 4.1: Summary of lithofacies descriptions .....	21
Table 4.2: Data set from the analyzed intervals.....	31

## Chapter 1: Introduction

### Rationale

In the Neuquén Basin, Argentina, several carbonate-rich intervals from slope to basin settings occur within the mixed siliciclastic-carbonate basinal deposits of the Late Jurassic to Early Cretaceous Vaca Muerta Formation (Figure 1.1). The most significant of these



**Figure 1.1. The Vaca Muerta Formation of the Neuquén Basin.** Left: Tithonian to earliest Valanginian paleogeographic reconstruction of the basin (modified from Zeller, 2013), with black arrows indicating the progradation direction of the Vaca Muerta-Quintuco mixed system. Lower right: lithostratigraphic units defined in Picún Leufú/Sierra de la Vaca Muerta outcrops

intervals, in terms of thickness and areal extension, is the Los Catutos Member (Mid-Late Tithonian) defined in the Sierra de la Vaca Muerta (Leanza and Zeiss 1990). The overall wedge-shape unit thins from south to north and consists of thick-bedded marine limestones with intercalations of marls and shales. Two different stratigraphic schemes have been used to explain the Los Catutos Member (Figure 1.2, A and B): Leanza et al (2011) represented

this unit as an isolated wedge in the slope, while Zeller (2013) attached it to platform carbonates within the Picún Leufú Formation (Mid-Late Tithonian). The two representations imply a different origin for the Los Catutos carbonates: pelagic in the first case, and periplatform in the second.

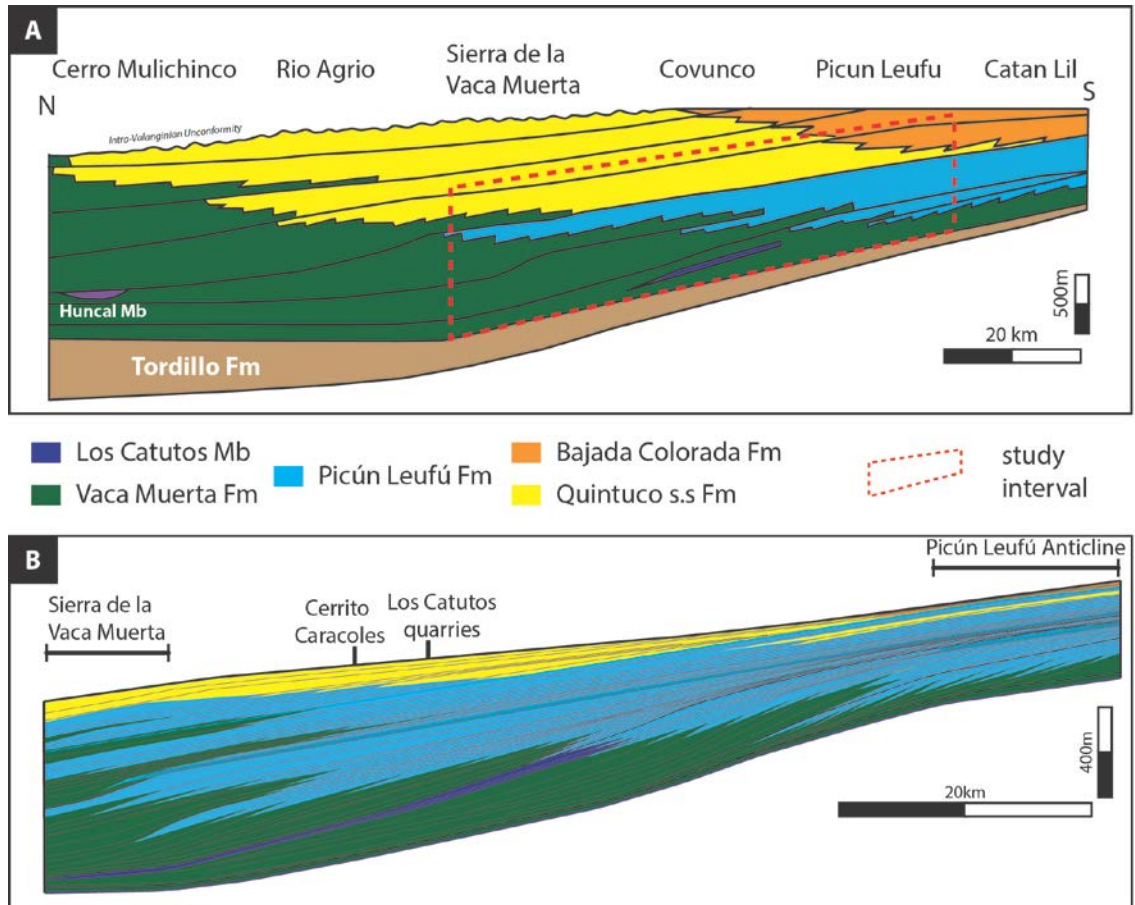


**Figure 1.2. The Los Catutos problem** (modified from Zeller 2013). A) Large-scale correlation from Leanza et al. (2011). B) Outcrop correlation from Zeller (2013, corresponding to the area indicated with the red box). The two cross-sections are comparable between Picún Leufú (south) and Sierra de la Vaca Muerta (north) outcrops shown in the map of Figure 1.1

Younger carbonate-rich intervals similar to the Los Catutos Member have been identified in the Puerta Curaco area (Figure 1.1). As in the case of the Los Catutos Member, the source of the carbonate mud that constitutes these intervals can be either pelagic or related to a carbonate platform. Intervals that are similar in lithology to the Picún Leufú

shelf carbonates, though younger, have been observed in the subsurface Quintuco Formation. This occurrence of carbonate-shelves and basinal carbonate-rich intervals, whether related or not to those carbonate shelves, at different stratigraphic positions within the basin point towards a recurring process.

As observed by Zeller (2013), sedimentary facies and carbonate-clastic partitioning in the subsurface Vaca Muerta-Quintuco system might be similar to what is observed in older intervals in outcrops. Hence, the detailed study of these carbonate-rich intervals in outcrops is fundamental to understand the mechanism behind their generation and to predict their stratigraphic distribution in the basin.

### **Working hypothesis and objectives**

Zeller (2013) proposed that carbonate production on the shelves of the Neuquén basin is related to an interplay between accommodation space and currents. During highstand periods when an increase in carbonate production in the shallow areas produces a decrease in the accommodation space along-shore currents are forced towards the basin, reducing siliciclastic input in the shallow-water areas.

In modern carbonate platforms, the increased carbonate production on the shelf during highstands results in a significant amount of export of carbonate mud from the platform into the basin (e.g. Schlager et al. 1994). The exported platform mud mixes with the pelagic carbonate forming the periplatform ooze that surrounds the platforms in a wedge shape thinning away from the platform.

The focus of this study will be on the basinal carbonate-rich intervals of different ages and will test the following hypothesis:

**“The carbonate-rich intervals are sourced from carbonate-rich shelves during times of sea-level highstands.”**

The approach for testing this hypothesis is the following: First the Los Catutos Member in Sierra de la Vaca Muerta will be studied and traced south towards the platform carbonates in Picún Leufú anticline. The younger basinal carbonates in Puerta Curaco area will be studied in regards to their stratigraphic distribution and composition to assess their origin and facies distribution. Through detailed logging and sampling, the identified carbonate-rich intervals will be characterized in terms of facies variability and stratal architecture, and placed within a biostratigraphic and sequence-stratigraphic framework.

The specific objectives of this study are to:

- Document the composition and lithofacies of the basinal carbonate-rich intervals at different stratigraphic positions in the more proximal setting in Sierra de la Vaca Muerta and in the more distal position in Puerta Curaco.
- Relate the observed lithofacies to depositional environments, and discuss the potential factors that control their deposition and variability.
- Compare the geochemical signature ( $\delta^{13}\text{C}$ ,  $\delta^{18}\text{O}$ ) of the Picún Leufú Formation and the Los Catutos Member as a way to determine whether the Picún Leufú shelf was the source of the Los Catutos basinal carbonates.
- Place the studied carbonate-rich intervals into a chrono- and sequence-stratigraphic framework.



## **The Neuquén Basin**

The Neuquén Basin is located in the eastern flank of the Andes in Argentina, between 32° and 40° south (Figure 1.1). It comprises a sedimentary succession from Late Triassic to Cenozoic that outcrops in the Andean Cordillera and remains relatively undeformed in the subsurface farther east (Legarreta and Gulisano 1989, Gulisano and Gutierrez Pleimling 1995, Vergani et al. 1995, among others).

Three tectono-stratigraphic stages can be recognized in the evolution of the basin:

- Late Triassic-Early Jurassic: This synrift stage was related to the extensional collapse of the Late Paleozoic orogenic belt in the western margin of Gondwana. During the rift period several relatively small and isolated basins were generated (e.g. Uliana and Biddle 1987, Uliana and Legarreta 1993, Vergani et al. 1995, Franzese and Spalletti 2001).
- Middle Jurassic-Early Cretaceous: This regional subsidence stage was caused by the retreating subduction system, resulting in a retro-arc basin that integrated previous depocenters (e.g. Uliana and Biddle 1987, Mpodozis and Ramos 1989, Legarreta and Gulisano 1989, Vergani et al. 1995). This stage was also punctuated by the local tectonic inversion of some previous extensional structures. For example, the Huincul High was likely active during this time and acted as an emerging positive topographic feature that isolated the southern part from the northern part of the Neuquén basin thereby controlling the distribution of the depositional systems at both sides (Vergani et al. 1995, Silvestro and Zubiri 2008, Mosquera et al. 2011).

- Late Cretaceous to present: This foreland basin stage is the result of the compressional Andean tectonics, and the development of the fold and thrust belt in the western side of the basin (Mpodozis and Ramos 1989, Vergani et al. 1995, Ramos and Folguera 2005, Howell et al. 2005, Tunik et al. 2010, among others)

The Vaca Muerta-Quintuco mixed system that is the focus of this study was deposited during the Middle Jurassic-Early Cretaceous retro-arc basin stage. During this period, the basin had a triangular shape, limited in the northeast by the San Rafael-Sierra Pintada system, and in the southeast by the North Patagonian massif (Figure 1.2). To the west, the development of a volcanic arc might have restricted intermittently the open connection with the proto-Pacific ocean through a combination of tectonic movements and eustatic oscillations (Howell et al. 2005).

### **Study interval**

The Vaca Muerta-Quintuco system (Figure 1.3) is a succession of mostly marine deposits related to a proto-Pacific transgression over previous continental deposits. The age of the system, between the Earliest Tithonian and the Earliest Valanginian, is based mainly on ammonite biostratigraphy (see review of paleontological content in Aguirre Urreta et al. 2014). The system consists of several lithostratigraphic units that have been defined differently by different authors. For the marine units that are part of this study, the criteria will be the same as applied by Leanza et al. (2011), from basin to shelf:

- Vaca Muerta Formation: It was originally defined by Weaver (1931) as Tithonian Strata but Fossa Mancini et al. (1938) replaced the former name with Vaca Muerta Formation. The type locality for the Formation is the western flank of the Sierra de

la Vaca Muerta (Leanza, 1973). The Vaca Muerta Formation consists of mudstones, marls and limestones with high organic content deposited in a marine off-shore environment with poorly-oxygenated bottom. Its age is Tithonian to Early Valanginian based on its ammonite content. The base of the unit is isochronous within the *Virgatosphinctes mendozanus* zone (Early Tithonian) while its top is diachronous getting younger towards the center of the basin (Leanza, 1973).

- Los Catutos Member: It was defined by Leanza and Zeiss (1990) in El Ministerio quarry, near Zapala. It is a carbonate-rich succession of up to 70m of tabular, marine, fossiliferous limestones interbedded with marls and shales. The age of this member is Middle-Late Tithonian based on its ammonite content with *Aulacosphinctes proximus* zone at the base and *Windhausenicerias internispinosum* zone at the top.
- Picún Leufú Formation (Leanza, 1973): It consists of limestones, claystones and sandstones deposited in a shallow-water shelf environment. The type locality is in the area where the national route 40 intersects the Picún Leufú stream. The age of this Formation is Late Tithonian to Early Berriasian based on its ammonite content (*Windhausenicerias internispinosum*, *Corongoceras alternans* and *Substeueroceras koeneni* zones).
- Quintuco *sensu stricto* Formation (Weaver, 1931 *pars*): It consists of the clastic mudstones with abundant bivalves and biogenic accumulations that outcrop in the Sierra de la Vaca Muerta between the Vaca Muerta Formation and the Intra-Valanginian unconformity. This Formation was deposited in a clastic shallow

marine shelf and nearshore environment, and is assigned to the Berriasian to Early Valanginian.

- Quintuco Formation (former Calcárea Formation, de Ferrariis 1947): This name is used extensively in the oil industry for a variety of lithologies similar to the Picún Leufú Formation lying in the subsurface between the Vaca Muerta Formation and the Mulichinco Formation. The unit consists of calcareous sandstones, oolitic and micritic limestones, calcareous mudstones, anhydrites and dolomites deposited in a mixed carbonate-siliciclastic shelf environment. Its age is assigned to the Tithonian to Early Valanginian.

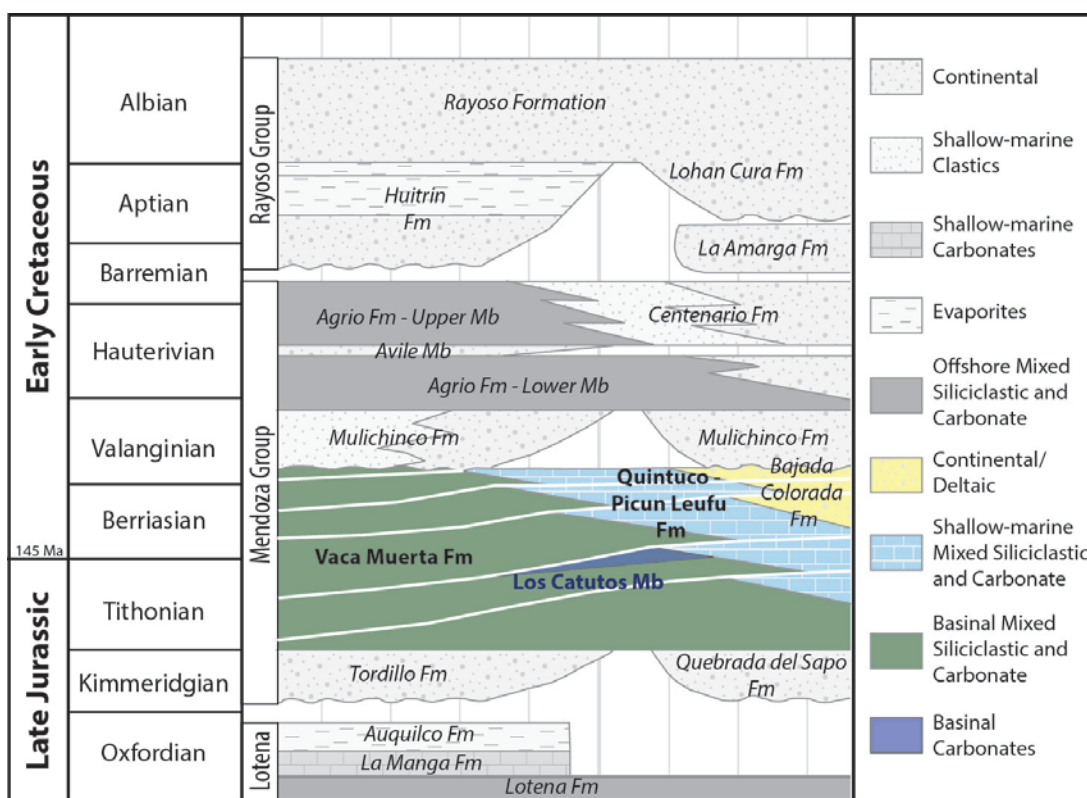


**Figure 1.3. Lithostratigraphic units.** Subdivision of the Late Jurassic-Early Cretaceous in the Neuquén basin. The prograding Quintuco-Vaca Muerta mixed system is highlighted in color (modified from Zeller 2013)

The contact between the Vaca Muerta Formation and the overlying Picún Leufú and Quintuco Formations are diachronous as the mixed carbonate-clastic shelf successions

prograde over the basinal strata (Figure 1.3; Leanza, 1973; Mitchum and Uliana, 1985; among others),

In the southern portion of the basin Zeller (2013) defined 8 (eight) depositional sequences within the prograding Vaca Muerta-Quintuco system both in outcrop and subsurface. In almost all of them the carbonate content increased towards the sequence tops. In some cases, these sequence tops were clearly carbonate-dominated, what Zeller (2013) attributed to a reduction of the accommodation space and the inhibition of the along-shelf current system that would be laterally supplying the clastic materials. One of the best examples of these carbonate-rich intervals, due to its thickness and extension, is the Los Catutos Member (Mid-Late Tithonian).

This sequence stratigraphic subdivision was carried to a more distal position in the basin in course of the Neuquen Basin research initiative of the CSL, of which the present work is one of the projects. At the Puerta Curaco reference section 11 depositional sequences were identified. As will be documented in this thesis, it was also possible to verify that the carbonate content increases towards the top of the cycles at all scales in this basinal position. In three of these sequences (7, 8 and 9) the regressive portion is clearly carbonate-dominated with similar characteristics to those of the Los Catutos Member.

## **Chapter 2: Data set**

The studied data set was collected in two reference locations (Figure 2.1): Picún Leufú – Sierra de la Vaca Muerta, to characterize the Mid-Late Tithonian carbonate-rich interval, and Puerta Curaco – Yesera del Tromen, to characterize the Mid-Late Tithonian expression in that basinal position and the younger (Berriasian-Valangian) carbonate-rich intervals. Several sections were logged in each location as part of a group initiative that includes the present work, and compared with published nearby sections of different authors to constrain the age of the logged successions.

### **Picún Leufú – Sierra de la Vaca Muerta**

In the two classic exposures –Picún Leufú and Sierra de la Vaca Muerta- Zeller (2013) documented for the first time the analogy between the outcrop stratal architecture and the seismic signature of the time-equivalent successions in the subsurface to the east. His sequence stratigraphic interpretation of the mixed system Vaca Muerta-Quintuco set the basis for the present work. Some of the sections logged during his dissertation were used as a starting point for the characterization of the Mid-Late Tithonian Los Catutos carbonate-rich interval and compared with similar sections from other authors to document the ammonite biostratigraphy, and re-sampled or re-analyzed as needed:

- Picún Leufú section (PLA) (Figure 2.2): It was used for comparison with an analogous section from Leanza (1973) to constrain the age of the carbonate platform. Also 48 plug samples of the platform mudstones and wackestones were analyzed for inorganic carbon isotopes to evaluate whether the Picún Leufú carbonate platform was the source of the Los Catutos carbonate mud.

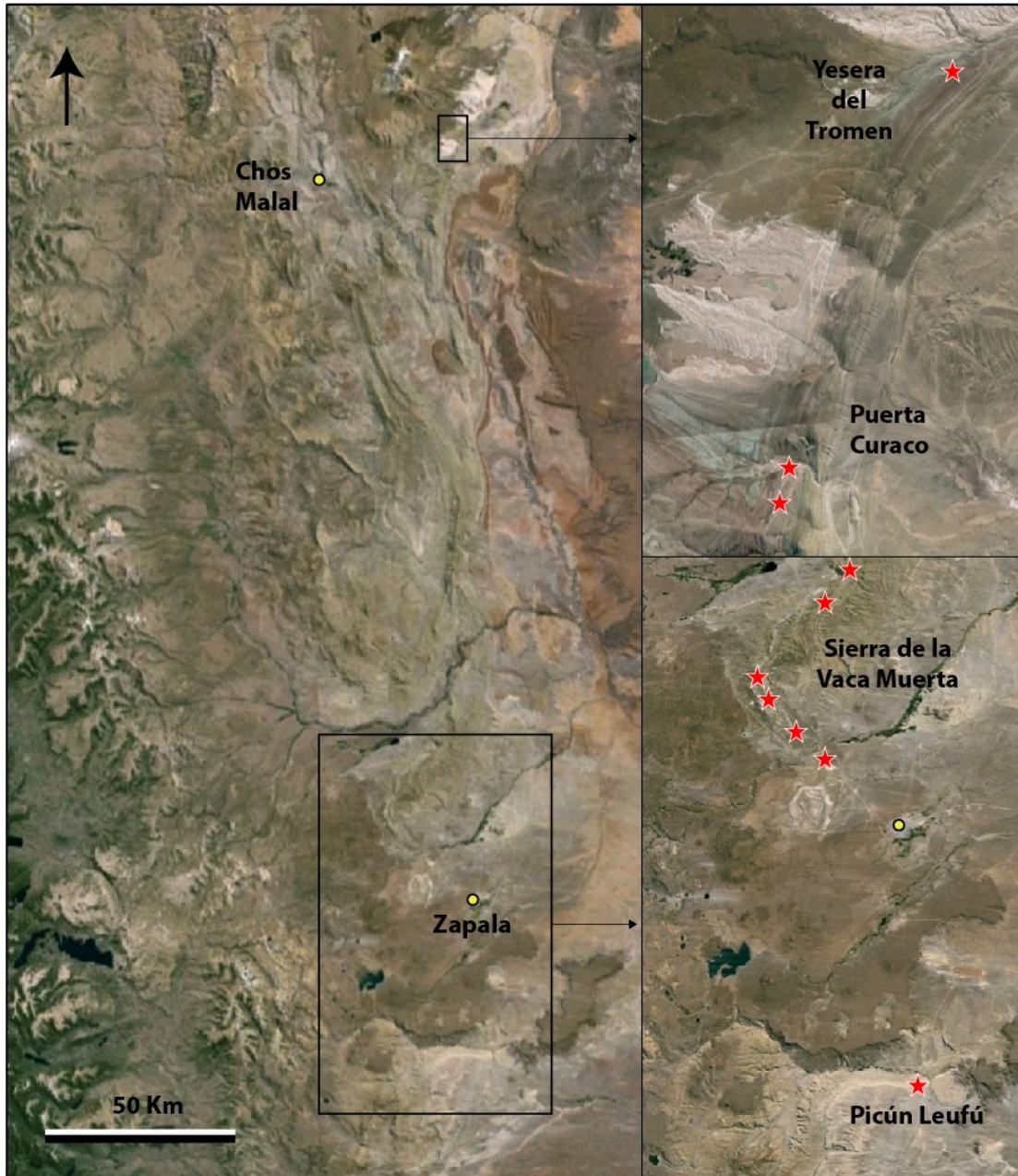


**Figure 2.1. Studied outcrop locations.** Red stars indicate the logged sections. The Picún Leufú section was taken from Zeller (2013)

- Cerrito Caracoles and El Ministerio quarry sections (Figure 2.2): These conceptual sections were compared with the ones from Leanza (1973), Leanza et al. (1977), Leanza and Hugo (1977), and Leanza and Zeiss (1990) to constrain the age of the Los Catutos carbonate-rich interval, and also compared with other sections in the present work to

evaluate the lateral facial variability. No samples were available from these sections, hence the comparison is just based on the logged profiles and related comments.

- Los Catutos road cut (WT section, Figure 2.2): This originally 20-meter section was extended above and below to lithologically characterize the passage between the Lower Member of Vaca Muerta Formation and the Los Catutos Member. The resultant section (WT) is approximately 70m thick. Additional samples were taken for microfacies characterization, resulting in a total of 30 thin sections. The thickness to the contact with the underlying Tordillo Formation was measured to ensure the positioning of the Los Catutos Member within the geometric framework. The top of the section was walked out between sections for exact correlation.

As part of the group initiative that includes the present work, 3 new sections were logged (Figure 2.2) to characterize carbonate-rich intervals in more distal positions. The type and amount of data collected varies from one section to another:

- ANG section: It is a 24-meter section that represents the base of the Los Catutos Member. Walking the top of the section from WT section ensures a precise correlation between the two sections. Key beds were sampled for microfacies analysis, obtaining a total of 5 thin sections to compare with nearby sections.

- MDC section (Mallin de los Caballos, Figure 2.2): The 147-meter section is measured from the contact with Tordillo Formation until the top of the Los Catutos carbonate-rich interval. It has the most complete data set, including gamma-ray measurement each meter, 124 samples taken at 1m-intervals for geochemical analysis (stable isotopes and TOC), 63 hand samples for microfacies characterization, and 14 1m-length cores. From that data set,





**Figure 2.2. Picún Leufú-Sierra de la Vaca Muerta outcrops.** Red stars point out to the logged sections that provided the data analyzed in this work. Black stars indicate other sections used for comparison

50 thin sections, 50 geochemical samples and 7 cores correspond to the Los Catutos interval and were analyzed as part of the present work.

- VM23 section: It is a 24-meter section through the entire Los Catutos carbonate-rich interval, which is much thinned in this distal position. As the thickness to the contact with Tordillo Formation was not measured; its position was estimated by comparison with the Mallin Quemado section from Leanza (1973). Samples were collected at approximately 1m-intervals, 23 of them for geochemical analysis and 18 for microfacies characterization.

### **Puerta Curaco – Yesera del Tromen**

The Vaca Muerta research team of the University of Miami logged several sections through the Vaca Muerta-Quintuco succession as the reference sections in this area, 8 in Puerta Curaco and 1 in Yesera del Tromen:

- Puerta Curaco (PC) sections (Figure 2.3): The 8 sections were correlated, and PC-6, 2, 7 and 4 were integrated into a single reference section (PC) that covers 760m between Tordillo and Mulichinco Formations. In addition to the detailed lithologic log, this section includes 1m-interval gamma-ray readings, TOC and isotope measurements. Hand samples were taken from key beds for microfacies characterization, and 1m-length cores were drilled in certain intervals to capture all lithofacies types. From this data set, 50 hand samples, 12 cores and 145 samples for geochemistry from sections PC-4 and 8 were used to characterize the 3 carbonate-rich intervals analyzed in this work (Berriasian-Early Valanginian). Geochemistry analysis was performed on 21 samples to characterize the top of the second sequence (top of sections PC-1 and 6), which is time-equivalent to the Los Catutos Mb (Mid-Late Tithonian).

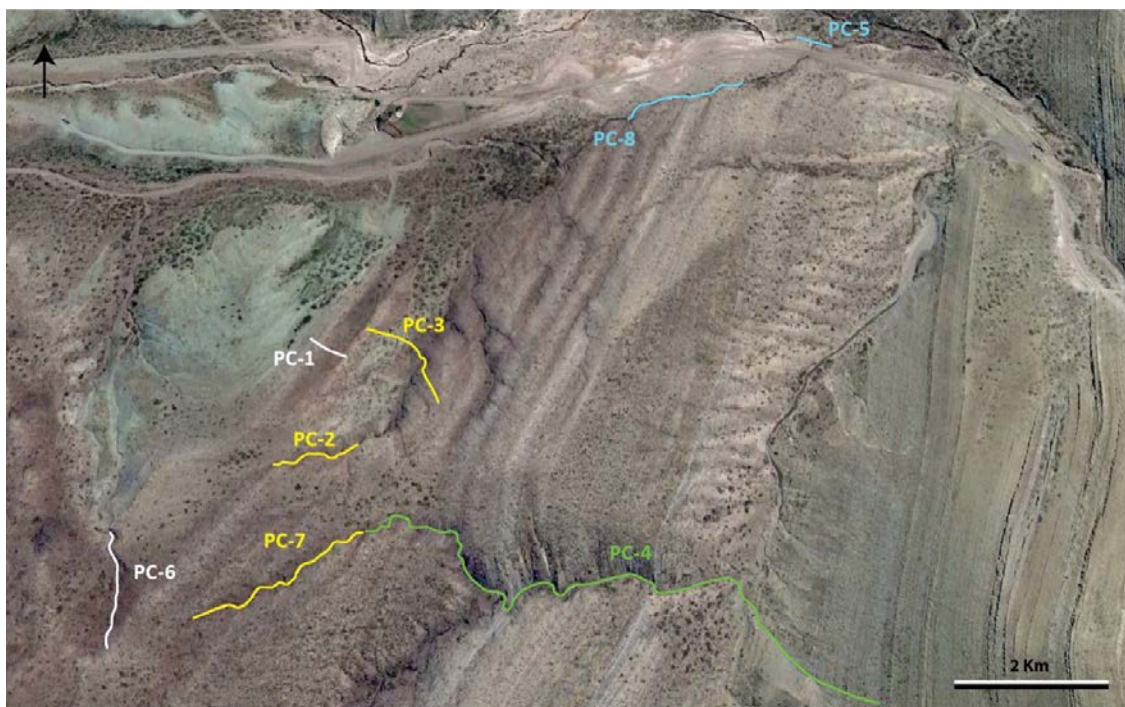


**Figure 2.3. Puerta Curaco outcrops.** Locations of the logged sections that were integrated into a PC reference section

- Yesera del Tromen section (YDT) (Figure 2.1): This section covers the 40m of the base of the Vaca Muerta Formation. The lithologic log is complemented by 1m-interval samples for geochemistry and TOC measurements. In addition, this section provides the biostratigraphic framework for the lower part of the PC reference section as it can be correlated to the biostratigraphic information provided by Aguirre Urreta et al (2014) in a nearby section.

An additional data source for this area are the well logs and core reports from El Trapial (Chevron) wells located approximately 40 km east of Puerta Curaco. Gamma-ray logs from these wells were compared with the outcrop GR for correlation. As there is no biostratigraphy published for Puerta Curaco outcrops, biostratigraphic reports from 17 cores drilled in 3 wells from El Trapial field were used to constrain the age of the sequences of the upper part of the PC reference section.

## **Chapter 3: Methods**

### **Data collection**

The sections were described in terms of lithology, rock color, texture after Dunham, sedimentary structures, and presence of fossils. Photos and GPS measurements were taken regularly. Small samples were collected in 1-meter intervals for geochemical analysis. Hand samples were taken at regular intervals, and from key beds for both microfacies characterization and geochemical analysis. Short cores were drilled from key intervals to characterize all lithotypes, with special focus on the more fissile portions where hand sample recovery is limited.

### **Lithofacies analysis**

The analysis of the lithofacies relies on the examination of outcrop beds, hand samples, and thin sections. The microfacies analysis conducted on thin sections under the light microscope helped validate and complement the outcrop lithofacies descriptions. This step was critical as most of the outcrop lithologies are mudstones in plain sight.

The studied carbonate-rich intervals were then divided into different lithofacies types according with their lithology, texture, sedimentary structures and components. Depositional environments were interpreted based on the observed lithofacies types and outcrop geometries.

### **Sequence stratigraphic analysis**

After each section was logged in outcrop, it was revisited and subdivided into cycles that follow the weathering profile: the transgressive portion and turnaround are typically

fissile and back-weathered, while the more cemented regressive tops tend to stick out more. These cycles defined in the field were subsequently grouped into cycle sets and sequences, which together produce the sequence-stratigraphic framework.

### **Biostratigraphy**

As Argentinian regulations forbid collecting fossils in the studied area, ages were assigned based on ammonite biostratigraphy compiled from the literature, in particular Leanza (1973), Leanza et al (1977), Leanza and Zeiss (1990), Aguirre Urreta et al (2014), and others. The most robust correlation was possible by comparing sections with ammonite stratigraphy to close-by sections measured for this study.

### **Geochemical analyses**

- **X-ray powder diffraction (XRD)**

This technique is based on the principle that monochromatic X-rays interfere constructively with a crystalline sample when conditions satisfy Bragg's Law:  $n\lambda=2d*\sin\theta$ , where the integer  $n$  is the "order" of reflection,  $\lambda$  is the wavelength of the incident X-rays,  $d$  is the interplanar spacing of the crystal and  $\theta$  is the angle of incidence. As a result of this interference diffracted rays are produced, detected and counted within an X-ray diffractometer. The sample is scanned through a range of  $2\theta$  angles to capture all possible diffraction directions of the lattice, as the powdered material is randomly oriented.

The samples were run in a PANalytical X'Pert PRO diffractometer and scanned through  $2\theta$  angles between 2 and 45. The resulting diffraction patterns were interpreted to qualitatively determine the main compounds in each sample.

- **Carbonate content**

The carbonate content was determined as part of measuring the organic material present in the samples. Approximately 0.5g of sample were initially weighted together with its beaker, and the carbonate present in the sample was dissolved in 10% HCl acid overnight to separate the organic material. The acidification of the samples was followed by 3 or 4 washes with DI water and decanting to remove the acid. The critical part of this process is that during decanting and changing the water no material is removed. The samples were then dried and the insoluble residue weighted, and its value subtracted from the initial weight of the sample. The resulting values represents the dissolved carbonate, which can be converted to percentage of carbonate (%CO<sub>3</sub>) originally in the sample.

- **Organic content**

After dissolution of the samples in 10% HCl, the insoluble residue was dried for at least 48hs until constant dry weight was achieved. The samples of the insoluble material were scrapped off the beakers, weighed and packed into tin capsules, and loaded into a Costech ECS 4010 where they were combusted. The resulting CO<sub>2</sub> gas was transferred to a Delta V Advantage elemental analyzer where the measured peak area was calibrated against the known weight of the carbon. As a result, the % organic carbon in the insoluble residue was obtained, and converted to %TOC by the following equation:

$$\% \text{TOC} = \frac{\text{organic C in insoluble residue (\%)} * \text{weight of insoluble residue (g)}}{\text{initial weight of sample (g)}}$$

- **$\delta^{13}\text{C}$  and  $\delta^{18}\text{O}$  isotopes**

Carbonate isotope ratios were measured via dissolution of the samples in phosphoric acid using the common acid bath method (Swart et al. 1991). The CO<sub>2</sub> gas produced by the reaction between the acid and the carbonate present in the samples was analyzed on a

Finnigan MAT 251. Each run included 25 samples, 3 standards at the beginning and 2 standards at the end. Data was corrected for any fractionation in the reference gas during the run, and reported relative to the Vienna Pee Dee Belemnite (VPDB) scale. The values of the CO<sub>2</sub> gas pressure were also reported for each sample.

The  $\delta^{13}\text{C}$  and  $\delta^{18}\text{O}$  were measured in all the available samples from MDC section and each 5m in the PC reference section, whether the samples were part of the carbonate-rich intervals or not. Samples with low carbonate content values ( $\% \text{CO}_3 < 11\%$ ) were disregarded.

## **Chapter 4: Results**

This chapter shows the results of the different analyses performed in the studied intervals: Los Catutos Member in Sierra de la Vaca Muerta (MDC and VM23) and three younger carbonate-rich intervals in Puerta Curaco (first, second and third interval). The first two sections of the chapter, Lithofacies and Geochemistry, present all the analyzed parameters that will be discussed in further detail in the subsequent sections. The Lithofacies Analysis section describes the different types of lithofacies identified in the entire stratigraphic sections (whether they belong to the analyzed intervals or not) in order to put the carbonate-rich intervals in context. The Geochemistry section provides an introduction to the geochemical variables of the entire investigated data set. Subsets of the data sorted by interval and position in the cycle are shown in Stratigraphic Distribution and Sequence Stratigraphy sections, respectively. The section on Stratigraphic Distribution examines first the vertical changes in lithofacies and the geochemical variations along the two main studied sections (MDC and PC), and then focus on the carbonate-rich intervals of different ages. In the case of the Los Catutos Member, lateral changes between MDC and VM23 are also evaluated. The section on Sequence Stratigraphy analyzes the lithofacies arrangement in cycles of different orders, and the geochemical variations within those cycles. The Correlation section integrates the litho, sequence and chrono-stratigraphic frameworks to show the correlation of the studied intervals, both amongst themselves and to sections from other authors.



## Lithofacies analysis

In the studied sections 12 lithofacies types were identified based on lithology, texture, main components, and sedimentary structures (Table 4.1):

lithofacies	texture	grain size	sorting	sedimentary structures	components
fissile clastic mudstones		mud to silt	well	mostly shattered, fissile, no bioturbation	quartz [a], clay [c], organic matter [a], ammonites [c-a], pyrite [c], fish scales [r-c], skeletal fragments [r] (radiolarians)
fissile carbonate mudstones	mudstone	mud to silt	well	fissile, no bioturbation	quartz [c], ammonites [c], organic matter [c], pyrite [c], skeletal fragments [r] (radiolarians, sponge spicules)
calcareous siltstones		silt to very fine sand	well	massive or thin bedded, moderately bioturbated	quartz [a], clay [c], plagioclase [r], skeletal fragments [c] (radiolarians, sponge spicules, shells, crinoids)
algal laminites	bindstone	mud to silt	well	microbial lamination	skeletal fragments [r] (radiolarians)
carbonate mudstone/wackestones	mudstone	mud, very fine sand	poor	massive, locally nodular, strongly bioturbated	quartz [c], organic matter [c], pyrite [c], ammonites [r-a], skeletal fragments [r] (radiolarians, sponge spicules)
peloidal wackestone/packstones	wackestone	mud, fine sand	poor	massive or slightly laminated, locally nodular, moderate to strongly bioturbated	peloids [c], quartz [r-c], skeletal fragments [c] (radiolarians, sponge spicules, shells), organic matter [c], pyrite [c]
skeletal wackestone/packstones	wackestone	mud, fine sand	poor	massive or slightly laminated, locally nodular, moderate to strongly bioturbated	skeletal fragments [a] (radiolarians, shells, crinoids), quartz [c], bivalves [c], ammonites [r-c]
crinoidal packstones	packstone	mud, medium sand	poor	massive or slightly laminated, locally nodular, moderate to strongly bioturbated	skeletal fragments [a] (radiolarians, sponge spicules, shells, crinoids), quartz [r]
massive calcareous sandstones		fine to medium sand	well	massive or thin bedded, moderately bioturbated	quartz [a], bivalves [r-c], skeletal fragments [r-c] (shells)
ash layers	crystalline	silt to coarse sand	moderate	generally laminated, occasionally cross-bedded, frequent ripples towards top, common bioturbation	crystalline calcite [a], opaque minerals [c], quartz [r-c], altered feldspars [r-c]
calcite veins	crystalline			fibrous	
dolomites	crystalline	mud	well	massive	crystalline dolomite [a]

**Table 4.1. Summary of lithofacies descriptions** for the investigated sections in Sierra de la Vaca Muerta (MDC and VM23) and Puerta Curaco (PC). Abbreviations for components are: a-abundant, c-common, r-rare

**Fissile clastic mudstones** (Figures 4.1-A and 4.2-A) are typically weathered, but show dark brown to black colors on fresh surfaces. Bioturbation is absent (or not visible), but organic matter is abundant. Along certain surfaces ammonites are abundant, and fish scales are less frequent. Skeletal fragments are rare and mostly limited to radiolarians. Commonly these dark shales grade upwards to more carbonate-rich mudstones.

**Fissile carbonate mudstones** (Figures 4.1-B and 4.2-B) are light brown to grey, and appear more weathered than the other carbonate-rich facies. Bioturbation is absent or not visible due to the fissile behavior, and organic matter is abundant. Ammonites can be concentrated along some surfaces. Skeletal fragments are rare, and mostly limited to radiolarians and sponge spicules. Frequently this facies is associated laterally with stratigraphically-aligned calcareous concretions of variable thickness, from centimeters to decimeters, and variable spacing, from isolated rounded concretions to almost continuous irregular beds.

**Calcareous siltstones** (Figures 4.1-C and 4.2-C) appear in layers of few centimeters, either massive or thin bedded, intercalated within the fissile carbonate mudstone facies. Occasionally siltstones grade upwards to very fine grained cross-bedded sandstones. Bioturbation is variable. Skeletal fragments are common; they are mostly radiolarians, sponge spicules and shells.

**Algal laminites** (Figures 4.1-D and 4.2-D). Beds with algal laminites are yellowish-brown on weathered surfaces and dark grey on fresh surfaces, laminated, and have an average thickness of 0.3m. Skeletal fragments are rare and consist of radiolarians.

**Massive carbonate mudstones/wackestones** (Figure 4.1-E) are massive or slightly laminated, yellowish-brown on weathered surfaces and dark grey on fresh surfaces.

Bioturbation is very strong, obliterating any previous structure. Organic matter is common. Ammonites are sometimes concentrated at the top of the beds, and other skeletal fragments are radiolarians and sponge spicules. Quartz is visible but the amount varies.

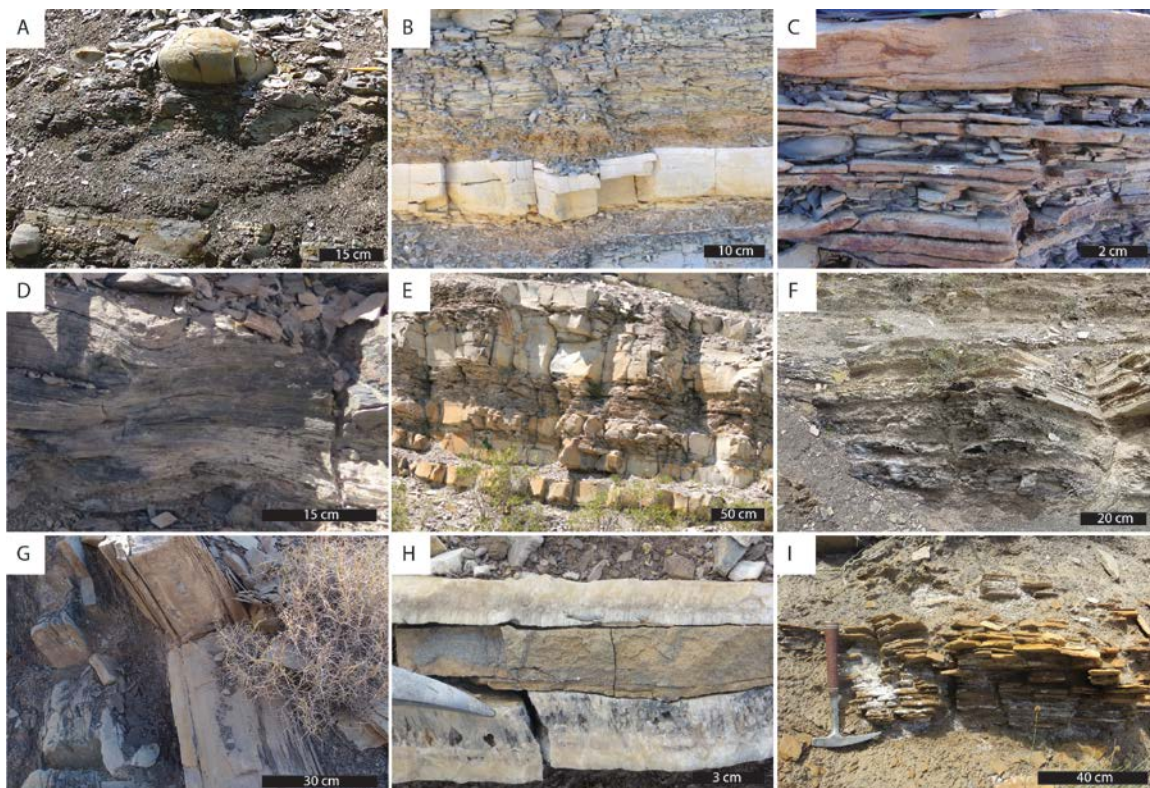


**Figure 4.1. Lithofacies in outcrops.** A) Fissile clastic mudstones, with more carbonate-rich intercalations associated with concretions. B) Fissile carbonate mudstones with volcanic intercalation. C) Siltstones grading to cross-stratified sandstones. D) Algal lamination. E) Massive mudstone/wackestones. F) Laminated peloidal wackestones. G) Massive to slightly laminated skeletal wackestone/packstones. H) Ash layer between calcite veins. I) Dolomitized bed.

**Peloidal wackestones/packstones** (Figures 4.1-F and 4.2-E) appear as massive or slightly laminated beds, yellowish-brown on weathered surfaces and dark grey on fresh surfaces. Bioturbation is moderate to strong, and organic matter is common. Peloids are very abundant and appear frequently compacted. Skeletal fragments are common and include radiolarians, sponge spicules, and shells. The clastic content, represented mostly by quartz, is variable.

**Skeletal wackestones/packstones** (Figures 4.1-G and 4.2-F) appear as massive or slightly laminated beds, with average thicknesses of 0.3 m, yellowish-brown on weathered surfaces and dark grey on fresh surfaces. Bioturbation is moderate to strong, and organic matter is common. Bivalves are common, and ammonites are sometimes concentrated at the top of the beds. Skeletal fragments are abundant and include radiolarians, sponge spicules, shells, and occasionally crinoids. The clastic content, usually quartz, is variable.

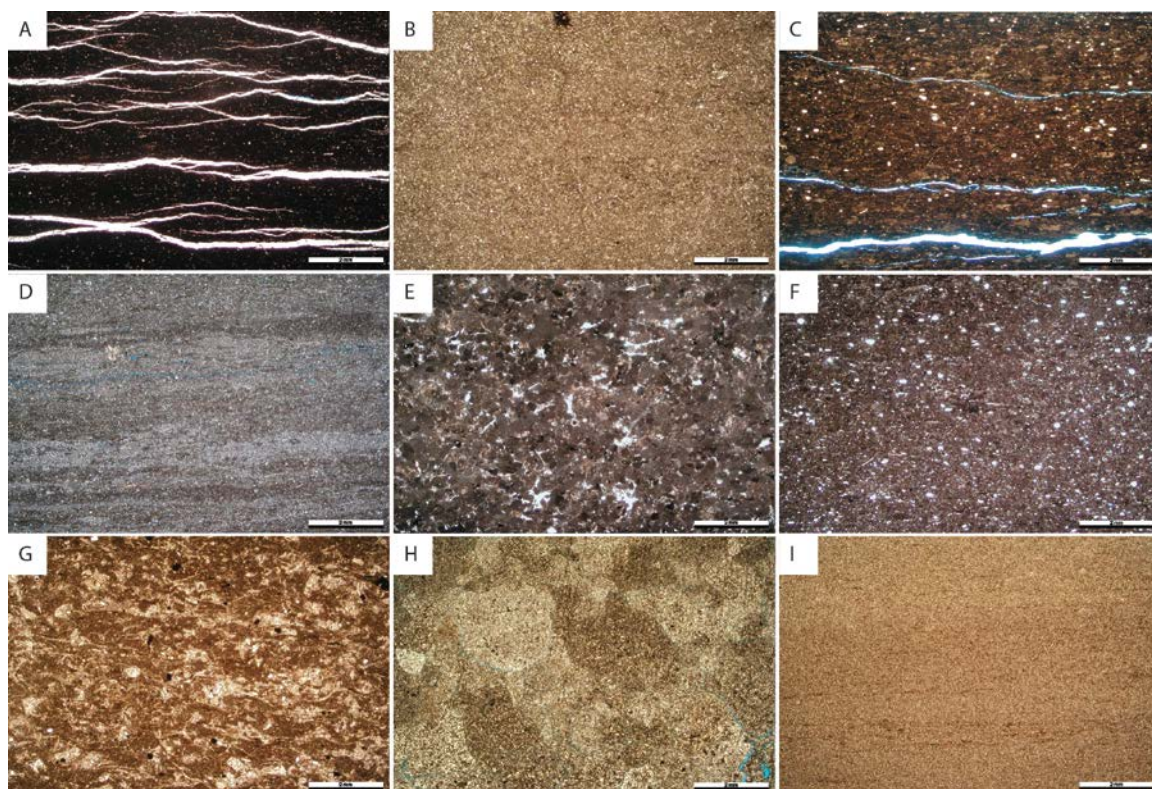


**Figure 4.2. Microfacies.** A) Fissile clastic mudstone. B) Carbonate mudstone. C) Calcareous silt with occasional radiolarians. D) Algal lamination. E) Peloidal packstone. F) Skeletal wackestone/packstone with abundant radiolarians. G) Crinoidal packstone. H) Coarse-grained crystalline structure in ash layer. I) Fine-grained crystalline structure in dolomitized bed. All scales are 2mm

**Crinoidal packstones** (Figure 4.2-G). Beds are yellowish-brown on weathered surfaces and dark grey on fresh surfaces, massive or slightly laminated, with an average thickness of 0.2m. Bioturbation is moderate to strong. Skeletal fragments are very abundant

and include crinoids, radiolarians, sponge spicules and shells. The clastic content, represented mostly by quartz, is variable.

**Massive calcareous sandstones** (Figure 4.1-C) are thin or medium bedded, with variable degree of bioturbation. Entire bivalves can be found as well as skeletal fragments of shells.

**Ash layers** (Figures 4.1-H and 4.2-H) appear as grey-greenish or orange layers with variable thickness from only a few centimeters to several decimeters. The orange layers are typically thinner and are reminiscent of bentonites. They disaggregate easily; hence no hand samples could be collected. The greyish layers are massive or normally graded beds, with sharp contacts and occasionally flute casts at the base. Cross bedding, ripples, and horizontal lamination are common, frequently disturbed by bioturbation that also produces a mix with the adjacent beds. Ash layers can resemble siltstones or sandstones due to their grain size and the presence of tractive structures, but in thin section this facies typically shows crystalline structure with common glass shards. In places crystals of quartz, altered feldspars, and clusters of opaque minerals can be identified within a devitrified matrix. Complete replacement of quartz crystals by calcite is very unlikely. It is more probable that quartz crystals were originally irregularly distributed within a glassy cloud. The more unstable portions would have been replaced by crystalline calcite, while the quartz-rich portions are preserved. These facies are sometimes associated with centimeter to decimeter-thick concretions. Lateral transitions between bentonite-type layers, concretions, and recrystallized beds with tractive structures are common.

**Calcite veins** (Figure 4.1-H) appear as several centimeter-thick, highly continuous layers of pure calcite within fissile clastic and carbonate-rich mudstones. Calcite veins are frequently associated with ash layers and concretions.

**Dolomitized beds and concretions** (Figures 4.1-I and 4.2-I) appear as either massive or laminated beds of 0.3m average thickness, or stratigraphically-aligned concretions of different sizes and shapes. Weathered surfaces are characteristically orange. In thin section they show a crystalline structure, and XRD analyses indicate an almost 100% dolomite composition. In the uppermost part of the Puerta Curaco section they are very fossiliferous, with bivalves, skeletal fragments and ammonites.

## Geochemistry

With the purpose of complementing the lithologic characterization of the analyzed sections and carbonate-rich intervals, carbonate (%CO<sub>3</sub>) and organic (%TOC) content, and carbon ( $\delta^{13}\text{C}_{\text{in}}$ ) and oxygen ( $\delta^{18}\text{O}$ ) isotope ratios were measured on 246 samples from Los Catutos Member in MDC and VM23, its time-equivalent expression in PC (where the Los Catutos Member is not present), and three younger carbonate-rich intervals in PC. Results are given in Table 4.2.

The complete data set from MDC and PC sections, which are the two most complete sections analyzed, is shown in Appendix A, and includes the data from the studied intervals (Table 4.2) and from the rest of the sections. In addition, isotope data from Picún Leufú carbonate platform plug samples is given in Appendix B.

Section	Interval/Unit	Cycle	Sample	Depth	CO <sub>3</sub> (%)	TOC (%)	$\delta^{13}\text{C}_{\text{in}}$ (‰)	$\delta^{18}\text{O}$ (‰)	
MDC	Los Cat	V	TOP	MDC4-13	146.80	91	0.16	0.94	-6.42
MDC	Los Cat	V	TOP	MDC4-12	145.80	82	0.26	4.04	-4.60
MDC	Los Cat	IV	TOP	MDC4-11	141.5	86	0.80	0.69	-5.96
MDC	Los Cat	IV	TOP	MDC4-10	139.7	88	0.79	0.86	-5.84

Section	Interval/Unit	Cycle		Sample	Depth	CO3 (%)	TOC (%)	$\delta^{13}\text{C}_{\text{in}}$ (‰)	$\delta^{18}\text{O}$ (‰)
MDC	Los Cat	IV	TOP	P_139	137.9	87	0.77	-0.09	-5.45
MDC	Los Cat	IV	TOP	MDC4-9	137.5	82	1.12	0.68	-6.17
MDC	Los Cat	IV	TOP	P_141	137.3	78	1.95	1.32	-5.18
MDC	Los Cat	IV	TOP	P_143	135	79		1.45	-6.87
MDC	Los Cat	IV	TOP	MDC4-8	134.5	84	1.23	0.83	-6.21
MDC	Los Cat	IV	TOP	P_145	134.2	76	1.53	1.31	-5.41
MDC	Los Cat	IV	R	MDC4-6	132.2	85	0.47	0.71	-6.03
MDC	Los Cat	IV	TOP	MDC4-5	131	71	1.57	-0.04	-5.71
MDC	Los Cat	IV	TOP	P_135	128.9	67	2.84	0.98	-6.53
MDC	Los Cat	IV	R	P_137	128.1	63	1.87	0.90	-6.01
MDC	Los Cat	IV	TOP	MDC4-4	127	67	1.09	0.70	-5.67
MDC	Los Cat	IV	MFS	MDC4-3	126	27	2.14	-0.28	-7.64
MDC	Los Cat	III	TOP	MDC4-2	124.5	81	0.79	1.17	-5.92
MDC	Los Cat	III	TOP	VM14-134	124.3	76	0.94	1.31	-5.01
MDC	Los Cat	III	TOP	MDC5-7	124	97	0.06	0.87	-5.89
MDC	Los Cat	III	TOP	P_130	124	78	1.07	1.32	-5.89
MDC	Los Cat	III	TOP	P_133	123.6	80	1.28	1.56	-6.38
MDC	Los Cat	III	TOP	VM14-133	123.4	77	1.25	1.50	-5.53
MDC	Los Cat	III	R	VM14-132	122.7	66	1.43	1.43	-6.50
MDC	Los Cat	III	TOP	MDC4-1	122.5	78	0.87	0.76	-6.40
MDC	Los Cat	III	TOP	VM14-131	122.25	71	1.03	1.25	-5.90
MDC	Los Cat	III	TOP	VM14-130	121.4	77	0.35	0.07	-6.50
MDC	Los Cat	III	TOP	MDC5-6	121	76	0.74	0.81	-6.07
MDC	Los Cat	III	R	VM14-129	120.6	77	0.22	0.49	-7.12
MDC	Los Cat	III	TOP	VM14-128	119.55	74	1.13	1.32	-7.00
MDC	Los Cat	III	TOP	MDC5-5	119	84	0.77	0.96	-6.48
MDC	Los Cat	III	TOP	VM14-127	118.7	79	1.22	1.29	-6.29
MDC	Los Cat	III	TOP	VM14-126	117.7	79	1.36	1.35	-7.48
MDC	Los Cat	III	TOP	VM14-125	116.9	84	1.01	1.04	-5.78
MDC	Los Cat	III	TOP	VM14-124	116	80	0.41	0.43	-6.01
MDC	Los Cat	III	TOP	VM14-135	115.9	79	0.95	1.24	-6.34
MDC	Los Cat	III	TOP	MDC5-4	115.8	74	1.19	1.01	-6.34
MDC	Los Cat	III	R	VM14-123	114.5	66	1.32	1.13	-5.81
MDC	Los Cat	III	R	VM14-122	113.3	60	1.38	0.60	-5.51
MDC	Los Cat	III	R	VM14-121	112.5	62	1.29	0.93	-5.71
MDC	Los Cat	III	TOP	VM14-119	110.6	66	1.03	0.61	-5.86
MDC	Los Cat	III	R	VM14-137	110	50	1.53	0.47	-5.87
MDC	Los Cat	III	T	VM14-118	109.5	29	2.82	-0.23	-6.24
MDC	Los Cat	III	TOP	MDC5-2	109	79	0.77	0.62	-6.16
MDC	Los Cat	III	TOP	MDC5-1	108	70	1.17	0.53	-5.53
MDC	Los Cat	II	TOP	VM14-115	106.5	82	0.98	0.82	-5.56
MDC	Los Cat	II	TOP	MDC2-13	106	84	0.60	1.17	-5.74
MDC	Los Cat	II	R	VM14-114	105.5	74	1.13	0.65	-6.43
MDC	Los Cat	II	R	MDC2-12	105.3	81	1.23	1.28	-5.11
MDC	Los Cat	II	R	VM14-113	104.6	79	2.21	1.05	-5.85
MDC	Los Cat	II	TOP	MDC2-11	104.5	82	0.58	0.33	-5.97
MDC	Los Cat	II	TOP	VM14-112	103.8	81	0.64	0.33	-5.43
MDC	Los Cat	II	TOP	MDC2-10	103.5	85	0.69	1.17	-5.10
MDC	Los Cat	II	TOP	VM14-111	103	83	0.70	0.93	-4.77
MDC	Los Cat	II	TOP	MDC2-9	102.5	85	0.76	1.09	-4.91
MDC	Los Cat	II	TOP	VM14-110	102.1	82	1.03	1.05	-5.09
MDC	Los Cat	II	TOP	MDC2-8	102	84	0.84	1.08	-4.99

Section	Interval/Unit	Cycle	Sample	Depth	CO3 (%)	TOC (%)	$\delta^{13}\text{C}_{\text{in}}$ (‰)	$\delta^{18}\text{O}$ (‰)	
MDC	Los Cat	II	TOP	MDC2-7	101.5	81	0.82	0.83	-5.50
MDC	Los Cat	II	TOP	VM14-109	101.4	70	1.31	0.79	-5.46
MDC	Los Cat	II	TOP	VM14-108	100.7	80	0.70	0.80	-4.83
MDC	Los Cat	II	TOP	MDC2-6	100	84	0.66	0.92	-4.73
MDC	Los Cat	II	TOP	VM14-107	99.75	78	0.30	0.34	-5.61
MDC	Los Cat	II	TOP	MDC2-5	99.5	82	0.85	0.85	-5.19
MDC	Los Cat	II	TOP	VM14-106	98.6	84	0.35	1.17	-5.17
MDC	Los Cat	II	TOP	MDC2-4	98.5	92	0.38	1.34	-4.94
MDC	Los Cat	II	R	VM14-105	97.4	64	1.65	0.10	-5.70
MDC	Los Cat	II	T	VM14-104	96.6	59	1.76	0.27	-5.34
MDC	Los Cat	II	T	VM14-103	95.9	49	2.53	-0.78	-6.36
MDC	Los Cat	II	T	VM14-102	94.7	44	1.42	-0.16	-4.88
MDC	Los Cat	II	TOP	MDC2-2	94.5	80	0.05	-0.19	-4.47
MDC	Los Cat	II	R	VM14-101	94.3	28	1.36	-2.21	-6.29
MDC	Los Cat	II	R	VM14-100	93.6	56	1.13	-0.25	-5.28
MDC	Los Cat	II	MFS	VM14-99	92.6	33	2.51	-0.50	-7.44
MDC	Los Cat	II	MFS	VM14-98	91.6	48	2.68	-1.38	-5.27
MDC	Los Cat	II	T	VM14-97	91.25	32	2.15	-0.48	-6.78
MDC	Los Cat	I	T	VM14-96	90.8	57	0.95	-1.26	-4.79
MDC	Los Cat	I	R	VM14-95	90.2	60	0.77	-0.36	-5.07
MDC	Los Cat	I	MFS	VM14-94	89.9	19	2.15	-1.07	-6.63
MDC	Los Cat	I	R	VM14-93	89.1	53	2.46		-7.68
MDC	Los Cat	I	T	VM14-92	88.2	48	2.32	-0.91	-6.23
MDC	Los Cat	I	T	VM14-91	87.25	37	2.98	-1.24	-6.23
MDC	Los Cat	I	MFS	VM14-90	86.45	22	2.12	-1.14	-6.06
MDC	Los Cat	I	MFS	VM14-89	85.55	10	1.96	-1.94	-8.46
MDC	Los Cat	I	TOP	VM14-87	84.6	58	1.77	-1.00	-6.33
MDC	Los Cat	I	TOP	MDC-GRL-1	84.3	59	1.34	-1.26	-6.12
MDC	Los Cat	I	TOP	VM14-86	83.25	66	1.84	-1.25	-6.14
MDC	Los Cat	I	TOP	VM14-85	82.25	82	0.38	0.47	-5.99
MDC	Los Cat	I	R	VM14-84	81.5	47	2.62	-1.40	-5.32
MDC	Los Cat	I	MFS	VM14-83	80.7	24	3.37	-1.60	-5.88
MDC	Los Cat	I	MFS	VM14-82	79.95	31	2.37	-1.50	-5.70
VM23	Los Cat	IV	R	VM23-21.6	21.6	90	0.37		-3.75
VM23	Los Cat	IV	TOP	VM23-20.5	20.5	83	1.06	-0.23	-8.25
VM23	Los Cat	IV	R	VM23-20	20	85	1.34	-0.33	-8.08
VM23	Los Cat	IV	R	VM23-19	19	72	2.75	0.31	-7.79
VM23	Los Cat	IV	R	VM23-18.2	18.2	68	2.22	-1.43	-7.48
VM23	Los Cat	IV	R	VM23-17	17	68	1.41	-0.62	-6.45
VM23	Los Cat	IV	MFS	VM23-16	16	48	2.05	-1.00	-8.26
VM23	Los Cat	IV	R	VM23-14.8	14.8	63	0.89	-0.77	-6.04
VM23	Los Cat	IV	R	VM23-13.5	13.5	61	2.52	-0.59	-7.97
VM23	Los Cat	IV	MFS	VM23-12.5	12.5	30	3.08	-1.01	-8.23
VM23	Los Cat	IV	MFS	VM23-12	12	35	1.24	-1.65	-8.43
VM23	Los Cat	III	R	VM23-10.9	10.9	83	0.89	-0.76	-5.80
VM23	Los Cat	III	R	VM23-9.6	9.6	86	1.05	-1.07	-6.37
VM23	Los Cat	III	R	VM23-8.5	8.5	90	0.68	-1.43	-6.54
VM23	Los Cat	III	R	VM23-7.6	7.6	87	0.75	-1.15	-6.78
VM23	Los Cat	III	R	VM23-6.6	6.6	83	0.72	-1.20	-6.64
VM23	Los Cat	III	R	VM23-5.6	5.6	70	1.09	-0.85	-6.20
VM23	Los Cat	III	R	VM23-4.7	4.7	64	1.48	-0.78	-7.50
VM23	Los Cat	III	R	VM23-4.5	4.5	54	1.95	-1.21	-7.61



Section	Interval/Unit	Cycle	Sample	Depth	CO3 (%)	TOC (%)	$\delta^{13}\text{C}_{\text{in}}$ (‰)	$\delta^{18}\text{O}$ (‰)	
VM23	Los Cat	III	MFS	VM23-3.8	3.8	36	2.82	-1.75	-8.44
VM23	Los Cat	III	T	VM23-2.1	2.1	56	1.94	-2.39	-7.49
VM23	Los Cat	III	MFS	VM23-1.6	1.6	32	4.45	-1.37	-8.54
PC	m-l Tith	TOP	PC02-6.2	56.2	67	1.97	-3.75	-8.77	
PC	m-l Tith	R	PC02-6	56	47	0.66	-2.54	-10.39	
PC	m-l Tith	R	PC02-5	55	19	1.65	-1.75	-8.98	
PC	m-l Tith	R	PC02-4	54	47	0.69	-2.37	-9.94	
PC	m-l Tith	R	PC02-3	53	44	1.30	-1.89	-9.90	
PC	m-l Tith	MFS	PC02-2	52	22	1.63	-3.09	-10.54	
PC	m-l Tith	T	PC02-1	51	28	1.15	-1.61	-10.35	
PC	m-l Tith	TOP	PC02-0	50	70	0.66	-0.21	-10.23	
PC	m-l Tith	R	PC06-49	49	35	1.79	-3.36	-10.52	
PC	m-l Tith	R	PC06-48.7	48.7	70	1.65	-2.47	-10.49	
PC	m-l Tith	R	PC06-48	48	21	2.01	-2.98	-13.91	
PC	m-l Tith	MFS	PC06-47	47	7	7.24			
PC	m-l Tith	T	PC06-46	46	37	2.04	-1.29	-13.19	
PC	m-l Tith	T	PC06-45	45	34	3.59	-5.19	-14.67	
PC	1st CO3	TOP	PC4-152.9	346.9	90	0.27	0.25	-6.62	
PC	1st CO3	TOP	P_115	346.9	85	0.75	-0.29	-8.24	
PC	1st CO3	TOP	PC4-155	346.9	82	0.45	-0.27	-7.02	
PC	1st CO3	R	P_117	346.4	79	0.46	-0.52	-7.99	
PC	1st CO3	TOP	PC4-152	346	77	1.25	-0.51	-6.99	
PC	1st CO3	TOP	PC4-154	345.9	68	0.61	-0.64	-7.89	
PC	1st CO3	TOP	P_123	345.4	77	1.23	-0.77	-8.21	
PC	1st CO3	R	PC4-151	345	45	1.87	-0.73	-7.47	
PC	1st CO3	R	P_125	344.7	67	1.84	-1.26	-8.10	
PC	1st CO3	MFS	PC4-150	344	48	1.90	-0.47	-7.50	
PC	1st CO3	TOP	P_119	343.1	73	1.09	-0.65	-7.84	
PC	1st CO3	TOP	PC4-149	343	65	1.17	-0.44	-7.81	
PC	1st CO3	MFS	P_121	342.2	52	1.11	-0.79	-7.96	
PC	1st CO3	MFS	PC4-148	342	53	1.78	-0.27	-7.21	
PC	1st CO3	TOP	PC4-147	341	65	1.35	-0.38	-7.99	
PC	1st CO3	TOP	PC4-146.8	340.8	88	0.21	-0.23	-5.47	
PC	1st CO3	R	PC4-146.2	340.2	81	0.13	-0.05	-5.28	
PC	1st CO3	R	PC4-146.1	340.1	85	0.11	-0.52	-5.55	
PC	1st CO3	R	PC4-145	339	83	0.46	-0.17	-7.79	
PC	1st CO3	TOP	PC4-144.1	338.1	83	0.65	-0.21	-6.54	
PC	1st CO3	TOP	PC4-144	338	58	1.61	-0.68	-7.81	
PC	1st CO3	TOP	PC4-143	337	64	1.34	-0.85	-7.14	
PC	1st CO3	MFS	PC4-142	336	58	2.09	-1.00	-7.98	
PC	1st CO3	TOP	P_60	335.3	82	0.58	-0.60	-8.30	
PC	1st CO3	TOP	PC4-141.1	335.1	95	0.13	0.78	-6.23	
PC	1st CO3	TOP	PC4-141	335	84	0.61	-0.11	-7.76	
PC	1st CO3	T	P_62	334.6	66	0.84	-0.59	-8.68	
PC	1st CO3	TOP	PC4-140	334	68	0.88	-0.57	-7.72	
PC	1st CO3	MFS	PC4-139	333	42	1.61	-0.56	-7.54	
PC	1st CO3	T	PC4-138	332	20	1.92	-1.00	-7.75	
PC	1st CO3	T	PC4-137	331	54	1.05	-1.40	-6.95	
PC	1st CO3	MFS	PC4-136	330	56	2.15	-0.96	-7.43	
PC	1st CO3	TOP	P_56	329.1	88	0.39	-1.23	-7.32	
PC	1st CO3	TOP	PC4-135	329	85	0.49	-0.73	-6.29	
PC	1st CO3	R	P_58	328.2	50	0.75	-0.86	-7.30	

Section	Interval/Unit	Cycle	Sample	Depth	CO3 (%)	TOC (%)	$\delta^{13}\text{C}_{\text{in}}$ (‰)	$\delta^{18}\text{O}$ (‰)
PC	2nd CO3	TOP	P_76	404.1	81	0.88	-0.84	-7.61
PC	2nd CO3	TOP	PC4-210	404	88	0.65	1.05	-7.19
PC	2nd CO3	R	P_78	403.5	48	2.00	-0.93	-7.56
PC	2nd CO3	R	PC4-209	403	47	2.29	-1.40	-8.27
PC	2nd CO3	T	PC4-208	402	36	2.97	-1.03	-7.10
PC	2nd CO3	R	PC4-207	401	50	2.55	-1.34	-6.02
PC	2nd CO3	MFS	PC4-206	400	31	2.00	-0.94	-8.29
PC	2nd CO3	TOP	PC4-204.9	398.9	78	0.68	1.31	-6.54
PC	2nd CO3	R	PC4-204	398	67	0.65	-0.67	-7.31
PC	2nd CO3	R	PC4-203	397	53	0.94	-0.88	-7.33
PC	2nd CO3	T	PC4-202	396	18	1.83	-0.65	-7.54
PC	2nd CO3	TOP	PC4-201.5	395.5	68	0.71	-0.71	-7.00
PC	2nd CO3	R	PC4-201	395	39	0.67	-0.93	-7.56
PC	2nd CO3	R	PC4-200	394	20	1.01	-1.53	-8.37
PC	2nd CO3	R	PC4-199	393	35	2.20	-1.12	-8.61
PC	2nd CO3	T	PC4-198	392	15	2.58	-1.00	-8.43
PC	2nd CO3	TOP	P_72	391.3	78	0.54	-0.44	-7.80
PC	2nd CO3	TOP	PC4-197.2	391.2	86	0.28	0.97	-6.26
PC	2nd CO3	TOP	PC4-197	391	73	0.54	-1.03	-7.51
PC	2nd CO3	MFS	PC4-196	390	26	1.25	-0.99	-8.39
PC	2nd CO3	R	PC4-195	389	59	1.27	-1.35	-5.91
PC	2nd CO3	R	PC4-194	388	29	1.35	-1.69	-8.16
PC	2nd CO3	T	PC4-193	387	29	2.60	-1.57	-8.33
PC	2nd CO3	R	PC4-192	386	20	1.18	-1.36	-7.50
PC	2nd CO3	MFS	PC4-191	385	26	1.89	-1.26	-7.61
PC	2nd CO3	T	PC4-190	384	33	0.92	-0.91	-6.71
PC	2nd CO3	T	PC4-189	383	36	2.27	-0.65	-7.39
PC	2nd CO3	TOP	PC4-188.6	382.6	86	0.31	1.21	-5.33
PC	2nd CO3	MFS	PC4-188	382	28	2.17	-0.60	-7.29
PC	2nd CO3	TOP	P_68	381.2	76	0.79	-0.76	-7.23
PC	2nd CO3	R	PC4-187	381	38	1.93	-0.27	-7.43
PC	2nd CO3	R	P_70	380.5	47	1.51	-0.01	-7.17
PC	2nd CO3	TOP	PC4-186.2	380.2	87	0.43	1.18	-5.35
PC	2nd CO3	TOP	PC4-185.3	379.3	86	0.49	0.99	-5.34
PC	2nd CO3	TOP	PC4-185	379	66	1.09	-0.56	-7.66
PC	2nd CO3	R	PC4-184	378	54	1.37	-0.62	-7.72
PC	2nd CO3	T	PC4-183	377	37	3.04	-0.95	-7.58
PC	2nd CO3	TOP	PC4-182	376	76	0.62	0.73	-5.99
PC	2nd CO3	MFS	PC4-181	375	41	2.51	-1.09	-7.92
PC	2nd CO3	T	PC4-180	374	32	1.87	-0.27	-7.67
PC	2nd CO3	MFS	PC4-179	373	39	2.66	-1.02	-8.10
PC	2nd CO3	MFS	PC4-178	372	41	4.31	-1.09	-7.71
PC	3rd CO3	TOP	PC4-323.5	517.5	81	0.89	0.23	-7.93
PC	3rd CO3	R	PC4-323	517	35	1.28	0.25	-7.14
PC	3rd CO3	T	PC4-322	516	61	1.01	0.08	-7.53
PC	3rd CO3	R	PC4-321	515	75	0.94	-0.20	-7.65
PC	3rd CO3	R	PC4-320.7	514.7	80	0.75	0.27	-7.79
PC	3rd CO3	R	PC4-320	514	46	0.94	-0.09	-7.26
PC	3rd CO3	T	PC4-319	513	50	0.60	-0.25	-7.52
PC	3rd CO3	TOP	PC4-318	512	51	0.64	-0.26	-7.77
PC	3rd CO3	MFS	PC4-317	511	42	1.77	0.02	-7.34
PC	3rd CO3	T	PC4-316	510	27	0.75	-0.24	-7.58

Section	Interval/Unit	Cycle	Sample	Depth	CO <sub>3</sub> (%)	TOC (%)	$\delta^{13}\text{C}_{\text{in}}$ (‰)	$\delta^{18}\text{O}$ (‰)
PC	3rd CO <sub>3</sub>	TOP	PC4-315	509	75	1.14	-0.09	-7.96
PC	3rd CO <sub>3</sub>	R	P_99	508.5	68	2.38	-0.52	-8.67
PC	3rd CO <sub>3</sub>	R	P_101	508.3	62	0.92	-0.05	-8.49
PC	3rd CO <sub>3</sub>	T	PC4-314	508	70	1.21	-0.48	-7.89
PC	3rd CO <sub>3</sub>	TOP	PC4-313	507	72	1.71	0.16	-7.74
PC	3rd CO <sub>3</sub>	T	PC4-312	506	60	1.55	0.01	-7.92
PC	3rd CO <sub>3</sub>	TOP	PC4-311	505	59	1.29	0.06	-7.52
PC	3rd CO <sub>3</sub>	R	PC4-310	504	60	1.13	0.18	-7.54
PC	3rd CO <sub>3</sub>	MFS	PC4-309	503	59	1.49	0.30	-7.49
PC	3rd CO <sub>3</sub>	TOP	PC4-308	502	61	1.88	-0.01	-7.64
PC	3rd CO <sub>3</sub>	R	PC4-307	501	66	1.09	0.18	-7.66
PC	3rd CO <sub>3</sub>	TOP	PC4-306	500	61	1.26	0.28	-7.84
PC	3rd CO <sub>3</sub>	R	PC4-305.5	499.5	74	0.66	-0.30	-7.78
PC	3rd CO <sub>3</sub>	MFS	PC4-305	499	32	1.88	-0.08	-7.50
PC	3rd CO <sub>3</sub>	R	PC4-304	498	43	0.69	-0.26	-7.76
PC	3rd CO <sub>3</sub>	TOP	PC4-303	497	53	1.17	0.37	-7.89
PC	3rd CO <sub>3</sub>	TOP	P_95	496.6	62	1.19	0.52	-8.13
PC	3rd CO <sub>3</sub>	R	PC4-302	496	57	1.26	0.18	-7.67
PC	3rd CO <sub>3</sub>	R	P_96	495.8	61	1.55	0.90	-7.88
PC	3rd CO <sub>3</sub>	R	PC4-301.7	495.7	69	1.28	0.08	-7.76
PC	3rd CO <sub>3</sub>	T	PC4-301	495	57	1.75	-0.06	-7.92
PC	3rd CO <sub>3</sub>	R	PC4-300	494	59	1.57	0.37	-7.78
PC	3rd CO <sub>3</sub>	R	PC4-299	493	54	1.92	0.03	-7.69
PC	3rd CO <sub>3</sub>	TOP	PC4-298	492	59	1.60	-0.11	-7.83
PC	3rd CO <sub>3</sub>	R	PC4-297	491	54	0.96	-0.08	-7.53
PC	3rd CO <sub>3</sub>	MFS	PC4-296	490	54	1.24	0.11	-7.94
PC	3rd CO <sub>3</sub>	TOP	PC4-295	489	65	1.29	0.09	-7.69
PC	3rd CO <sub>3</sub>	TOP	P_91	488.1	75	0.92	0.12	-8.06
PC	3rd CO <sub>3</sub>	R	PC4-294	488	70	1.21	0.10	-8.11
PC	3rd CO <sub>3</sub>	R	P_93	487.6	64	1.56	0.21	-7.63
PC	3rd CO <sub>3</sub>	MFS	PC4-293	487	32	3.17	-0.12	-7.53
PC	3rd CO <sub>3</sub>	T	PC4-292	486	45	3.54	-0.56	-8.18
PC	3rd CO <sub>3</sub>	R	PC4-291	485	37	2.05	-0.15	-7.79
PC	3rd CO <sub>3</sub>	MFS	PC4-290	484	31	2.85	-0.02	-7.17

**Table 4.2. Data set from the analyzed intervals:** Los Catutos (Los Cat) in MDC and VM23 sections, the three younger carbonate-rich intervals (1<sup>st</sup>, 2<sup>nd</sup> and 3<sup>rd</sup> CO<sub>3</sub>) in PC, and the mid-late Tithonian (m-l Tith) in PC. Cycle column indicates the position of each sample within the basic cycles defined in the field: top (TOP), regressive (R), maximum flooding (MFS) and transgressive (T)

Histograms in Figure 4.3 show the distribution of each of the analyzed variables for the entire data set. Within the measured ranges, the best representation of the majority of the data is provided by the 5<sup>th</sup> and 95<sup>th</sup> percentiles (P<sub>05</sub> and P<sub>95</sub>, respectively). Hence, all the ranges reported subsequently in text are P<sub>05</sub> and P<sub>95</sub> ranges. The actual minimum-

maximum ranges, as well as other statistical parameters, are provided in tables accompanying the histograms in the corresponding figures.

The carbonate content of the studied intervals is high varying between 25% (P<sub>05</sub>) and 87% (P<sub>95</sub>) with a mean value of 61% (Figure 4.3). Most of the TOC values fall between 0.32% and 2.83% (P<sub>05</sub> and P<sub>95</sub>, respectively) and the mean is 1.38%. The measured carbon isotopes ratios ( $\delta^{13}\text{C}_{\text{in}}$ ) show values between -1.75 (P<sub>05</sub>) and 1.3‰ (P<sub>95</sub>) with a mean of -0.24‰. Most  $\delta^{18}\text{O}$  values are between -8.75 (P<sub>05</sub>) and -5.08‰ (P<sub>95</sub>) and the mean value is -7.07‰.

The carbon isotopic composition ( $\delta^{13}\text{C}_{\text{in}}$ ) of marine carbonates reflects the isotopic composition of dissolved inorganic carbon (DIC) species that are mostly independent of changes in temperature during diagenesis (Anderson and Arthur 1983; Grossman & Ku 1986; Romanek et al 1992; among others). Therefore burial diagenesis should not have led to a significant change in the carbon isotope signature of the bulk sediment. Conversely, oxygen isotopes values are likely to be reset during diagenesis due to the strong temperature-dependent fractionation factor between water and calcite (Anderson and Arthur 1983; Weissert & Channell 1989; among others). The highly negative  $\delta^{18}\text{O}$  values measured in this work are not considered to be primary signatures. The possibility of other diagenetic changes affecting the measured  $\delta^{13}\text{C}$  values are evaluated in Chapter 5 – Discussion.

A cross-plot of carbonate content (%CO<sub>3</sub>) versus total organic carbon (%TOC) shows that TOC decreases when carbonate content increases (Figure 4.4). This trend is better developed in the carbonate-rich samples, while clastic-rich compositions show more

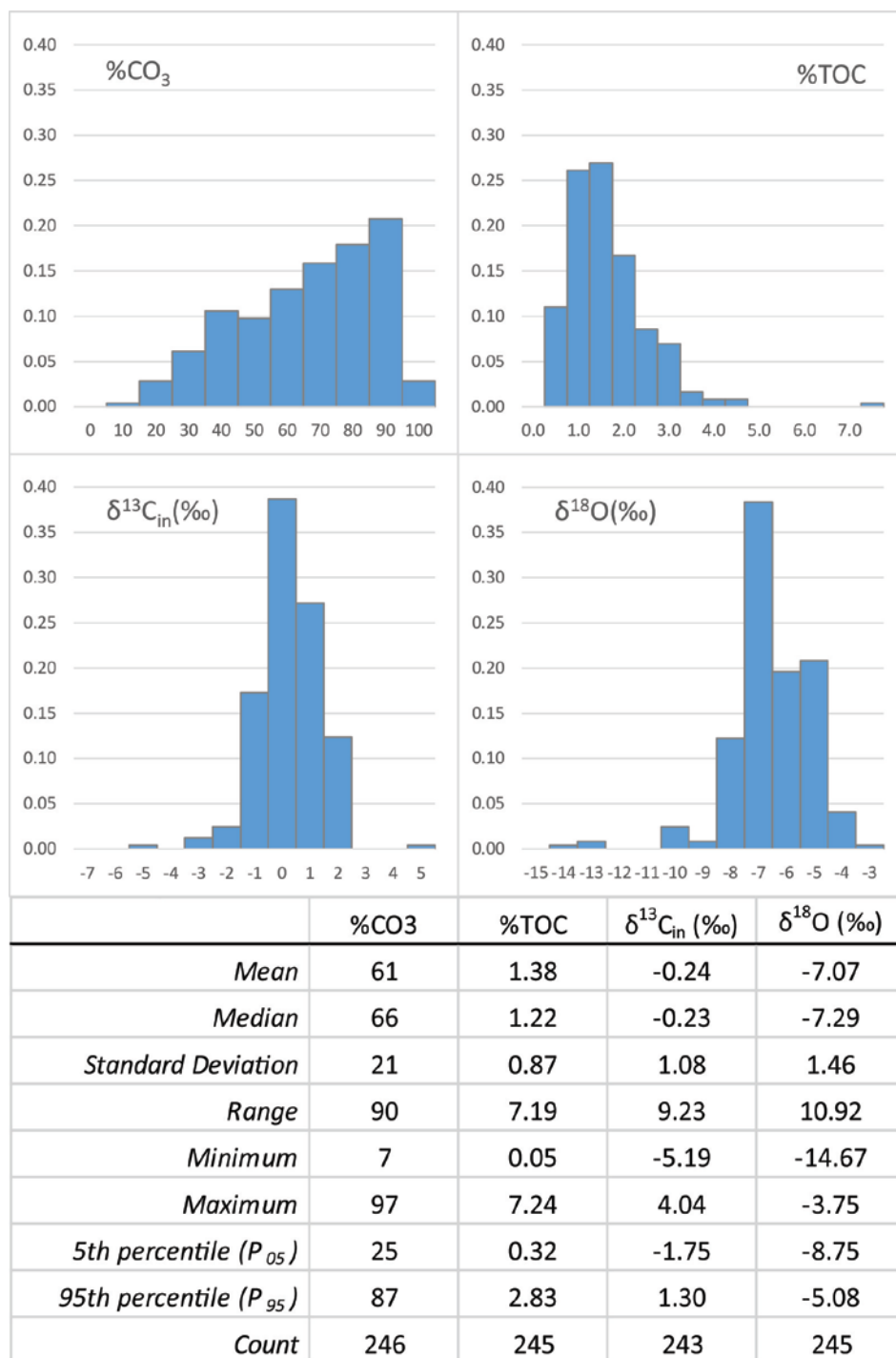


**Figure 4.3. General statistics of the chemical proxies measured.** Above: histograms of carbonate ( $\% \text{CO}_3$ ) and organic content (TOC), and stable isotope ratios ( $\delta^{13}\text{C}_{\text{in}}$  and  $\delta^{18}\text{O}$ ). Below: statistical summary of the data

scattered TOC values. Carbonate content ( $\% \text{CO}_3$ ) plotted versus carbon isotope ratios ( $\delta^{13}\text{C}_{\text{in}}$ ) shows that  $\delta^{13}\text{C}_{\text{in}}$  values tend to increase with increasing carbonate content (Figure

4.4). The observed trend is weak but become more pronounced when the geochemical signature is examined within transgressive and regressive hemicycles (see Sequence Stratigraphy section, this Chapter).

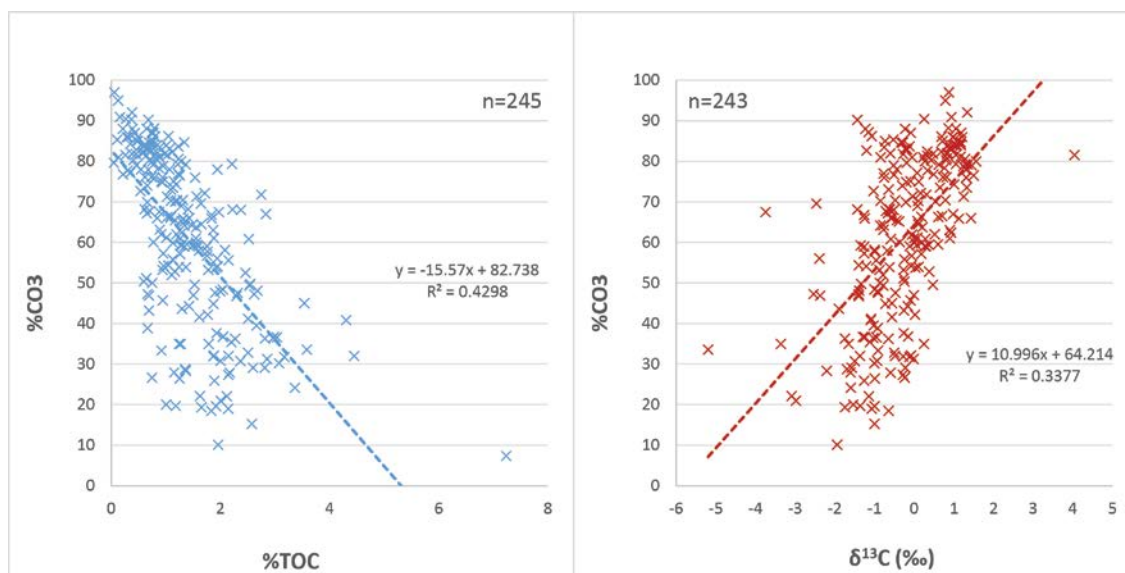














**Figure 4.4. %CO<sub>3</sub> plotted versus %TOC and  $\delta^{13}C_{in}$  for the analyzed intervals.** Organic content (TOC) decreases when carbonate content (%CO<sub>3</sub>) increases. Carbon isotope ratios ( $\delta^{13}C_{in}$ ) increase when carbonate content increases. **n** indicates the number of samples

### Stratigraphic distribution
















Several sections along the Sierra de la Vaca Muerta (Figures 2.1 and 2.2) were analyzed to characterize the vertical and lateral facial variability as well as the geometry of the Los Catutos carbonate-rich interval. Among the studied sections, the most complete in terms of thickness and data is the Mallín de los Caballos (MDC), which is well-exposed along a steep-walled gully. In other sections such as WT and ANG only the lower portion of the carbonate-rich interval is exposed. The VM23 section provides the lithologic content of the distal portion of the carbonate-rich interval within the Sierra de la Vaca Muerta. The most distal expression for the same time is represented by the Mid-Late Tithonian interval in

Puerta Curaco (PC) area (Figures 2.1 and 2.3) where the Los Catutos Member is not present. The PC reference section, however, provides the vertical facies variability of three other carbonate-rich intervals younger than Los Catutos.

The subsequent paragraphs describe first the general characteristics of the Los Catutos Member as defined by Leanza and Zeiss (1990, 1994), and then concentrate in the sections analyzed in this study: MDC and VM23 from Sierra de la Vaca Muerta, and PC from Puerta Curaco. Figure 4.5 shows the main lithologic types, sedimentary structures and fossils involved in the descriptions.

	Ash layer
	Calcite veins (beef)
	Crystalline, dolomitized
	Wackestone/packstone
	Carbonate mudstone
	Stratigraphically-aligned concretion
	Fissile carbonate mudstone (CO <sub>3</sub> >60%)
	Fissile carbonate mudstone, TOC >2%
	Fissile clastic mudstone (0-60% CO <sub>3</sub> )
	Fissile clastic mudstone, TOC >2%
	Siltstone
	Sandstone

Parallel lamination		Gastropods	
Cross-bedding		Ammonites	
Fosets		Oysters	
Algal lamination		Skeletal fragments	
Bioturbation		Bivalve fragments	
Nodules / small concretions		Reptile bones	
Slumps		Spicules	
		Fish Scales	

**Figure 4.5. Section legend.** The indicated elements are common to all the stratigraphic sections described in this work

### **Los Catutos Member (mid-late Tithonian) in Sierra de la Vaca Muerta**

In the area of Los Catutos (El Ministerio, Los Catutos and other quarries, Figure 2.2) Leanza and Zeiss (1990, 1994) recognized a carbonate-rich interval within the Vaca Muerta Formation and defined it as the Los Catutos Member. Leanza and Hugo (2005) mentioned that this carbonate interval is part of a gently dipping sigmoidal clinoform prograding towards the north along the Sierra de la Vaca Muerta. In the type locality, Los Catutos was described as a 70 m-thick package that starts approximately 150m above the contact with the Tordillo Formation. Near Mallin Quemado, 27km to the north, the base of the interval is approximately 30 m above the same contact and the thickness of the interval is significantly reduced (Leanza and Hugo 2005).

In El Ministerio quarry, the Los Catutos Member contains 5 fossiliferous limestone levels (x+a, x, y, z and w) intercalated with marls (Leanza and Zeiss 1990). The limestones consist of bioclastic and peloidal wackestones and packstones, more massive in the 2 lower levels and more laminated in the upper 3 (*Plattenkalk* limestones). The preservation of the fossils varies from fragmented ammonites in the lower levels to well-preserved faunas in the laminated ones, including a large variety of cephalopods, reptiles, fishes and turtles (Gasparini et al 1987, among others). Based on its ammonite content, Leanza and Zeiss (1990, 1994) assigned the unit to the *W. internispinosum* zone, but they also mention that the lower level could belong to the *A. proximus* zone (Figure 4.6).

### **MDC section**

The 150m-thick MDC section was logged from the top of the underlying Tordillo Formation to the top of the Los Catutos Member. Ages in this section were determined



from the published ammonite biostratigraphy (Figure 4.6). According with Leanza and Zeiss (1990, 1994), and other authors, the succession of the Vaca Muerta Formation underlying the Los Catutos Member includes the *V.mendozanus*, *P.zitteli* and the lower part of the *A.proximus* ammonite zones. The upper part of the *A.proximus* zone extends up to the lower unit of the Los Catutos Member, while the rest of the carbonate-rich interval is constrained within the *W.internispinosum* ammonite zone (Leanza and Zeiss 1990, 1994).

	Edad	Zonas Andinas	Zonas del Tethys
VALANGINIANO	Tardío (pars)	<i>O. (Viluceras) permolestus</i>	<i>Neocomites peregrinus</i>
		<i>Karakaschiceras attenuatum</i>	<i>Saynoceras verrucosum</i>
	Tempr.	<i>O. atherstoni</i>	<i>Karakaschiceras inostranzewi</i>
		<i>Lissonia riveroi</i>	<i>Neocomites neocomiensisformis</i>
		<i>Thurmanniceras pertransiens</i>	
BERRIASIANO	Tardío	<i>Spiticeras damesi</i>	<i>Subthurmannia boissieri</i>
	Medio	<i>Argentinceras noduliferum</i>	<i>Subthurmannia occitanica</i>
	Tempr.	<i>Substeueroceras koeneni</i>	<i>Berriasella jacobi</i>
TITHONIANO	Tardío	<i>Corongoceras alternans</i>	<i>Durangites</i>
		<i>Windhauseniceras internispinosum</i>	<i>Micracanthoceras microcanthum</i>
		<i>Aulacosphinctes proximus</i>	<i>Micracanthoceras ponti/ Burckhardtceras peroni</i>
	Medio	<i>Pseudolissoceras zitteli</i>	<i>Semiformiceras fallauxi</i>
		<i>Virgatosphinctes mendozanus</i>	<i>Semiformiceras semiforme</i>
	Tempr.		<i>Semiformiceras darwini</i>
			<i>Hybonoticeras hybonotum</i>

**Figure 4.6. Ammonite zones** (from Aguirre Urreta et al. 2014). The chart includes the correlation between Andean and Tethyan zones

The MDC stratigraphic section and the outcrop expression of the described lithologies are shown in Figure 4.7. The Vaca Muerta Formation starts above the contact with the cross-bedded sandstones of the Tordillo Formation (Figure 4.7-A) with a few decimeter-thick mudstone/wackestone beds with ammonites (Figure 4.7-B). Above these limestone beds, the Formation is mostly clastic, consisting of poorly-exposed fissile and organic-rich clastic mudstones that intercalate with thin-bedded siltstones grading to massive fine sandstone layers (Figure 4.7-C). This 8m-thick and relatively coarse clastic interval is followed by poorly exposed, dark, fissile and clastic-rich mudstone facies with variable carbonate content and abundant organic matter. Above, thin bedded mudstone/wackestones intercalations are common, with abundant ammonites and associated isolated or stratigraphically-aligned concretions of variable sizes (Figure 4.7-D). The subsequent 40m-interval is dominated by dark, fissile and organic-rich clastic mudstones that are punctuated by either concretions or thin layers of carbonate mudstone/wackestones. Recrystallized ash layers are common throughout the interval. They are sometimes lens-shaped and with tractive structures (Figure 4.7-E). Upwards the succession is dominated by thick and closely spaced, massive and laterally highly-continuous skeletal wackestone/packstone beds that characterize the Los Catutos Member (Figure 4.7-F).

The Los Catutos Member in MDC is 65m thick and starts approximately 80m above the contact with the Tordillo Fm (Figure 4.7). It can be subdivided into 5 units (I – V) based on the thickness, texture, sedimentary structures and composition of the beds. Units I through III outcrop along a gully with good exposure, while Unit IV and specially Unit V that constitute the top of the hill are more weathered and/or covered by vegetation.

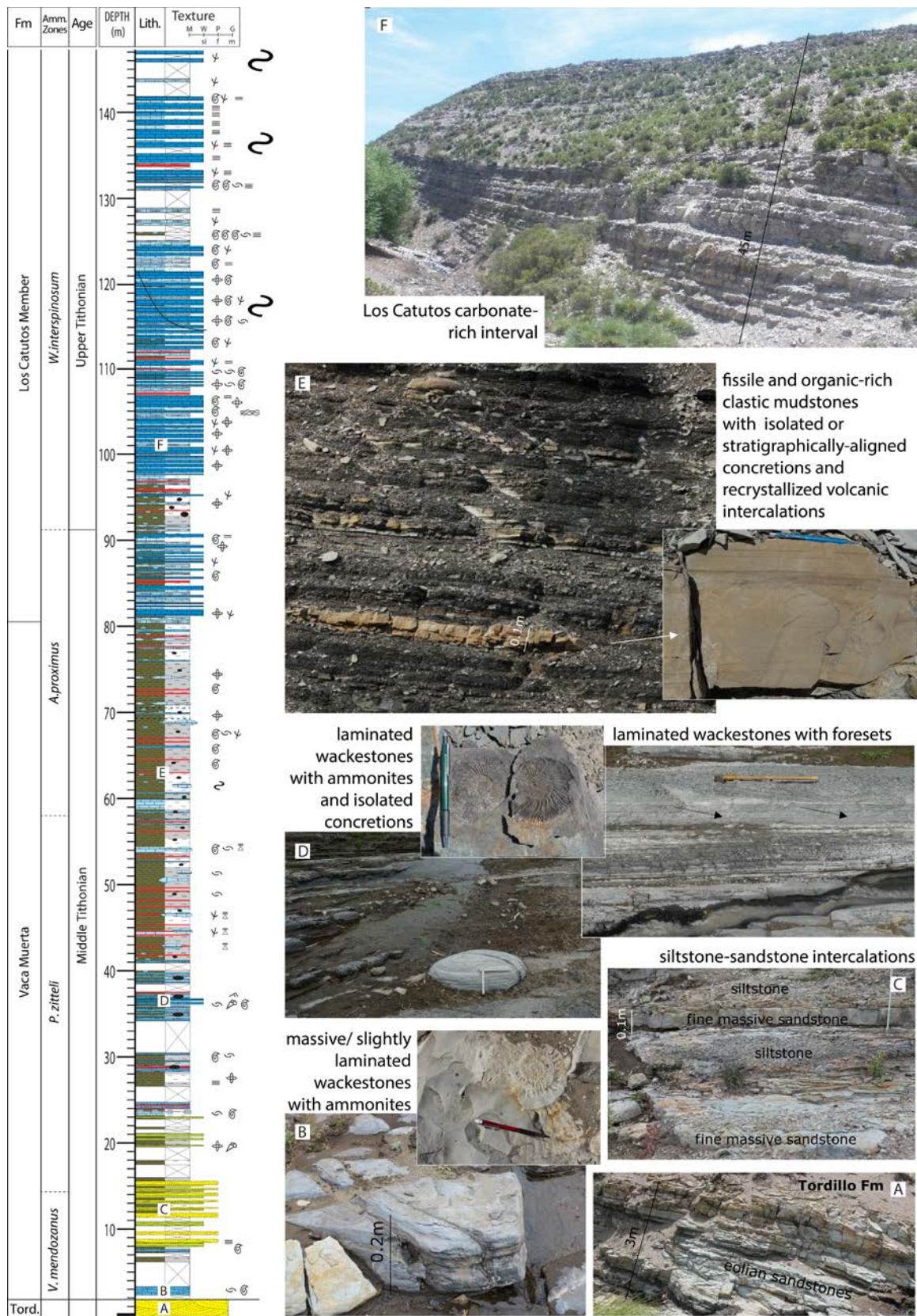
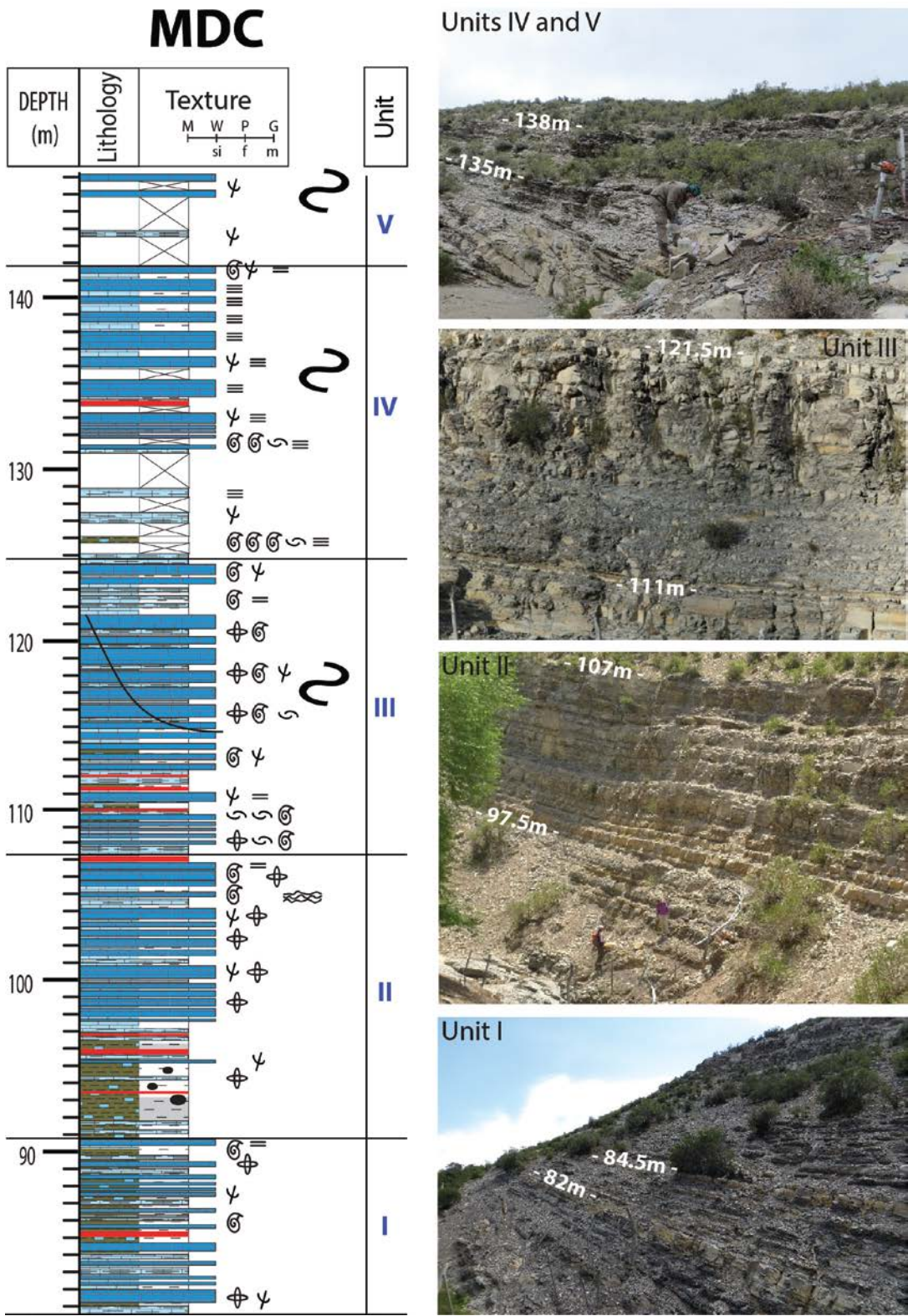


Figure 4.7. MDC section. See lithological description in the text

The stratigraphic section of Los Catutos in MDC is shown in Figure 4.8. Each unit starts with a clastic-rich portion dominated by fissile clastic or carbonate mudstones sometimes associated with isolated concretions (Unit II) and frequently poorly exposed (Units IV and V). The fissile mudstone facies intercalate with occasional ash layers and with massive mudstone/wackestone or skeletal wackestone/packstone beds. The carbonate beds become thicker and more frequent upwards within each unit. The thickness of the carbonate beds is high throughout most of the interval (~0.6m, and up to 1m), except in Unit I and the lower part of Unit II (~0.25m). Conversely, the fissile intercalations are thicker in Unit I and the lower part of unit II (~0.5m) and very thin or absent in the other units. The carbonate-rich facies appear either as massive and highly bioturbated beds (Units I to III) or laminated beds with minor bioturbation (Units IV and V), and usually have ammonites and shell fragments (Figure 4.9). The skeletal content is lower in massive mudstone/wackestones of Units I and II, and higher in Units III to V that are dominated by skeletal wackestone/packstones (Figure 4.10). Plug porosity measurements from short cores within Units II, III and IV range between 1 and 2%.

In the upper Units (III to V) slump scars, moved strata and channelized features, downcutting into the normal bedding, are common (Figure 4.11). The largest scar in Unit III cuts through 7m of the succession with a width of at least 40m (Figure 4.11-B). Other smaller scars are also asymmetrical with a clean listric shape on one side, typically cutting through 2 or 3m of the succession and with variable width of 10-20m (Figure 4.11-A). The strata onlapping the scar consist of the same material that is being cut, with the exception of a crinoidal packstone facies that has only been identified near the base inside of these features but not outside.



**Figure 4.8. Los Catutos Member in MDC.** Detail of the carbonate-rich interval, subdivided into 5 units (I to V), and outcrop expression of those units

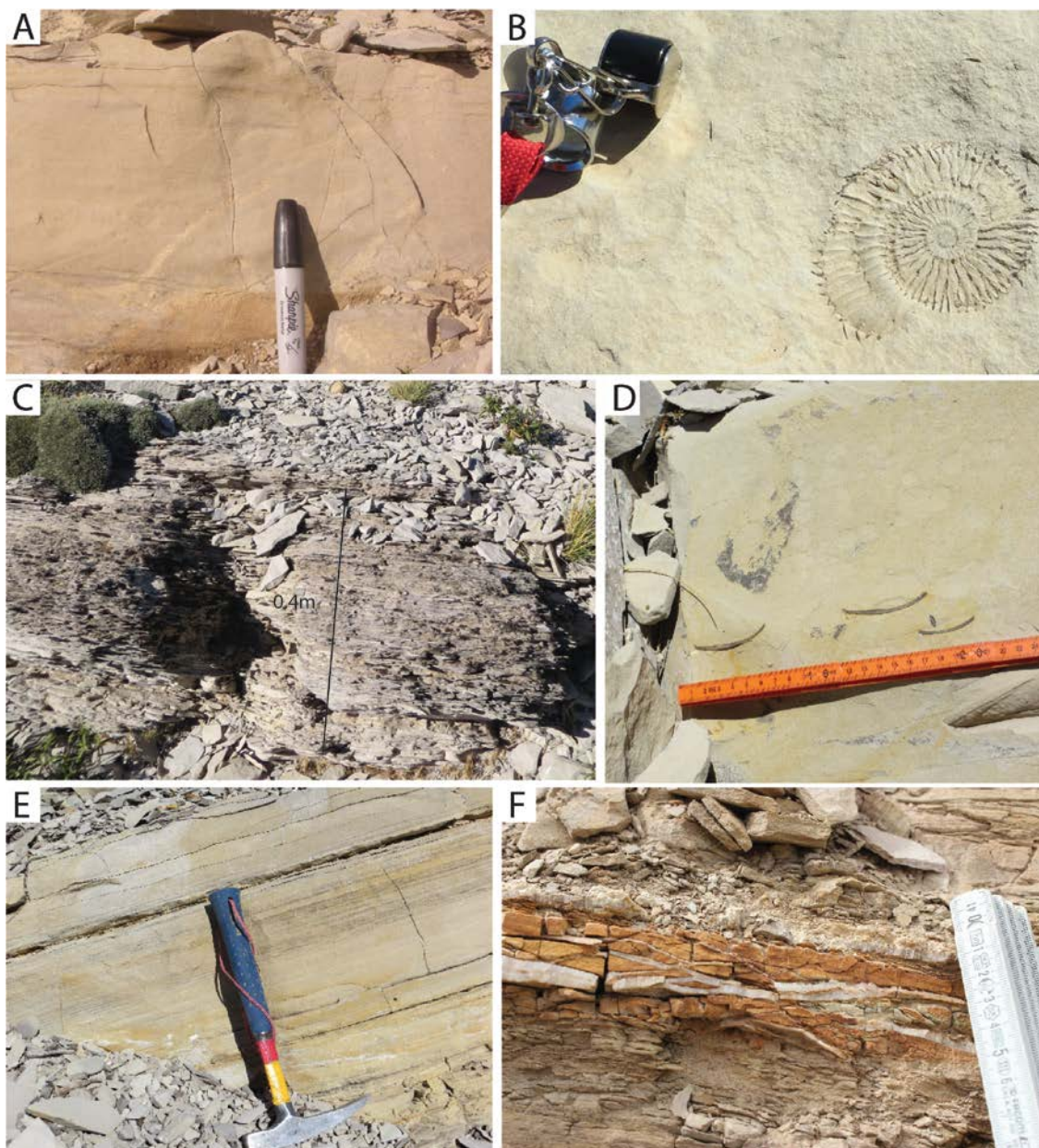


**Figure 4.9. Outcrop facies of Los Catutos in MDC.** A) Massive mudstone/wackestones characteristic of units I to III. B) Ammonites commonly found at the top of the beds. C) Laminated skeletal wackestone/packstones, characteristic of Units IV and V. D) Shell fragments identified within Unit I. E) Algal laminites near the top of Unit II. F) Ash layers and calcite veins occasionally intercalated within the carbonate beds

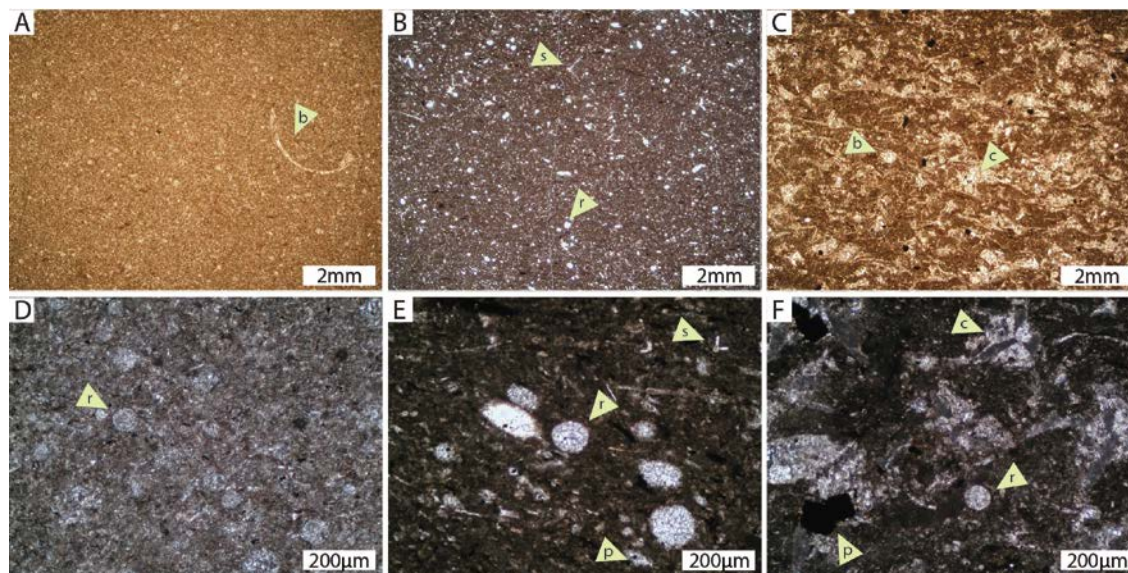


**Figure 4.10. Microfacies of Los Catutos in MDC.** A-D) Massive mudstone/wackestones with micritized radiolarians and occasional bivalve fragments. B-E) Skeletal wackestone/packestones with abundant radiolarians (*r*) and sponge spicules (*s*). C-F) Crinoidal (*Saccocoma*) packstones with crinoids (*c*), radiolarians and common pyrite (*p*)

The geochemical characterization of the Los Catutos Member in MDC is presented in Figures 4.12 to 4.15. The vertical variation of the analyzed parameters can be observed in Figure 4.12. Within each unit, carbonate content and carbon isotopes ratios tend to increase upwards while organic content shows the opposite behavior. These overall trends are clearer in Units II and III that have larger number of samples (30 and 28, respectively), both from fissile and massive facies.

Figure 4.13 shows the statistical summary and histograms of the analyzed parameters (%CO<sub>3</sub>, %TOC and δ<sup>13</sup>C<sub>in</sub>) for the whole interval and for each of the units. No individual statistics are provided for Unit V, as only 2 samples were recovered. However, the statistics of the whole interval includes the 89 available samples from Units I to V.

The distribution of the analyzed parameters show differences and similarities between the units (Figure 4.13). Unit I, where fissile and organic-rich clastic facies are dominant



**Figure 4.11. Moved strata in los Catutos in MDC.** Channelized feature (A) and slump scar (B) observed near the top of Unit III

and carbonate-rich intercalations are relatively thin (Figure 4.8), has the lowest carbonate and the highest organic content. The bulk of the values (P<sub>05</sub>-P<sub>95</sub>) falls between 16% and 71%CO<sub>3</sub> with a mean of 45%, and between 0.65% and 3.1%TOC with a mean of 1.96%. Unit II shows a clear bimodal distribution (Figures 4.13 and 4.14) in agreement with its subdivision in a clastic-rich lower part and a carbonate-rich top (Figure 4.8). The lower part of the unit has the lowest %CO<sub>3</sub> and highest %TOC with mean values of 46% and 1.91% respectively. Conversely, the upper and carbonate-rich part shows mean values of 82% CO<sub>3</sub> and 0.8%TOC. Isotope ratios ( $\delta^{13}\text{C}_{\text{in}}$ ) tend to be lower in the clastic-rich portion



(mean value of -0.6‰) and show more positive values in the carbonate-rich portion (mean 0.85‰). Units III and IV present similar distributions to those of unit II (Figure 4.13), though the bimodal distribution is not as clear due to the under-sampling of the clastic-rich facies.

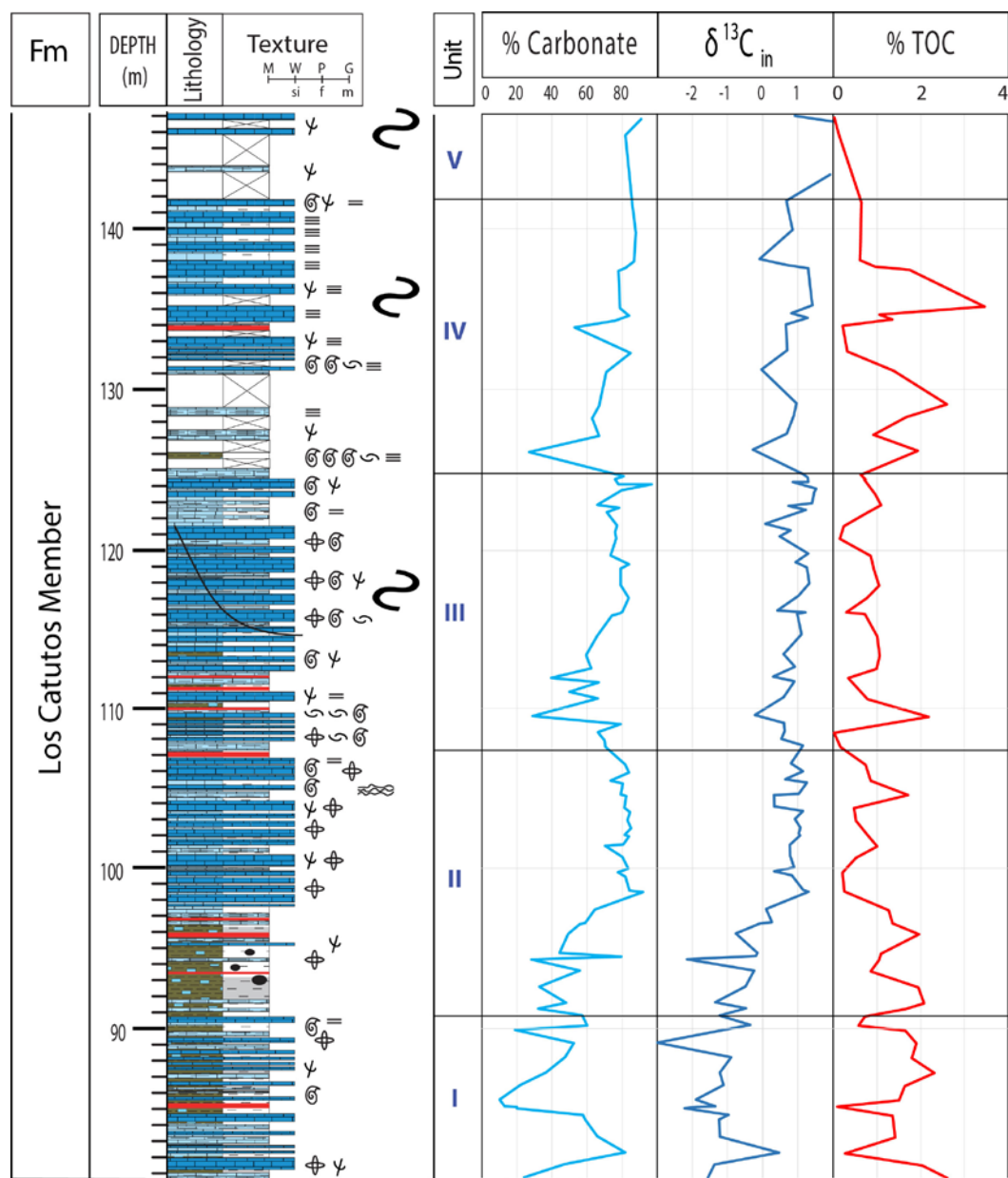


**Figure 4.12. Geochemical variations within Los Catutos in MDC.** Carbonate content (%CO<sub>3</sub>), carbon isotope ratios ( $\delta^{13}C_{in}$ ) and organic content (%TOC) curves. Sampling distance is usually 1m

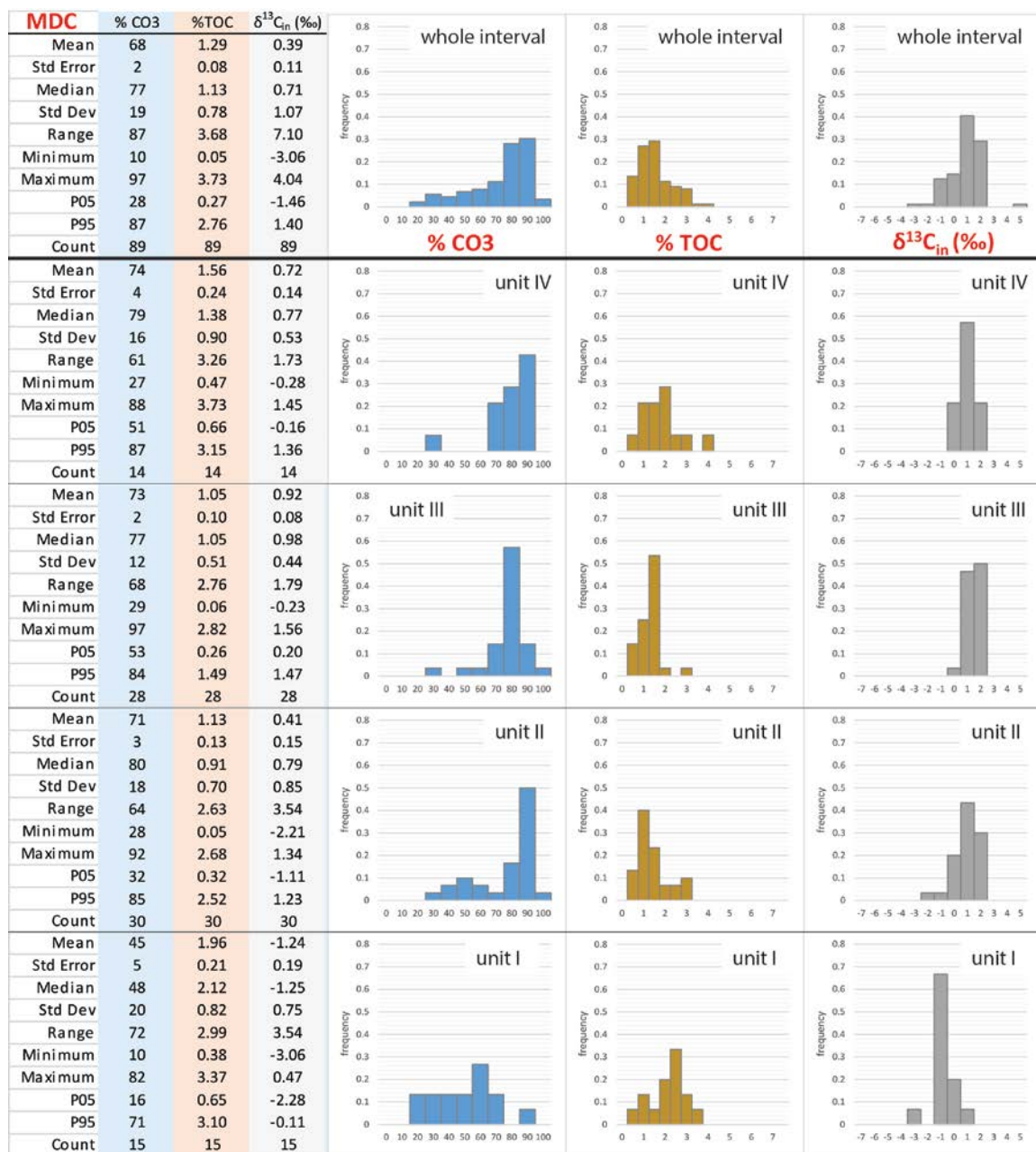


**Figure 4.13. Data analysis of Los Catutos in MDC.** Top row: whole-interval statistics. Subsequent rows: subsets of the data by Unit

In all the analyzed units the more clastic-rich portions are more organic-rich, and an increase in the carbonate content is accompanied by a decrease in the organic content (Figures 4.12, 4.13 and 4.14). A cross-plot of carbonate (%CO<sub>3</sub>) versus organic content (%TOC) shows an inverse trend that is usually better developed in the carbonate-rich samples, while clastic-rich compositions show more disperse TOC values (Figure 4.15).

Carbonate content (%CO<sub>3</sub>) plotted versus carbon isotope ratios ( $\delta^{13}\text{C}_{\text{in}}$ ) shows that  $\delta^{13}\text{C}_{\text{in}}$  values tend to become less negative or even positive with increasing carbonate content (Figure 4.15). In some cases, trends are very weak ( $R^2 \sim 0.1$  or  $0.2$ ), but they become more robust when data is sorted by position within the cycle (see Sequence Stratigraphy section, this Chapter). These observations are valid both for the whole interval and individual units.

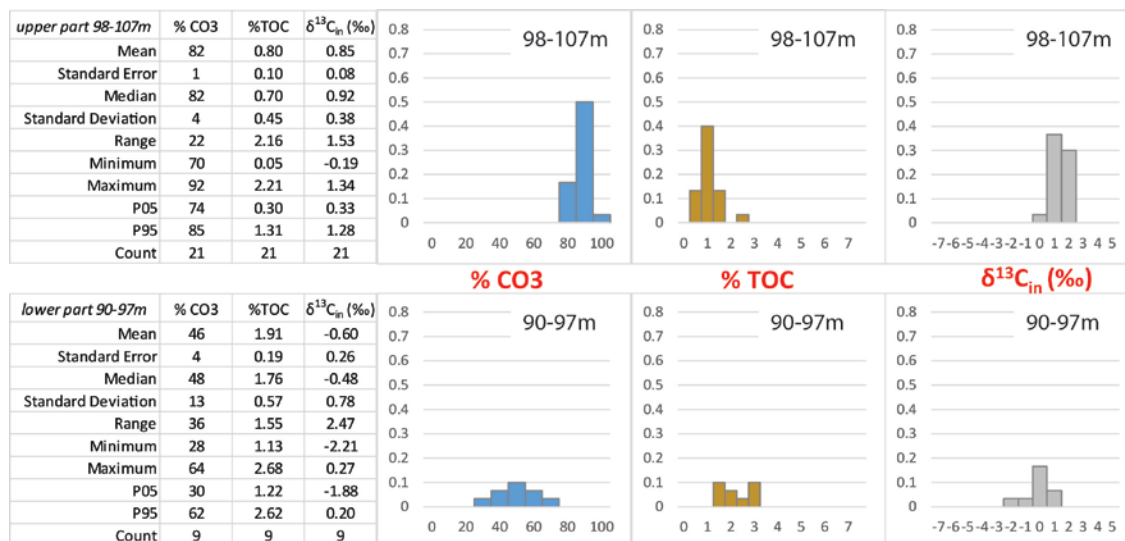


**Figure 4.14. Data analysis of Unit II in MDC.** The characteristic subdivision of the unit into a clastic and organic-rich lower part and a carbonate-rich top results in bimodal distributions of the analyzed parameters

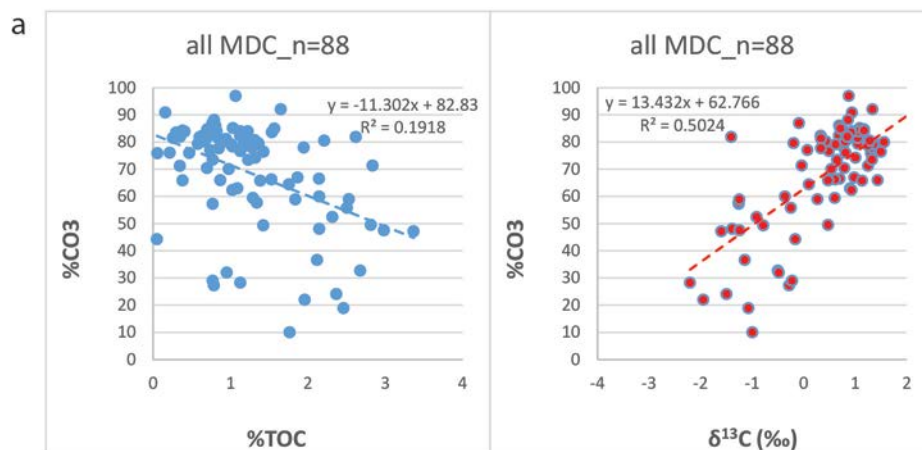
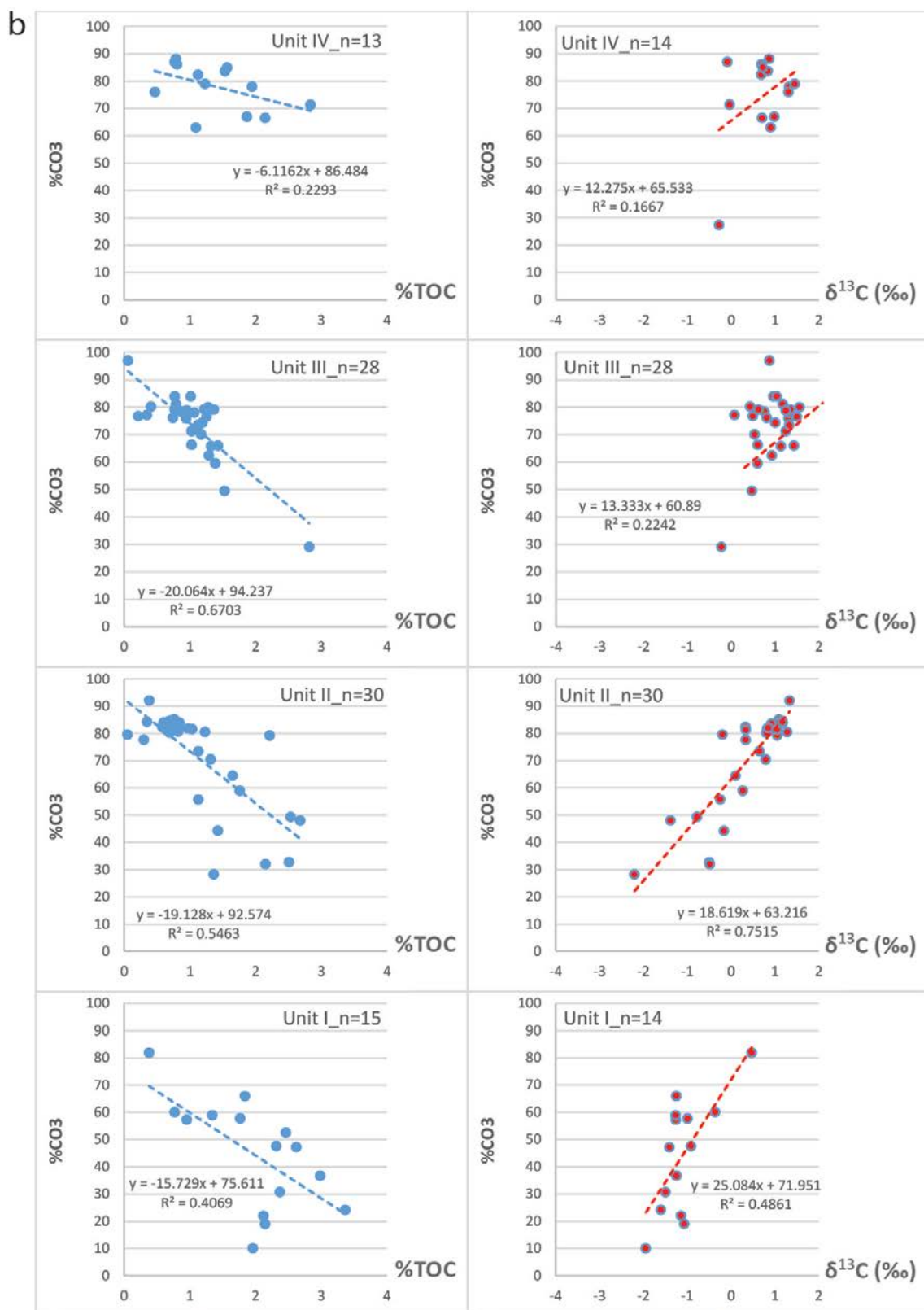


**Figure 4.15. %CO<sub>3</sub> plotted vs %TOC and  $\delta^{13}\text{C}_{\text{in}}$  for Los Catutos in MDC.** The whole interval (a) and individual units (b, next page) display an inverse relationship between carbonate content and TOC, and a slightly direct relation between carbonate and  $\delta^{13}\text{C}$  values. The 2 samples from unit V are plotted together with the data of the whole interval



### **VM23 section**

The carbonate-rich interval of the Los Catutos Member in VM23 is 22m thick. Its position above the contact with the Tordillo Formation is estimated to be around 50m (see Correlations, this Chapter). The succession can be subdivided into 2 (or 3, see Lateral Variations within the Los Catutos Member, this Chapter) units that start with fissile clastic and carbonate mudstone facies with associated concretions, and thin skeletal wackestone/packstone intercalations (Figure 4.16). The skeletal wackestone/packstone beds become thicker (~0.3m, and up to 0.8m) and more frequent towards the top of both units (Figure 4.16) where occasionally crinoidal packstones can also be identified. The increase in thickness and frequency of the carbonate beds is accompanied with a decrease in thickness of the fissile and clastic-rich intercalations. Carbonate beds tend to be more massive in the lower unit and more laminated in the upper one. The presence of ammonites and shell fragments is more frequent in the lower unit (Figure 4.17). Micritized radiolarians and silt-size quartz are present in both fissile mudstone and skeletal wackestone/packstone facies (Figure 4.18).

The geochemical characterization of the Los Catutos carbonate-rich interval in VM23 is presented in Figures 4.19 to 4.21. The vertical variation of the analyzed parameters can be observed in Figure 4.19. Within each unit, carbonate content and carbon isotopes ratios tend to increase upwards while organic content shows the opposite behavior.

Figure 4.20 shows the statistical summary and histograms of the analyzed parameters (%CO<sub>3</sub>, %TOC and  $\delta^{13}\text{C}_{\text{in}}$ ) for the whole interval and for each of the units. The distributions are similar for both units, and show a slight bimodality in concert with their clastic-rich lower part and carbonate-rich top. The P<sub>05</sub>-P<sub>95</sub> values for the whole interval fall

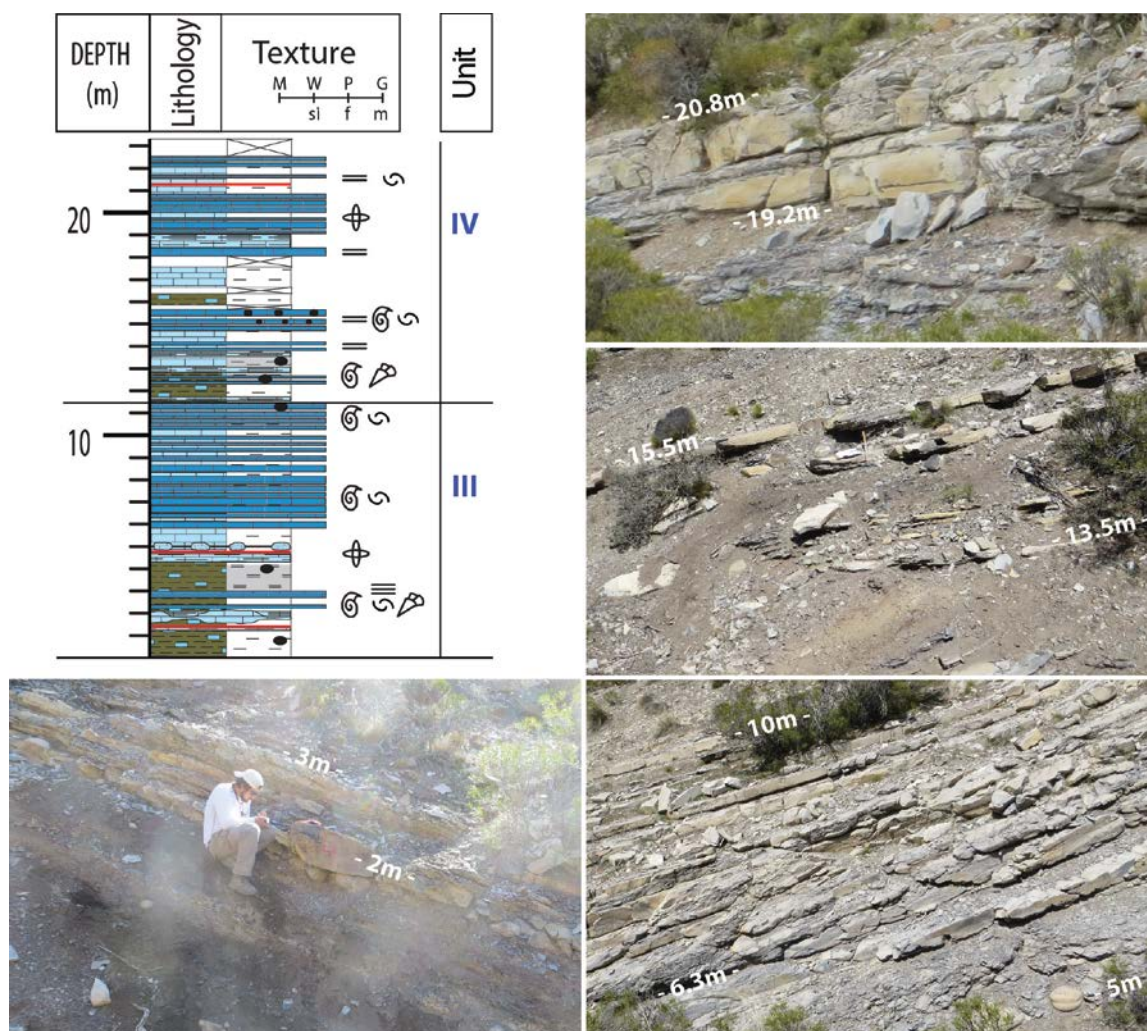


**Figure 4.16. Los Catutos Member in VM23.** Detail of the carbonate-rich interval subdivided into 2 units (III and IV), and outcrop expressions of those units

between 32% and 90%CO<sub>3</sub> with a mean of 66%, between 0.69% and 3.07%TOC with a mean of 1.67%, and between -1.75‰ and -0.23‰δ<sup>13</sup>C with a mean of -1.25‰.

A cross-plot of carbonate (%CO<sub>3</sub>) versus organic content (%TOC) shows an inverse trend that is better developed in the carbonate-rich samples (Figure 4.21). Carbonate content (%CO<sub>3</sub>) plotted versus carbon isotope ratios (δ<sup>13</sup>C<sub>in</sub>) shows no clear correlation in the case of the lower unit (R<sup>2</sup> = 0.18), affecting the statistics of the whole interval (R<sup>2</sup> = 0.15), while the upper unit displays a clearer positive trend between %CO<sub>3</sub> and δ<sup>13</sup>C (R<sup>2</sup> = 0.43).

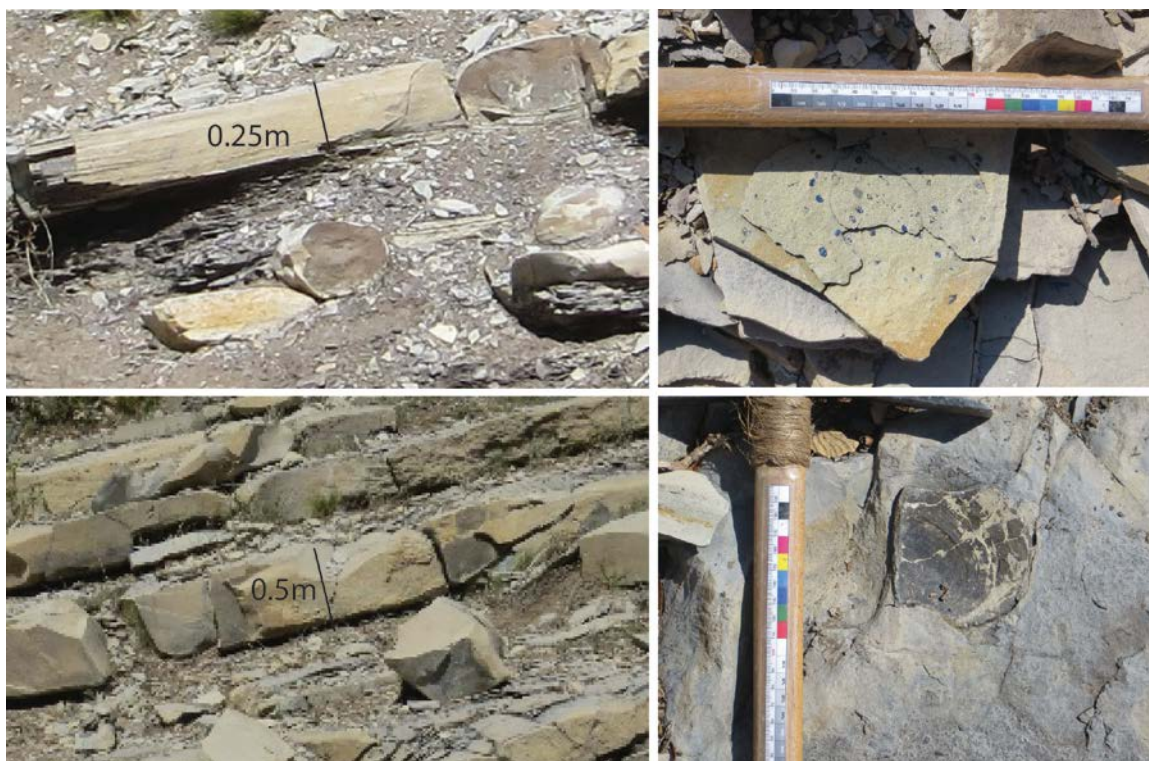


**Figure 4.17. Outcrop facies of Los Catutos in VM23.** A) Laminated wackestone/packstones with associated concretions, near the base of Unit IV. B) Fish scales occasionally observed at the top of the beds. C) Massive wackestone/packstones at the top of Unit III. D) Bivalve shells within the massive beds of Unit III

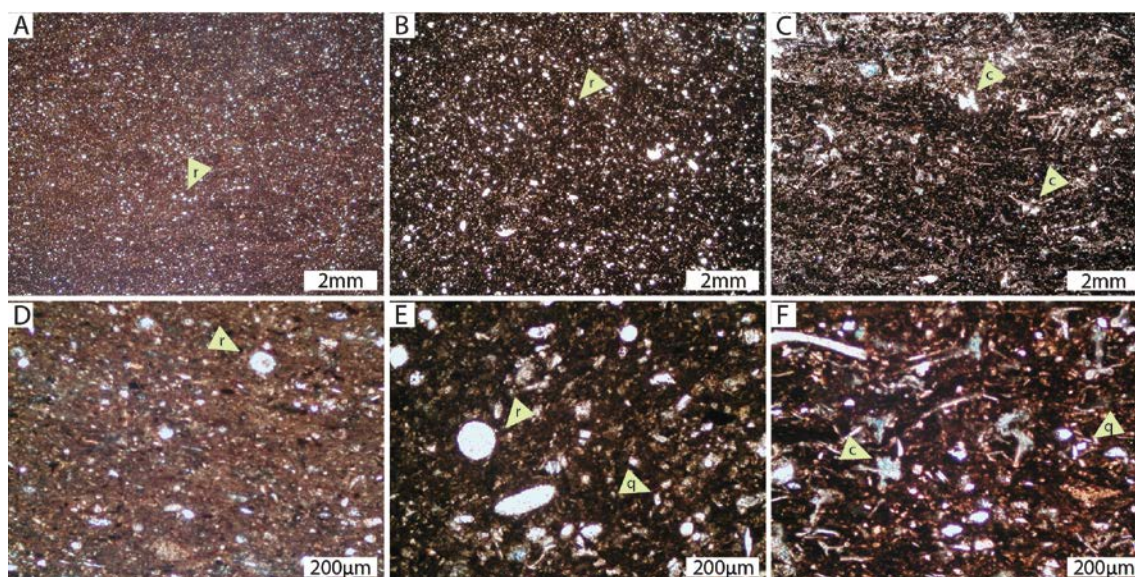


**Figure 4.18. Microfacies of Los Catutos in VM23.** A-D) Calcareous siltstones with radiolarians (r). B-E) Clastic-rich skeletal wackestone/ packstones with abundant radiolarians (r) and quartz (q). C-F) Clastic-rich crinoidal (*Saccocoma*) packstones with crinoids (c) and abundant quartz (q)

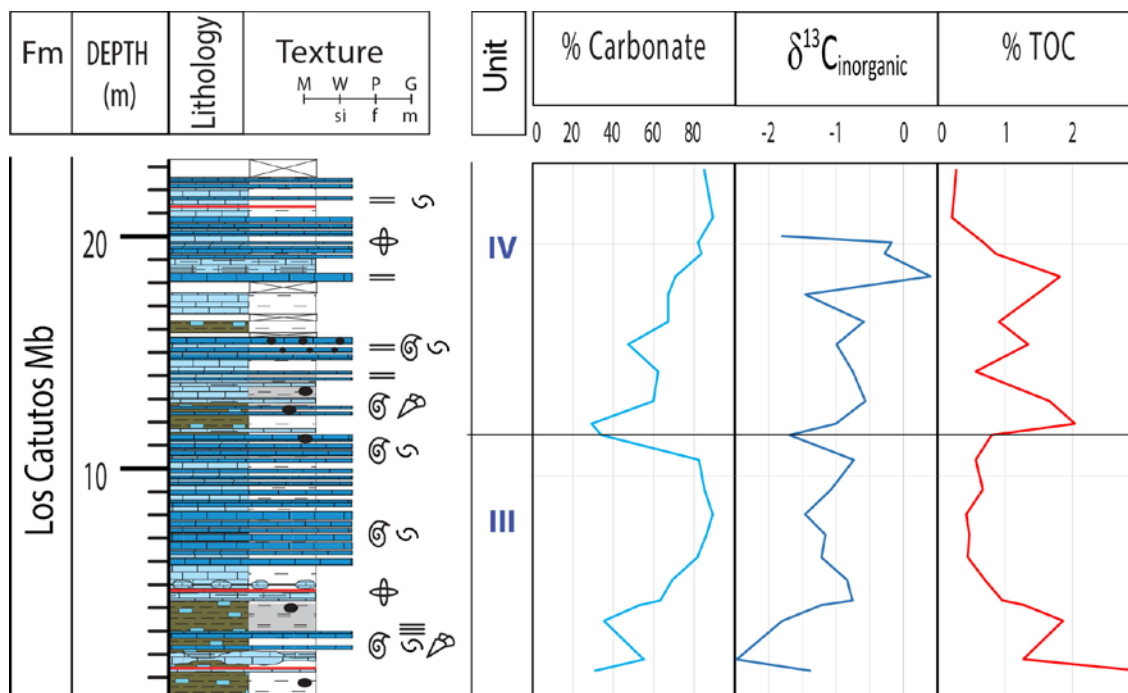


**Figure 4.19. Geochemical variations within Los Catutos in VM23.** Carbonate content (%CO<sub>3</sub>), carbon isotope ratios ( $\delta^{13}C_{in}$ ) and organic content (%TOC) curves. Sampling distance is usually 1m

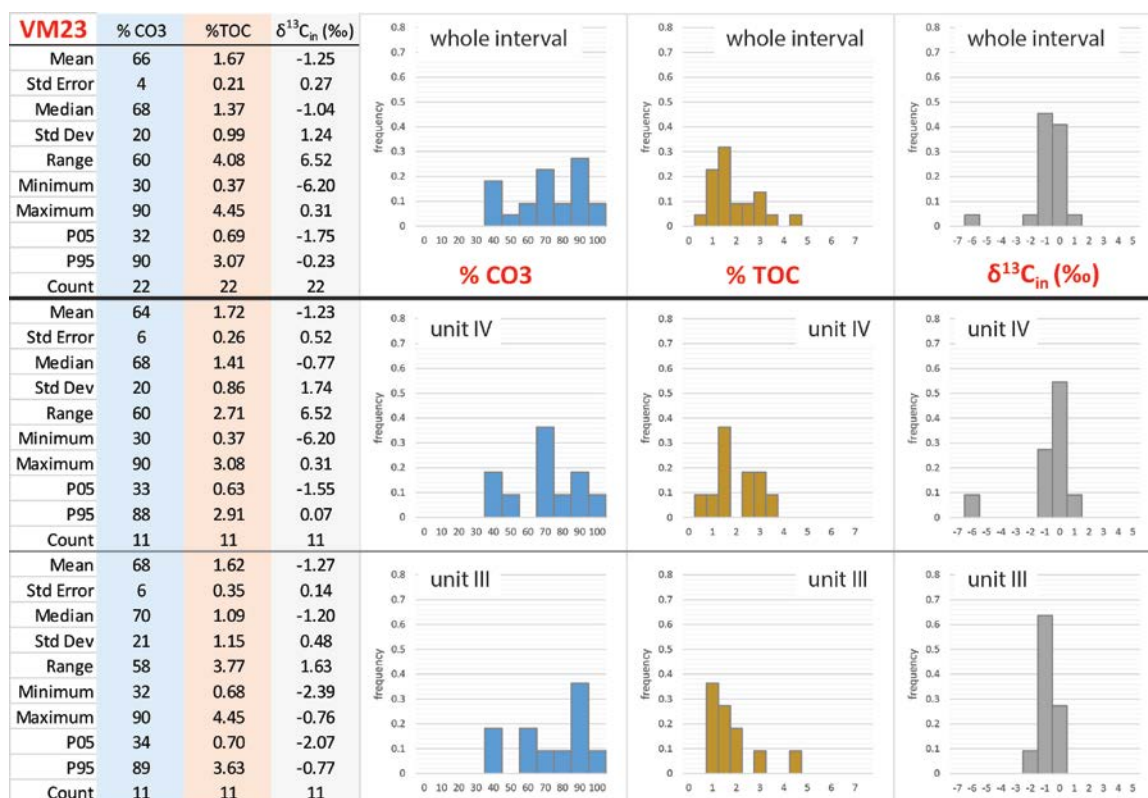


**Figure 4.20. Data analysis of Los Catutos in VM23.** Top row: whole-interval statistics. Subsequent rows: subsets of the data by Unit



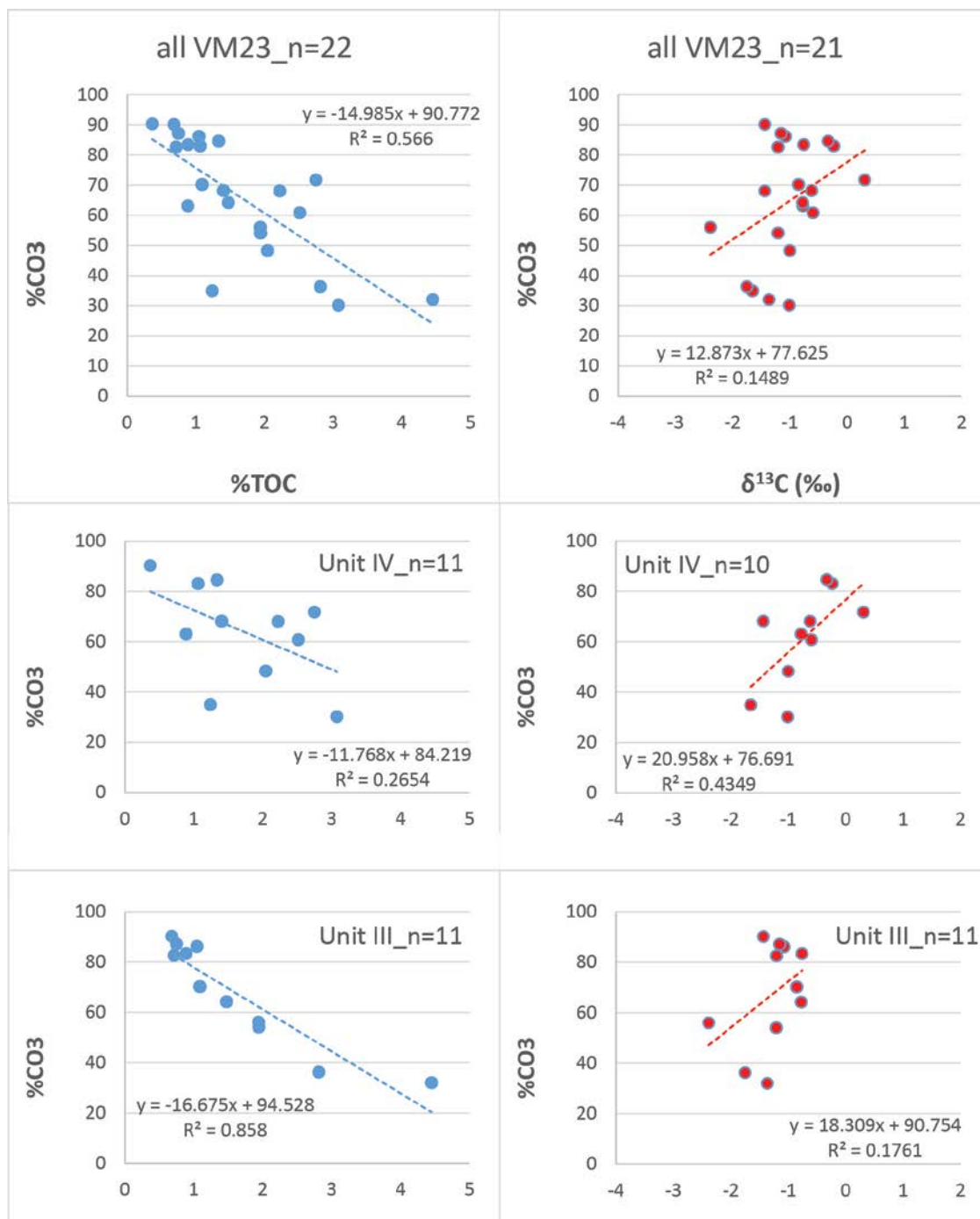


**Figure 4.21. %CO<sub>3</sub> plotted vs %TOC and δ<sup>13</sup>C<sub>in</sub> for Los Catutos in VM23.**  
 Top row: data of the whole interval plotted together. Subsequent rows: data separated by unit

### **Lateral variations within the Los Catutos Member**

The studied sections are 12km apart: MDC in the southern portion of the Sierra de la Vaca Muerta and VM23 near its northern end (Figure 4.22). Two possible correlation scenarios are shown between the two sections, considering that, from the 5 units defined in MDC, either 2 or 3 units present in VM23. Independently of the chosen scenario, a significant reduction in the total thickness of the Los Catutos Member is observed between MDC (65m) and VM23 (22m). The thinning of the whole interval and units is accompanied by a reduction in the thickness of individual carbonate beds, from average values of 0.6m in MDC to less than 0.3m in VM23. Conversely the fissile clastic-rich intercalations are thicker in VM23 than in MDC.

The lateral change of the carbonate-rich interval observed between MDC and VM23 is produced by a lateral change in facies, and a decrease in thickness and frequency of carbonate beds (Figure 4.22). The MDC section is dominated by thick and massive carbonate beds with very thin clastic and organic-rich intercalations, while in VM23 the fissile clastic and organic-rich portions are more common. Another significant difference between the two sections is the presence of slump scars, moved strata and channelized features in the upper units in MDC that suggest a relatively more proximal, slope setting.

The thinning of the Los Catutos Member along the Sierra de la Vaca Muerta, from El Ministerio quarry in the south, where Los Catutos was defined, to VM23 in the north, can also be traced on satellite images (Figure 4.23). Successive close-up views of different outcrops of the Los Catutos show the decrease in number of the white carbonate-rich bands that correspond to each of the identified units. From the 5 units observed in MDC, only 2

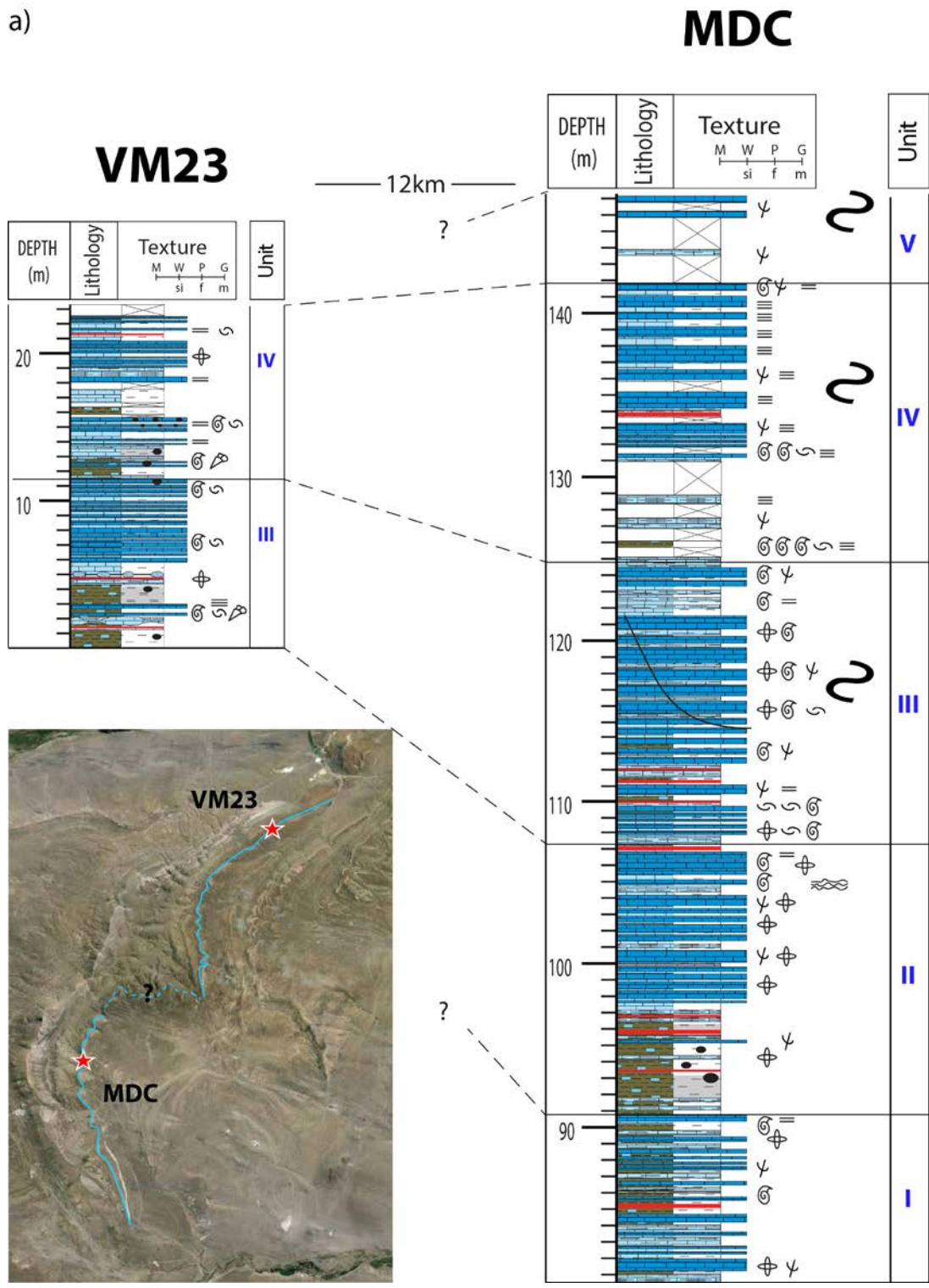
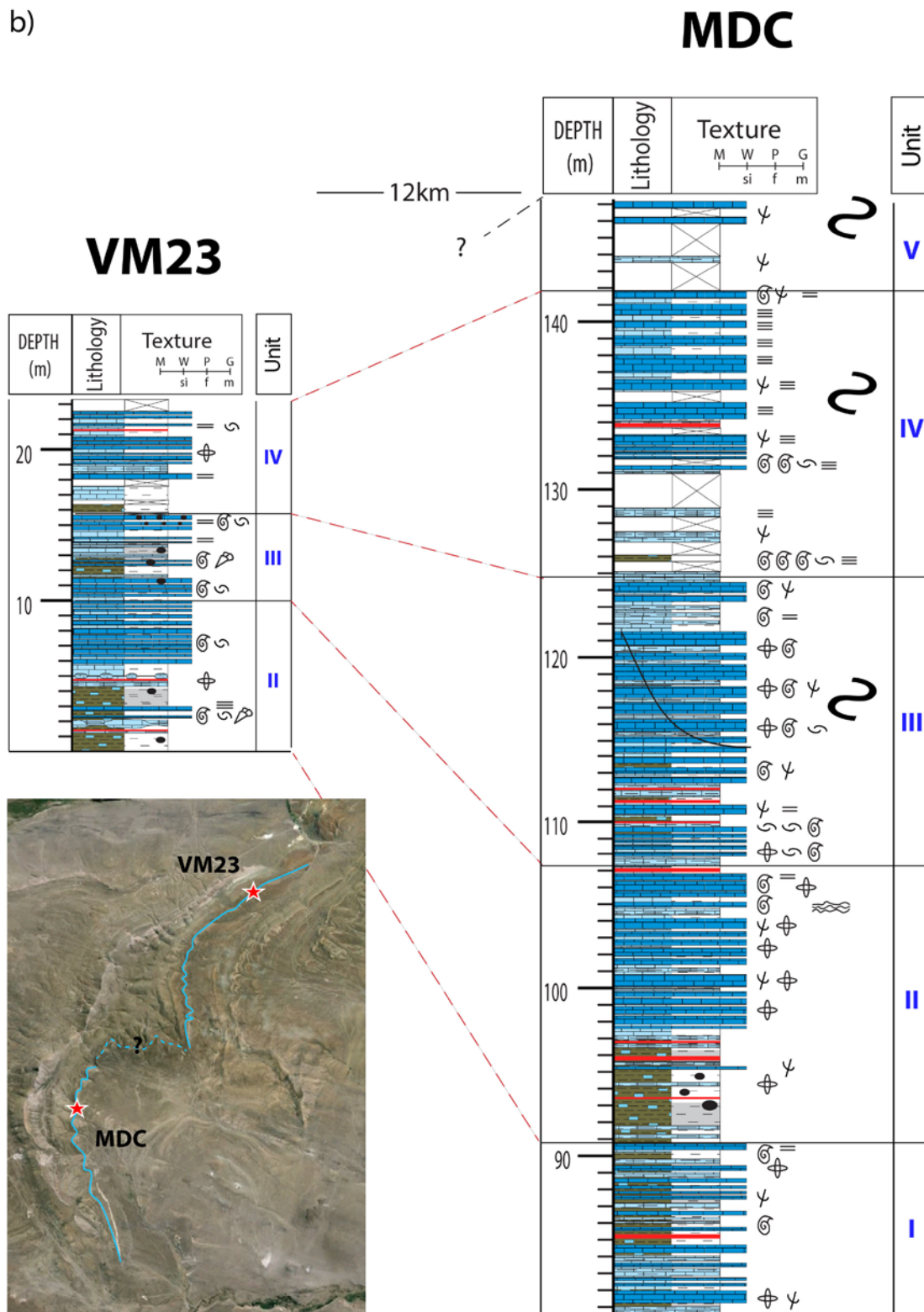


**Figure 4.22. Lateral lithological variations within Los Catutos (MDC-VM23).** Two models of correlation are presented, depending on how many of the units defined in MDC still preserve a carbonate-rich character in VM23: 2 (a) or 3 (b, next page). Independently of the preferred model, the thickness of the Los Catutos Member decreases significantly towards north

b)



seem to remain in VM23. However, the quality of the image is poor in VM23 location, and alternatively 3 bands might be interpreted. Additionally, the continuity of the exposures is

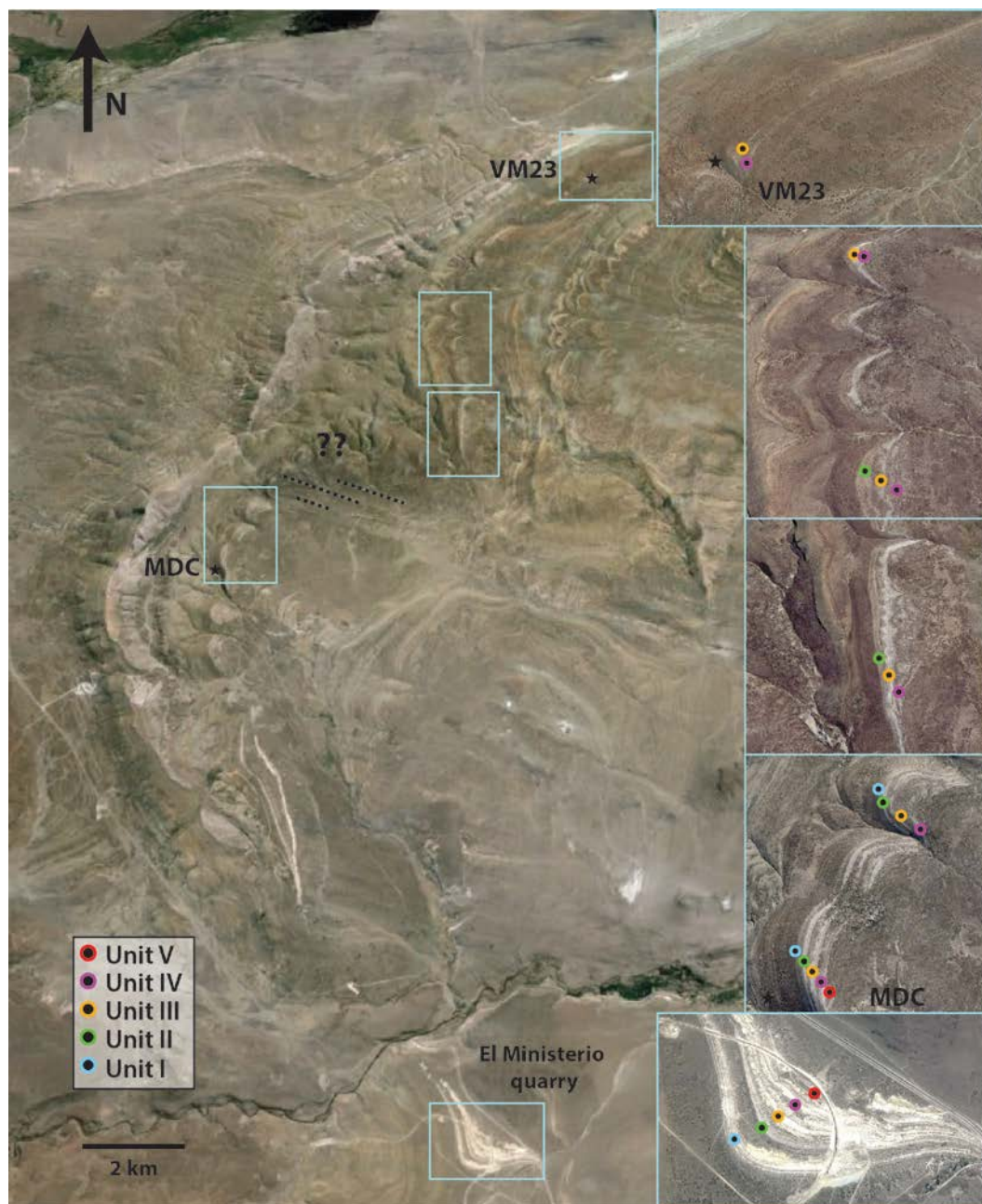


**Figure 4.23. Tracing Los Catutos on satellite image.** The carbonate interval outcrops along the Sierra de la Vaca Muerta as a series of white bands that attenuate and disappear towards north. Between MDC and VM23 a faulted area with poor exposures is indicated with question marks. The boxes are closer views of different outcrops. Colored dots indicate the units in which the interval was subdivided

lost in a faulted area between the two sections. Nevertheless, it is still possible to observe the attenuation of the units north from MDC as they pass laterally from carbonate-rich (white) to clastic-rich facies (darker colors). Among the two correlation scenarios, the first is the one preferred, in which only Units III and IV preserve the carbonate-rich character in the distal setting represented by VM23. The commonly laminated character of the skeletal wackestone/packstone beds and the presence of crinoids (*Saccocoma*), only observed in the upper units in MDC, support this interpretation.

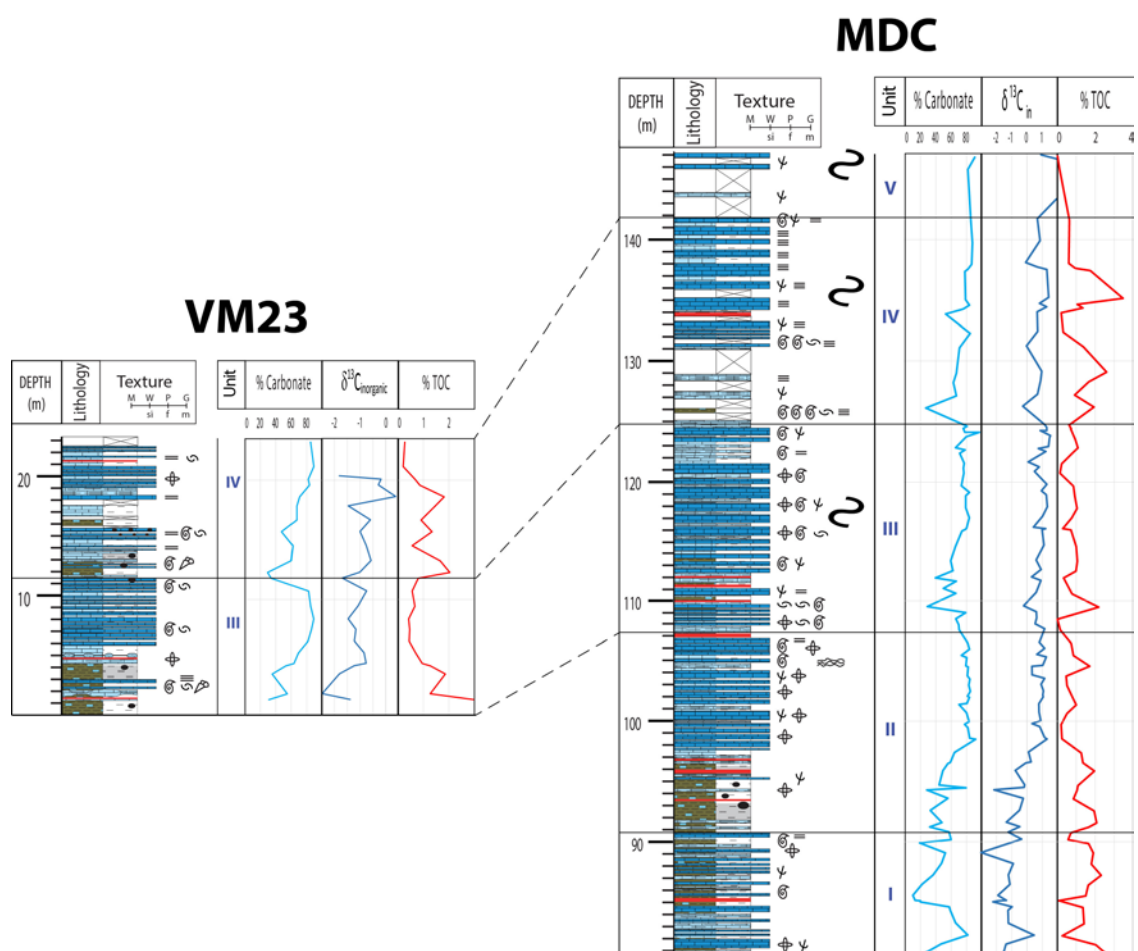


**Figure 4.24. Lateral geochemical variations within Los Catutos (MDC-VM23).** Carbonate content (%CO<sub>3</sub>), carbon isotope ratios ( $\delta^{13}C_{in}$ ) and organic content (%TOC) curves are shown for comparison between the 2 sections

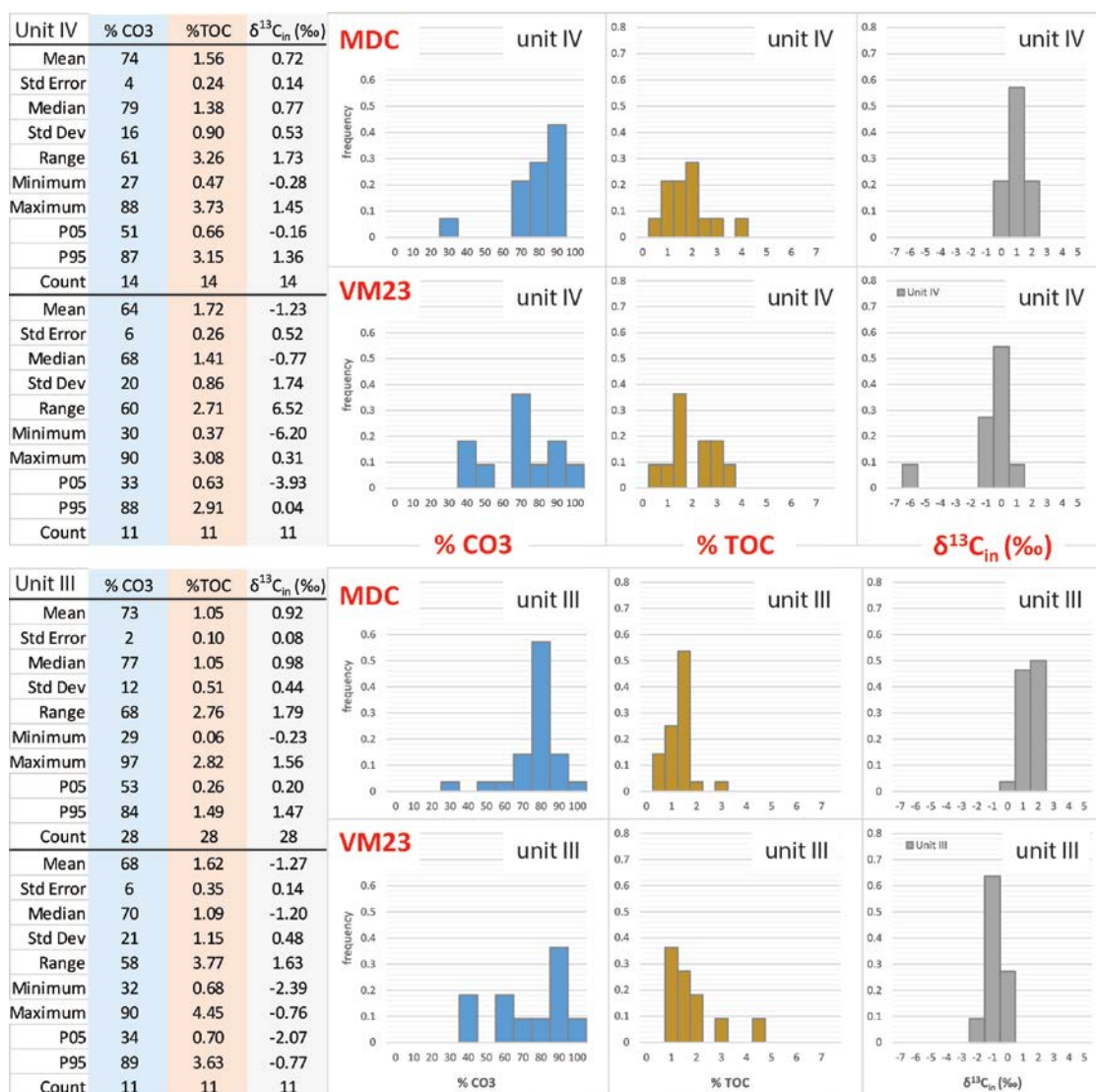


**Figure 4.25. Geochemical comparison of Units III and IV (MDC-VM23).** Upper rows: data from Unit IV. Lower rows: data from Unit III. Carbonate content and isotope ratios show higher values in MDC than in VM23. The organic content displays the opposite behavior

The geochemical characterization of the Los Catutos interval between MDC and VM23 sections show similarities and differences (Figure 4.24). In both cases there is an upward increase in carbonate content (%CO<sub>3</sub>) within the units accompanied by a reduction in organic content (TOC) and less negative or positive  $\delta^{13}C$  values. Cross-plots of CO<sub>3</sub> vs TOC and CO<sub>3</sub> vs  $\delta^{13}C$  (Figures 4.15 and 4.21) show that TOC decreases and  $\delta^{13}C$  increases

with increasing carbonate content, both for individual units and whole intervals in MDC and VM23.

As a result of the lateral change in facies between MDC and VM23, lateral variations in the analyzed geochemical parameters can be observed between correlated units (Figure 4.25). In units III/IV, mean carbonate content decreases from 73/74% in MDC to 64/68% in VM23, while mean  $\delta^{13}\text{C}$  values become more negative from 0.92/0.72‰ in MDC to -1.27/-1.23 in VM23. Lateral variations in organic content were also observed, from mean TOC values of 1.05/1.56% in MDC to 1.62/1.72% in VM23.

### **The younger carbonate-rich intervals in Puerta Curaco**

In the area of Puerta Curaco (PC), three carbonate-rich intervals were identified within the Vaca Muerta Formation. Though younger than the Los Catutos Member, they show similar characteristics to those observed in VM23. The following paragraphs describe first the entire PC succession, and then focus in the lithological and geochemical characteristics of the carbonate-rich intervals. The Los Catutos Member is not present in this distal position, but its time-equivalent interval (mid-late Tithonian) will be also studied to evaluate the lateral facial and geochemical changes that take place along a clinof orm.

### **PC reference section**

The 765m-thick PC reference section was logged from the contact with the underlying lacustrine facies of Tordillo Formation to the cross-bedded sandstones at the base of Mulichinco Formation (Figure 4.26). Ages for the basal portion of this section were estimated based on the ammonite zonation from a 120m succession from Yesera del



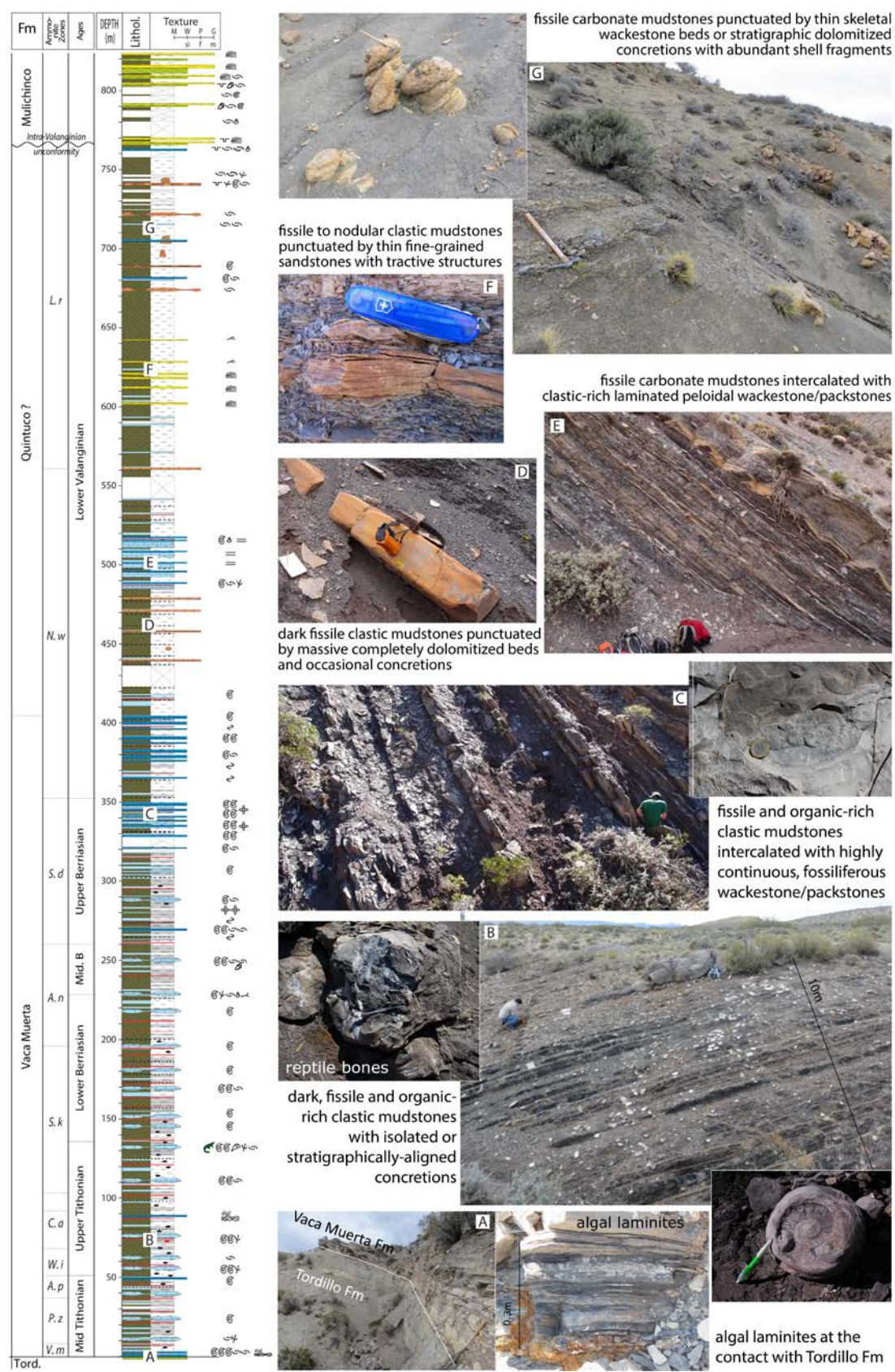


**Figure 4.26. PC reference section.** See lithological description in the text

Tromen (Aguirre Urreta et al., 2014) (Figure 4.27). The published section includes all the Tithonian ammonite zones (Figure 4.6), whose boundaries were translated into the PC section assuming the same thickness for both successions. For the upper part of the PC section, ages were assigned based on biostratigraphic internal reports from cores and side-wall cores from El Trapial wells (Chevron). Gamma ray (GR) logs from those wells were compared to field GR measured in Puerta Curaco (see GR correlation in Appendix C), to translate the ammonite zones (Aguirre Urreta and Vennari, 2013) and the ages obtained from a calcispheres and calpionellids zonation (Kietzmann and Ambrosio, 2014).

The succession in PC starts with a characteristic bed with algal laminations (Figure 4.26-A) and a fossiliferous packstone. The subsequent 250m are dominated by dark, fissile and organic-rich clastic mudstones punctuated by carbonate-rich layers (Figure 4.26-B). The carbonate-rich intercalations are mostly stratigraphically-aligned mudstone/wackestone concretions that are up to 1m thick and may contain ammonites, bivalves, fish scales, and rarely gastropods and reptile bones. Occasionally the carbonate-rich intercalations are thin and massive skeletal mudstone/wackestone beds. Isolated concretions, ash layers and calcite veins are also common.

Upwards, the concretions gradually disappear and the carbonate-rich intercalations consist of massive or slightly laminated skeletal wackestone/packstone beds with abundant ammonites (Figure 4.26-C). Between 328-349m and 373-404m in the section, the carbonate beds become thicker and more frequent. These two carbonate-rich intervals, plus one between 485 – 518 m, are the focus of this study. Above, the system is dominated by fissile clastic mudstones punctuated by massive and completely dolomitized carbonate

beds and concretions (Figure 4.26-D). The carbonate content increases between 485 and 518m, forming a third carbonate-rich interval with frequent intercalations of thin and

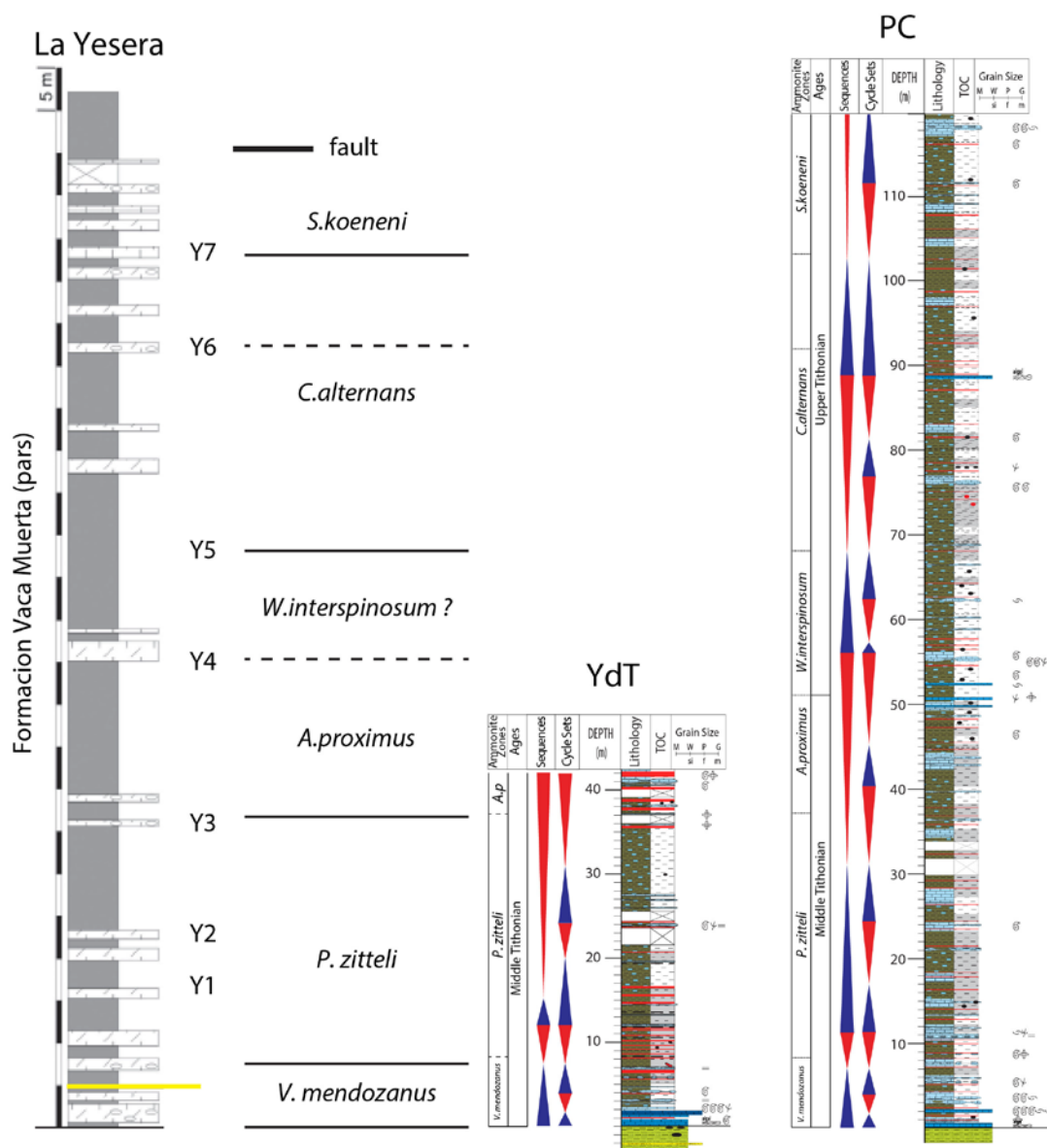


**Figure 4.27. Ages of the lower part of the succession in PC.** The ammonite zones were translated from a section in Yesera del Tromen (Aguirre Urreta et al 2014)

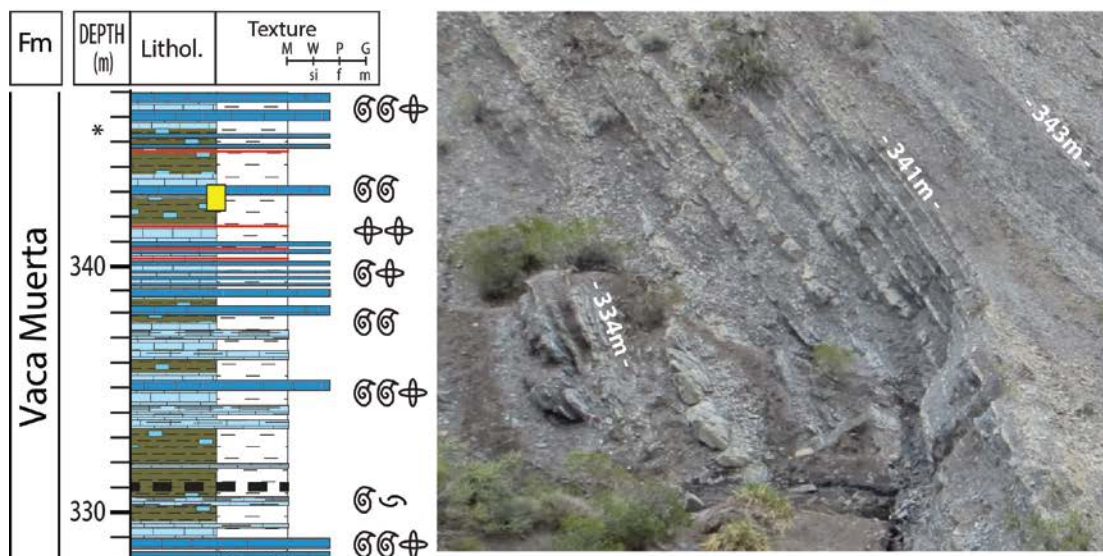
laminated peloidal wackestone beds (Figure 4.26-E). Upwards in the succession, the same pattern of dolomitized intercalations followed by laminated wackestones is repeated but significantly less developed and poorly exposed.

Above 595m, the system is dominated by fissile to nodular clastic mudstones punctuated by thin and fine-grained sandstone beds with frequent cross-bedded structures (Figure 4.26-F). The sandstone intercalations disappear gradually upwards, and thin skeletal wackestone beds with associated dolomitized concretions become common (Figure 4.26-G). The system changes abruptly around 765m where thick, cross bedded sandstones with load cast structures and abundant oysters characterize the base of the Mulichinco Fm.

### **First carbonate-rich interval**

The first carbonate-rich interval in the PC section (328-349m) consists of an alternation of fissile organic-rich clastic mudstones and massive or slightly laminated skeletal or peloidal wackestone/packstones with abundant ammonites (Figure 4.28). The massive carbonate beds have an average thickness of 0.3m and are commonly bioturbated. Porosities of this interval measured on plugs from short cores show values of 1-8% with an average of 4.79%.

The geochemical parameters of the interval show a slightly bimodal distribution of carbonate content, a relatively wide scatter of TOC values, and a very narrow range of  $\delta^{13}\text{C}$  compositions (Figure 4.29). The 5<sup>th</sup>-95<sup>th</sup> percentiles of the analyzed parameters are 44%/89%  $\text{CO}_3$ , 0.13%/1.97% TOC, and  $-1.24\text{‰}/+0.04\text{‰}$   $\delta^{13}\text{C}$ , with mean values of 69%  $\text{CO}_3$ , 1% TOC and  $-0.55\text{‰}$   $\delta^{13}\text{C}$ . Cross-plots of  $\text{CO}_3$  vs TOC and  $\text{CO}_3$  vs  $\delta^{13}\text{C}$  show that TOC decreases and  $\delta^{13}\text{C}$  increases with increasing carbonate content. The latter correlation is weak ( $R^2 = 0.27$ ), but becomes significant when samples are analyzed relatively to their position in the cycle (see section Sequence Stratigraphy, this Chapter).



### First carbonate-rich interval - Upper Berriasian (*S.damesi* zone)

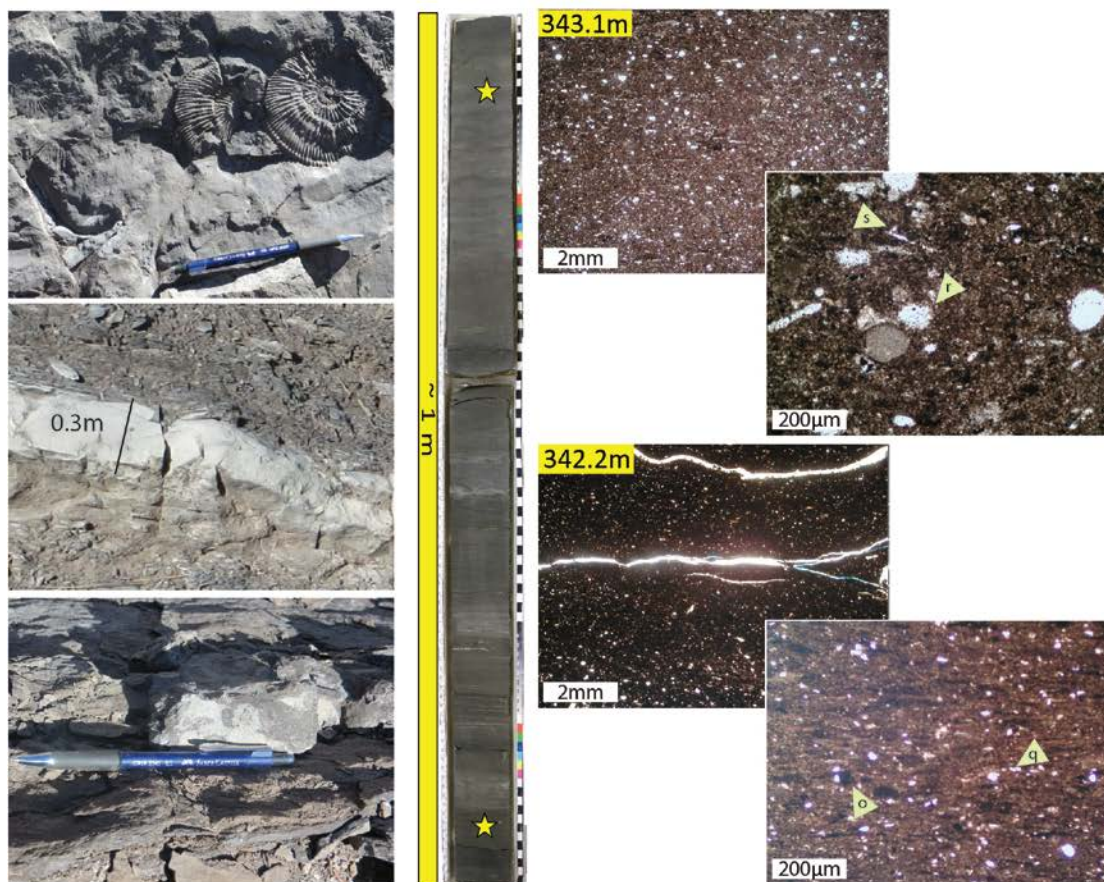


**Figure 4.28. Lithology of the 1<sup>st</sup> carbonate-rich interval in PC.** The yellow rectangle in the lithologic section represents the position of the short core shown below. The short core cut through a massive and bioturbated skeletal wackestone/packstone with radiolarians (*r*) and sponge spicules (*s*), and reached the fissile clastic (*q*-quartz) and organic-rich (*o*-organic matter) mudstones below

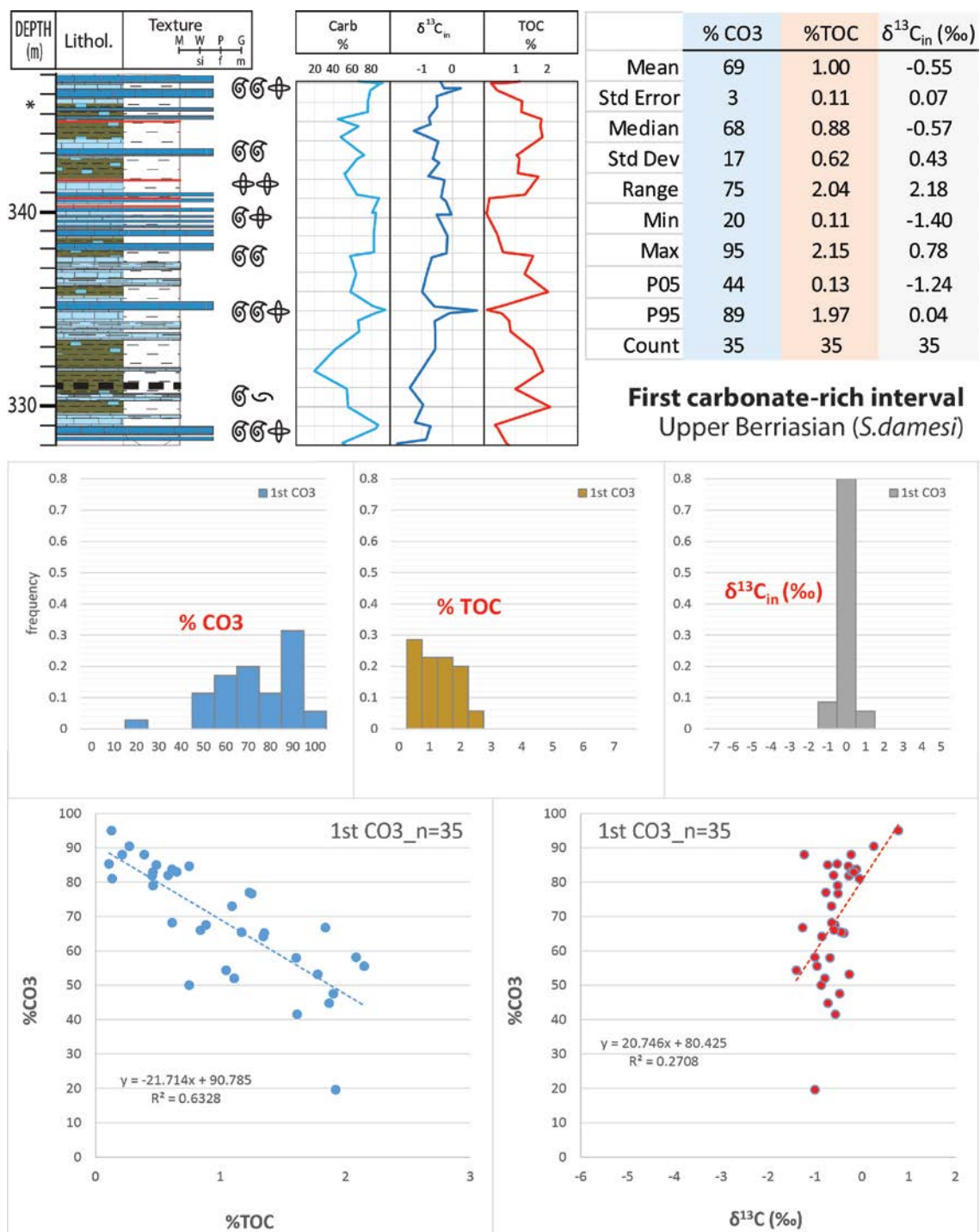


**Figure 4.29. Geochemistry of the 1<sup>st</sup> carbonate-rich interval in PC.**  
See comments in the text

### **Second carbonate-rich interval**

The second carbonate-rich interval (373-404m) is characterized by the alternation of fissile organic-rich clastic mudstones and massive or slightly laminated peloidal wackestone/packstones with abundant ammonites (Figure 4.30). The massive carbonate beds are on average 0.2m-thick with moderate bioturbation. Porosities of this interval show values of 1-10% with an average of 5.73%.

The interval displays slightly bimodal distributions for all the analyzed geochemical parameters, especially in case of the carbonate content (Figure 4.31). The bimodality responds to the alternation of fissile organic-rich clastic mudstones and carbonate beds. The bulk of the values ( $P_5$ - $P_{95}$ ) for the analyzed parameters fall between 20%/86%  $\text{CO}_3$ , 0.43%/2.95% TOC, and -1.53‰/+1.18 ‰  $\delta^{13}\text{C}$ . Mean values are 50%  $\text{CO}_3$ , 1.52% TOC and -0.6‰  $\delta^{13}\text{C}$ . There is an inverse correlation between % $\text{CO}_3$  and TOC, and a direct one between  $\text{CO}_3$  and  $\delta^{13}\text{C}$ .

### **Third carbonate-rich interval**

The third carbonate-rich interval (485-518m) typically shows an alternation of fissile carbonate mudstones with laminated peloidal wackestone/packstones (Figure 4.32). The boundaries between these two facies are often gradual, with a small difference in carbonate content. As a result, the overall character of the interval is very homogenous. Bioturbation is rare and fossil content is scarce and generally limited to radiolarians. Porosities measured on plugs from short cores show values of 1-10% with an average of 5.73%.

The distributions of the analyzed geochemical parameters show  $P_5$ / $P_{95}$  ranges of 32%/75%  $\text{CO}_3$ , 0.66%/2.78% TOC and -0.45‰/+0.37‰  $\delta^{13}\text{C}$ , and mean values of 57%

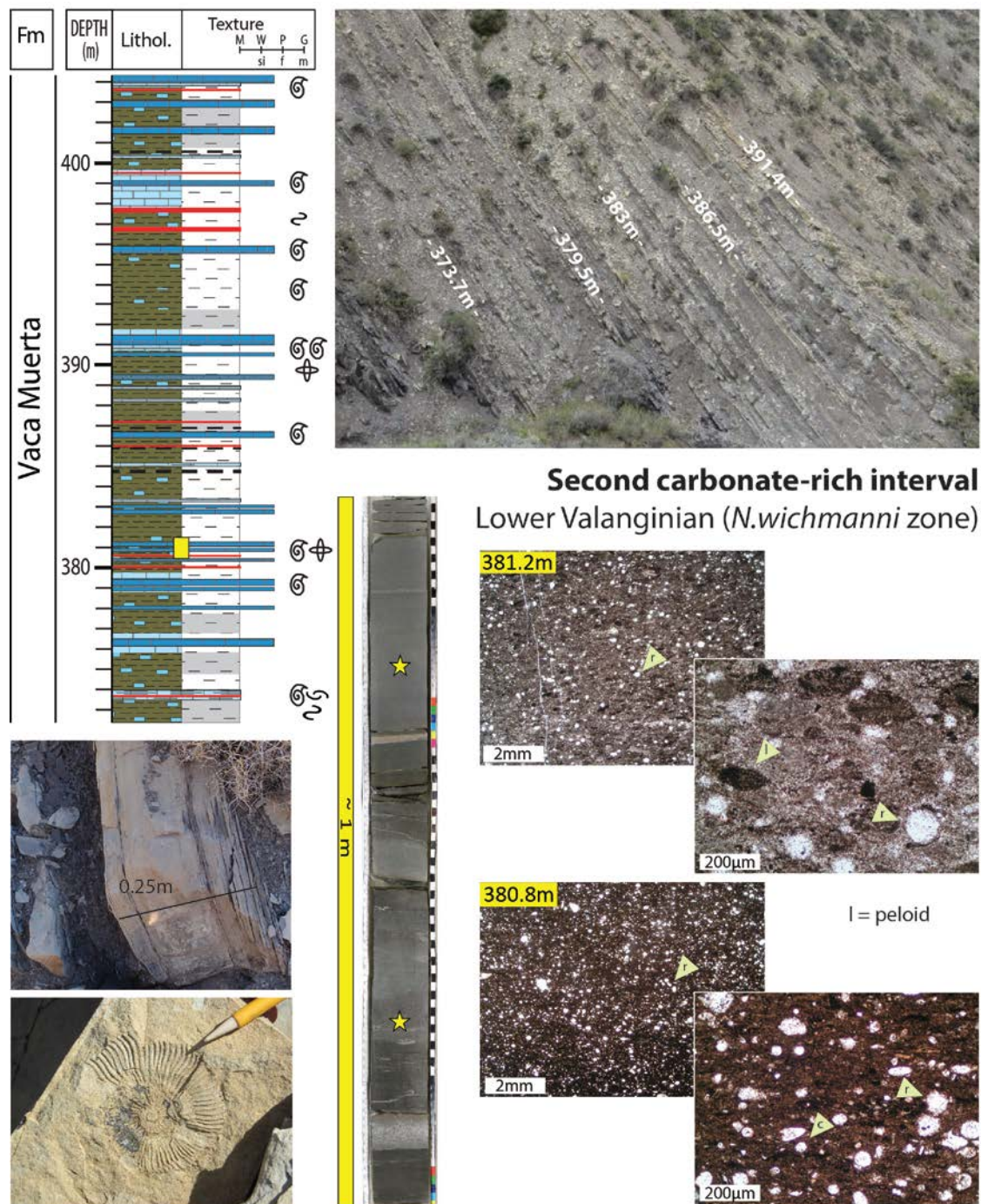
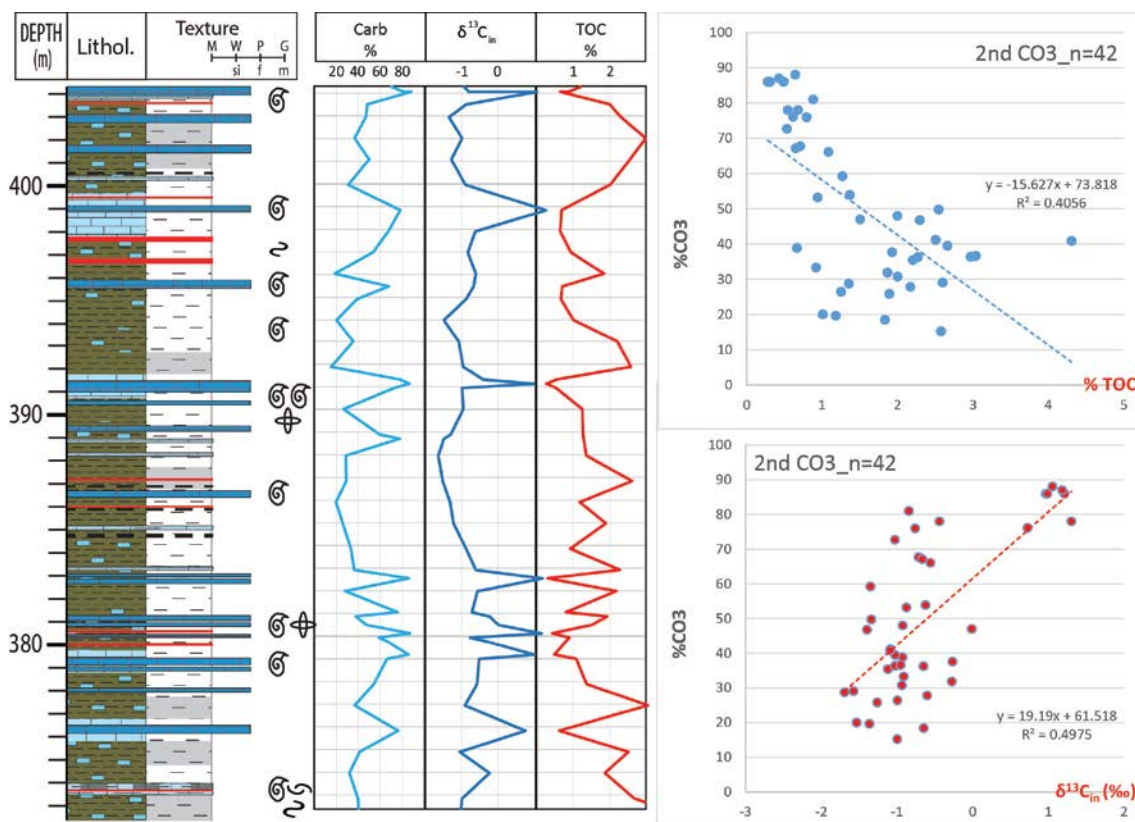


**Figure 4.30. Lithology of the 2<sup>nd</sup> carbonate-rich interval in PC.** The yellow rectangle in the lithologic section represents the position of the short core shown below. The core cut first through a massive peloidal wackestone/packstone with abundant peloids (l) and radiolarians (r), then a skeletal wackestone with abundant radiolarians (r) and calcispheres (c), and a volcanic rich layer near the bottom





### Second carbonate-rich interval - Lower Valanginian (*N.wichmanni*)

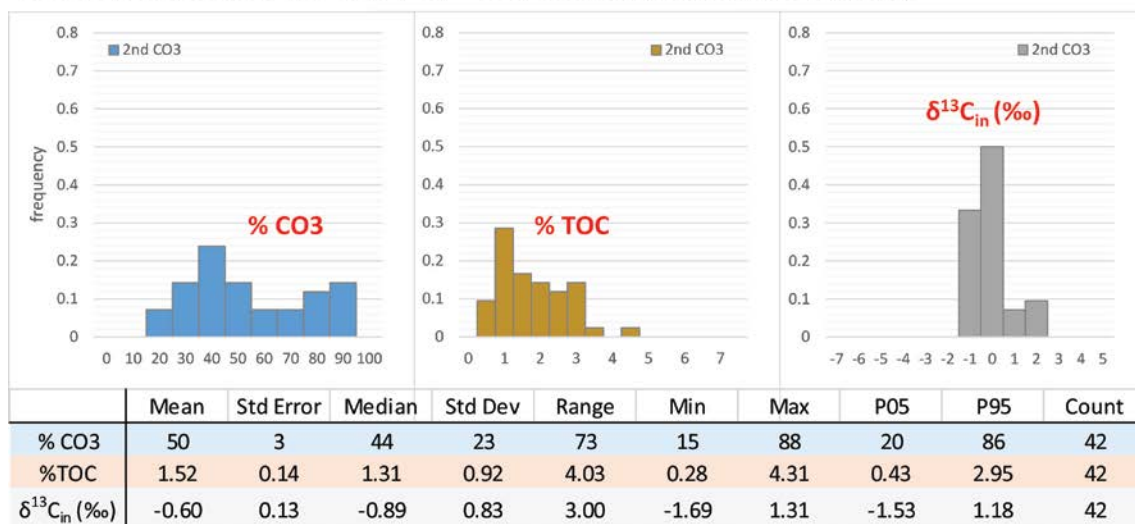


**Figure 4.31. Geochemistry of the 2<sup>nd</sup> carbonate-rich interval in PC.**  
See comments in the text

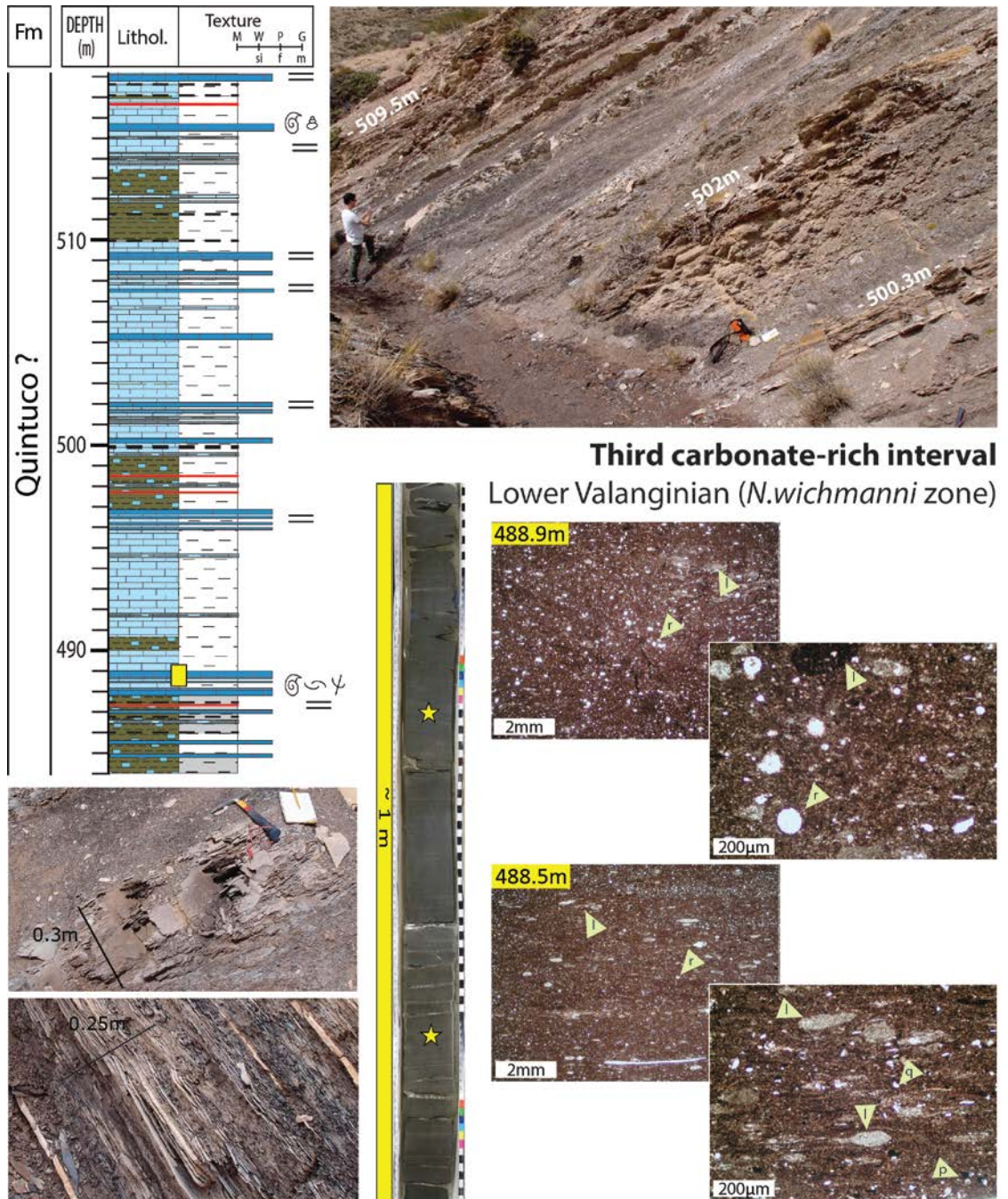
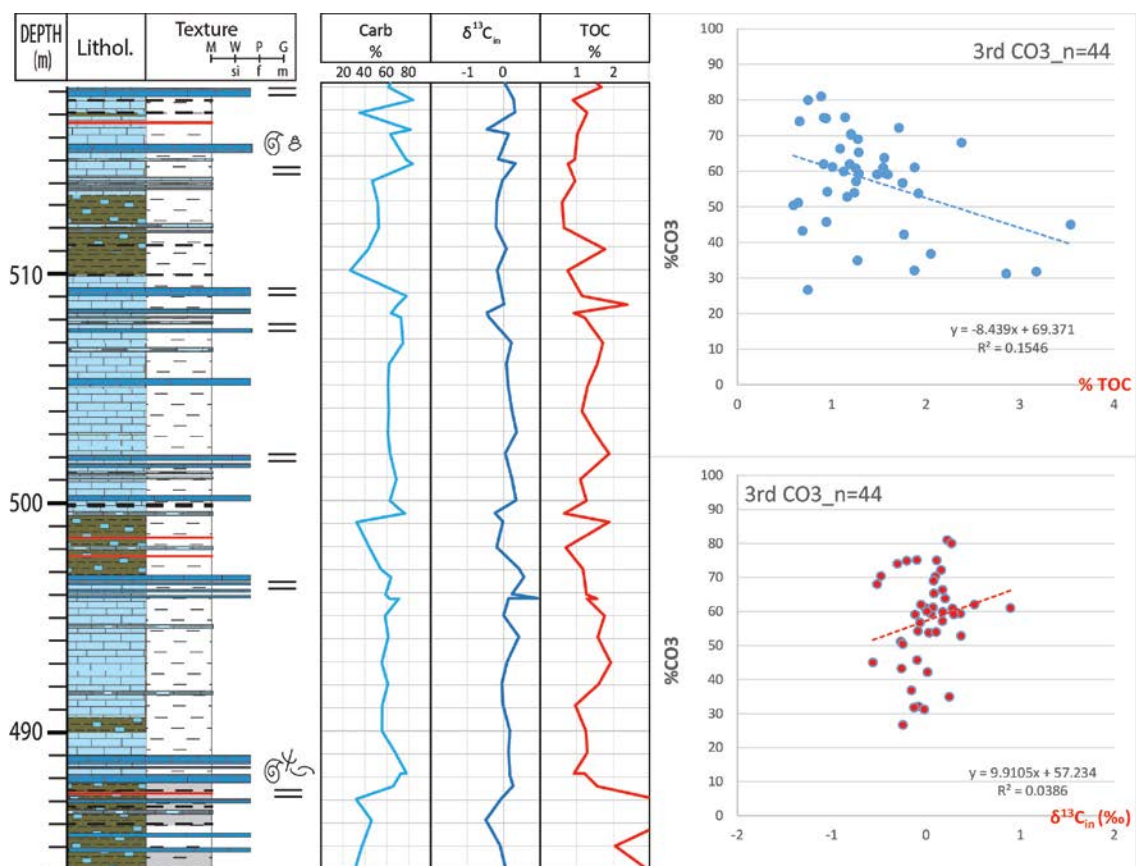


**Figure 4.32. Lithology of the 3<sup>rd</sup> carbonate-rich interval in PC.** The yellow rectangle in the lithologic section represents the position of the short core shown below. The core cut first through a massive skeletal wackestone with abundant radiolarians (*r*) and occasional peloids (*l*), and a laminated peloidal wackestone below, with abundant peloids (*l*)



### Third carbonate-rich interval - Lower Valanginian (*N.wichmanni*)

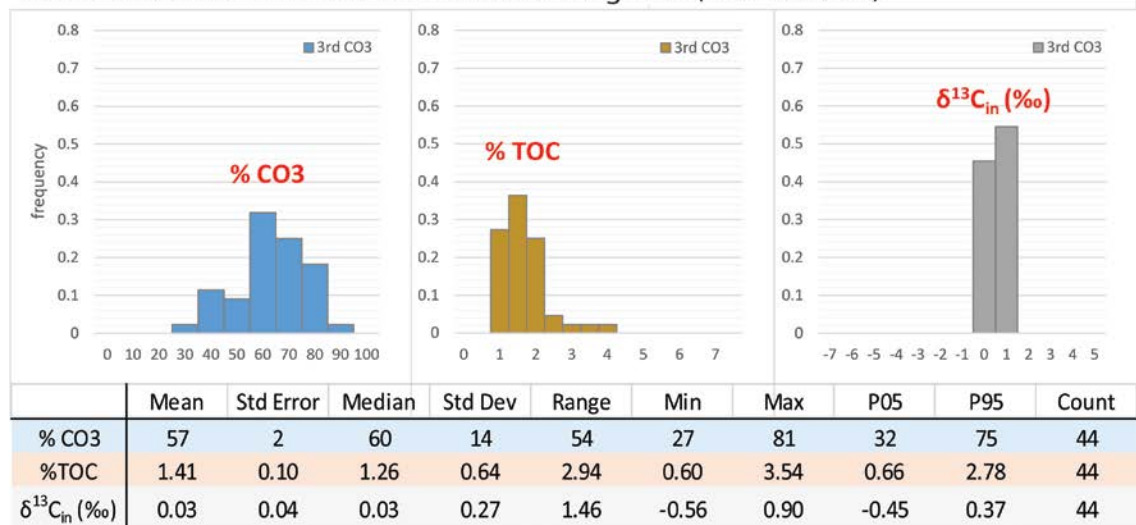


**Figure 4.33. Geochemistry of the 3<sup>rd</sup> carbonate-rich interval in PC.**  
See comments in the text

CO<sub>3</sub>, 1.41%TOC and 0.03‰ δ<sup>13</sup>C (Figure 4.33). Cross-plots of CO<sub>3</sub> vs TOC and CO<sub>3</sub> vs δ<sup>13</sup>C show weak trends of decreasing TOC and increasing δ<sup>13</sup>C with increasing carbonate content. As mentioned for previous intervals, the observed slightly weak trends become stronger when the data is subset by transgressive and regressive hemicycles (see section Sequence Stratigraphy, this Chapter).

### **The mid-late Tithonian in PC**

The mid-late Tithonian interval in PC (~45-56m) is not a carbonate-rich interval, but its description is also included as part of this work because it represents the same time-interval as Los Catutos Member but in a more distal position. Hence, its characterization provides an insight into the lateral facial and geochemical variations that take place along a clinoform, from a relatively proximal setting in Sierra de la Vaca Muerta to a position 150km further into the basin (PC section).

The mid-late Tithonian in PC is dominated by dark, fissile and organic-rich clastic mudstones commonly associated with isolated concretions (Figure 4.34). The clastic mudstone facies are punctuated by stratigraphically-aligned concretions or, less frequently, by thin carbonate wackestone/packstone beds. The concretions are 0.3-0.6m-thick skeletal wackestones with abundant radiolarians and ammonites. The carbonate beds are 0.2m-thick skeletal wackestone/packstones with abundant crinoids, or peloidal wackestones with abundant radiolarians (Figure 4.34). Ash layers and calcite veins are common. Porosities measured on samples of the skeletal wackestone/packstones show values of 4-8%.

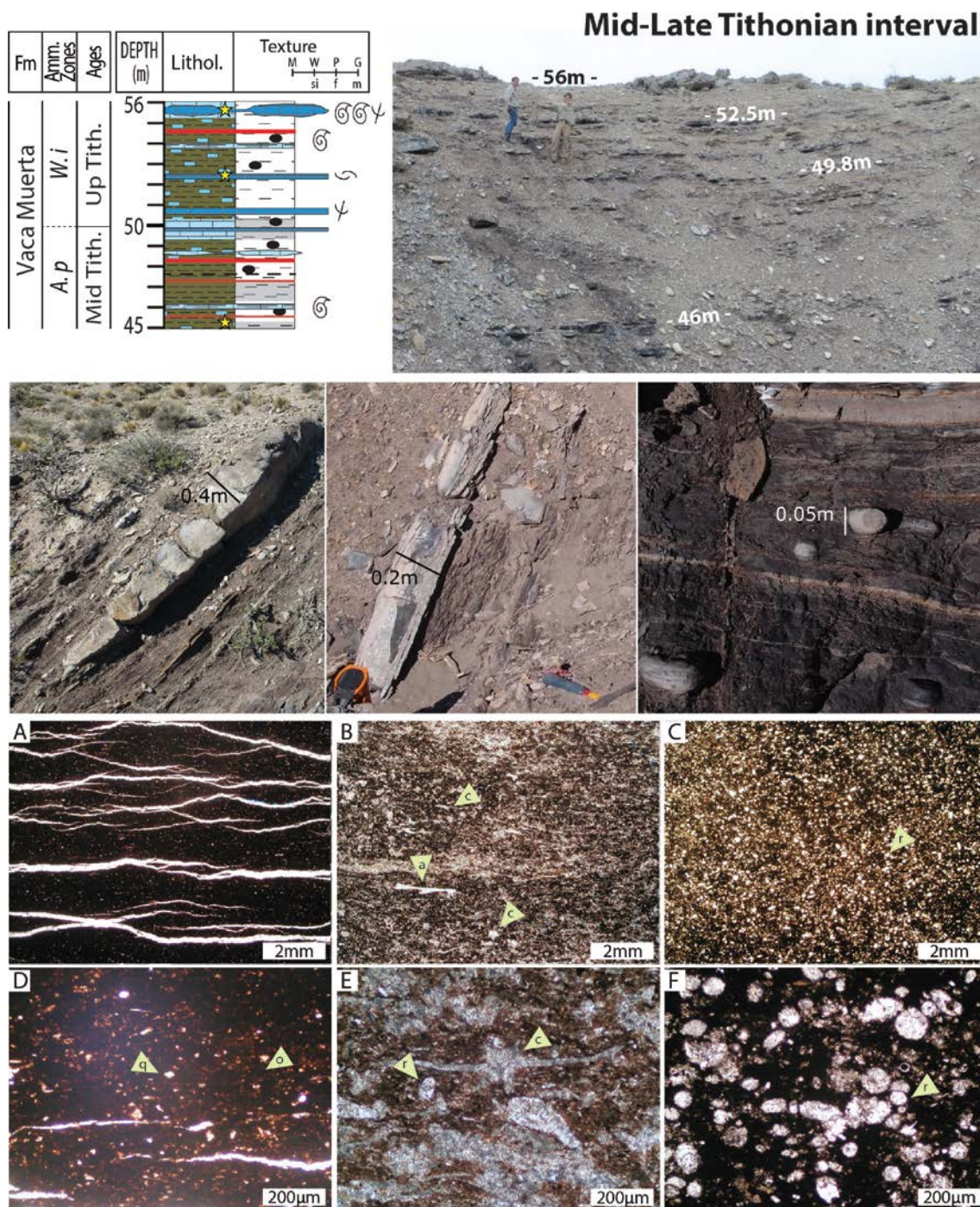
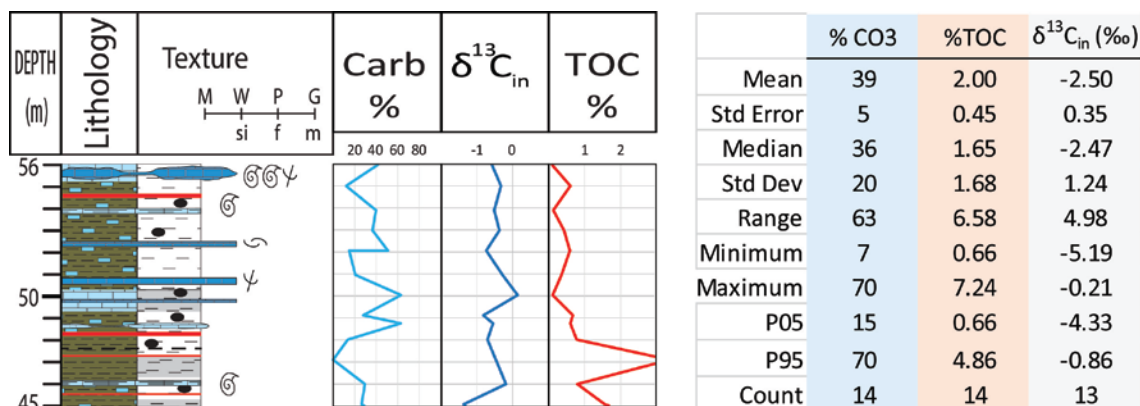


**Figure 4.34. Lithology of the mid-late Tithonian interval in PC.** Carbonate-rich intercalations (second row) can be either stratigraphically aligned concretions (left) or thin massive beds (middle). Small isolated concretions (right) are also common. Characteristic microfacies are dominantly clastic (q-quartz) and organic-rich (o-organic matter) mudstones, and less commonly crinoidal packstone beds or radiolarian wackestone/packstone concretions [crinoids (c), radiolarians (r), ammonite aptichus (a)]



### Mid-Late Tithonian interval (*A.proximus*, *W.internispinosum*)

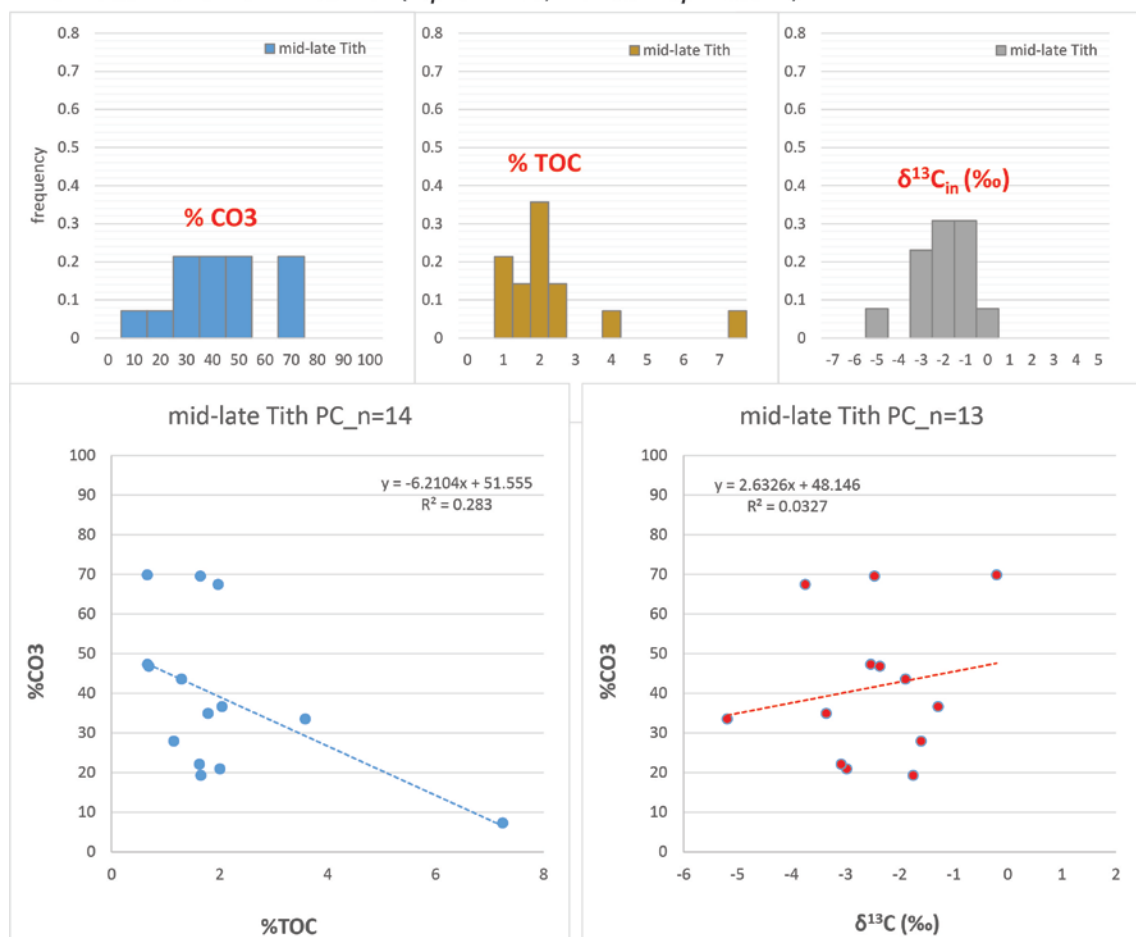


**Figure 4.35. Geochemistry of the mid-late Tithonian interval in PC.**  
See comments in the text

The interval has a very low carbonate content, relatively high TOC and very negative  $\delta^{13}C$ , with mean values of 39%, 2% and -2.5‰ respectively (Figure 4.35). The bulk of the values (P<sub>5</sub>-P<sub>95</sub>) fall between 15% and 70% CO<sub>3</sub>, 0.66% and 4.86%TOC, and -4.33‰ and

-0.86‰  $\delta^{13}\text{C}$ . Cross-plots of  $\text{CO}_3$  vs TOC and  $\text{CO}_3$  vs  $\delta^{13}\text{C}$  show a very weak trend of decreasing TOC with increasing carbonate content ( $R^2 = 0.28$ ), and almost no correlation between carbonate content and  $\delta^{13}\text{C}$  ( $R^2 = 0.03$ ).

## **Sequence stratigraphy**

### **Cycles and cycle sets**

The lithofacies are arranged in cyclic patterns of different orders that can be clearly identified in the analyzed intervals (Figures 4.36, 4.38, 4.40, 4.42, 4.44 and 4.46). Each cycle is subdivided into a transgressive and regressive hemicycle, with an interval of maximum flooding in between. The top of the regressive hemicycle represents the cycle boundary.

Basic cycles defined in the field are characterized by the rhythmic alternation of clastic-rich and carbonate-rich layers. A fissile clastic-rich portion dominates the transgressive hemicycle, the zone of maximum flooding and the beginning of the regressive hemicycle, while a carbonate-rich portion forms the top of the cycles. The vertical variation of lithofacies types result in a characteristic weathering profile where the fissile portion is back weathered and the carbonate-rich tops stick out.

The rhythmic alternation of clastic-rich and carbonate-rich layers have different expressions in different intervals. In Los Catutos in MDC, the carbonate-rich tops dominate most of the cycles and are represented by thick (>0.6m-thick) skeletal carbonate beds, while the fissile, clastic and organic-rich intercalations are relatively thin or absent (Figure 4.36). The regressive portion (R) of the cycles is characterized by high carbonate content, low TOC, and less negative or more positive  $\delta^{13}\text{C}$  values, while the opposite is observed

in the transgressive portions (T) (Figure 4.37). Mean values are 75 (R) and 36 (T) % CO<sub>3</sub>, 1.04 (R) and 2.26 (T) % TOC, and 0.72 (R) and -0.89 (T) ‰ δ<sup>13</sup>C.

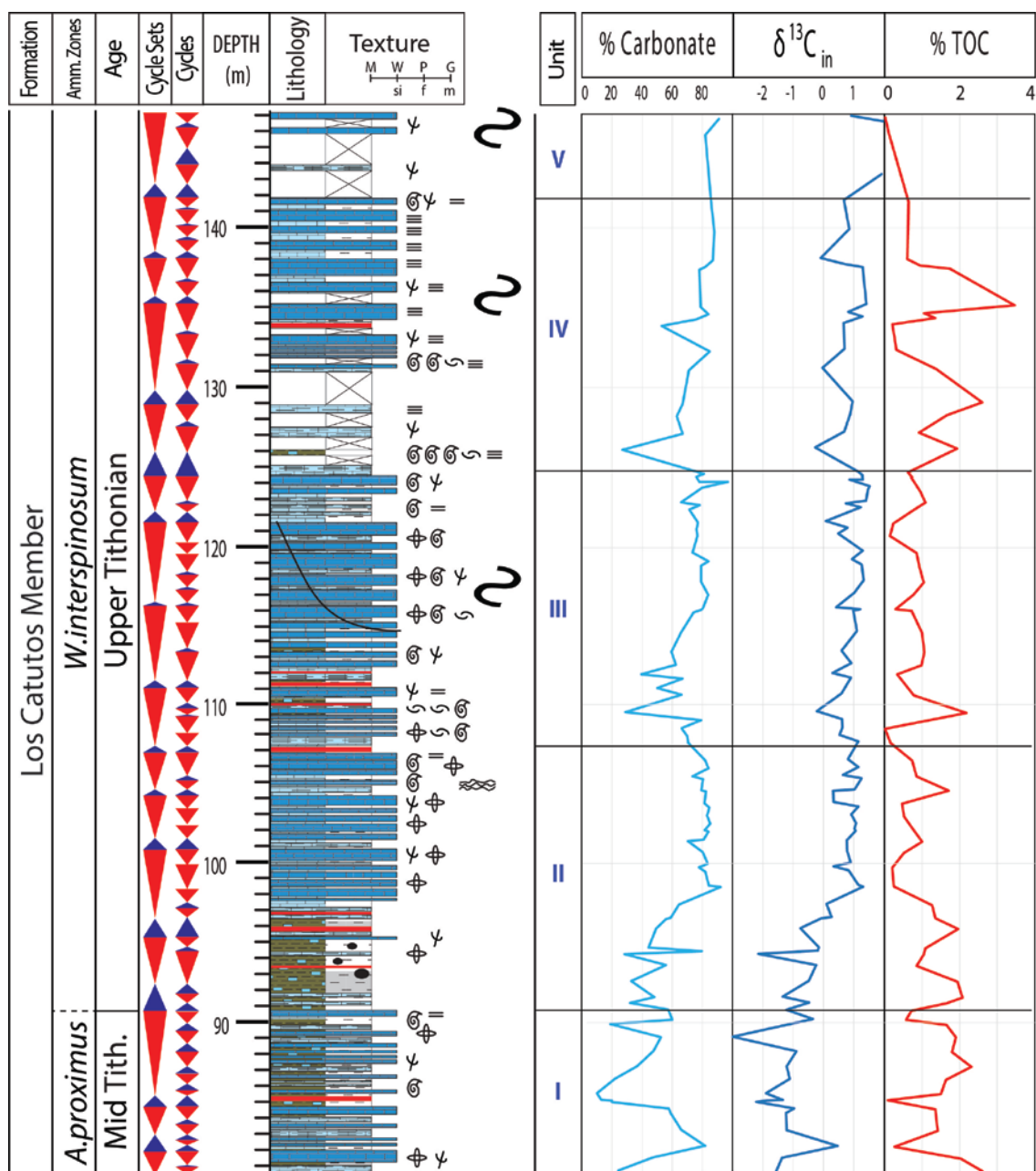


**Figure 4.36. Cycles of Los Catutos in MDC.** Field cycles and cycle sets are shown next to the lithologic section

In the Los Catutos interval in VM23, the fissile, clastic and organic-rich portions are thicker than in MDC, and the skeletal carbonate-rich tops are represented by thinner (0.2-0.3m-thick) carbonate beds (Figure 4.38). This results in overall lower carbonate content,



higher TOC, and more negative  $\delta^{13}\text{C}$  values than in MDC (Figure 4.39). As in MDC, the regressive portion (R) of the cycles is characterized by high carbonate content, low TOC, and less negative or more positive  $\delta^{13}\text{C}$  values, while the opposite is observed in the transgressive portions (T). Mean values in VM23 are 76 (R) and 40 (T) %CO<sub>3</sub>, 1.32 (R) and 2.60 (T) %TOC, and -0.81 (R) and -1.53 (T) ‰  $\delta^{13}\text{C}$ .

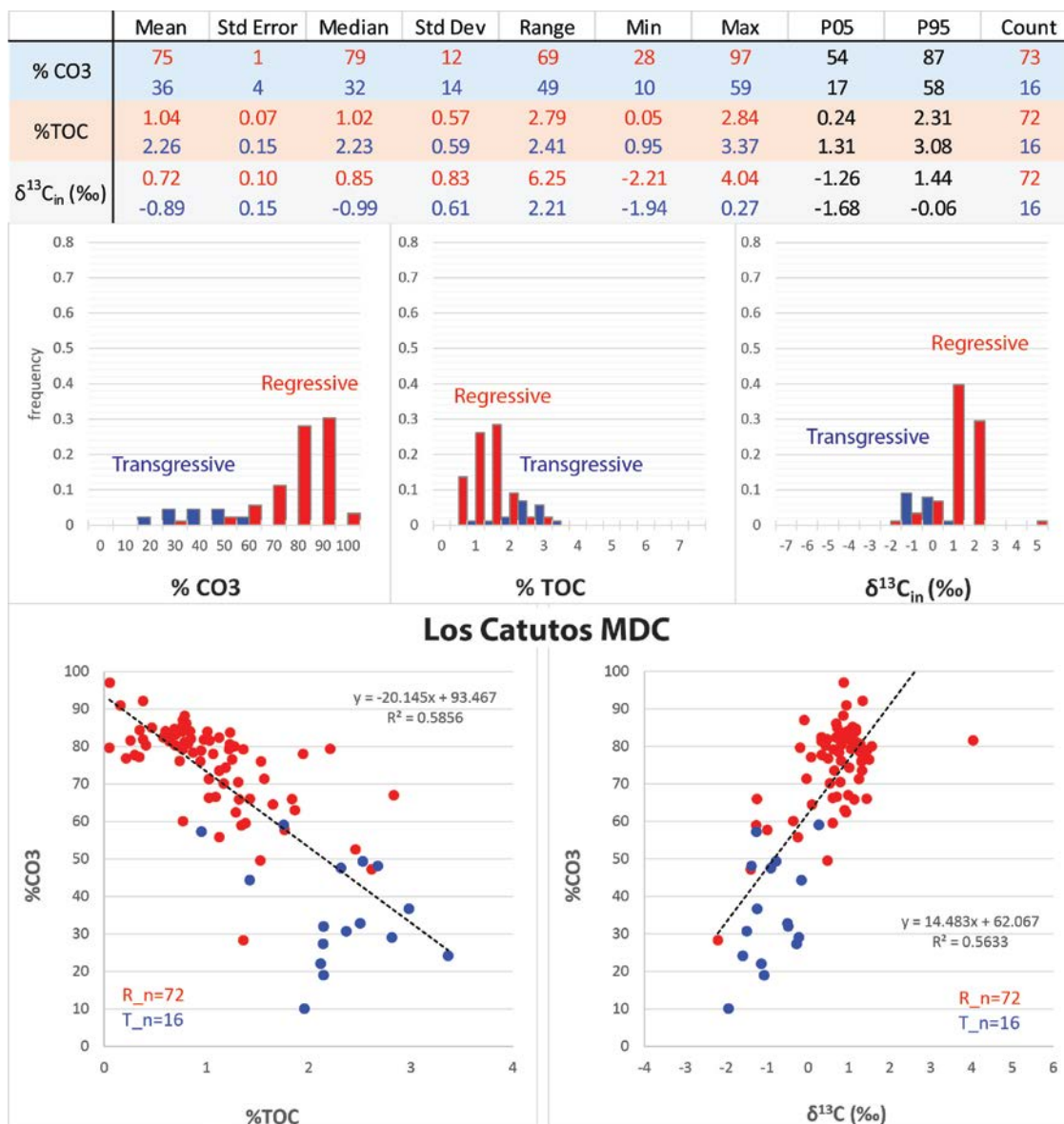


**Figure 4.37. Geochemical signature of cycles -Los Catutos, MDC.** Samples are grouped according to their position in the cycle: TOP and R samples (see Table 4.2) correspond to the Regressive hemicycle (in red), T and MFS (see Table 4.2) correspond to the Transgressive hemicycle (in blue). See other comments in the text

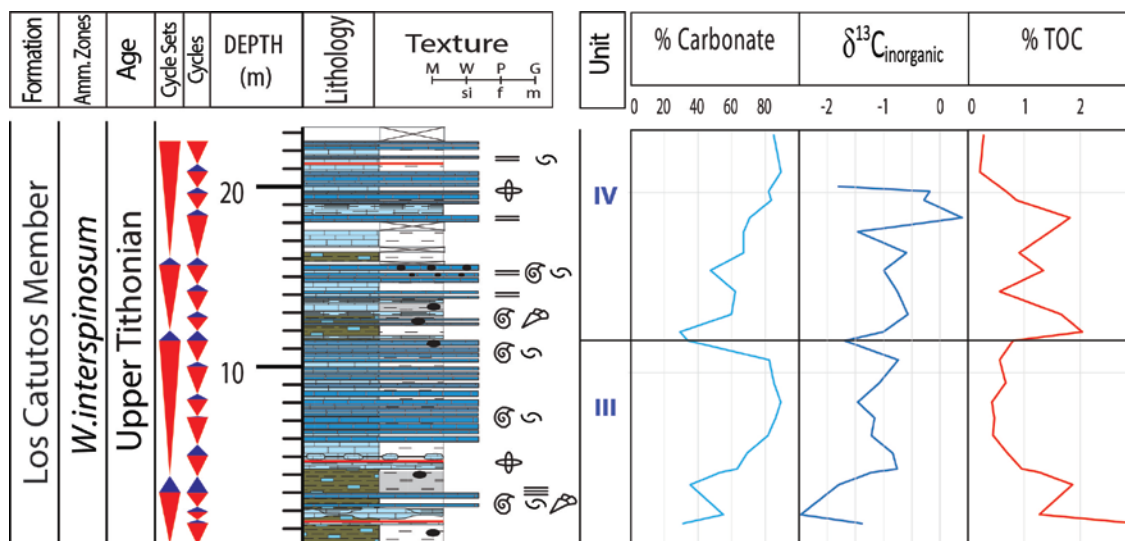


**Figure 4.38. Cycles of Los Catutos in VM23.** Field cycles and cycle sets are shown next to the lithologic section

The three carbonate-rich intervals studied in PC have cycles similar to those of Los Catutos in VM23 (Figures 4.40, 4.42 and 4.44). The fissile, clastic and organic-rich portions are relatively thick, while the skeletal carbonate-rich tops are represented by thin (0.2-0.3m-thick) carbonate beds. As observed in other intervals, the regressive portion (R) of the cycles is characterized by high carbonate content, low TOC, and less negative or more positive  $\delta^{13}\text{C}$  values, while the opposite occurs in the transgressive portions (T) (Figures 4.41, 4.43 and 4.45). In the first carbonate-rich interval, mean values are 76 (R) and 50 (T) % $\text{CO}_3$ , 0.80 (R) and 1.61 (T) %TOC, and -0.47 (R) and -0.78 (T) ‰  $\delta^{13}\text{C}$ . The second carbonate-rich interval is more clastic and organic-rich, both in the transgressive and regressive portions of the cycles, with mean values of 61 (R) and 31 (T) % $\text{CO}_3$ , 1.07 (R) and 2.32 (T) %TOC, and -0.41 (R) and -0.94 (T) ‰  $\delta^{13}\text{C}$ . The differences between transgressive and regressive hemicycles are smaller in the third carbonate-rich interval,

with mean values of 62 (R) and 48 (T) %CO<sub>3</sub>, 1.26 (R) and 1.75 (T) %TOC, and 0.08 (R) and -0.10 (T) ‰ δ<sup>13</sup>C.

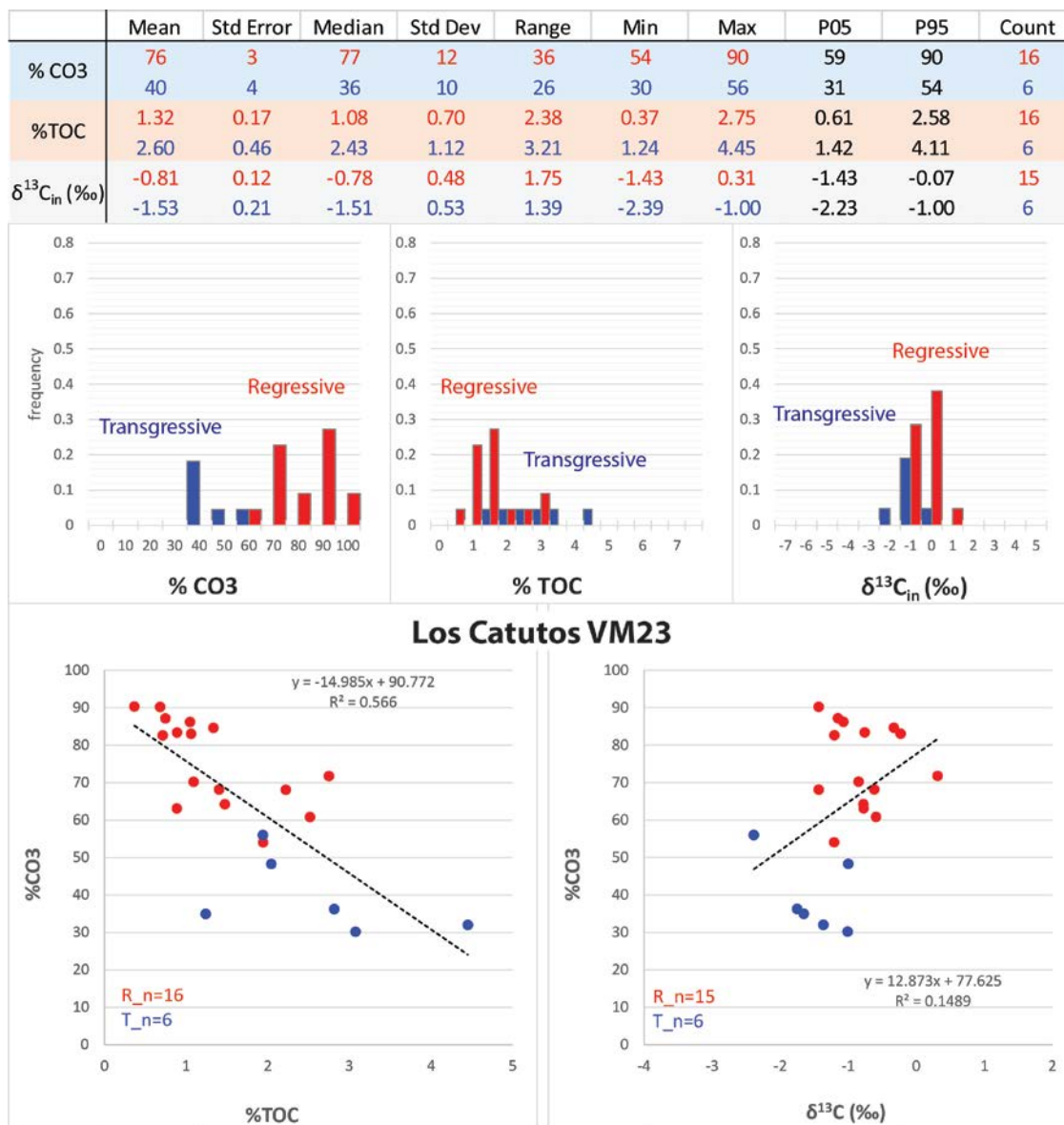


**Figure 4.39. Geochemical signature of cycles -Los Catutos, VM23.** Samples are grouped according to their position in the cycle: TOP and R samples (see Table 4.2) correspond to the Regressive hemicycle (in red), T and MFS (see Table 4.2) correspond to the Transgressive hemicycle (in blue). See other comments in the text

Cycles of the mid-late Tithonian interval in PC are dominated by the fissile clastic-rich portions (Figure 4.46). The carbonate rich tops are rarely represented by continuous carbonate beds, and instead stratigraphically-aligned concretions are frequent. As observed

in the other intervals, the regressive portion (R) of the cycles is characterized by high carbonate content, low TOC, and less negative  $\delta^{13}\text{C}$  values, while the opposite occurs in the transgressive portions (T) (Figures 4.47). Mean values are 47 (R) and 26 (T) % $\text{CO}_3$ , 1.38 (R) and 3.13 (T) %TOC, and -2.37 (R) and -2.79 (T) ‰  $\delta^{13}\text{C}$ .

### First carbonate-rich interval

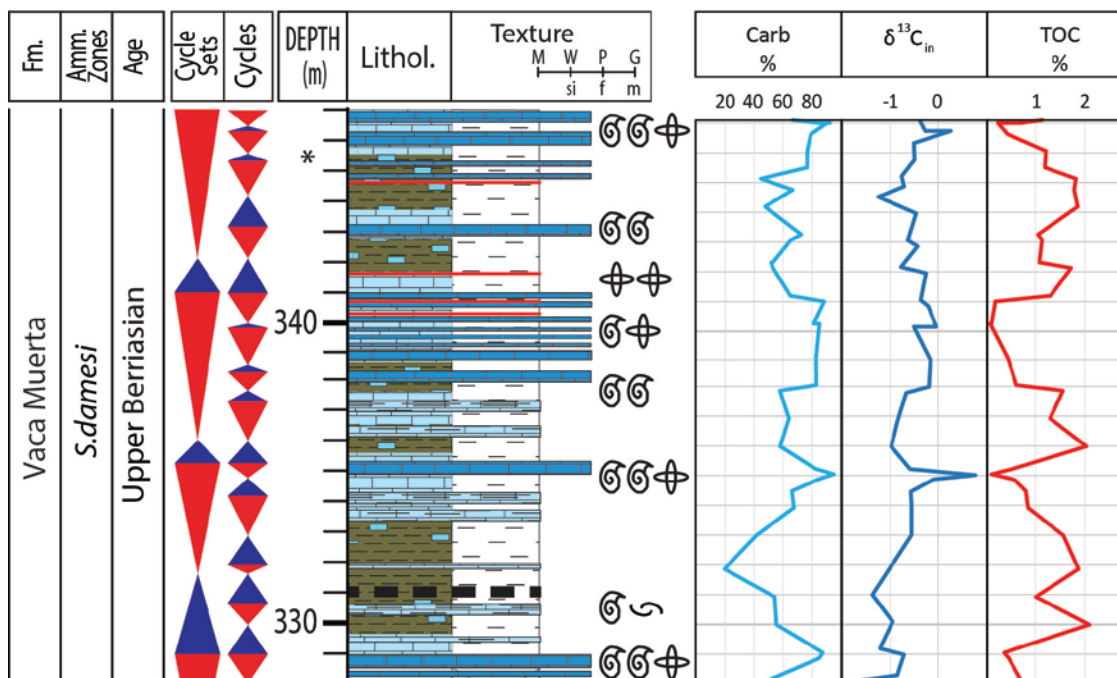


**Figure 4.40.** Cycles of the 1<sup>st</sup> carbonate-rich interval in PC. Field cycles and cycle sets are shown next to the lithologic section

The vertical stacking of the basic cycles reinforce the described patterns in the 6 analyzed intervals, as the regressive portion of the cycle sets is marked by an increase in the thickness and frequency of carbonate beds (Figures 4.36, 4.38, 4.40, 4.42, 4.44 and 4.46). The increase in frequency of carbonate beds results in an increase in carbonate and skeletal content. Additionally, the observed relations between % $\text{CO}_3$  and %TOC, and % $\text{CO}_3$  and  $\delta^{13}\text{C}$ , result in less negative or even positive  $\delta^{13}\text{C}$  values, and a decrease in the TOC content towards the top of the cycle sets. These relations are common to all the

analyzed intervals, but are much weaker in the case of the mid-late Tithonian interval, which is not carbonate-rich.

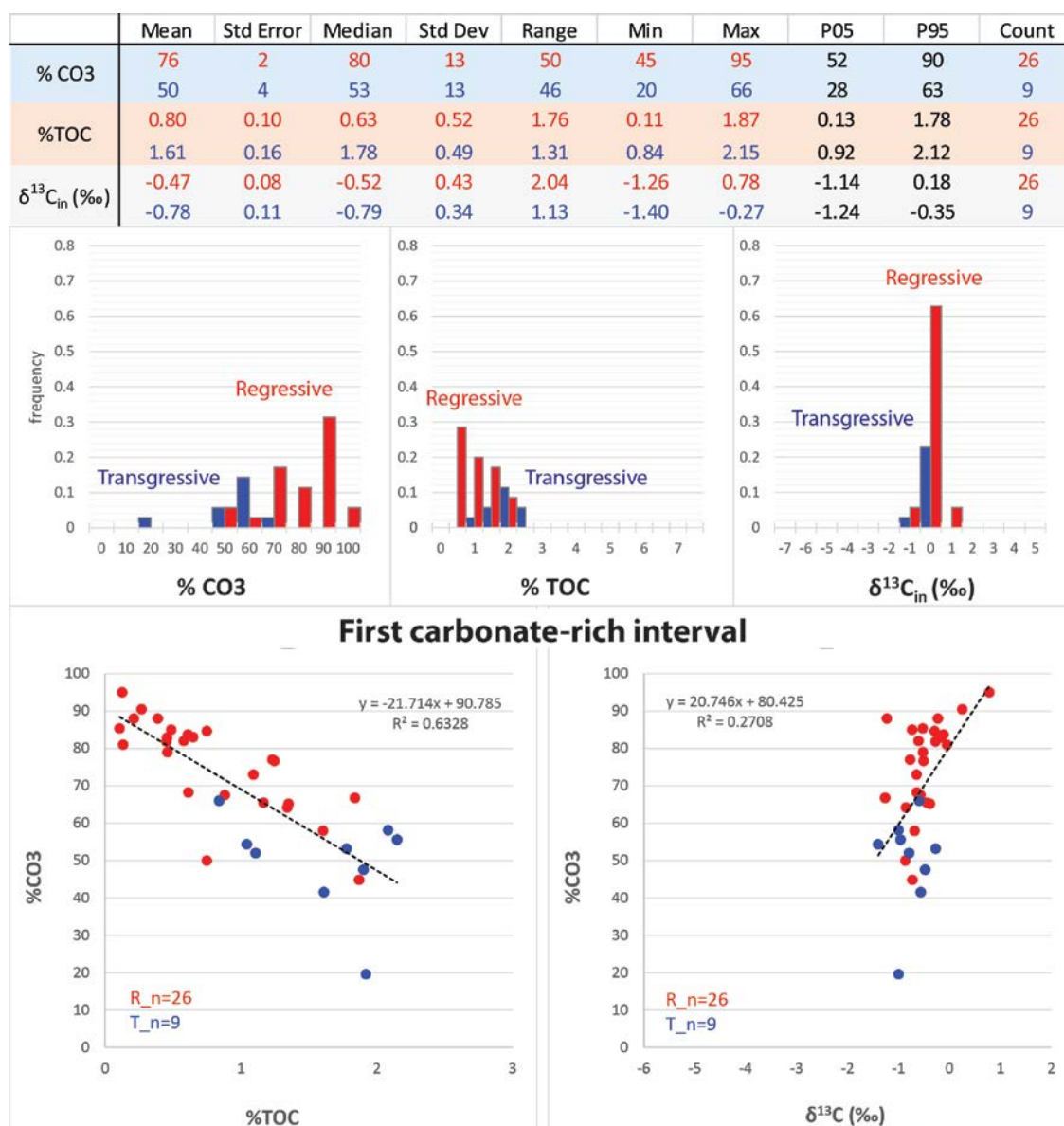


**Figure 4.41. Geochemical signature of cycles -1<sup>st</sup> carbonate-rich interval, PC.** Samples are grouped according to their position in the cycle: TOP and R samples (see Table 4.2) correspond to the Regressive hemicycle (in red), T and MFS (see Table 4.2) correspond to the Transgressive hemicycle (in blue). See other comments in the text

## Second carbonate-rich interval

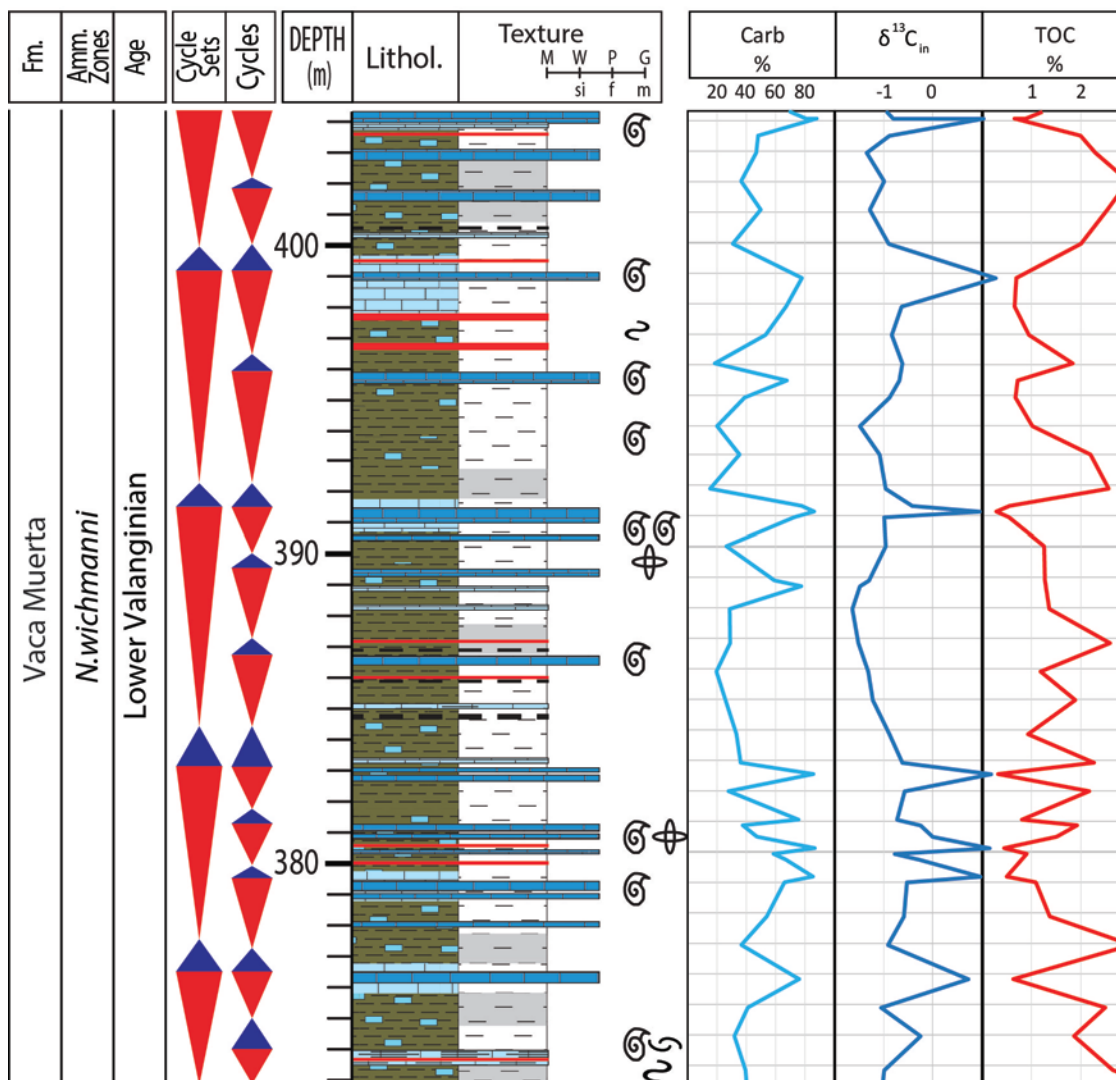


**Figure 4.42.** Cycles of the 2<sup>nd</sup> carbonate-rich interval in PC. Field cycles and cycle sets are shown next to the lithologic section

A lateral change in cycle character is observed when comparing time-equivalent intervals, as Los Catutos in MDC and VM23, and the mid-late Tithonian in PC (Figures 4.36, 4.38 and 4.46). Cycles of the Los Catutos interval are carbonate-dominated in MDC, and have thicker clastic-rich portions and thinner carbonate tops in VM23. In PC, where the Los Catutos carbonate-rich interval is not present, cycles of the time-equivalent interval

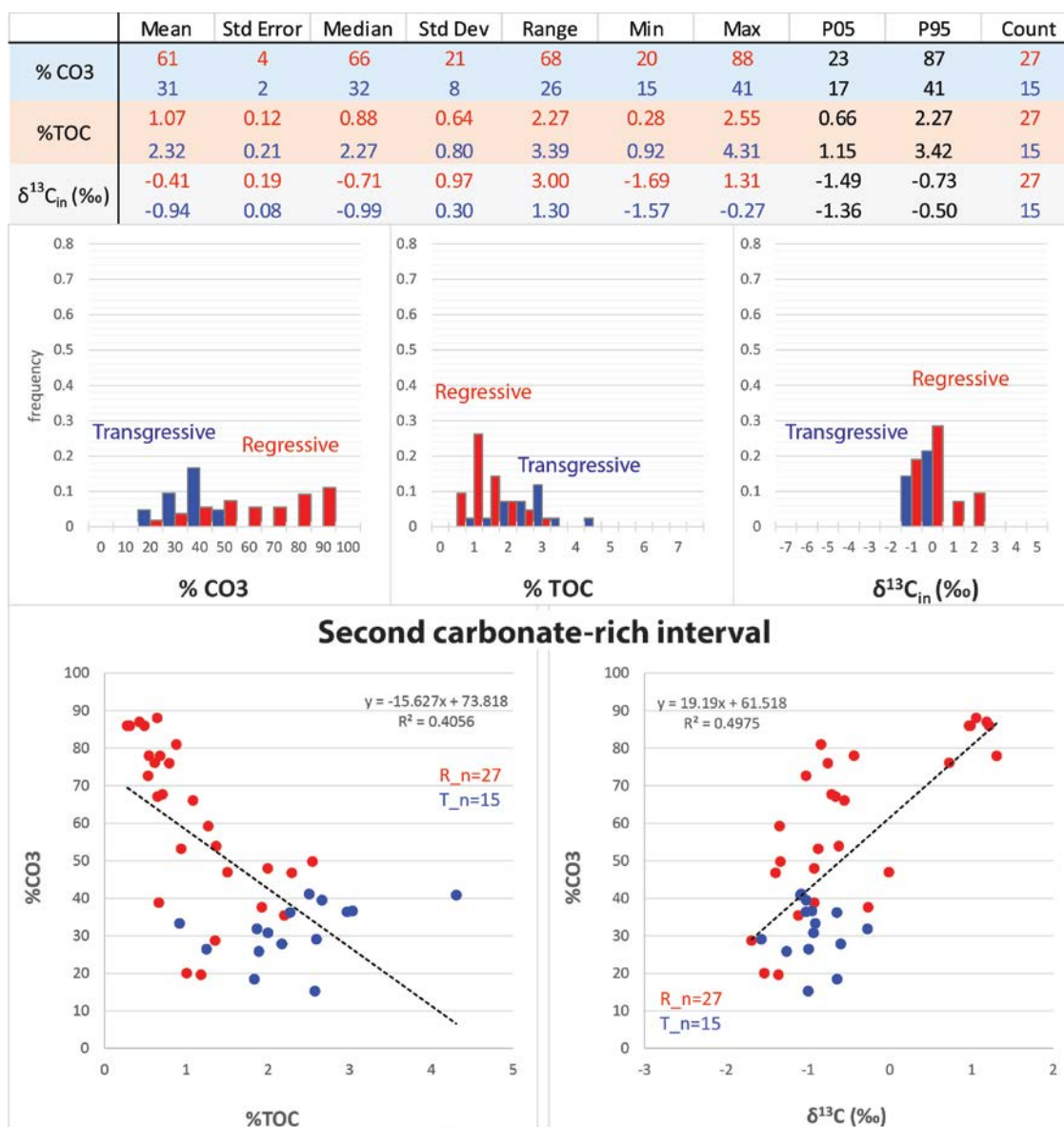


**Figure 4.43. Geochemical signature of cycles -2<sup>nd</sup> carbonate interval, PC.** Samples are grouped according to their position in the cycle: TOP and R samples (see Table 4.2) correspond to the Regressive hemicycle (in red), T and MFS (see Table 4.2) correspond to the Transgressive hemicycle (in blue). See other comments in the text

are clastic-dominated, commonly with stratigraphically-aligned concretions at the cycle tops. This proximal-distal decrease in the thickness and frequency of the carbonate-rich tops is accompanied by an increase in the clastic content of the individual beds, as observed between correlatable units in MDC and VM23 (Figure 4.25). This results in a decrease in

the overall carbonate content of the cycles, more negative  $\delta^{13}\text{C}_{\text{in}}$  values, and relatively higher TOC in more basinal settings.

### Third carbonate-rich interval

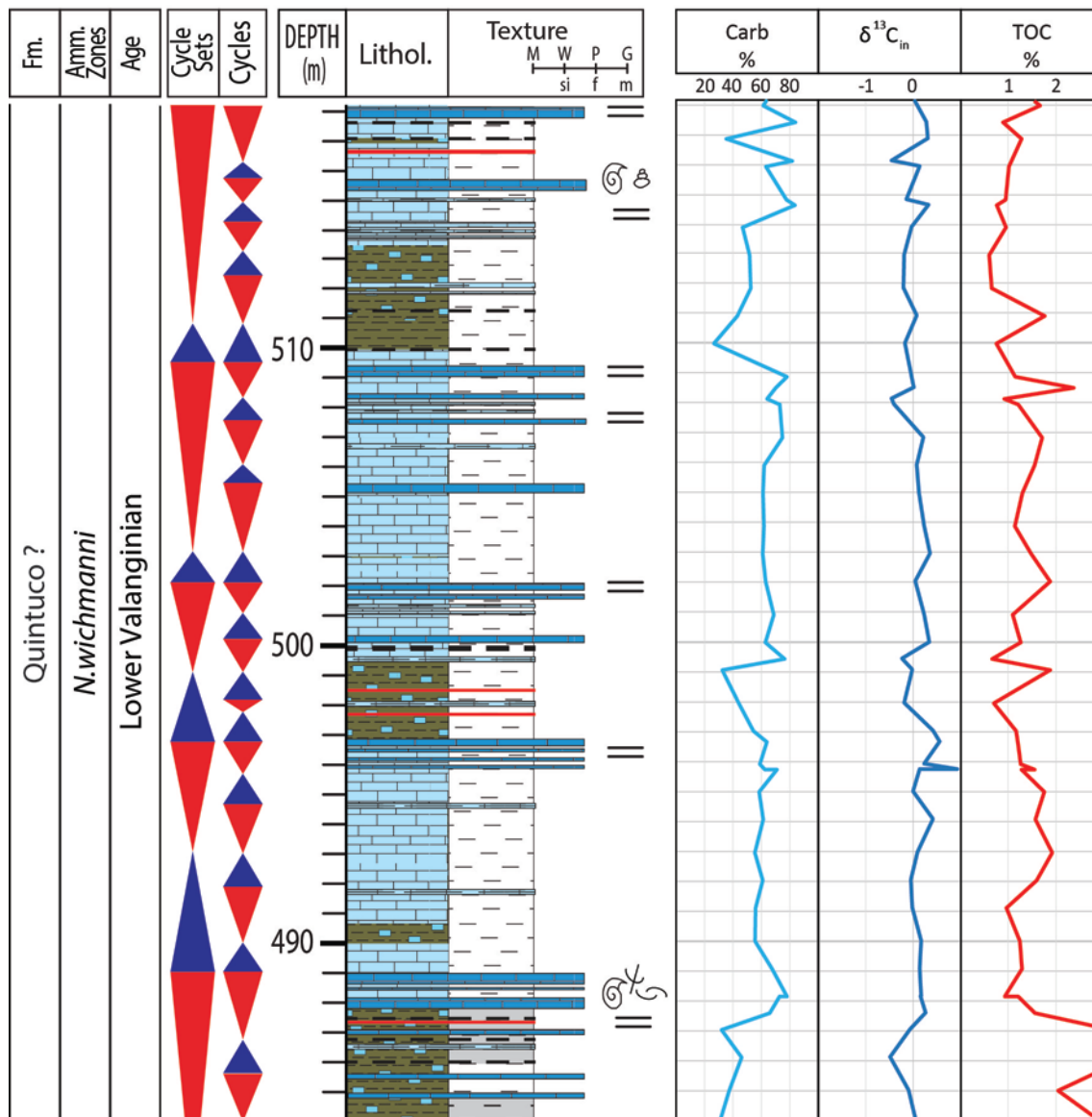


**Figure 4.44.** Cycles of the 3<sup>rd</sup> carbonate-rich interval in PC. Field cycles and cycle sets are shown next to the lithologic section



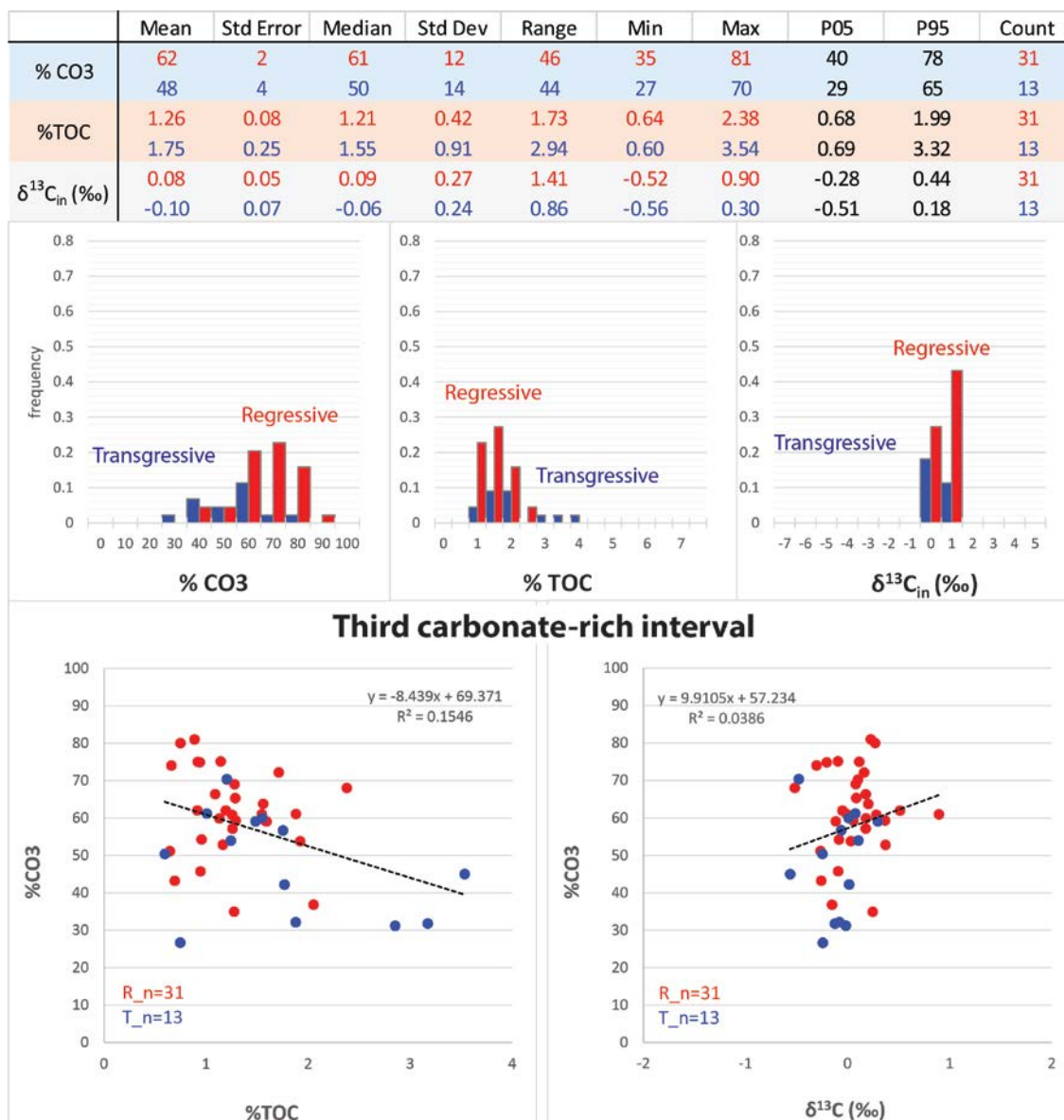


**Figure 4.45. Geochemical signature of cycles -3<sup>rd</sup> carbonate interval, PC.** Samples are grouped according to their position in the cycle: TOP and R samples (see Table 4.2) correspond to the Regressive hemicycle (in red), T and MFS (see Table 4.2) correspond to the Transgressive hemicycle (in blue). See other comments in the text

## Mid-late Tithonian interval

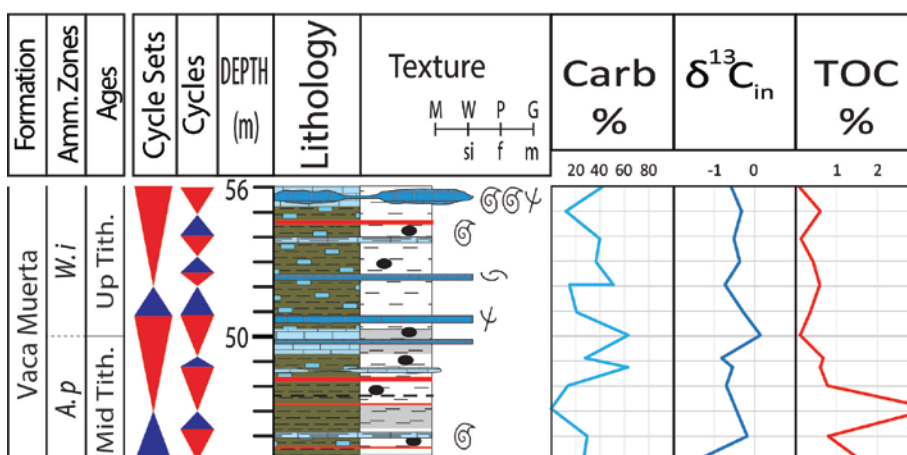


**Figure 4.46.** Cycles of the mid-late Tithonian interval in PC. Field cycles and cycle sets are shown next to the lithologic section

	Mean	Std Error	Median	Std Dev	Range	Min	Max	P05	P95	Count
% CO <sub>3</sub>	47	7	47	20	51	19	70	20	70	9
% TOC	1.38	0.19	1.65	0.57	1.35	0.66	2.01	0.66	1.99	9
$\delta^{13}\text{C}_{\text{in}}$ (‰)	-2.37	0.34	-2.47	1.03	3.54	-3.75	-0.21	-3.59	-0.83	9
	-2.79	0.89	-2.35	1.78	3.90	-5.19	-1.29	-4.88	-1.34	4

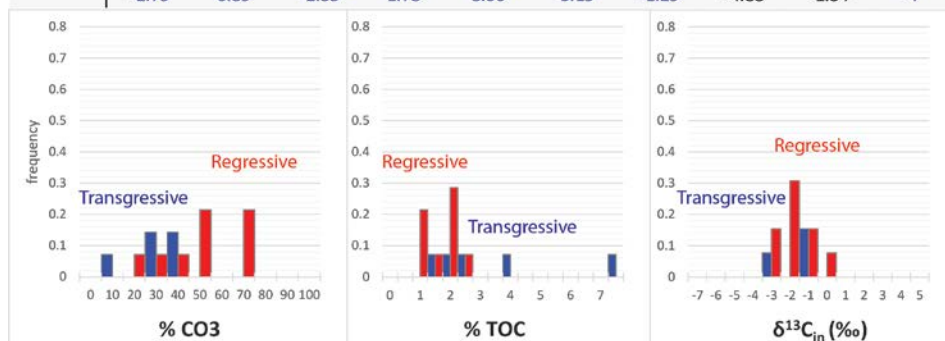
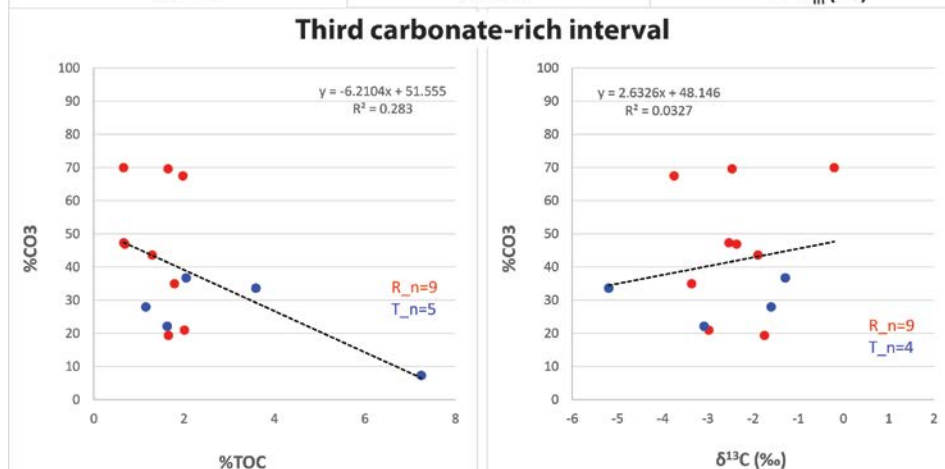


**Figure 4.47.** Geochemical signature of cycles - mid-late Tithonian, PC. Samples are grouped according to their position in the cycle: TOP and R samples (see Table 4.2) correspond to the Regressive hemicycle (in red), T and MFS (see Table 4.2) correspond to the Transgressive hemicycle (in blue). See other comments in the text



### **Sequences in Sierra de la Vaca Muerta**

In the MDC section, where the succession is complete from the contact with the underlying Tordillo Formation, the basic cycles can be nested into two sequences: 1 and 2 (Figure 4.48). The first sequence has a mixed and organic-rich transgressive portion, and a clastic-dominated top, while the second sequence has a clastic and organic-rich transgressive portion, and a carbonate-rich top.

Sequence 1 starts with a carbonate mudstone/wackestone bed with ammonites, above the contact with the eolian cross-bedded sandstones of the Tordillo Formation. The transgressive portion consists mostly of poorly exposed fissile and organic-rich clastic mudstones. The turnaround is placed at approximately 4m above the contact with the Tordillo Formation, where the carbonate content is very low and TOC shows very high values. The regressive portion of the sequence is characterized by an intercalation of siltstones and massive fine sandstones.

Sequence 2 starts approximately 14m above the contact with the Tordillo Formation, with poorly exposed fissile and organic-rich clastic mudstones with thin siltstone layers and mudstone/wackestone beds. The carbonate-rich intercalations are frequently associated with isolated or stratigraphically-aligned concretions. Upwards in the section, the maximum flooding zone is dominated by the organic-rich clastic mudstone facies with isolated concretions and frequent volcanic intercalations. In the regressive portion of this sequence, the carbonate content increases together with an increase in frequency and thickness of the carbonate beds. Towards the top of the sequence, thin fissile carbonate mudstones alternate with thick massive or slightly laminated wackestone/ packstones that characterize the Los Catutos Member.

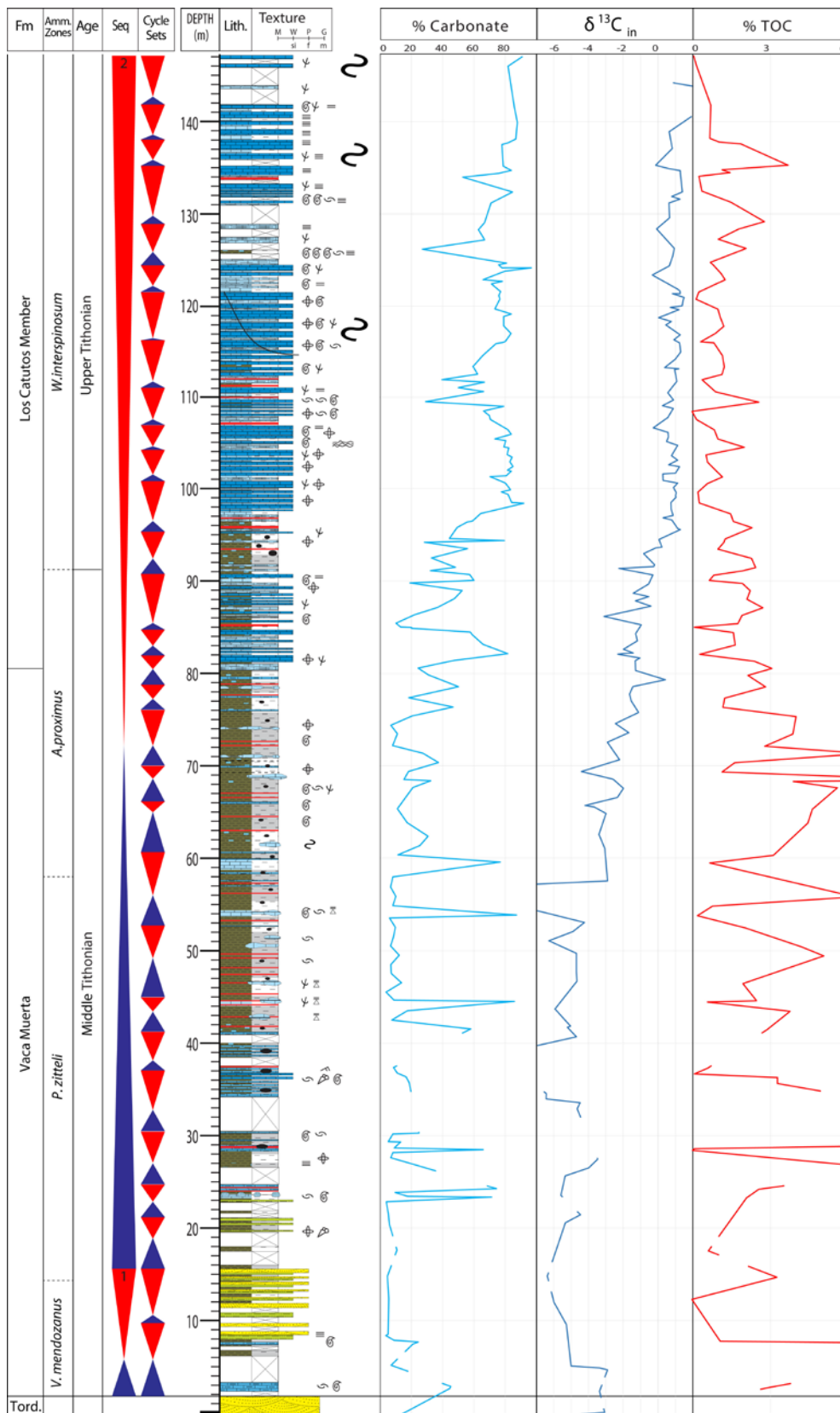


**Figure 4.48. Cycles and sequences in MDC section.** See comments in the text

The carbonate content curve shows a significant increase towards the top of Sequence 2, from < 20% CO<sub>3</sub> in the transgressive portion that ends at 72m to ~80% CO<sub>3</sub> in the carbonate-rich top. The TOC curve displays the opposite behavior, with the higher values (>3% TOC) in the transgressive, maximum flooding and early regressive portions, decreasing to ~1% TOC in the Los Catutos carbonate-rich interval. The δ<sup>13</sup>C curve follows the CO<sub>3</sub> increasing trend, from very negative values (near -5‰ δ<sup>13</sup>C) in the transgressive and maximum flooding surface to positive values (~1 ‰ δ<sup>13</sup>C) in the carbonate-rich top of the sequence 2.

### **Sequences in Puerta Curaco**

In the PC section the basic cycles can be nested into 11 sequences (Figure 4.49). Sequence 1 starts with algal laminites at the contact with Tordillo Formation and passes upwards to skeletal wackestones and packstones. Above, the transgressive portion up to the maximum flooding zone at 8m is dominated by fissile and organic-rich clastic mudstones with isolated small-size concretions or nodules. The regressive portion of the sequence is represented by stratigraphically-aligned concretions.

Sequences 2 to 6 (Figure 4.49) have transgressive portions dominated by cyclic intercalations of clastic and carbonate-rich mudstones. Both have a fissile character, a high organic content, and are commonly accompanied by isolated small-size concretions or nodules. The only carbonate-rich intercalations are stratigraphically-aligned concretions of variable size or thin skeletal wackestone/packstone beds that increase in frequency within the regressive portion. The overall stacking shows an upward increase in the presence of carbonate beds while concretions become less frequent. Ash layers and calcite veins are

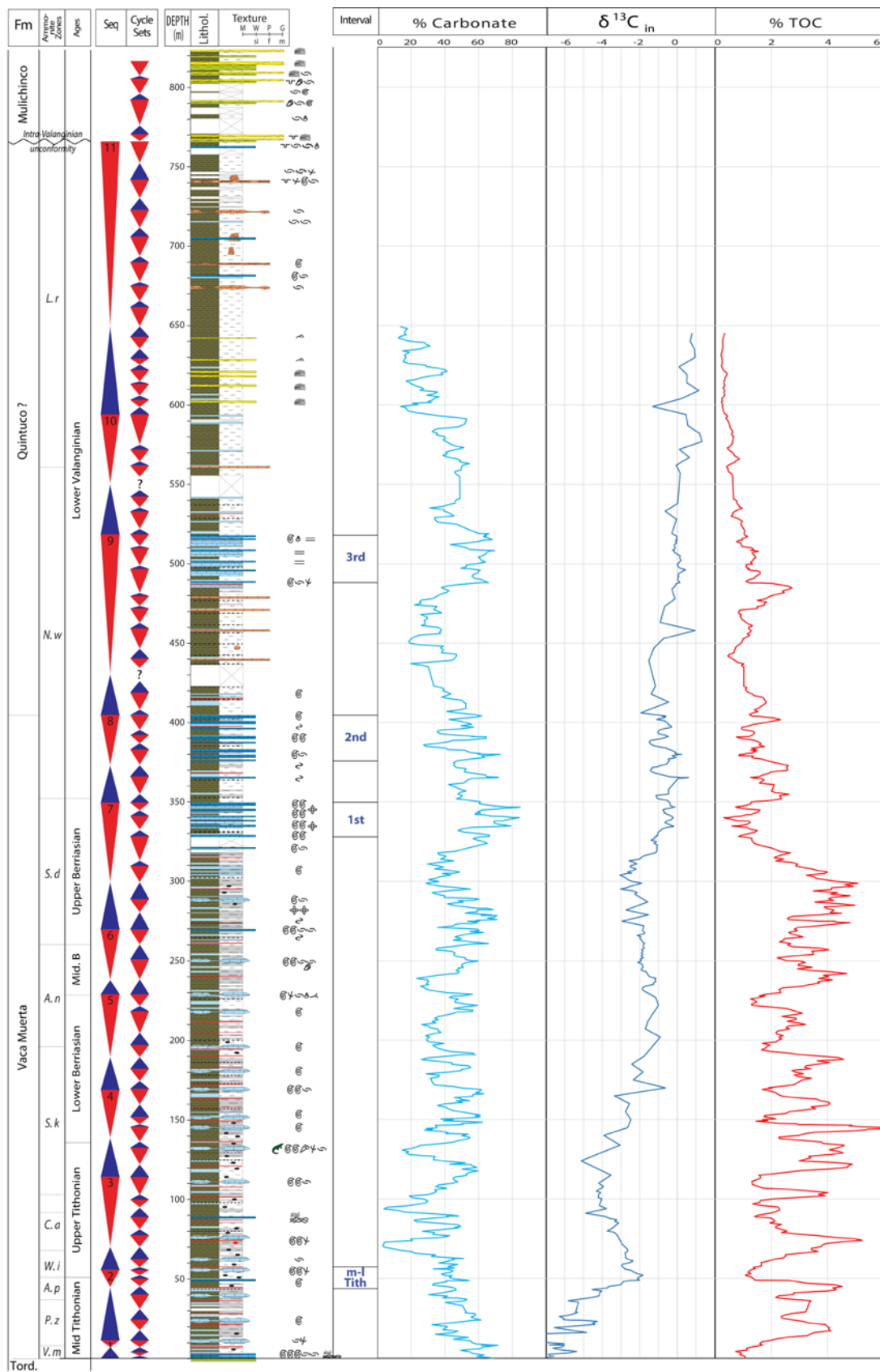


**Figure 4.49. Cycles and sequences in PC section.** See comments in the text

common throughout. The top of sequence 2 at 56m is the top of the Mid-Late Tithonian interval analyzed as part of this study.

Sequences 7 and 8 (Figure 4.49) start with fissile clastic and carbonate mudstones with high organic content, similarly as in the previous sequences. However, the regressive portions show a significant increase in carbonate and skeletal content, and an increase in frequency of carbonate beds. The carbonate-rich top portions of sequences 7 and 8 are the first and second carbonate-rich intervals of this study.

Sequences 9 and 10 (Figure 4.49) have a transgressive portion dominated by fissile clastic and carbonate mudstones with significantly lower organic content than the previous sequences. The turnaround is characterized by the highest clastic content within the fissile background, and intercalations of relatively thick and completely dolomitized beds. Towards the top, the system becomes more carbonate-rich with frequent intercalations of peloidal wackestone/packstones. These characteristics are better developed in sequence 9, whose top at 518m is the top of the third carbonate-rich interval under study.

Sequence 11 starts with a very clastic-rich transgressive portion represented by fissile very clay-rich mudstones intercalated with siltstones and fine-grained sandstones with tractive structures (Figure 4.49). The organic content is very low. The regressive portion is characterized by an increase in carbonate content together with an increase in the frequency of carbonate beds and concretions, sometimes completely dolomitized, containing abundant bivalve infauna.

The geochemical parameters (%CO<sub>3</sub>, %TOC, and  $\delta^{13}\text{C}$ ) show distinctive characteristics along the section (Figure 4.49). Carbonate content shows minimum values near the maximum flooding surfaces of all sequences, and maximum values near the tops.

In the regressive portion of sequences 1 to 6, maximum values are between 40% and 60% CO<sub>3</sub>, and typically correspond to stratigraphically-aligned concretions. In the regressive portion of sequences 7, 8 and 9, maximum values are between 60% and 80% CO<sub>3</sub>, and correspond to highly continuous carbonate beds within the studied carbonate-rich intervals.

The TOC curve shows oscillations between 1.5% and 5% in sequences 1 to 8, and between 0.5% and 1.5% in sequences 9 to 11 (Figure 4.49). Lower TOC values are found at the carbonate-rich tops of cycle sets and sequences, while maximum values tend to coincide with transgressive and maximum flooding zones. This behavior is clearer in the lower and organic-rich sequences. Major intervals of high TOC are observed near the maximum flooding zone of sequences 2, 4 and 7.

The  $\delta^{13}\text{C}$  curve shows at least 3 clear cyclic variations within an overall increasing trend: ~20-130m, 130-300m, and 300-440m (Figure 4.49). Within the 3 identified cycles, the minimum values coincide with the transgressive or maximum flooding zones of sequences 2, 4, 7 and 9, while maximum values are observed at the tops of sequences 2, 5, and 7-8. The minimum values of sequences 2, 4 and 7 (~20m, 130m and 300m) also correspond to major intervals of high TOC.

The  $\delta^{13}\text{C}$  curve (Figure 4.49) starts with very negative values (-7 to -6‰) above the contact with the underlying Tordillo Formation. No clear trends are observed in the first 20m. The first clear cycle starts with very negative values (near -6‰) in the transgressive portion of sequence 2. A pronounced increase in  $\delta^{13}\text{C}$  is observed between 20 and 50m, up to -2‰ at the top of sequence 2. The positive trend is followed by a shift towards more negative values (down to -5‰) near the maximum flooding zone of sequence 4 (~130m). The second cycle starts with a positive trend, up to -1‰ at the top of sequence 5, and is



followed by a minor shift towards more negative values (-3‰) near the maximum flooding zone of sequence 7 (~300m). The third cycle starts with a positive trend, up to values between -1 and 0 at the first carbonate-rich interval. A rather constant composition is observed up to the top of the second carbonate-rich interval (~400m). Above, a slight decrease is observed towards more negative values (-1.5‰) near the maximum flooding zone of sequence 9 (~440m). The third cycle is followed by a shift towards 0‰ that coincide with the third carbonate-rich interval. After the top of sequence 9, trends are less clear and values increase slightly up to 1‰ near the clastic-rich portion at the base of sequence 11.

### **Correlations**

According to the estimated ages, the analyzed sections were correlated among themselves and with sections from other authors. Units I to V of Los Catutos Member in MDC can be correlated to the 5 limestone levels (x+a, x, y, z and w) described by Leanza and Zeiss (1990, 1994) in the Los Catutos type locality (Figure 4.50). Towards the north of the Sierra de la Vaca Muerta, the whole interval and units become thinner, and only the carbonate-rich Units III and IV are interpreted to remain in VM23 (Figure 4.23). The progressive loss of the carbonate-rich character towards more distal settings reaches its maximum expression in PC, where the Los Catutos Mb is not present and instead a clastic-dominated interval is observed (mid-late Tithonian interval in PC).

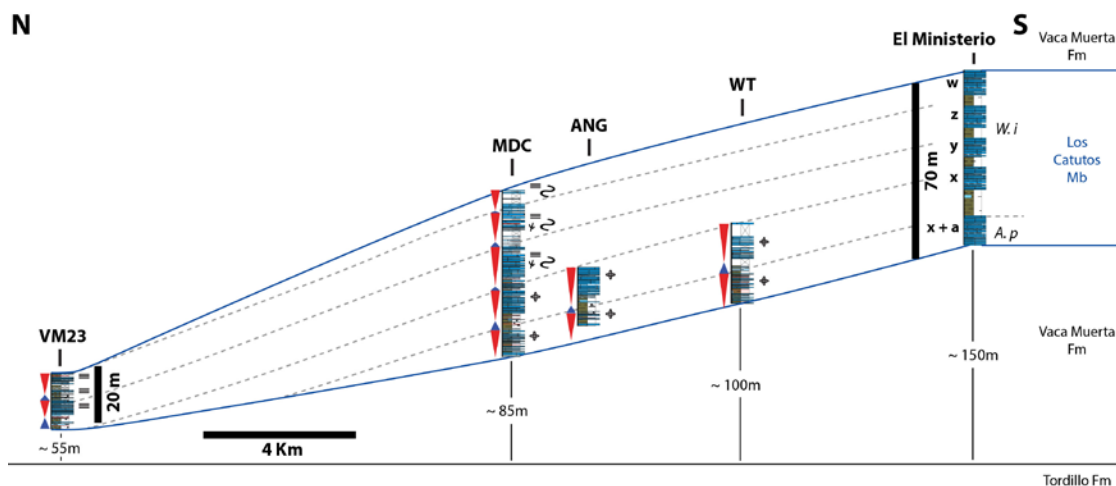


**Figure 4.50. Los Catutos cliniform.** Correlation of the Los Catutos Member from its type locality in El Ministerio quarry (lithological section modified from Leanza and Zeiss 1990, 1994) to the north of the Sierra de la Vaca Muerta. Northward, the thickness of the Los Catutos Member decreases and the height above the underlying Tordillo Formation also decreases

Sequences 1 and 2 in MDC and PC were correlated based not only on their common mid-late Tithonian age and ammonite zones, but also on their similar carbon isotope signature (Figure 4.51). In both sections, the  $\delta^{13}\text{C}$  curve starts with relatively low and negative values in Sequence 1, with the minimum compositions in the transgressive portion of Sequence 2. A clear positive trend accompanies the regressive portion of Sequence 2. The maximum values are reached at the top of this sequence, which corresponds to the carbonate-rich interval of Los Catutos Member in MDC, and the clastic-dominated mid-late Tithonian interval in PC.

Sequences 1 to 8 in PC coincide with the 8 sequences defined by Zeller (2013) in Sierra de la Vaca Muerta. Within this context, the first carbonate-rich interval at the top of sequence 7 in PC, which corresponds to the *S. damesi* zone, can be correlated to a mixed shelf in the south (Zeller, 2013). The second carbonate-rich interval, at the top of sequence 8, corresponds to the *N. wichmanni* zone, and can be correlated to a clastic-dominated shelf

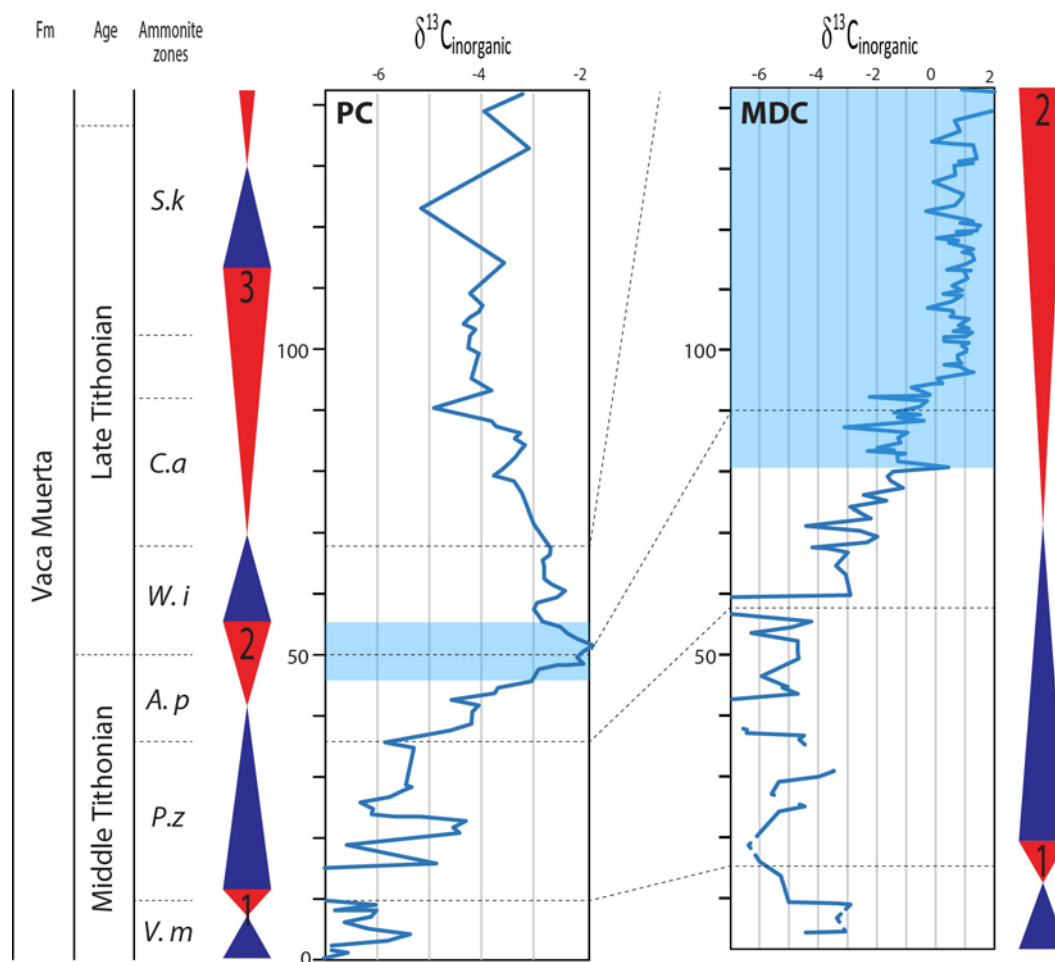


**Figure 4.51. Isotope stratigraphy.** Correlation of Sequences 1 and 2 between PC and MDC. The Los Catutos Member in MDC and its time-equivalent succession in PC are shown in light blue

in the south (Zeller, 2013). The high clastic content of this sequence would be related to the tectonic inversion of the Huincul High (Zeller, 2013), and might account for the high clastic content observed within the fissile intercalations of the second carbonate-rich interval in PC. Sequences 9 to 11 in PC correspond to the younger portions of the prograding system that is filling the basin, hence they were not identified in the relatively proximal location represented by the Sierra de la Vaca Muerta.

## **Chapter 5: Discussion and implications**

The studied carbonate-rich intervals show vertical and lateral variations in different orders of cyclicity. In this chapter, the potential factors that control those variations are discussed to understand the origin and sources of the carbonate material. This analysis is reinforced by the subsequent interpretation of the  $\delta^{13}\text{C}$  signature observed both within the carbonate-rich intervals and along the entire PC reference section. Finally, the implications for hydrocarbon exploration and production are briefly examined.

### **Facies and chemical partitioning in the carbonate-rich intervals**

In all analyzed carbonate-rich intervals, carbonate content increases towards the top of the cycles and units, accompanied with a slight increase in  $\delta^{13}\text{C}$  values, while organic content decreases. This trend is even more pronounced when the geochemical signal is investigated in the transgressive and regressive hemicycles (Figure 5.1). The cross-plot of %CO<sub>3</sub> vs %TOC for all the carbonate intervals shows a clear inverse trend, with more scatter of the values in samples with a lower carbonate content. The cross-plot of %CO<sub>3</sub> vs  $\delta^{13}\text{C}$  shows a direct trend, with less negative or even positive values towards the cycle tops (Figure 5.1). The CO<sub>3</sub>- $\delta^{13}\text{C}$  trend ( $R^2= 0.34$ ) is weaker than the trend observed between carbonate and organic content ( $R^2= 0.46$ ), but was observed consistently in all the studied intervals.

The carbonate transgressive-regressive partitioning within the cycles of the analyzed intervals (Figure 5.1) coincides with the observations of Zeller (2013). In the mixed Vaca Muerta-Quintuco system, carbonates and siliciclastics coexist indicating a constantly active carbonate factory and clastic input but with variable rates. Zeller (2013, 2015)

explained the increase in carbonate content towards the top of the cycles with sea level variations; during highstands, carbonate production increasingly reduces the accommodation space thus inhibiting the along-shelf current system that would be laterally supplying clastic materials. The increased carbonate content is the combined product of increase in the carbonate production and reduction of the admixture of clastics. As a consequence, the siliciclastic content is depth-dependent and varies along the depositional profile. If water depth is too shallow, frictional forces prevent the development of currents that need certain depth to develop an effective strength.

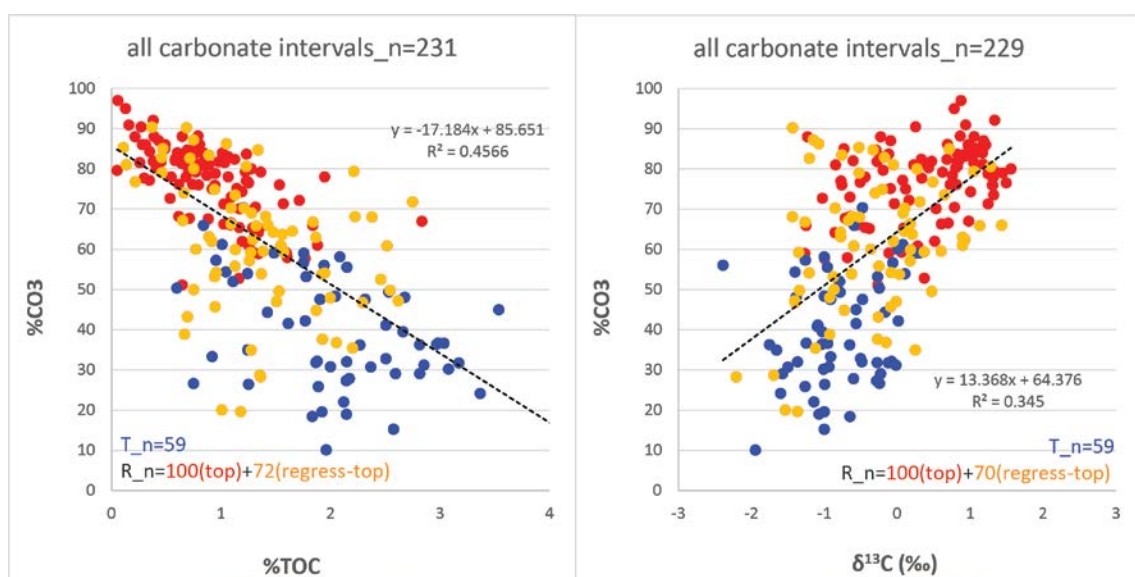


**Figure 5.1. %CO<sub>3</sub> plotted vs %TOC and δ<sup>13</sup>C<sub>in</sub> for the carbonate-rich intervals.** A clear trend of increasing %CO<sub>3</sub> and δ<sup>13</sup>C can be observed towards the top of the cycles. The TOC shows the opposite behavior, decreasing towards the top of the cycles. Samples are colored relative to their position within the cycle: samples from transgressive hemicycles (T) are in blue, while those from regressive hemicycles (R) are shown in yellow (regressive part of the cycle, excluding top) and red (only tops of the cycles)

### Lateral variability of the carbonate-rich intervals

The most significant carbonate-rich interval within the Vaca Muerta Formation, in terms of thickness and areal extension, is the Los Catutos Member in the Sierra de la Vaca

Muerta. In its type locality, this unit is thought to have been deposited in approximately 30 to 50m water-depths with relatively quiet bottom conditions that allowed the preservation of a variety of faunas (Leanza and Zeiss, 1990). The faunal content with ammonites, radiolarians and nannoplankton point to open marine conditions (Leanza and Zeiss 1990, Scasso et al 2005, among others). Poorly oxygenated bottoms were suggested by Leanza and Zeiss (1994) and others, because of the preservation of organic matter in certain places.

Within the Los Catutos Member in MDC and VM23, differences in thickness and facies assemblage within the cycles, cycle sets and sequences document a proximal-distal trend. MDC is the more proximal position on the slope near the shelf break or the break to a distally steepening of the ramp, as indicated by the presence of slump scars and channelized features (Figure 5.2-A). The thinner VM23 section, with a decrease in the frequency and thickness of the carbonate beds and a relative increase in the proportion of clastic components, represents a more distal setting (Figure 5.2-B). In Puerta Curaco, 150km north from the Sierra de la Vaca Muerta, the time-equivalent succession of the Los Catutos Member (the Mid-Late Tithonian interval) is mostly a clastic-rich succession (Figure 5.2-C). Here, cycles are dominated by the organic-rich and clastic facies frequently associated with concretions, and only punctuated by thin carbonate beds. This shows that the carbonate deposit pinches out and does not reach the basin center.

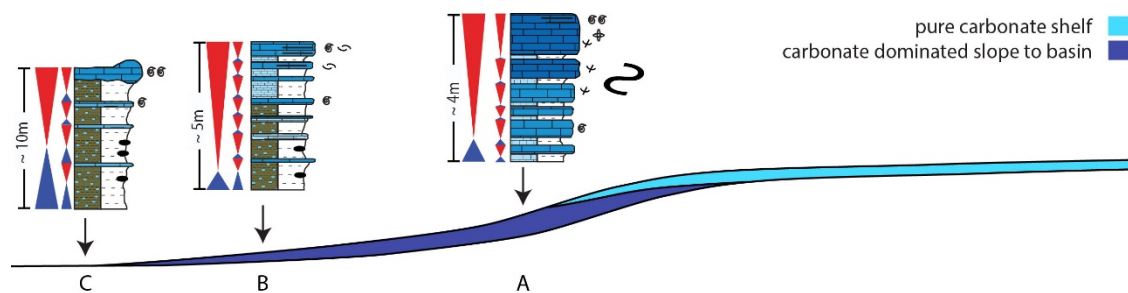


**Figure 5.2. Proximal-distal variations in cycles of the studied intervals.**  
Conceptual cycles and cycle sets are shown for different positions along a clinoform

Carbonate-rich intervals are, however, identified in PC section at a higher position in the succession. Though younger, these intervals are very similar to Los Catutos facies in VM23 (Figure 5.2-B).

### **The source issue**

As observed by Schlager et al. (1994) and other authors, modern carbonate platforms shed significant amounts of carbonate sediment during highstand periods as opposed to what is observed in clastic systems (Vail et al., 1977). Schlager et al. (1994) suggest two main reasons for highstand shedding: the first is the increase in the productivity area of the platforms when flooded, and the second is the extensive lithification that takes place during lowstands making carbonate platforms resistant to mechanical erosion.

The exported sediment mixes with pelagic carbonate producing a deposit called periplatform ooze (Schlager and James, 1978). The periplatform deposits are characterized by a mixture of shallow-water and pelagic components in its coarse-grain fraction, and probably also in its mud fraction since whole units and individual beds thin away from the platform (Wilson, 1969). Its highstand origin is supported by the presence of skeletal fragments that are generated on the platform in a context of high productivity. In contrast, lowstand periods would be dominated by plankton grains and a clastic sedimentation due to the increased erosion of the hinterland.

The main carbonate-rich interval studied, the Los Catutos Member, shows the following characteristics analogous to a periplatform ooze (Figure 5.3):

- A significant decrease in thickness of beds and intervals between proximal and distal positions, accompanied by an overall decrease in carbonate content. The variations

in thickness and carbonate content between MDC and VM23 indicate that fine lime mud is transported into the basin from an active shelf/ramp. If the mud were only produced by pelagic organisms, the thickness of the Los Catutos deposit and their carbonate content would be similar in MDC and VM23.

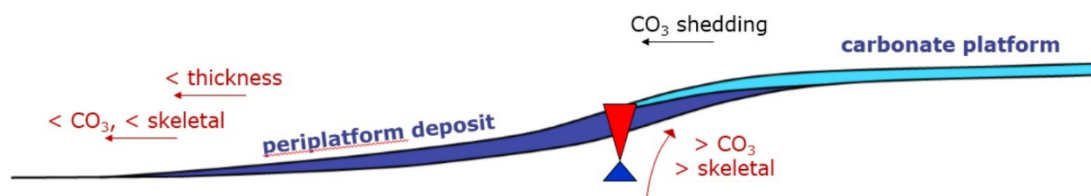


**Figure 5.3. Periplatform deposits.** The conceptual scheme shows the proximal-distal variation of the analyzed parameters. Platform shedding produces a wedge-shaped periplatform deposit with a basinward decrease in carbonate content. The process of mud export is enhanced during highstands, due to the increase in productivity, resulting in carbonate and skeletal-rich tops of cycles

- An increase in carbonate content towards the top of the cycles points towards a highstand origin of this interval. The increase in carbonate content within the Los Catutos cycles and cycle sets is not just related to an increase in diagenesis and cementation due to low sedimentation rate, but also to an increase in the skeletal content. The higher skeletal content, and the increase in frequency and thickness of carbonate beds towards the top of the cycles could be related to either one or a combination of the following factors: a higher productivity in the shelf, a decrease in the clastic input, or a change in the deep-current system, which are all related to highstand conditions.

These characteristics of the Los Catutos Member suggest a periplatform origin for this interval. During a highstand phase in the Mid-Late Tithonian, increased productivity on the shelf would have caused significant shedding of carbonate mud into the basin. The exported mud would have been accumulated as a wedge-shaped periplatform deposit thinning and decreasing its carbonate content from south to north as observed between



MDC and VM23. Based on the similarities between Los Catutos in VM23 and younger carbonate-rich intervals in PC, it is also possible to interpret a distal periplatform position for these intervals.

The provided evidences support the hypothesis that the studied carbonate-rich basinal intervals were sourced from carbonate-rich shelves during sea level highstands. The question of which specific platform is shedding the mud that constitutes each of these carbonate-rich intervals remains.

### **The platform sources**

In the case of the Los Catutos Member, with its wedge-shape thinning towards the north, the source of the carbonate mud must be located south of the Los Catutos area. During the Mid-Late Tithonian, a carbonate platform developed in the area of Picún Leufú, 40km south from the Los Catutos deposits.

The Picún Leufú carbonate platform forms a steep edged exposure along the Picún Leufú Anticline (Figure 2.2). It was first described by Leanza (1973), as part of the Picún Leufú Formation, as a 15m-thick interval of yellowish-white oolitic limestones with abundant bivalves. Zeller (2013) described it as approximately 20m of continuous almost exclusively carbonate strata (Figure 5.4). This pure carbonate interval consists mostly of packstones to floatstones from a shallow tidal environment, in some cases heavily bioturbated with a nodular appearance (Spalletti et al 2000, Zeller 2013). Zeller (2013) observed internal subhorizontal stratification and bed thinning towards the north, indicating a low-angle progradation pattern. The top of the interval was interpreted as a

sequence boundary with subaerial exposure, which turned into a flooding surface and hardground during the subsequent transgression (Zeller 2013).

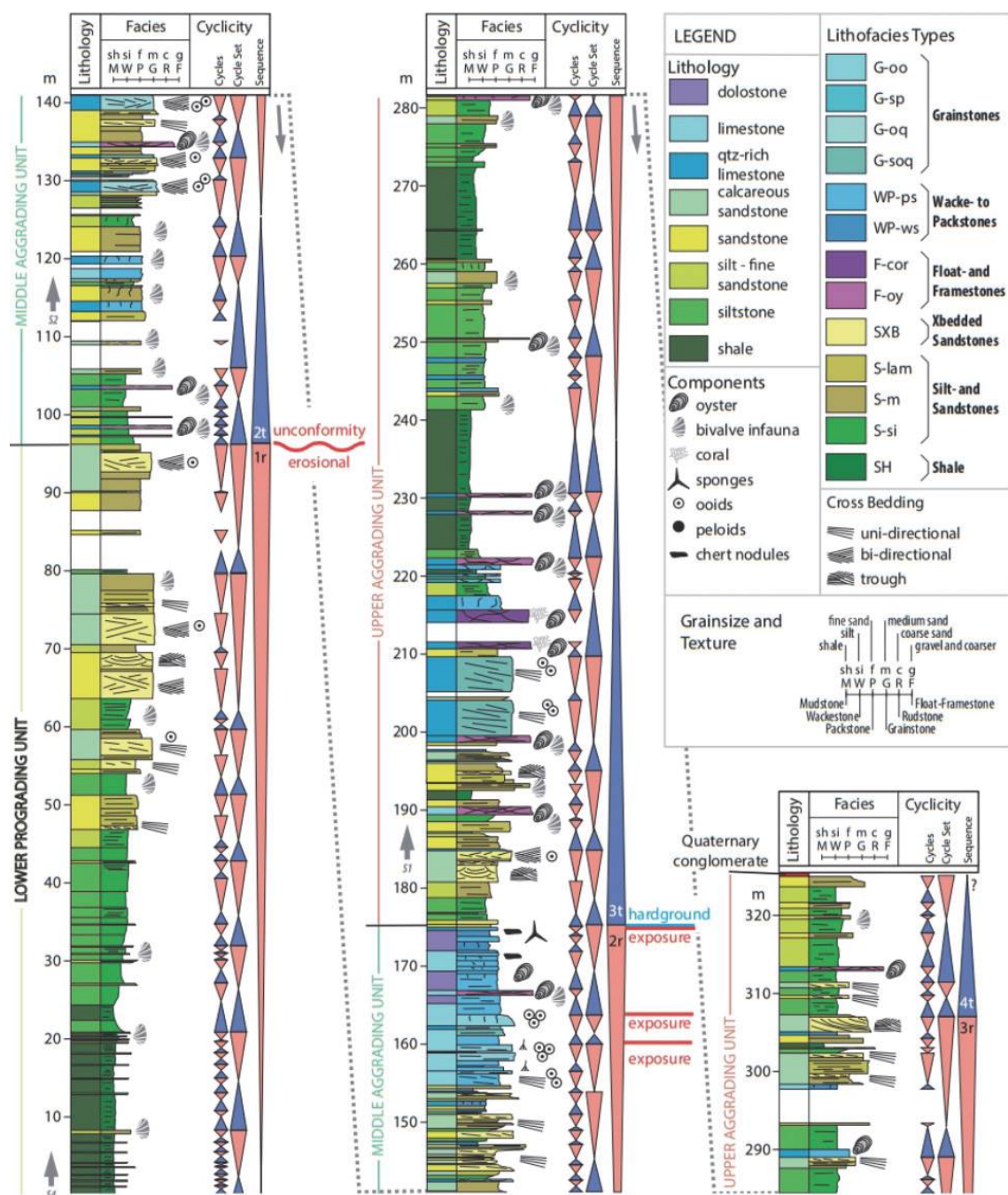


**Figure 5.4. Composite section from Picún Leufú Anticline (Zeller, 2013).** The pure carbonate interval interpreted as the Picún Leufú carbonate shelf is located between 155 and 175m.

Zeller (2013) considered that the 20m of pure platform carbonates from the Picún Leufú Formation must have been related to specific environmental conditions that isolated the platform from the siliciclastic input by one of two mechanisms: either long-lived highstand settings, in which subsidence and carbonate production are in equilibrium, preventing the development of siliciclastic input by currents, or a sudden climatic change to more arid conditions that limited the weathering and erosion in the hinterland. This platform generated in exceptional conditions of almost no clastic input and high productivity would have exported a significant amount of carbonate mud into periplatform positions. The resultant deposit would have had a wedge-shape, thinning towards the north away from the source.

Outcrops between the Picún Leufú anticline and the Sierra de la Vaca Muerta are not continuous and it is not possible to observe the transition from the shelf to its genetically-related periplatform deposit. In the Los Catutos area, Kietzmann et al (2014) described the presence of oolitic grainstones in the upper portion of the Los Catutos Member, which are the highest-energy facies described within this interval so far. These shallow water, high energy facies could be the missing link between the Picún Leufú and the Sierra de la Vaca Muerta areas, representing the progradation of the carbonate platform facies into the basin.

Another piece of evidence in favor of a genetic link between the Picún Leufú Formation and the Los Catutos Member is the similar age of both successions. No precise age for this platform deposit was available in the literature, yet it can be constrained by references to underlying or overlying deposits. The base of the Picún Leufú Formation was interpreted as to be contained within the *A. proximus* zone (Leanza 1973, Leanza and Hugo 1977) or the *W. internispinosum* zone (Leanza 1993). Deposits above the pure-carbonate interval

were interpreted to be within the *C. alternans* zone (Leanza 1973, Leanza and Hugo 1977, Leanza 1993). Hence, the age of the Picún Leufú carbonate platform would be constrained between the *A. proximus* or *W. internispinosum* zones and the *C. alternans* zone. This time-interval is close to the age of the Los Catutos Member, comprising the late *A. proximus* zone and most of the *W. internispinosum* zone (Leanza and Zeiss 1990, 1994).

Based on the analyzed evidences, the Picún Leufú carbonate platform is interpreted as the source of the Los Catutos periplatform deposits (Figure 5.5). The stratigraphic scheme of Zeller (2013) (Figure 1.2) in which the Los Catutos Member was attached to the Picún Leufú Formation is preferred over the scheme of Leanza et al (2011). In the latter, a pelagic origin seems to be suggested by placing the Los Catutos Member as an isolated wedge between slope to basinal deposits of the Vaca Muerta Formation.

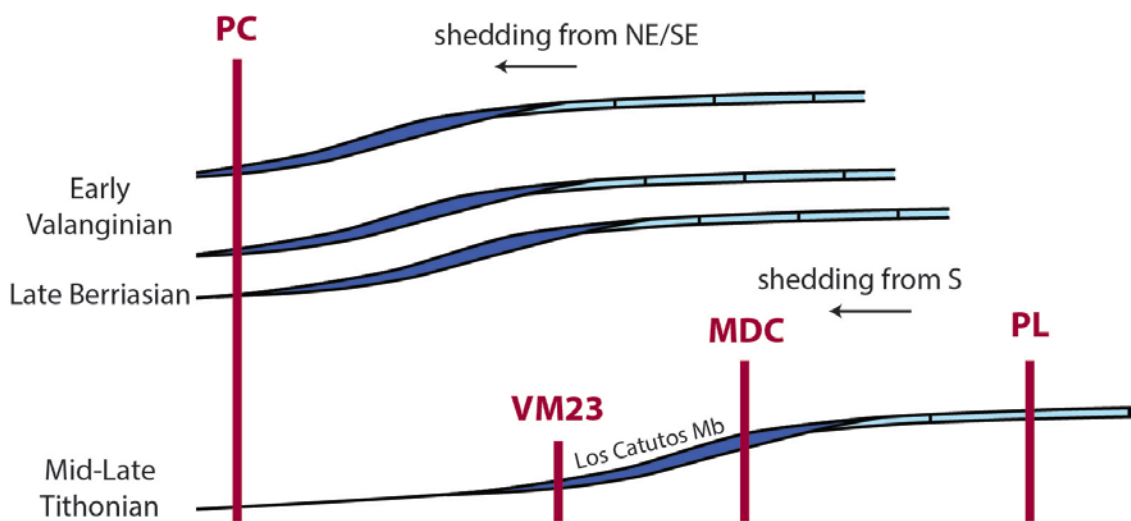


**Figure 5.5. Proposed origin of the carbonate-rich intervals.** The studied intervals interpreted as periplatform deposits are shown in dark blue. The lime mud would be shed from a carbonate platform (pale blue) during highstands.

In the case of the younger carbonate-rich intervals, whose geometries were not analyzed in this work, the source of the carbonate mud must be located in a direction other than the south. The Sierra de la Vaca Muerta Late Berriasian-Early Valanginian succession

is mostly clastic-rich (Zeller 2013) and no carbonate shelves have been described there. However, deposits similar to the Picún Leufú Formation, though younger, have been described in the subsurface Quintuco-Loma Montosa Formation (Uliana and Legarreta 1993, Carozzi et al. 1993, among others). This suggests that the younger carbonate-rich intervals were probably sourced from the east.

### **Carbon isotope ratios**

Carbon isotope ratios measured on time-equivalent mudstone/wackestone samples from Picún Leufú, the Los Catutos Member in MDC and VM23, and the mid-late Tithonian interval in PC show a clear proximal-distal trend (Figure 5.6). The most positive values correspond to Picún Leufú pure-carbonate shelf samples, with a P<sub>5</sub>-P<sub>95</sub> range from +1.11‰ to +2.59‰, and a mean value of +1.95‰ (see data and statistics in Appendix B). In a near-slope position (MDC), the P<sub>5</sub>-P<sub>95</sub> range falls between -1.46‰ and +1.4‰ (see data and statistics in Chapter 4), with the negative values being influenced by samples from unit I (mean -1.24‰), while values slightly above 0‰ are characteristic of the upper units (mean +0.72‰). Values in a distal periplatform position (VM23) are similar to those of unit I in MDC, ranging from -1.75‰ to -0.23‰ with a mean of -1.25‰. The most negative isotopic compositions were measured on samples of the mid-late Tithonian interval in the most distal position (PC). Here the P<sub>5</sub>-P<sub>95</sub> values range between -4.33‰ and -0.86‰, with a mean of -2.5‰.

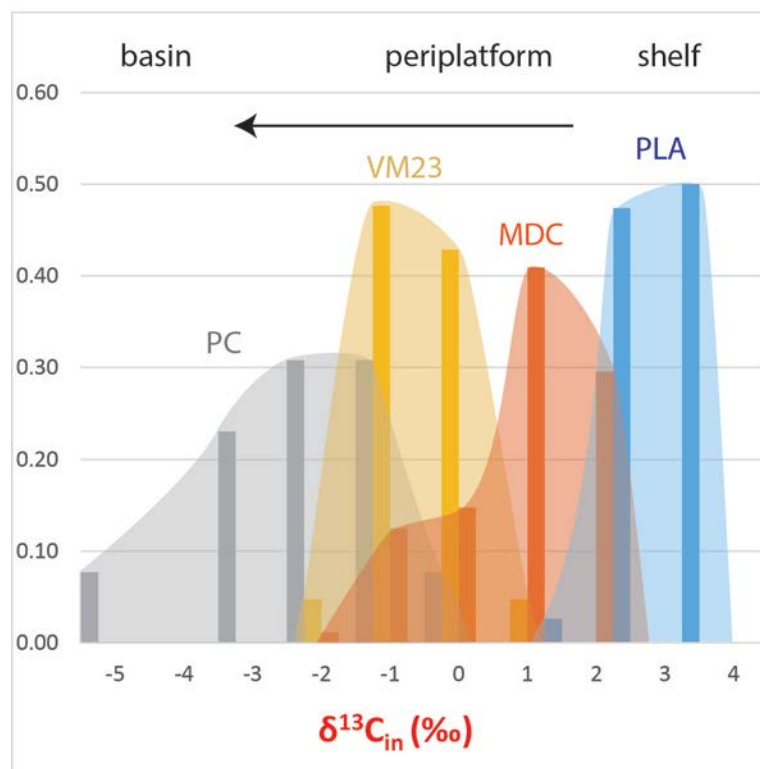


**Figure 5.6. Proximal-distal isotope trend.** The  $\delta^{13}\text{C}$  values are positive in samples from the Picún Leufú carbonate platform (blue), become less positive in samples from the upper units of Los Catutos in MDC (red), are slightly negative in samples of Los Catutos in VM23 (yellow), and increasingly negative in samples from the mid-late Tithonian interval in PC (grey)

The gradual decrease in the  $\delta^{13}\text{C}$  values from the shelf towards more basinal positions can be explained by the mixing of different carbon sources, and/or by diagenetic alteration. In the first case, the proximal-distal trend could be reflecting the mixture of  $\delta^{13}\text{C}$ -rich platform sediments and pelagic material, analogously to what was observed by Swart and Eberli (2005) in modern sediments on the western margin of the Great Bahama Bank (GBB). These authors attributed the isotope enrichment of the platform sediments to a combination of dominantly aragonite composition of the carbonates, and high level of photosynthesis in the shallow waters of GBB. However, the mid-late Tithonian corresponds to the beginning of the Calcite II period (e.g. Hardie 1996, Stanley and Hardie 1998) for which an  $m\text{Mg}/\text{Ca} \sim 1.5$  is estimated (Hardie 1996, Horita et al 2002), and calcite,

not aragonite, would be the dominant carbonate produced. Additionally, Picún Leufú is described as a heterozoan-dominated fabric (Zeller 2013) in which photosynthetic organisms are not expected to play such an important role as they do in GBB.

Furthermore, most of the  $\delta^{13}\text{C}$  compositions of Tithonian sea waters mentioned in the literature range between 0 and +2 (e.g. Weissert and Channel 1989, Weissert and Mohr 1996, Veizer et al 1999, Follmi et al 2006, Zak et al 2011). These values include both bulk and belemnite measurements, and come either from pelagic, periplatform or platform deposits in the Tethyan and Boreal realms. The relatively narrow range represented by those measurements coincide with the  $\delta^{13}\text{C}$  signature of the Picún Leufú carbonate platform samples (mean +1.95‰) and with most of the data from the proximal periplatform deposits of Los Catutos in MDC and in Los Catutos area (Scasso et al 2002, 2005). However, most of the data from distal periplatform (VM23) and basinal (mid-late Tithonian in PC) deposits show consistent values between 0‰ and -4.33‰, increasingly negative towards more distal settings. These negative values deviate from sea water isotopic composition observed in Tithonian samples in other parts of the world.

An alternative explanation for the isotopically negative values is the diagenetic alteration produced in a context of dysoxic bottom waters and high productivity of the surface waters (Figure 5.7). In a marine basin, biogenic particles produced near the surface sink through the water column and undergo remineralization, either during sinking or when reaching the sea bottom. In both cases, and whether the degradation of the organic matter takes place in the presence of oxygen (1) or in anoxic conditions (2), the result will be isotopically negative alkalinity. The  $\text{HCO}_3^-$  thus generated will combine with  $\text{Ca}^{2+}$  from the sea water to produce isotopically negative carbonates. This process take place normally

in modern oceans and is enhanced by the stratification of the waters (e.g. Gruszczynski 1998, Saltzman and Thomas 2012).

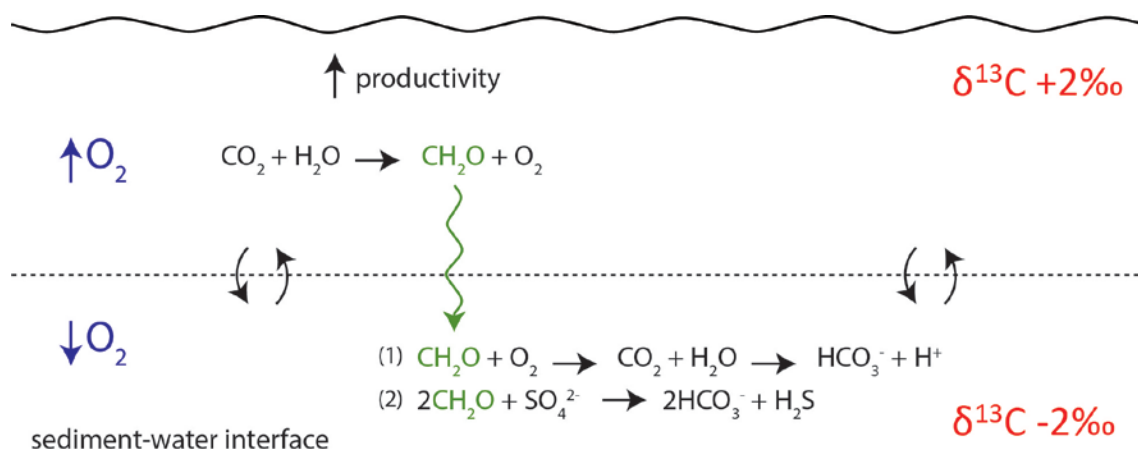


**Figure 5.7. Model of stratified waters.** Proposed explanation for the increasingly-negative values along a proximal-distal trend, and increasingly positive values towards the top of the cycles. Organic matter (in green) sinks through the water column and is degraded in the presence of oxygen (1) or sulfate (2), resulting in poorly oxygenated bottom waters with more negative carbon isotope signatures. The mix with isotopically-positive carbonate materials exported from the shelf results in variable compositions, depending on the relative distance to the carbonate source. The enhancement of the shedding process during highstands results in more positive  $\delta^{13}\text{C}$  values towards the top of the cycles

The driving force behind the high production of organic matter is the high productivity of the waters, which in turn depends on the availability of nutrients (e.g. Saltzman and Thomas 2012). In the case of the Tithonian deposits of the Neuquén Basin, upwelling has been proposed as the main supplier of nutrients (Gasparini et al 1997). However,  $\delta^{15}\text{N}$  compositions (measured as part of the group initiative that includes the present work) show values between  $-2.35\text{‰}$  and  $0.41\text{‰}$  (see statistics in Appendix D) that are far from the expected  $+7\text{‰}$  or higher estimated for upwelling zones (Giraud et al 2003, Emeis et al 2009, among others). Instead, our values resemble more what is expected for nutrient input from dust ( $\sim 0\text{‰}$ ; Swart, *personal communication*). Whatever the reason behind the high supply of nutrients in the Vaca Muerta Formation, many authors have provided evidences of a



stratified water column with anoxic or dysoxic bottom waters and high productivity in surface waters: high organic matter content, presence of phosphate concentrations, dominance of planktonic/nektonic organisms and relative absence of benthic organisms, abundance of well-preserved marine reptile skeletons, and low bioturbation (Leanza 1973, Uliana and Legarreta 1993, Gasparini et al 1997).

In a context of stratified waters, a depth-related variation in the anoxic/suboxic conditions might account for the increasingly negative values observed along a proximal-distal trend. Additionally, the introduction of platform allochems with isotopically positive values, more abundant in more proximal areas, might drive the resultant isotopic signal towards more positive values, increasing the vertical gradient (Saltzman and Thomas 2012). Hence, this process will also result in a mixing trend, but instead of taking place between platform and pelagic compositions as in GBB, it will be produced between normal isotopic values from shallow waters and diagenetically altered compositions from deeper water settings.

The  $\delta^{13}\text{C}$  variations observed within the cycles (more negative compositions in transgressive hemicycles and less negative or positive in regressive hemicycles) can also be explained by the mixing between normal and diagenetically-altered isotopic compositions. The increased platform productivity and export of carbonate materials during sea level highstands may account not only for the increased carbonate and skeletal content towards the top of the cycles, but also for the more positive isotopic values. Additionally, if a periodic mixing between water layers occurs, it may drive the system from dominantly-anoxic during transgressions (as evidenced by the higher organic content

and lack of bioturbation in transgressive hemicycles) to more oxygen-rich during regressions (as evidenced by the frequent bioturbation observed at the cycle tops).

A similar cyclic behavior is observed at a lower order (Figure 5.8). The  $\delta^{13}\text{C}$  curve from PC section shows at least 3 clear cyclic variations within an overall positive trend (see detailed description in Chapter 4 – Sequence Stratigraphy). Within the 3 cycles, the turning points from negative to positive trends coincide with transgressive or maximum flooding zones at sequences 2, 4, 7 and 9, and in some cases (sequences 2, 4 and 7) also with major TOC accumulations and highest GR values (Figure 5.8). Additionally, the minimum near the flooding zone of sequence 4 coincide with the estimated position of the Tithonian-Berriasian boundary. The turning points from positive to negative trends coincide with the tops of sequences 2, 5 and 8.

This cyclic behavior, characterized by the most negative values near maximum flooding zones and less negative or positive values at the top of the sequences, is consistent with the higher-order cycle observations presented in previous paragraphs, but contradicts those interpretations that associate maximum isotopic values to global periods of organic matter sequestration (e.g. Arthur et al 1987, Fisher et al 2005, Jenkyns 2010, Gertsch et al 2010, Morettini et al 2015). However, examples of high deposition and preservation of organic matter displaying negative shifts in  $\delta^{13}\text{C}$  values are also mentioned in the literature (Menegatti et al 1998, Jenkyns 2003).

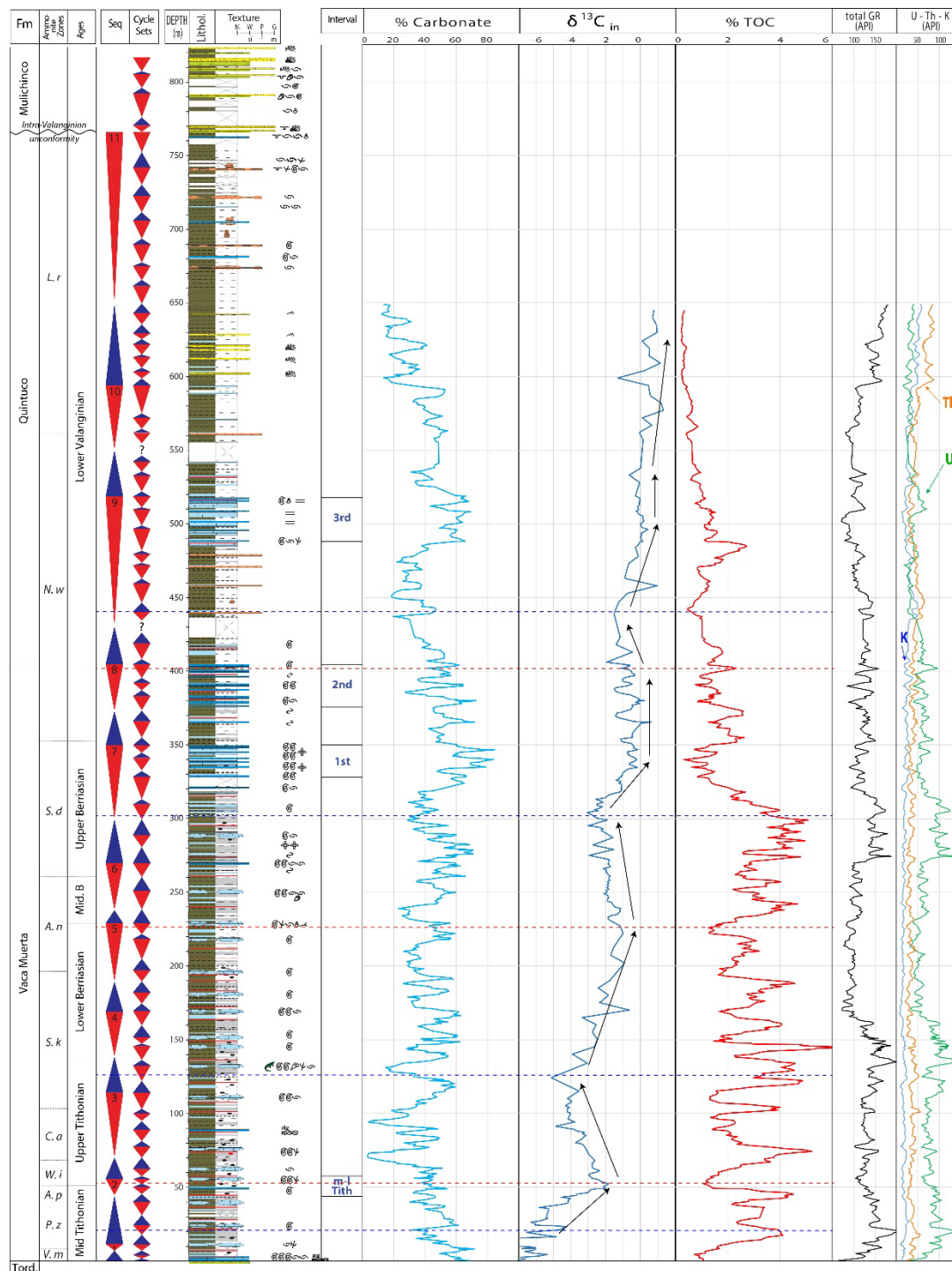


**Figure 5.8.  $\delta^{13}C$  variations within the Tithonian-Valanginian succession in PC.** At least 3 clear cyclic variations are observed, limited by blue dotted lines. The blue lines represent the turning points from negative to positive trends, and coincide with transgressive or maximum flooding zones (sequences 2, 4, 7 and 9). In the case of the first three, they also correspond to major high TOC and high GR intervals. The red dotted lines represent the turning points from positive to negative trends, and coincide with the top of sequences 2, 5 and 8

The overall positive trend observed in PC, from -6‰ to 1‰, also differs from the relatively constant or slightly negative trends, between +2‰ and +1‰, described by several authors for the Tithonian-Valanginian interval in the Tethyan realm (e.g. Weissert and Channel 1989, Lini et al 1992, Follmi et al 2006). Nevertheless, most of the cited works come from relatively thin and condensed sections, and consist of relatively limited data sets. In contrast, the overall high sedimentation rates within Vaca Muerta Formation provide a detailed record of measurements that supports the present interpretations. The analyzed  $\delta^{13}\text{C}$  curve from PC covers 650m of continuous sedimentary succession from middle and late Tithonian age (and probably also from part of the early Tithonian, according with ammonite zonation) to earliest Valanginian. Also, the 1m or 5m –sampling in PC section allows a high density of data points (371) to statistically support the observations.

### **Implications for hydrocarbon exploration and production**

Due to their inherent brittleness, carbonate-rich intervals can be preferred locations for hydraulic fracturing in unconventional reservoirs (e.g. Rickman et al 2008, Zehnder 2007). Hence, understanding their lateral facies variability and stratigraphic distribution is important to determine preferred fracking locations in the subsurface. However, if carbonate-rich intervals exceed a certain thickness, they might act as a barrier to fracture propagation.

The characterization of the studied carbonate-rich intervals provides insight into the thickness variability of individual limestone beds, the amount and organic-richness of intercalated mudstones, and the thickness of entire intervals. In proximal positions like the

Los Catutos in MDC, where the whole interval is more than 60m-thick, the carbonate beds can reach thickness as in excess of 1m and the intercalated mudstones are generally thin. Here, it is very likely that the carbonate-rich intervals act as fracking barriers. Also, the low porosities (1-2%) measured in this proximal position rule these carbonates out as conventional reservoirs.

In the case of the Los Catutos in VM23 and the younger carbonate-rich intervals in PC, the entire interval is approximately 20-30m thick. Carbonate beds are 0.2 to 0.3m-thick, and the intercalated organic-rich mudstones range between 1 to 2m in thickness. The organic content in the mudstone intercalations varies between 1 and 4%TOC. The higher values are observed in the second carbonate-rich interval in PC (375-404m). Porosities in these intervals vary between 1 and 13%, with average values for the first and second carbonate-rich intervals in PC near 5%, and near 9% for the third carbonate-rich interval. Based on these characteristics, the distal portion of the periplatform carbonate deposits might be considered to be potential sweet spots in unconventional exploration and production.

## **Chapter 6: Conclusions**

The study was the documentation of facial heterogeneities within carbonate-rich intervals of Vaca Muerta Formation, to understand their origin and stratigraphic distribution. The facies and geochemical analysis of key sections provided very strong evidence that the carbonate-rich intervals within the Vaca Muerta Formation are sourced from shallow-water carbonate platforms, and thus can be considered periplatform deposits. The Los Catutos Member (mid-late Tithonian) is most likely sourced from the Picún Leufú shelf. Three younger carbonate-rich intervals were discovered in the basin center and measured in the Puerta Curaco section. These younger intervals probably have their source areas in the east, in platform carbonates that are not exposed but were reported from the subsurface. All carbonate-rich interval, including the Los Catutos Member, are placed in the regressive portions of depositional sequences, which makes their position and location predictable in geophysical subsurface data.

The specific results that lead to these findings are:

- Cycles within the carbonate-rich intervals have a clastic and organic-rich transgressive hemicycle, and a carbonate and skeletal-rich top. The transgressive portion and the turnaround typically are fissile clastic mudstones. The top portion of the cycles consists of massive or slightly laminated, skeletal or peloidal wackestone/packstones. None of the cycles was ever exposed. Like the motif in the cycles, the carbonate and skeletal content increase towards the tops of cycle sets and sequences, produced by an increase in frequency and/or thickness of carbonate beds.
- The increased carbonate content in the regressive part of the cycles, cycles set and sequences, interpreted to be deposited during relative sea level highstands, gives strong

evidence of highstand shedding from active carbonate shelves surrounding the Neuquén basin. As a result, the occurrence of the carbonate-rich intervals is predictable within the sequence stratigraphic framework.

- Proximal-distal variations within the carbonate-rich interval of the Los Catutos Member in the Sierra de la Vaca Muerta, from proximal (MDC) to distal (VM23) positions, involve a decrease in carbonate and skeletal content, and a concomitant decrease in thickness and frequency of carbonate-rich beds in the regressive portion of the cycles, cycle sets and sequences. Simultaneously, an increase in the fissile, clastic and organic-rich facies is observed in the transgressive portions. Together, the proximal-distal thinning, and the decrease in carbonate and skeletal content of the carbonate succession indicate a periplatform origin of the Los Catutos Member.

- The source of the Los Catutos is presumed to be in the south, as suggested by the thinning of this interval towards the north. The Picún Leufú carbonate platform is situated 50km farther south, and also has a mid-late Tithonian age. Hence, a genetic link is proposed between the Los Catutos periplatform deposits and the Picún Leufú platform carbonates.

- The Los Catutos Member does not extend towards the distal basin. In the Puerta Curaco section, the time equivalent strata is devoid of periplatform carbonates but consists of clastic and organic-rich cycles, with only concretions on the cycle tops and occasionally thin carbonate beds.

- In the distal basin, Catutos-like carbonate rich-intervals occur at three younger stratigraphic levels: one in the late Upper Berriasian and two in the early Lower Valanginian. These three intervals show similar characteristics to distal facies of the Los

Catutos Member at VM23 section in the Sierra de la Vaca Muerta. Based on the similarity in composition and facies, they are also interpreted as distal periplatform deposits.

- The source of the younger intervals identified in Puerta Curaco is likely to be from the east, based on two lines of evidence. First, no carbonate platforms exist in the south during the Late Berriasian-Early Valanginian. Second, shallow-water deposits similar but younger than the Picún Leufú carbonate platform have been described in subsurface northeast and southeast of the Puerta Curaco outcrops.

- The isotope signature of the Los Catutos carbonate-rich interval reinforces the observed proximal-distal trend between MDC and VM23, and the genetic link to the Picún Leufú carbonate platform. The younger carbonate-rich intervals from Puerta Curaco show similar values to those of Los Catutos in VM23, indicating a similar position relatively distal to a carbonate shelf.

- Distal periplatform deposits in the Los Catutos Member at VM23 and the younger carbonate-rich intervals in PC are mainly composed of relatively thick organic-rich mudstone cycles capped by thin carbonate beds, and might be potential sweet spots for unconventional exploration and production. In proximal positions, on the other hand, where the entire interval and individual beds are thicker and where the intercalated organic-rich mudstones are very thin, the periplatform deposits might act as fracking barriers.



## Works cited

- Afsar, F. (2010) Einfluss petrographischer Merkmale auf akustische Geschwindigkeiten in gemischt siliziklastisch-karbonatischen Gesteinen (Picún Leufú-Formation, Neuquén Becken, Argentinien). *Master-Thesis*. Universität Bremen.
- Aguirre Urreta, M.B. and Vennari, V.V. (2013) Amonites y bioestratigrafía de la Formación Vaca Muerta en tres pozos de El Trapial. *Chevron internal report*.
- Aguirre Urreta, M.B., Vennari, V.V., Lescano, M., Naipauer, M., Concheyro, A. and Ramos, V.A. (2014) Bioestratigrafía y Geocronología de Alta Resolución de la Formación Vaca Muerta, Cuenca Neuquina. *IX Congreso de Exploración y Desarrollo de Hidrocarburos*. Mendoza. Trabajos Técnicos 2, 245-268.
- Anderson, T.F. and Arthur M.A. (1983) Stable Isotopes of Oxygen and Carbon and their Application to Sedimentologic and Paleoenvironmental Problems. In: *Stable isotopes in sedimentary geology, 10* (Eds Arthur, M.A., Anderson, T.F., Kaplan, I.R., Veizer, J. and Land, L.S.), SEPM Short Course, 1-151.
- Arthur, M.A., Zachos, J.C. and Jones, D.S. (1987) Primary Productivity and the Cretaceous/Tertiary Boundary Event in the Oceans. *Cretaceous Research*, 8, 43-54.
- Carozzi, A.V., Orchueta, A. and Rodriguez Schelotto, M.L. (1993) Depositional Models of the Lower Cretaceous Quintuco-Loma Montosa Formation, Neuquén Basin, Argentina. *Journal of Petroleum Geology*, 16 (4), 421-450.
- De Ferrariis, C. (1947) Edad del arco o dorsal antigua del Neuquén oriental de acuerdo con la estratigrafía de la zona inmediata. *Revista de la Sociedad Geológica Argentina*, 2 (3), 256- 283.
- Eberli, G.P., Rodríguez Blanco, L., Weger, R.J., Tengalia, M.R., Rueda, L. and McNeill, D.F. (2015) Establishing a Basinal Reference Section in the Neuquén Basin, Argentina. *CSL Sponsor's Meeting 2015*, CSL internal presentation.
- Emeis, K-C., Struck, U., Leipe, T. and Ferdelman, T.G. (2009) Variability in upwelling intensity and nutrient regime in the coastal upwelling system offshore Namibia: results from sediment archives. *International Journal of Earth Sciences (Geologische Rundschau)*, 98, 309–326.
- Fantin, M.A., Crousse, L., Cuervo, S., Vallejo, D., Gonzalez Tomassini, F., Reijenstein, H. and Lipinski, C. (2014) Vaca Muerta Stratigraphy in central Neuquén Basin : Impact on emergent unconventional project. *Unconventional Resources Technology Conference*, Denver, Colorado, USA.

Fisher, J.K., Price, G., Hart, M.B. and Leng, M.J. (2005) Stable isotope analysis of the Cenomanian-Turonian (Late Cretaceous) oceanic anoxic event in the Crimea. *Cretaceous Research*, 26, 853-863.

Follmi, K.B., Goldet, A., Bodin, S. and Linder, P. (2006) Interactions between environmental change and shallow water carbonate buildup along the northern Tethyan margin and their impact on the Early Cretaceous carbon isotope record. *Paleoceanography*, 21, 4211.

Fossa Mancini, E., Feruglio, E. and Yussen de Campana J. (1938). Una reunión de geólogos de YPF y el problema de la terminología estratigráfica. *Boletín de Informaciones Petroleras*, 15 (171), 1-67.

Franzese, J.R. and Spalletti, L.A. (2001) Late Triassic- Early Jurassic continental extension in Southwestern Gondwana: Tectonic segmentation and pre-break-up rifting. *Journal of South American Earth Sciences*, 14, 257-270.

Gasparini, Z., Spalletti, L. and De La Fuente, M. (1997) Tithonian Marine Reptiles of the Western Neuquén Basin, Argentina. Facies and Palaeoenvironments. *Geobios*, 30 (5), 701-712.

Gertsch, B., Adatte, T., Keller, G., Aziz, A., Tantawy, A.M., Berner, Z., Mort, H.P. and Fleitmann D. (2010) Middle and late Cenomanian oceanic anoxic events in shallow and deeper shelf environments of western Morocco. *Sedimentology*, 57, 1430-1462.

Giraud, X., Bertrand, P., Garçon, V. and Dadou I. (2003) Interpretation of the nitrogen isotopic signal variations in the Mauritanian upwelling with a 2D physical-biogeochemical model. *Global Biogeochemical Cycles*, 17 (2), 1059.

Gonzalez Tomassini, F., Kietzmann, D.A. and Fantin, M.A. (2014). Estratigrafía y análisis de facies Vaca Muerta en el área de El Trapial. *Actas IX Congreso de Exploración y Desarrollo de Hidrocarburos*.

Grossman, E.L. and Ku, T. (1986) Oxygen and Carbon Isotope Fractionation in Biogenic Aragonite: Temperature Effects. *Chemical Geology (Isotope Geoscience Section)*, 59, 59-74.

Gruszczynski, M. (1998) Chemistry of Jurassic seas and its bearing on the existing organic life. *Acta Geologica Polonica*, 48 (1), 1-29.

Gulisano, C.A. and Gutiérrez-Pleimling, A.R. (1995) The Jurassic of the Neuquén Basin, a) Neuquén Province. In: *International Congress on Jurassic Stratigraphy and Geology No. 4*, Field guide, Serie E, Asociación Geológica Argentina: 111 p. Buenos Aires.

Hardie, L.A. (1996) Secular variation in seawater chemistry: An explanation for the coupled secular variation in the mineralogies of marine limestones and potash evaporates over the past 600 m.y. *Geology*, 24 (3), 279-283.

Horita J., Zimmermann, H. and Holland, H.D. (2002) Chemical evolution of seawater during the Phanerozoic: Implications from the record of marine evaporites. *Geochimica et Cosmochimica Acta*, 66 (21), 3733–3756.

Howell, J.A., Schwarz, E., Spalletti, L.A. and Veiga, G.D. (2005) The Neuquén Basin: an overview. *Geological Society, London, Special Publications*, 252, 1-14.

Jenkyns, H.C. (2003) Evidence for rapid climate change in the Mesozoic-Palaeogene greenhouse world. *Philosophical Transactions of the Royal Society A*, 361, 1885-1916.

Jenkyns, H.C. (2010) Geochemistry of oceanic anoxic events. *Geochemistry, Geophysics, Geosystems*. 11 (3), 1-30.

Kernan, H. (2013) Electrofacies, Elemental Composition, and Source Rock Characteristics along Seismic Reflectors of Vaca Muerta Formation in the Loma La Lata Area, Neuquén Basin, Argentina. *MSc Thesis*. Colorado School of Mines.

Kernan, H. and Sonnenberg, S. (2015) Sequence Stacking and Reservoir Facies of a Vaca Muerta Shale Outcrop, Puerta Curaco, Neuquén Basin, Argentina. *AAPG Search and Discovery Article #90166*. AAPG International Conference and Exhibition, Cartagena, Colombia.

Kietzmann, D.A. and Ambrosio, A.L. (2014) Estudio bioestratigráfico integrado basado en calciesferas y calpionellidos. Formación Vaca Muerta. *Chevron internal report*.

Kietzmann, D.A., Ambrosio, A.L., Suriano J., Alonso S., Vennari V.V., Aguirre-Urreta M.B., Depine G. and Repol D. (2014) Variaciones de facies de las secuencias basales de la Formación Vaca Muerta en su localidad tipo (Sierra de la Vaca Muerta), cuenca Neuquina. *IX Congreso de Exploración y Desarrollo de Hidrocarburos, Mendoza*. Trabajos Técnicos 2, 299-317.

Larriestra, C. and Merino, R. (2014) High resolution non-destructive chemostratigraphy of Vaca Muerta Formation, Argentina: new evidence of black shale sedimentary features. *AAPG Search and Discovery Article #41310*. AAPG Annual Convention and Exhibition, Houston TX.

Leanza, H.A. (1973) Estudio sobre los cambios faciales de los estratos limítrofes Jurásico-Cretácicos entre Loncopué y Picún Leufú, provincia de Neuquén, República Argentina. *Revista de la Asociación Geológica Argentina*, XXVIII (2), 97–132.

Leanza, H.A. (1977) Estratigrafía del grupo Mendoza con especial referencia a la formación Vaca Muerta entre los paralelos 35° y 40° L.S., cuenca Neuquina-Mendocina. *Revista de la Asociación Geológica Argentina*, XXXII (3), 190–208.

Leanza, H.A. and Hugo C.A. (1977) Sucesión de amonites y edad de la formación Vaca Muerta y Sincrónicas entre los paralelos 35° y 40° L.S., cuenca Neuquina-Mendocina. *Revista de la Asociación Geológica Argentina*, XXXII (4), 248–264.

Leanza, H.A. and Hugo C.A. (2005) Hoja Geológica 3669-I, Zapala. *Instituto de Geología y Recursos Minerales, Servicio Geológico Minero Argentino*. Boletín 275.

Leanza, H.A. and Zeiss, A. (1990) Upper Jurassic Lithographic Limestones from Argentina (Neuquén Basin): Stratigraphy and Fossils. *Facies*, 22, 169–186.

Leanza, H.A. and Zeiss, A. (1994) The "Lithographic Limestones" of Zapala (Central Argentina) and their Ammonite Fauna. *Geobios*, 16, 245-250.

Leanza, H.A., Sattler, F., Martínez, R.S. and Carbone, O. (2011) La Formación Vaca Muerta y equivalentes (Jurásico tardío-Cretácico temprano) en la Cuenca Neuquina. In: *Congreso Geológico Argentino, No. 18* (Eds H. Leanza, J. Vallés, C. Arregui, J.C. Danieli). *Geología y Recursos Naturales de la provincia del Neuquén*, 12, 113-129. Neuquén.

Legarreta, L. and Gulisano, C.A. (1989) Análisis estratigráfico secuencial de la cuenca Neuquina (Triásico Superior-Terciario Inferior). En: *Cuencas Sedimentarias Argentinas* (Eds G.A. Chebli y L.A. Spalletti), Instituto Miguel Lillo, Universidad Nacional de Tucumán, *Serie de Correlación Geológica*, 6, 221-244, San Miguel de Tucumán.

Lini, A., Weissert H. and Erba, E. (1992) The Valanginian carbon isotope event: a first episode of greenhouse climate conditions during the Cretaceous. *Terra Nova*, 4 (3), 374-385.

Menegatti, A.P., Weissert, H., Brown, R.S., Tyson, R.V., Farrimond, P., Strasser, A. and Caron, M. (1998) High-resolution  $\delta^{13}\text{C}$  stratigraphy through the early Aptian "Livello Selli" of the Alpine Tethys. *Paleoceanography*, 13 (5), 530-545.

Mitchum, R.M.Jr. and Uliana, M.A. (1985) Seismic Stratigraphy of Carbonate Depositional Sequences, Upper Jurassic-Lower Cretaceous, Neuquen Basin, Argentina. AAPG Memoir 39, 255-274.

Morettini, E., Godino, G., Smith, L.B. and Massafarro, J.L. (2015) The Vaca Muerta-Quintuco Mixed Depositional System: New Insights from Carbon Stable Isotopes ( $\delta^{13}\text{C}_{\text{carb}}$  and  $\delta^{13}\text{C}_{\text{org}}$ ) and Geochemical Data at the Jurassic-Cretaceous Boundary (Neuquén Basin, West Argentina). *AAPG Search and Discovery Article #90216*. AAPG Annual Convention and Exhibition, Denver, CO.

Mosquera, A., Silvestro, J., Ramos, V., Alarcón, M. and Zubiri, M. (2011) La estructura de la Dorsal de Huincul. In: *Geología y Recursos Naturales de la Provincia del Neuquén* (Eds H.A. Leanza, C. Arregui, O. Carbone, J.C. Danieli and J.M. Vallés), *Relatorio del 18º Congreso Geológico Argentino, Neuquén*, 385-398.

Mpodozis, C. and Ramos, V.A. (1989) The Andes of Chile and Argentina. In: *Geology of the Andes and its relation to hydrocarbon and mineral resources* (Eds G.E. Ericksen, M.T. Cañas Pinochet and J.A. Reinemund). *Circum-Pacific Council for Energy and Mineral Resources, Earth Sciences Series*, 11, Houston, Texas, USA.

Ramos, V.A. and Folguera, A. (2005) Tectonic evolution of the Andes of Neuquén: constraints derived from the magmatic arc and foreland deformation. *Geological Society, London, Special Publications*, 252 (1), 15–35.

Riccardi, A.C. (1988) The Cretaceous System of southern South America. *Geological Society of America, Memoir* 168, 1-161.

Rickman, R., Mullen, M., Petre, E., Grieser, B. and Kundert, D. (2008) A practical use of shale petrophysics for stimulation design optimization: all shale plays are not clones of the Barnett shale. *SPE 115258*, SPE ATCE, Denver, CO.

Romanek, C.S., Grossman, E.L. and Morse, J.W. (1992) Carbon Isotopic fractionation in synthetic aragonite and calcite: Effects of temperature and precipitation rate. *Geochimica et Cosmochimica Acta*, 56, 419-430.

Saltzman, M.R. (2012) Carbon and oxygen isotope stratigraphy of the Lower Mississippian (Kinderhookian–lower Osagean), western United States: Implications for seawater chemistry and glaciation. *Geological Society of America Bulletin*, 114 (1), 96-108.

Saltzman, M.R. and Thomas, E. (2012) Carbon Isotope Stratigraphy. In: *The Geologic Time Scale 2012* (Eds Gradstein, F.M., Ogg, J.G., Schmitz, M.D. and Ogg, G.M.), Elsevier, Oxford, 207–232.

Scasso, R.A., Alonso, M.S., Lanes, S., Villar, H.J. and Laffitte, G. (2005) Geochemistry and petrology of a Middle Tithonian limestone-marl rhythmite in the Neuquén Basin, Argentina: depositional and burial history. In: *The Neuquén Basin, Argentina: A Case Study in Sequence Stratigraphy and Basin Dynamics* (Eds Veiga, G.D., Spalletti, L.A., Howell, J.A. and Schwarz, E.). *Geological Society, London, Special Publications*, 252, 207-229.

Scasso, R.A., Alonso, M.S., Lanés, S., Villar, H.J. and Lippai, H. (2002) Petrología y geoquímica de una ritmita marga-caliza del Hemisferio Austral: El Miembro Los Catutos (Formación Vaca Muerta, Tithoniano medio de la Cuenca Neuquina). *Revista de la Asociación Geológica Argentina*, 57 (2), 143–159.

Schlager, W. and James, N.P. (1978) Low-magnesian calcite limestones forming at the deep-sea floor, Tongue of the Ocean, Bahamas. *Sedimentology*, 25, 675-702.

Schlager, W., Riejmer, J.J.G. and Droxler, A. (1994) Highstand shedding of carbonate platforms. *Journal of Sedimentary Research*, 64 (3), 270-281.

Silvestro, J. and Zubiri, M. (2008) Convergencia oblicua: Modelo estructural alternativo para la dorsal Neuquina (39°S) - Neuquén. *Revista de la Asociación Geológica Argentina*, 63 (1), 49-64.

Spalletti, L.A., Franzese, J.R., Matheos, S.D. and Schwarz, E. (2000) Sequence stratigraphy of a tidally dominated carbonate-siliciclastic ramp; the Tithonian-Early Berriasian of the Southern Neuquén Basin, Argentina. *Journal of the Geological Society, London*, 157, 433-446.

Spalletti, L.A., Schwarz, E. and Veiga, G.D. (2014) Geoquímica inorgánica como indicador de procedencia y ambiente sedimentario en sucesiones de lutitas negras: los depósitos transgresivos titonianos (Formación Vaca Muerta) de la Cuenca Neuquina, Argentina. *Andean Geology*, 41 (2), 401-435.

Stanely, S.M. and Hardie L.A. (1998) Secular oscillations in the carbonate mineralogy of reef-building and sediment-producing organisms driven by tectonically forced shifts in seawater chemistry. *Palaeogeography, Palaeoclimatology, Palaeoecology*, 144, 3-19.

Swart, P.K. and Eberli G.P. (2005) The nature of the  $\delta^{13}\text{C}$  of periplatform sediments: Implications for stratigraphy and the global carbon cycle. *Sedimentary Geology*, 175, 115-129.

Swart, P.K., Burns, S.J. and Leder, J.J. (1991) Fractionation of the stable isotopes of oxygen and carbon in carbon dioxide during the reaction of calcite with phosphoric acid as a function of temperature and technique. *Chemical Geology*, 86, 89-96.

Tunik, M., Folguera, A., Naipauer, M., Pimentel, M. and Ramos, V.A. (2010) Early uplift and orogenic deformation in the Neuquén Basin: Constraints on the Andean uplift from U-Pb and Hf isotopic data of detrital zircons. *Tectonophysics*, 489 (1-4), 258-273.

Uliana, M.A. and Biddle, K.T. (1987) Permian to late Cenozoic evolution of northern Patagonia: main tectonic events, magmatic activity and depositional trends. *Gondwana Six: Structure, Tectonics and Geophysics*, 271-286.

Uliana, M.A. and Legarreta, L. (1993) Hydrocarbons Habitat in a Triassic-to-Cretaceous Sub-Andean Setting: Neuquén Basin, Argentina. *Journal of Petroleum Geology*, 16 (4), 397-420.

Vail, P.R., Mitchum, R.M., Todd, R.G., Widmier, J.M., Thompson, S., Sangree, J.B., Bubb, J.N. and Hatlelid, W.G. (1977) Seismic stratigraphy and global changes of sea level.

In: *Seismic Stratigraphy – Application to Hydrocarbon Exploration* (Ed C.E. Payton, C.E.). *AAPG Memoir*, 26, 49-212.

Veizer, J., Ala, D., Azmy, K., Bruckschen, P., Buhl, D., Bruhn, F., Carden, G.A.F., Diener, A., Ebner, S., Godderis, Y., Jasper, T., Korte, C., Pawellek, F., Podlaha O.G. and Strauss H. (1999)  $^{87}\text{Sr}/^{86}\text{Sr}$ ,  $\delta^{13}\text{C}$  and  $\delta^{18}\text{O}$  evolution of Phanerozoic seawater. *Chemical Geology*, 161, 59–88.

Vennari, V.V., Alvarez, P.P., and Aguirre-Urreta, M.B. (2012) A new species of *Andiceras Krantz* (Cephalopoda: Ammonoidea) from the Late Jurassic-Early Cretaceous of the Neuquén Basin, Mendoza, Argentina. Systematics and Biostratigraphy. *Andean Geology*, 39 (1), 92–105.

Vergani, G.D., Tankard, A., Belotti, H.J., and Welsink, H.J. (1995) Tectonic Evolution and Paleogeography of the Neuquén Basin, Argentina. *Petroleum Basins of South America, Memoir*, 62, 383–402.

Weaver, C.E. (1931) Paleontology of the Jurassic and Cretaceous of west central Argentina. *Memoir University Washington*, 1, 1-469.

Weissert, H. and Channell, J.E.T. (1989) Tethyan Carbonate Carbon Isotope Stratigraphy across the Jurassic-Cretaceous boundary: An Indicator of Decelerated Global Carbon Cycling? *Paleoceanography*, 4 (4), 483-494.

Weissert, H. and Mohr (1996) Late Jurassic climate and its impact on carbon cycling. *Palaeogeography, Palaeoclimatology, Palaeoecology*, 122, 27-43.

Wilson, J.L. (1969) Microfacies and sedimentary structures in “deeper water” lime mudstones. In: *Depositional Environments in Carbonate Rocks* (Ed G.M. Friedman), 14, 4-19.

Zak, K., Košťák, M., Man, O., Zakharov, V.A., Rogov M.A., Pruner P., Rohovec, J., Dzyuba, O.S., Mazuch, M. (2011) Comparison of carbonate C and O stable isotope records across the Jurassic/Cretaceous boundary in the Tethyan and Boreal Realms. *Palaeogeography, Palaeoclimatology, Palaeoecology*, 299, 83-96.

Zehnder, A.T. (2007) Lecture Notes on Fracture Mechanics. Cornell University.

Zeller, M. (2013) Facies, Geometries and Sequence Stratigraphy of the Mixed Carbonate-Siliciclastic Quintuco-Vaca Muerta System in the Neuquén Basin, Argentina: An Integrated Approach. *Open Access Dissertations*. Paper 1099.

Zeller, M., Verwer, K., Eberli, G.P., Massaferró, J.L., Schwarz, E. and Spalletti, L.A. (2015) Depositional controls on mixed carbonate-siliciclastic cycles and sequences on gently inclined shelf profiles. *Sedimentology*, Accepted article.

## APPENDIX A

### Complete data set from MDC and PC sections

Section	Sample	Depth	CO <sub>3</sub> (%)	TOC (%)	$\delta^{13}\text{C}_{\text{in}}$ (‰)
MDC	MDC4-13	146.8	91	0.16	0.94
MDC	MDC4-12	145.8	82	0.26	
MDC	MDC4-11	141.5	86	0.80	0.69
MDC	MDC4-10	139.7	88	0.79	0.86
MDC	P_139	137.9	87	0.77	-0.09
MDC	MDC4-9	137.5	82	1.12	0.68
MDC	P_141	137.3	78	1.95	1.32
MDC	P_143	135	79		1.45
MDC	MDC4-8	134.5	84	1.23	0.83
MDC	P_145	134.2	76	1.53	1.31
MDC	MDC4-6	132.2	85	0.47	0.71
MDC	MDC4-5	131	71	1.57	-0.04
MDC	P_135	128.9	67	2.84	0.98
MDC	P_137	128.1	63	1.87	0.90
MDC	MDC4-4	127	67	1.09	0.70
MDC	MDC4-3	126	27	2.14	-0.28
MDC	MDC4-2	124.5	81	0.79	1.17
MDC	VM14-134	124.3	76	0.94	1.31
MDC	MDC5-7	124	97	0.06	0.87
MDC	P_130	124	78	1.07	1.32
MDC	P_133	123.6	80	1.28	1.56
MDC	VM14-133	123.4	77	1.25	1.50
MDC	VM14-132	122.7	66	1.43	1.43
MDC	MDC4-1	122.5	78	0.87	0.76
MDC	VM14-131	122.25	71	1.03	1.25
MDC	VM14-130	121.4	77	0.35	0.07
MDC	MDC5-6	121	76	0.74	0.81
MDC	VM14-129	120.6	77	0.22	0.49
MDC	VM14-128	119.55	74	1.13	1.32
MDC	MDC5-5	119	84	0.77	0.96
MDC	VM14-127	118.7	79	1.22	1.29
MDC	VM14-126	117.7	79	1.36	1.35
MDC	VM14-125	116.9	84	1.01	1.04
MDC	VM14-124	116	80	0.41	0.43
MDC	VM14-135	115.9	79	0.95	1.24
MDC	MDC5-4	115.8	74	1.19	1.01
MDC	VM14-123	114.5	66	1.32	1.13
MDC	VM14-122	113.3	60	1.38	0.60
MDC	VM14-121	112.5	62	1.29	0.93
MDC	VM14-119	110.6	66	1.03	0.61
MDC	VM14-137	110	50	1.53	0.47
MDC	VM14-118	109.5	29	2.82	-0.23
MDC	MDC5-2	109	79	0.77	0.62
MDC	MDC5-1	108	70	1.17	0.53
MDC	VM14-115	106.5	82	0.98	0.82
MDC	MDC2-13	106	84	0.60	1.17
MDC	VM14-114	105.5	74	1.13	0.65
MDC	MDC2-12	105.3	81	1.23	1.28



Section	Sample	Depth	CO3 (%)	TOC (%)	$\delta^{13}\text{C}_{\text{in}}$ (‰)
MDC	VM14-113	104.6	79	2.21	1.05
MDC	MDC2-11	104.5	82	0.58	0.33
MDC	VM14-112	103.8	81	0.64	0.33
MDC	MDC2-10	103.5	85	0.69	1.17
MDC	VM14-111	103	83	0.70	0.93
MDC	MDC2-9	102.5	85	0.76	1.09
MDC	VM14-110	102.1	82	1.03	1.05
MDC	MDC2-8	102	84	0.84	1.08
MDC	MDC2-7	101.5	81	0.82	0.83
MDC	VM14-109	101.4	70	1.31	0.79
MDC	VM14-108	100.7	80	0.70	0.80
MDC	MDC2-6	100	84	0.66	0.92
MDC	VM14-107	99.75	78	0.30	0.34
MDC	MDC2-5	99.5	82	0.85	0.85
MDC	VM14-106	98.6	84	0.35	1.17
MDC	MDC2-4	98.5	92	0.38	1.34
MDC	VM14-105	97.4	64	1.65	0.10
MDC	VM14-104	96.6	59	1.76	0.27
MDC	VM14-103	95.9	49	2.53	-0.78
MDC	VM14-102	94.7	44	1.42	-0.16
MDC	MDC2-2	94.5	80		-0.19
MDC	VM14-101	94.3	28	1.36	-2.21
MDC	VM14-100	93.6	56	1.13	-0.25
MDC	VM14-99	92.6	33	2.51	-0.50
MDC	VM14-98	91.6	48	2.68	-1.38
MDC	VM14-97	91.25	32	2.15	-0.48
MDC	VM14-96	90.8	57	0.95	-1.26
MDC	VM14-95	90.2	60	0.77	-0.36
MDC	VM14-94	89.9	19	2.15	-1.07
MDC	VM14-93	89.1	53	2.46	
MDC	VM14-92	88.2	48	2.32	-0.91
MDC	VM14-91	87.25	37	2.98	-1.24
MDC	VM14-90	86.45	22	2.12	-1.14
MDC	VM14-89	85.55	10	1.96	-1.94
MDC	VM14-88	85.15	13	0.14	-1.38
MDC	VM14-87	84.6	58	1.77	-1.00
MDC	MDC-GRL-1	84.3	59	1.34	-1.26
MDC	VM14-86	83.25	66	1.84	-1.25
MDC	VM14-85	82.25	82	0.38	0.47
MDC	VM14-84	81.5	47	2.62	-1.40
MDC	VM14-83	80.7	24	3.37	-1.60
MDC	VM14-82	79.95	31	2.37	-1.50
MDC	VM14-81	78.7	50	3.10	-1.08
MDC	VM14-80	77.5	18	1.40	-2.41
MDC	VM14-79	76.5	47	1.33	-1.64
MDC	VM14-78	75.5	20	4.35	-2.88
MDC	VM14-77	74.5	7	3.08	
MDC	VM14-76	73.6	11	4.22	-2.18
MDC	VM14-75	72.3	8	3.05	-4.38
MDC	VM14-74	71.5	27	7.18	-2.55
MDC	VM14-73	70.5	37	1.81	-1.95
MDC	VM14-72	69.5	18	1.30	-2.30
MDC	VM14-71	68.65	15	10.01	-4.16

Section	Sample	Depth	CO3 (%)	TOC (%)	$\delta^{13}\text{C}_{\text{in}}$ (‰)
MDC	VM14-70	68.5	32	4.25	-3.63
MDC	VM14-69	67.8	21	6.07	-2.95
MDC	VM14-68	65.5	11	5.03	-3.36
MDC	VM14-67	64	17	4.84	-3.02
MDC	VM14-66	62.5	31	1.84	
MDC	VM14-65	61.5	25	1.54	
MDC	VM14-64	60.5	11	3.41	-2.86
MDC	VM14-63	59.7	77	0.78	-12.14
MDC	VM14-62	58.1	8	4.36	
MDC	VM14-61	57	7	9.31	
MDC	VM14-60	56	10	6.79	-4.20
MDC	VM14-59	55	8	0.90	-4.87
MDC	VM14-58	54	87	0.28	-6.24
MDC	VM14-57	53.65	6	2.65	
MDC	VM14-56	52.65	10	2.26	-4.66
MDC	VM14-55	51.65	8	4.79	
MDC	VM14-54	50.65	6	4.55	-4.66
MDC	VM14-53	49.65	12	5.50	-4.62
MDC	VM14-52	48.65	7	6.70	
MDC	VM14-51	47.65	7	9.33	
MDC	VM14-50	46.65	14	2.16	-5.89
MDC	VM14-49	45.65	4	0.62	
MDC	VM14-47	44.8	9	2.72	-4.99
MDC	VM14-48	44.65	86	0.70	-5.18
MDC	VM14-46	43.65	17	4.12	-4.66
MDC	VM14-45	42.65	7	5.78	
MDC	VM14-44	41.65	58	3.15	-9.33
MDC	VM14-43	37.5	9	0.70	-6.39
MDC	VM14-42	36.9	11	0.15	-6.40
MDC	VM14-41	36.5	16	3.59	-4.44
MDC	VM14-40	35.85	18	3.59	-4.61
MDC	VM14-39	35	8	11.33	
MDC	VM14-38	33.9	13	15.57	-3.94
MDC	VM14-37	30.4	25	15.45	-3.43
MDC	VM14-36	29.5	5	6.30	
MDC	VM14-35	28.8	9	0.15	-4.97
MDC	VM14-34	28.6	66	0.08	-5.30
MDC	VM14-33	28.3	8	9.46	
MDC	VM14-32	27.75	7	2.41	
MDC	VM14-31	26.5	32	8.67	-5.55
MDC	VM14-28	24.4	75	2.81	-4.43
MDC	VM14-27	24.1	17	7.35	
MDC	VM14-30	24	9	0.09	
MDC	VM14-29	23.5	72	2.31	-5.29
MDC	VM14-26	23	4	0.10	
MDC	VM14-25	21.7	5	0.38	
MDC	VM14-24	20.5	6	3.88	
MDC	VM14-23	17.75	11	0.73	-6.33
MDC	VM14-22	14.9	4	3.56	-5.94
MDC	VM14-21	12.5	5	0.05	-5.23
MDC	VM14-20	8.65	5	0.09	
MDC	VM14-19	8.5	4	0.81	
MDC	VM14-18	8	9	1.21	-4.97

Section	Sample	Depth	CO3 (%)	TOC (%)	$\delta^{13}\text{C}_{\text{in}}$ (‰)
MDC	VM14-17	7.8	24	7.87	-3.33
MDC	VM14-16	7.6	21	11.42	-2.87
MDC	VM14-15	5.3	7	8.13	-3.32
MDC	VM14-14	3	45	3.27	-3.03
MDC	VM14-13	2.8	44	2.89	-4.38
PC	PC04-455	649	17		
PC	PC04-454	648	14		
PC	PC04-453	647	10		
PC	PC04-452	646	30		
PC	PC04-451	645	14	0.51	0.77
PC	PC04-450	644	15	0.32	
PC	PC04-449	643	11	0.23	
PC	PC04-448	642	15	0.24	
PC	PC04-447	641	12	0.25	
PC	PC04-446	640	9	0.40	0.67
PC	PC04-445	639	30	0.24	
PC	PC04-444	638	24	0.23	
PC	PC04-443	637	66	0.27	
PC	PC04-442	636	14	0.22	
PC	PC04-441	635	21	0.47	0.90
PC	PC04-440	634	14	0.18	
PC	PC04-439	633	11	0.19	
PC	PC04-438	632	14	0.20	
PC	PC04-437	631	34	0.19	
PC	PC04-436	630	12	0.38	0.93
PC	PC04-435	629	9	0.16	
PC	PC04-433	627	16	0.30	
PC	PC04-432	626	12	0.23	
PC	PC04-431	625	28	0.25	
PC	PC04-430	624	26	0.30	0.08
PC	PC04-429	623	61	0.08	
PC	PC04-428	622	18	0.35	
PC	PC04-427	621	49	0.35	
PC	PC04-426	620	44	0.45	
PC	PC04-425	619	34	0.58	0.51
PC	PC04-424	618	44	0.43	
PC	PC04-423	617	23	0.31	
PC	PC04-422	616	13	0.19	
PC	PC04-421	615	17	0.28	
PC	PC04-420	614	18	0.59	0.49
PC	PC04-419	613	15	0.23	
PC	PC04-418	612	33	0.32	
PC	PC04-417	611	18	0.26	
PC	PC04-416	610	28	0.32	
PC	PC04-415	609	33	0.32	1.13
PC	PC04-414	608	24	0.43	
PC	PC04-413	607	22	0.41	
PC	PC04-412	606	70	0.10	
PC	PC04-411	605	19	0.50	
PC	PC04-410	604	11	0.29	0.22
PC	PC04-409	603	61	0.09	
PC	PC04-408	602	8	0.20	

Section	Sample	Depth	CO3 (%)	TOC (%)	$\delta^{13}\text{C}_{\text{in}}$ (‰)
PC	PC04-407.5	601.5	65		
PC	PC04-407	601	5	0.22	
PC	PC04-406	600	21	0.36	
PC	PC04-405	599	4	0.36	-1.32
PC	PC04-404	598	26	0.20	
PC	PC04-403	597	13	0.16	
PC	PC04-402	596	22	0.27	
PC	PC04-401	595	22	0.45	
PC	PC04-400	594	12	0.45	0.44
PC	PC04-399	593	47	0.30	
PC	PC04-398	592	49	0.55	
PC	PC04-397	591	53	0.51	
PC	PC04-394	588	73	0.15	
PC	PC04-393	587	43	0.65	0.55
PC	PC04-392	586	42	0.74	
PC	PC04-391	585	38	0.57	
PC	PC04-390	584	43	0.58	
PC	PC04-389	583	13	0.31	
PC	PC04-388	582	31	0.89	1.17
PC	PC04-387	581	37	0.81	
PC	PC04-386	580	53	0.43	
PC	PC04-385	579	41	0.61	
PC	PC04-384	578	36	0.61	
PC	PC04-383	577	34	0.75	1.30
PC	PC04-382	576	31	0.89	
PC	PC04-381	575	59	0.26	
PC	PC04-380	574	50	0.66	
PC	PC04-379	573	43	0.34	
PC	PC04-378	572	49	0.55	0.09
PC	PC04-377	571	54	0.37	
PC	PC04-376	570	40	0.50	
PC	PC04-375	569	30		
PC	PC04-374	568	29	0.98	
PC	PC04-373	567	54	0.81	0.63
PC	PC04-372	566	41	0.90	
PC	PC04-371	565	57	0.96	
PC	PC04-370	564	53	0.73	
PC	PC04-369	563	43	0.34	
PC	PC04-368	562	51	0.65	-0.08
PC	PC04-367	561	70	0.15	
PC	PC04-366	560	38	0.45	
PC	PC04-365	559	48	0.49	
PC	PC04-364	558	42	0.56	
PC	PC04-363	557	51	0.66	0.13
PC	PC04-362	556	51	0.34	
PC	PC04-361	555	39	0.83	
PC	PC04-347	541	52	0.70	
PC	PC04-346	540	51	0.61	
PC	PC04-344	538	51	0.86	0.00
PC	PC04-343	537	39	0.88	
PC	PC04-342	536	37	0.92	
PC	PC04-341	535	31	1.01	
PC	PC04-340	534	35	0.71	

Section	Sample	Depth	CO3 (%)	TOC (%)	$\delta^{13}\text{C}_{\text{in}}$ (‰)
PC	PC04-339	533	13	1.38	-0.66
PC	PC04-338	532	81	0.04	
PC	PC04-337	531	37	0.45	
PC	PC04-336	530	45	0.60	
PC	PC04-335	529	42	0.74	
PC	PC04-334	528	21	1.08	-0.06
PC	PC04-333	527	25	1.00	
PC	PC04-332	526	36	0.95	
PC	PC04-331	525	50	1.15	
PC	PC04-327	521	48	0.60	
PC	PC04-325	519	73	0.95	-0.30
PC	PC04-324.75	518.75	69		
PC	PC04-324	518	59	1.67	
PC	PC04-323.5	517.5	81	0.89	0.23
PC	PC04-323	517	35	1.28	0.25
PC	PC04-322.2	516.2	79		-0.52
PC	PC04-322	516	61	1.01	0.08
PC	PC04-321	515	75	0.94	-0.20
PC	PC04-320.7	514.7	80	0.75	0.27
PC	PC04-320	514	46	0.94	-0.09
PC	PC04-319	513	50	0.60	-0.25
PC	PC04-318	512	51	0.64	-0.26
PC	PC04-317	511	42	1.77	0.02
PC	PC04-316	510	27	0.75	-0.24
PC	PC04-315	509	75	1.14	-0.09
PC	P-99h	508.5	68	2.38	-0.05
PC	P-101h	508.3	62	0.92	-0.52
PC	PC04-314	508	70	1.21	-0.48
PC	PC04-313	507	72	1.71	0.16
PC	PC04-312	506	60	1.55	0.01
PC	PC04-311	505	59	1.29	0.06
PC	PC04-310	504	60	1.13	0.18
PC	PC04-309	503	59	1.49	0.30
PC	PC04-308	502	61	1.88	-0.01
PC	PC04-307	501	66	1.09	0.18
PC	PC04-306	500	61	1.26	0.28
PC	PC04-305.5	499.5	74	0.66	-0.30
PC	PC04-305	499	32	1.88	-0.08
PC	PC04-304	498	43	0.69	-0.26
PC	PC04-303	497	53	1.17	0.37
PC	P-95h	496.6	62	1.19	0.52
PC	PC04-302	496	57	1.26	0.18
PC	P-96h	495.8	61	1.55	0.90
PC	PC04-301.7	495.7	69	1.28	0.08
PC	PC04-301	495	57	1.75	-0.06
PC	PC04-300	494	59	1.57	0.37
PC	PC04-299	493	54	1.92	0.03
PC	PC04-298	492	59	1.60	-0.11
PC	PC04-297	491	54	0.96	-0.08
PC	PC04-296	490	54	1.24	0.11
PC	PC04-295	489	65	1.29	0.09
PC	P-91h	488.1	75	0.92	0.12
PC	PC04-294	488	70	1.21	0.10

Section	Sample	Depth	CO3 (%)	TOC (%)	$\delta^{13}\text{C}_{\text{in}}$ (‰)
PC	P-93h	487.6	64	1.56	0.21
PC	PC04-293	487	32	3.17	-0.12
PC	PC04-292	486	45	3.54	-0.56
PC	PC04-291	485	37	2.05	-0.15
PC	PC04-290	484	31	2.85	-0.02
PC	PC04-289	483	45	2.24	
PC	PC04-288	482	40	2.67	
PC	PC04-287	481	59	2.35	
PC	PC04-286	480	30	2.37	
PC	PC04-284	478	15	1.71	-0.14
PC	PC04-283	477	36	1.05	
PC	PC04-282	476	24	1.53	
PC	PC04-281	475	24	0.96	
PC	PC04-280	474	26	4.07	
PC	PC04-279	473	18	1.27	-0.70
PC	PC04-278	472	17	1.04	
PC	PC04-277	471	91	0.20	
PC	PC04-276	470	18	1.08	
PC	PC04-275	469	22	0.91	
PC	PC04-274	468	32	1.04	-0.81
PC	PC04-273	467	27	1.01	
PC	PC04-272	466	28	0.70	
PC	PC04-271	465	30	0.84	
PC	PC04-270	464	31	1.12	
PC	PC04-269	463	29	1.21	-0.92
PC	PC04-268	462	19	1.39	
PC	PC04-267	461	32	1.01	
PC	PC04-266	460	30	1.43	
PC	PC04-265	459	19	1.75	
PC	PC04-264	458	78	0.47	0.93
PC	PC04-263	457	28	1.49	
PC	PC04-262	456	35	1.34	
PC	PC04-261	455	25	1.26	
PC	PC04-260	454	21	1.23	
PC	PC04-259	453	16	0.91	-0.75
PC	PC04-257	451	13	0.95	
PC	PC04-256	450	26	0.72	
PC	PC04-255	449	16	1.04	
PC	PC04-254	448	24	1.03	
PC	PC04-253	447	42	0.52	-1.25
PC	PC04-251.7	445.7	88		
PC	PC04-250	444	17	0.55	
PC	PC04-249	443	25	0.48	
PC	PC04-248	442	19	0.78	
PC	PC04-246	440	86	0.22	
PC	PC04-245.2	439.2	89	0.28	
PC	PC04-245	439	10	1.50	-1.53
PC	PC04-244	438	17	0.75	
PC	PC04-243	437	16	0.93	
PC	PC04-242	436	19	0.57	
PC	PC04-241	435	36	1.43	
PC	PC04-229	423	45	1.06	-1.18
PC	PC04-228	422	34	1.18	

Section	Sample	Depth	CO3 (%)	TOC (%)	$\delta^{13}\text{C}_{\text{in}}$ (‰)
PC	PC04-227	421	33	0.95	
PC	PC04-226	420	42	1.13	
PC	PC04-225	419	42	1.14	
PC	PC04-224	418	43	1.33	-1.41
PC	PC04-223	417	47	1.49	
PC	PC04-222	416	43	1.70	
PC	PC04-221	415	30	1.32	
PC	PC04-220	414	27	2.81	
PC	PC04-219	413	72	1.51	-0.47
PC	PC04-218	412	77	1.67	
PC	PC04-215	409	48	1.89	
PC	PC04-214	408	38	1.18	
PC	PC04-213	407	27	1.47	
PC	PC04-212	406	56	0.85	-1.96
PC	PC04-211	405	36	2.31	
PC	P-76h	404.1	81	0.88	-0.84
PC	PC04-210	404	88	0.65	1.05
PC	P-78h	403.5	48	2.00	-0.93
PC	PC04-209	403	47	2.29	-1.40
PC	PC04-208	402	36	2.97	-1.03
PC	PC04-207	401	50	2.55	-1.34
PC	PC04-206	400	31	2.00	-0.94
PC	PC04-204.9	398.9	78	0.68	1.31
PC	PC04-204	398	67	0.65	-0.67
PC	PC04-203	397	53	0.94	-0.88
PC	PC04-202	396	18	1.83	-0.65
PC	PC04-201.5	395.5	68	0.71	-0.71
PC	PC04-201	395	39	0.67	-0.93
PC	PC04-200	394	20	1.01	-1.53
PC	PC04-199	393	35	2.20	-1.12
PC	PC04-198	392	15	2.58	-1.00
PC	P-72h	391.3	78	0.54	-0.44
PC	PC04-197.2	391.2	86	0.28	0.97
PC	PC04-197	391	73	0.54	-1.03
PC	PC04-196	390	26	1.25	-0.99
PC	PC04-195	389	59	1.27	-1.35
PC	PC04-194.8	388.8	77		-1.54
PC	PC04-194	388	29	1.35	-1.69
PC	PC04-193	387	29	2.60	-1.57
PC	PC04-192	386	20	1.18	-1.36
PC	PC04-191	385	26	1.89	-1.26
PC	PC04-190	384	33	0.92	-0.91
PC	PC04-189	383	36	2.27	-0.65
PC	PC04-188.6	382.6	86	0.31	1.21
PC	PC04-188	382	28	2.17	-0.60
PC	P-68h	381.2	76	0.79	-0.76
PC	PC04-187	381	38	1.93	-0.27
PC	P-70h	380.5	47	1.51	-0.01
PC	PC04-186.2	380.2	87	0.43	1.18
PC	PC04-186	380	59	0.90	-0.80
PC	PC04-185.9	379.9	67		-0.30
PC	PC04-185.3	379.3	86	0.49	0.99
PC	PC04-185	379	66	1.09	-0.56

Section	Sample	Depth	CO3 (%)	TOC (%)	$\delta^{13}\text{C}_{\text{in}}$ (‰)
PC	PC04-184	378	54	1.37	-0.62
PC	PC04-183	377	37	3.04	-0.95
PC	PC04-182	376	76	0.62	0.73
PC	PC04-181	375	41	2.51	-1.09
PC	PC04-180	374	32	1.87	-0.27
PC	PC04-179	373	39	2.66	-1.02
PC	PC04-178	372	41	4.31	-1.09
PC	PC04-177.6	371.6	73		-0.98
PC	PC04-177	371	47	1.83	-2.17
PC	PC04-176	370	34	2.23	-1.54
PC	PC04-175	369	69	1.98	-0.96
PC	PC04-174	368	38	2.74	-1.63
PC	PC04-173	367	71	1.28	-0.57
PC	PC04-172	366	71	1.44	-1.21
PC	PC04-171.6	365.6	73	1.12	0.50
PC	PC04-171.4	365.4	72	1.30	0.75
PC	P-64h	365.3	70	1.27	-0.36
PC	PC04-171	365	57	2.33	-0.91
PC	P-66h	364.9	85	0.68	2.67
PC	PC04-170	364	22	1.61	
PC	PC04-168	362	46	2.35	
PC	PC04-167	361	59	1.90	
PC	PC04-164	358	44	1.44	-0.48
PC	PC04-163	357	41	3.35	
PC	PC04-162	356	57	1.31	
PC	PC04-161	355	62	2.14	-0.77
PC	PC04-160	354	41	2.54	-2.82
PC	PC04-159	353	39	3.98	-1.04
PC	PC04-158	352	52	1.63	-0.66
PC	PC04-157	351	54	1.55	-0.32
PC	PC04-156	350	49	2.26	-0.43
PC	PC04-155	349	82	0.45	-0.27
PC	PC04-154	348	68	0.61	-0.64
PC	PC04-153	347	49	1.59	-0.33
PC	PC04-152.9	346.9	90	0.27	0.25
PC	P-115h	346.9	85	0.75	-0.29
PC	P-117h	346.4	79	0.46	-0.52
PC	PC04-152	346	77	1.25	-0.51
PC	P-123h	345.4	77	1.23	-0.77
PC	PC04-151	345	45	1.87	-0.73
PC	P-125h	344.7	67	1.84	-1.26
PC	PC04-150	344	48	1.90	-0.47
PC	P-119h	343.1	73	1.09	-0.65
PC	PC04-149	343	65	1.17	-0.44
PC	P-121h	342.2	52	1.11	-0.79
PC	P-121h	342.2	53		-0.79
PC	PC04-148	342	53	1.78	-0.27
PC	PC04-147	341	65	1.35	-0.38
PC	PC04-146.8	340.8	88	0.21	-0.23
PC	PC04-146.2	340.2	81	0.13	-0.05
PC	PC04-146.1	340.1	85	0.11	-0.52
PC	PC04-145	339	83	0.46	-0.17
PC	PC04-144.1	338.1	83	0.65	-0.21



Section	Sample	Depth	CO <sub>3</sub> (%)	TOC (%)	$\delta^{13}\text{C}_{\text{in}}$ (‰)
PC	PC04-144	338	58	1.61	-0.68
PC	PC04-143	337	64	1.34	-0.85
PC	PC04-142	336	58	2.09	-1.00
PC	P-60h	335.3	82	0.58	-0.60
PC	PC04-141.1	335.1	95	0.13	0.78
PC	PC04-141	335	84	0.61	-0.11
PC	P-62h	334.6	66	0.84	-0.59
PC	PC04-140	334	68	0.88	-0.57
PC	PC04-139	333	42	1.61	-0.56
PC	PC04-138	332	20	1.92	-1.00
PC	PC04-137	331	54	1.05	-1.40
PC	PC04-136	330	56	2.15	-0.96
PC	P-56h	329.1	88	0.39	-1.23
PC	PC04-135	329	85	0.49	-0.73
PC	P-58h	328.2	50	0.75	-0.86
PC	PC04-134	328	55	0.89	-1.81
PC	PC04-133	327	55	1.79	-0.87
PC	PC04-132	326	57	1.72	-1.85
PC	PC04-131	325	67	1.51	-0.73
PC	PC04-130	324	64	0.70	-1.80
PC	PC04-129	323	74	1.16	-0.33
PC	PC04-127	321	64	1.91	-1.59
PC	PC04-126	320			
PC	PC04-125	319	38	2.49	-1.03
PC	PC04-124	318	30	3.91	-0.75
PC	PC04-123	317	24	2.21	-1.81
PC	PC04-122	316	23	3.04	-0.70
PC	PC04-121	315	67	0.50	-3.41
PC	PC04-120	314	58	1.70	-2.36
PC	PC04-119	313	25	3.20	-1.46
PC	PC04-118	312	14	3.95	-2.09
PC	PC04-117	311	62	1.63	-3.60
PC	PC04-116	310	25	3.27	-2.09
PC	PC04-115	309	22	2.89	-1.56
PC	PC04-114	308	57	2.74	-3.16
PC	PC04-113	307	30	5.04	-2.11
PC	PC04-112	306	36	3.48	-2.11
PC	PC04-111.2	305.2	69		-2.79
PC	PC04-111	305	51	4.21	-3.09
PC	PC04-110	304	42	4.79	-2.09
PC	PC04-109	303	-6	2.18	-3.23
PC	PC04-108	302	61	1.77	-4.22
PC	PC04-107	301	38	4.88	-1.82
PC	PC04-106	300	37	4.50	-2.23
PC	PC04-105	299	21	6.51	-1.72
PC	PC04-104	298	25	4.24	-2.09
PC	PC04-103	297	22	5.64	-1.71
PC	PC04-102.1	296.1	53		-2.99
PC	PC04-102	296	69	2.45	-3.92
PC	PC04-101.1	295.1	71		-2.84
PC	PC04-101	295	23	6.09	-2.01
PC	PC04-100	294	60	2.56	-3.36
PC	PC04-99	293	31	4.23	-2.47

Section	Sample	Depth	CO3 (%)	TOC (%)	$\delta^{13}\text{C}_{\text{in}}$ (‰)
PC	PC04-98	292	19	2.37	-1.25
PC	PC04-97	291	29	6.83	
PC	PC04-96	290	35	4.79	
PC	PC04-95.6	289.6	85		
PC	PC04-95	289	30	6.09	
PC	PC04-94.2	288.2	89	0.82	
PC	PC04-94.01	288.01	62	1.90	
PC	PC04-93	287	21	7.74	-1.60
PC	PC04-92	286	36	3.95	
PC	PC04-91	285	44	3.58	
PC	PC04-90	284	43	5.30	
PC	PC04-89.1	283.1	77		
PC	PC04-89	283	61	4.60	
PC	PC04-88.1	282.1	73		
PC	PC04-88	282	60	2.25	-2.75
PC	PC04-87	281	44	4.30	
PC	PC04-86.5	280.5	47	4.94	
PC	PC04-86	280	73	4.85	
PC	PC04-85.5	279.5	48	4.40	
PC	PC04-85	279	49	4.32	-1.54
PC	PC04-84.5	278.5	85	1.75	
PC	PC04-84	278	41	3.45	
PC	PC04-83.5	277.5	95		
PC	PC04-83	277	43	2.62	
PC	PC04-82	276	82	1.82	
PC	PC04-81.5	275.5	64	3.42	
PC	PC04-81	275	69	1.87	-2.95
PC	PC04-80.9	274.9	33	6.51	
PC	PC04-80.4	274.4	54	5.15	
PC	PC04-80	274	47	4.67	
PC	PC04-79.5t	273.5	78		
PC	PC04-79.5b	273.5	85		
PC	PC04-79	273	20	3.51	
PC	PC04-78	272	15	4.50	-1.80
PC	PC04-77	271	33	3.09	
PC	PC04-76.7	270.7	78		
PC	PC04-76	270	31	2.75	
PC	PC04-75	269	75	1.00	-0.67
PC	PC04-74.4	268.4	79		
PC	PC04-74	268	38	2.94	-2.01
PC	PC04-73	267	51	5.08	-1.91
PC	PC04-72	266	70	1.50	-2.43
PC	PC04-71	265	30	3.20	-1.80
PC	PC04-70	264	55	2.18	-2.53
PC	PC04-69	263	24	3.83	-1.15
PC	PC04-68.6	262.6	70		
PC	PC04-68	262	46	1.78	-2.10
PC	PC04-67	261	65	1.40	-2.02
PC	PC04-66.8b	260.8	75		
PC	PC04-66.8t	260.8	73		
PC	PC04-66	260	49	2.39	-1.62
PC	PC04-65	259	26	4.25	-1.86
PC	PC04-64	258	32	3.23	-1.53

Section	Sample	Depth	CO3 (%)	TOC (%)	$\delta^{13}\text{C}_{\text{in}}$ (‰)
PC	PC04-63	257	35	2.72	-2.14
PC	PC04-62	256	35	6.42	-1.69
PC	PC04-61	255	45	3.83	-2.35
PC	PC04-60	254	74	1.25	-1.51
PC	PC04-59	253	42	3.44	-2.00
PC	PC04-58	252	30	2.79	-1.73
PC	PC04-57	251	41	2.38	-2.12
PC	PC04-56.2	250.2	75	1.34	
PC	PC04-56	250	59	2.10	-1.78
PC	PC04-55	249	50	4.29	-2.28
PC	PC04-54	248	40	5.15	-1.69
PC	PC04-53	247	41	3.40	
PC	PC04-52	246	61	0.12	-2.67
PC	PC04-51.7	245.7	56		
PC	PC04-51	245	25	2.05	-1.06
PC	PC04-50	244	41	6.77	-1.50
PC	PC04-49	243	64	2.53	-2.61
PC	PC04-48	242	47	5.73	-1.79
PC	PC04-47.8	241.8	66		
PC	PC04-47	241	17	3.91	
PC	PC04-46	240	22	4.76	-1.36
PC	PC04-45	239	24	2.58	-0.83
PC	PC04-44	238	21	3.51	-0.95
PC	PC04-43	237	32	3.91	-0.81
PC	PC04-42	236	50	6.32	-2.08
PC	PC04-41	235	24	2.18	-1.15
PC	PC04-40	234	18	2.88	-1.40
PC	PC04-39	233	26	1.68	-1.08
PC	PC04-38	232	9	2.73	-2.81
PC	PC04-37	231	62	2.75	-2.87
PC	PC04-36	230	33	1.45	
PC	PC04-35	229	41	3.10	
PC	PC04-34	228	60	1.82	
PC	PC04-33.9	227.9	84	0.10	
PC	PC04-33	227	29	1.42	-1.18
PC	PC04-32	226	11	2.53	
PC	PC04-31	225	28	2.24	
PC	PC04-30	224	87	0.09	
PC	PC04-29	223	76	0.88	
PC	PC04-28	222	26	1.74	-1.00
PC	PC04-27	221	41	1.67	
PC	PC04-26	220	67	2.20	
PC	PC04-25	219	43	3.50	
PC	PC04-24	218	49	3.69	
PC	PC04-23.9	217.9	83		
PC	PC04-23	217	37	2.90	-1.31
PC	PC04-22	216	26	2.47	
PC	PC04-21	215	29	3.13	
PC	PC04-20	214	33	1.94	
PC	PC04-19	213	56	1.64	
PC	PC04-18	212	26	5.40	-1.58
PC	PC04-17	211	38	2.48	
PC	PC04-16	210	10	1.53	

Section	Sample	Depth	CO3 (%)	TOC (%)	$\delta^{13}\text{C}_{\text{in}}$ (‰)
PC	PC04-15	209	43	3.83	
PC	PC04-14	208	14	3.05	
PC	PC04-13	207	46	2.32	-1.71
PC	PC04-12	206	41	2.05	
PC	PC04-11	205	35	2.18	
PC	PC04-10	204	43	1.80	
PC	PC04-9	203	23	2.62	
PC	PC04-8	202	20	2.43	-0.92
PC	PC04-7	201	22	3.22	
PC	PC04-6	200	47	1.40	
PC	PC04-5	199	35	2.35	
PC	PC04-4	198	22	1.99	
PC	PC04-3	197	27	2.04	
PC	PC04-2	196	65	0.80	
PC	PC04-1	195	15	2.68	
PC	PC04-0	194	42	1.87	
PC	PC03-135	193	30	1.65	
PC	PC03-134	192	45	1.36	
PC	PC03-133.1b	191.11	84		
PC	PC03-133.1a	191.1	84		
PC	PC03-133	191	39	2.34	
PC	PC03-132	190	39	6.08	-1.78
PC	PC03-131	189	6	3.66	
PC	PC03-130	188	34	5.77	
PC	PC03-129	187	33	4.38	
PC	PC03-128	186	18	3.25	
PC	PC03-127.5	185.5	78		
PC	PC03-127	185	54	1.35	-2.43
PC	PC03-126	184	40	5.87	
PC	PC03-125	183	31	3.60	
PC	PC03-124	182	67	2.43	
PC	PC03-123.9	181.9	85		
PC	PC03-123	181	38	2.90	
PC	PC03-122	180	27	2.45	-1.83
PC	PC03-121	179	30	2.46	
PC	PC03-120	178	30	4.08	
PC	PC03-119	177	19	4.00	
PC	PC03-118	176	77	1.28	
PC	PC03-117	175	25	3.29	-2.36
PC	PC03-116	174			
PC	PC03-115	173	5	4.69	
PC	PC03-114	172	34	2.43	
PC	PC03-113	171	22	3.01	
PC	PC03-112.1	170.1	83	0.76	
PC	PC03-112	170	79	1.11	-0.65
PC	PC03-111	169	30	2.33	
PC	PC03-110	168	41	3.07	
PC	PC03-109	167	76	1.25	
PC	PC03-108.3	166.3	78		
PC	PC03-108	166	67	2.14	
PC	PC03-107	165	54	2.11	-3.35
PC	PC03-106	164	9	2.73	
PC	PC03-105.5	163.5	76		

Section	Sample	Depth	CO3 (%)	TOC (%)	$\delta^{13}\text{C}_{\text{in}}$ (‰)
PC	PC03-105	163	22	3.70	
PC	PC03-104b	162.1	87		
PC	PC03-104	162	52	3.23	
PC	PC03-103	161	36	6.53	
PC	PC03-102	160	37	2.64	-2.55
PC	PC03-101	159	40	4.43	
PC	PC03-100	158	34	3.81	
PC	PC03-99	157	30	2.82	
PC	PC03-98	156	57	3.57	
PC	PC03-97	155	49	3.51	-2.77
PC	PC03-96	154	52	1.83	
PC	PC03-95	153	61	1.53	
PC	PC03-94.5	152.5	59	2.39	
PC	PC03-94	152	83	0.78	
PC	PC03-93.5	151.5	35	2.42	
PC	PC03-93	151	67	1.71	
PC	PC03-92.5	150.5	45	2.18	
PC	PC03-92.1	150.1	20		
PC	PC03-92	150	21	3.21	-2.48
PC	PC03-91.5	149.5	60	1.40	
PC	PC03-91	149	78	0.04	
PC	PC03-90.5	148.5	16	2.69	
PC	PC03-90	148	77		
PC	PC03-89.6	147.6	80	0.08	
PC	PC03-89.5	147.5	34	4.94	
PC	PC03-89	147	42	3.75	
PC	PC03-88.5	146.5	22	3.15	
PC	PC03-88	146	62	3.13	
PC	PC03-87.5	145.5	11	9.69	
PC	PC03-87	145	39	4.47	-2.66
PC	PC03-86.5	144.5	40	6.43	
PC	PC03-86	144	24	8.70	
PC	PC03-85.5	143.5	32	3.75	
PC	PC03-85	143	30	4.11	
PC	PC03-84	142	15	4.06	
PC	PC03-83.3b	141.31	78		
PC	PC03-83.3a	141.3	55		
PC	PC03-83	141	25	4.01	
PC	PC03-82	140	52	1.89	-3.92
PC	PC03-81	139	58	1.91	
PC	PC03-80	138	60	3.16	
PC	PC03-79	137	79	0.51	
PC	PC03-78	136	21	4.18	
PC	PC03-77	135	24	5.70	
PC	PC03-76	134	38	5.59	-3.07
PC	PC03-75	133	25	3.51	
PC	PC03-74	132	19	4.31	
PC	PC03-73	131	11	3.71	
PC	PC03-72	130	8	4.70	
PC	PC03-71	129	11	4.35	
PC	PC03-70	128	44	5.25	
PC	PC03-69	127	11	5.05	
PC	PC03-68	126	23	1.33	

Section	Sample	Depth	CO3 (%)	TOC (%)	$\delta^{13}\text{C}_{\text{in}}$ (‰)
PC	PC03-67	125	82	0.88	
PC	PC03-66	124	8	4.74	-5.13
PC	PC03-65	123	41	4.12	
PC	PC03-64	122	43	4.06	
PC	PC03-63.8	121.8	85		
PC	PC03-63	121	37	7.84	
PC	PC03-62	120	70	3.94	
PC	PC03-61	119	47	4.01	
PC	PC03-60	118	56	4.11	
PC	PC02-67	117	41	0.99	
PC	PC02-66.5	116.5	84		
PC	PC02-66	116	45	2.39	
PC	PC02-65	115	42	1.70	-3.53
PC	PC02-64	114	50	1.42	
PC	PC02-63	113	42	1.39	
PC	PC02-62	112	49	1.32	
PC	PC02-61	111	40	2.29	
PC	PC02-60	110	46	0.88	-3.93
PC	PC02-59	109	61	0.74	
PC	PC02-58	108	25	1.54	-4.49
PC	PC02-57	107	10	1.26	-3.90
PC	PC02-56	106	30	3.32	-3.87
PC	PC02-55	105	80	1.71	-3.97
PC	PC02-54	104	25	5.97	-4.75
PC	PC02-53	103	31	5.08	-5.07
PC	PC02-52	102	3	4.21	
PC	PC02-51	101	10	1.58	-2.79
PC	PC02-50	100	25	3.03	-4.35
PC	PC02-49	99	37	1.05	
PC	PC02-48	98	64	0.63	
PC	PC02-47	97	14	1.84	
PC	PC02-46	96	4	1.51	-4.16
PC	PC02-45	95	6	1.73	
PC	PC02-44	94	2	2.70	-3.78
PC	PC02-43	93	3	3.55	
PC	PC02-42	92	4	2.08	
PC	PC02-41	91	45	1.50	-4.89
PC	PC02-40	90	25	1.03	
PC	PC02-39.4	89.4	75	1.76	
PC	PC02-39	89	21	1.57	-2.39
PC	PC02-38	88	9	1.56	-3.35
PC	PC02-37	87	29	1.21	-4.46
PC	PC02-36	86	25	3.97	-3.36
PC	PC02-35	85	24	2.26	-2.55
PC	PC02-34	84	27	1.77	-2.96
PC	PC02-33	83	77	0.69	-2.35
PC	PC02-32.2	82.2	83		
PC	PC02-32	82	35	3.31	-4.90
PC	PC02-31	81	7	3.03	-3.84
PC	PC02-30	80	37	2.09	-3.08
PC	PC02-29	79	30	2.79	-3.65
PC	PC02-28	78	24	1.72	
PC	PC02-27	77	71	2.30	-3.19

Section	Sample	Depth	CO3 (%)	TOC (%)	$\delta^{13}\text{C}_{\text{in}}$ (‰)
PC	PC02-26	76	3	6.01	
PC	PC02-25.8	75.8	86		
PC	PC02-25	75	4	5.56	
PC	PC02-24	74	4	5.69	
PC	PC02-23	73	2	5.55	
PC	PC02-21.9	71.9	7	3.68	-2.97
PC	PC02-21	71	4	2.37	
PC	PC02-20	70	2	2.68	
PC	PC02-19	69	1	5.01	
PC	PC02-18	68	3	5.42	-3.02
PC	PC02-17	67	34	1.84	-1.92
PC	PC02-16	66	23	2.39	-2.16
PC	PC02-15	65	44	3.82	-3.26
PC	PC02-14	64	6	2.31	-3.66
PC	PC02-13.3	63.3	66		
PC	PC02-13	63	22	2.31	-2.88
PC	PC02-12.8	62.8	71		
PC	PC02-12	62	25	1.88	-1.86
PC	PC02-11	61	32	2.00	-2.17
PC	PC02-10	60	29	2.12	-2.57
PC	PC02-9	59	51	1.23	-2.38
PC	PC02-8	58	46	1.05	-3.65
PC	PC02-7.6	57.6	81		
PC	PC02-7	57	4	1.95	
PC	PC02-6.6	56.6	28		
PC	PC02-6.2	56.2	67	1.97	-3.75
PC	PC02-6	56	47	0.66	-2.54
PC	PC02-5	55	19	1.65	-1.75
PC	PC02-4	54	47	0.69	-2.37
PC	PC02-3	53	44	1.30	-1.89
PC	PC02-2.05	52.05	58		
PC	PC02-2	52	22	1.63	-3.09
PC	PC02-1	51	28	1.15	-1.61
PC	PC02-0	50	70	0.66	-0.21
PC	PC06-49	49	35	1.79	-3.36
PC	PC06-48.7	48.7	70	1.65	-2.47
PC	PC06-48	48	21	2.01	-2.98
PC	PC06-47	47	7	7.24	
PC	PC06-46	46	37	2.04	-1.29
PC	PC06-45	45	34	3.59	-5.19
PC	PC06-44	44	65	6.63	-3.14
PC	PC06-43	43	69	3.38	-5.69
PC	PC06-42	42	26	5.56	-3.32
PC	PC06-41	41	40	2.72	-5.36
PC	PC06-40	40	16	1.96	
PC	PC06-39	39	36	0.53	-2.60
PC	PC06-38	38	34	3.40	-3.76
PC	PC06-37.9	37.9	82		
PC	PC06-37	37	26	2.83	
PC	PC06-36	36	59	2.20	-5.81
PC	PC06-35	35	64	4.26	-5.27
PC	PC06-33	33	26	4.57	
PC	PC06-29	29	25	3.09	-4.45

Section	Sample	Depth	CO <sub>3</sub> (%)	TOC (%)	$\delta^{13}\text{C}_{\text{in}}$ (‰)
PC	PC06-28.5	28.5	79		-4.93
PC	PC06-28	28	69	2.69	-6.67
PC	PC06-27	27	62	1.71	-5.21
PC	PC06-26	26	56	2.00	-6.03
PC	PC06-25	25	26	3.01	-5.78
PC	PC06-24	24	65	2.45	-7.80
PC	PC06-23.8	23.8	80		-5.38
PC	PC06-23	23	29	2.93	-3.78
PC	PC06-22	22	25	3.26	-3.37
PC	PC06-21	21	39	4.17	-3.46
PC	PC06-20	20	30	4.17	
PC	PC06-19	19	39	5.37	-6.55
PC	PC06-18	18	74	3.21	
PC	PC06-17	17	19	3.67	
PC	PC06-16	16	31	4.04	-4.84
PC	PC06-15	15	75	4.53	-7.47
PC	PC06-14	14	23	2.55	
PC	PC06-13	13	24	2.46	-4.77
PC	PC06-12	12	71	3.00	-14.55
PC	PC06-11	11	76	0.65	-7.45
PC	PC06-10	10	31	2.47	-4.66
PC	PC06-9.01	9.01	74		-7.12
PC	PC06-9	9	27	1.32	-3.49
PC	PC06-8.1	8.1	84		-7.44
PC	PC06-8	8	89	0.94	
PC	PC06-7	7	24	2.63	-8.56
PC	PC06-6	6	76	1.22	-3.12
PC	PC06-5	5	38	0.73	-4.04
PC	PC06-4	4	80	0.19	-9.96
PC	PC06-3	3	30	1.06	-5.14
PC	PC06-2	2	50	0.46	-4.62
PC	PC06-1	1	84	2.28	-5.22
PC	PC06-0.1	0.1	72	0.50	-11.26



APPENDIX B

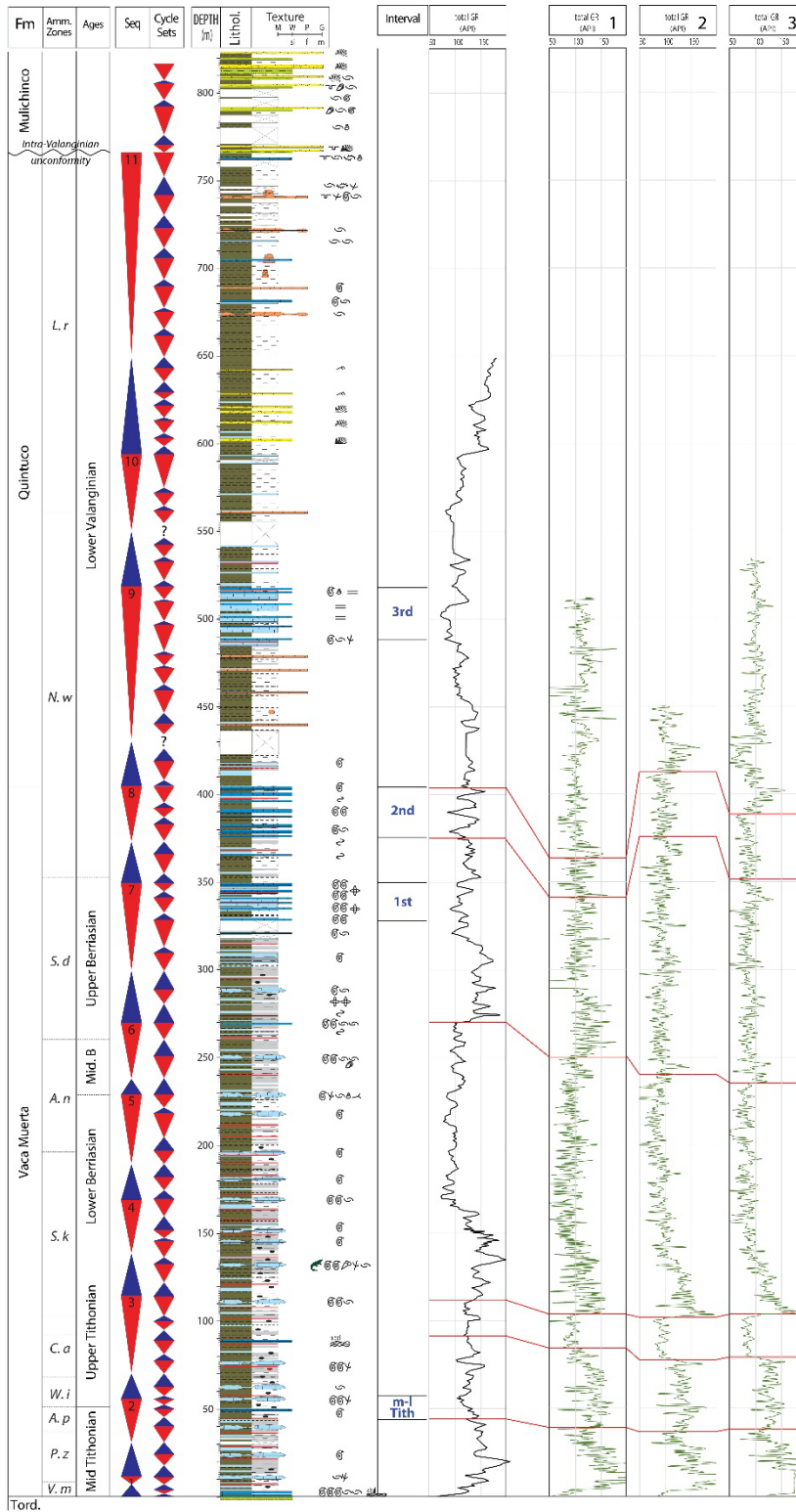
**Isotope data from mudstone/wackestone plug samples from Picún Leufú carbonate platform**

Section	Sample	$\delta^{13}\text{C}_{\text{in}}$ (‰)	$\delta^{18}\text{O}$ (‰)
B1	67	1.38	-3.47
B1	68	1.91	-2.89
B1	70	2.30	-4.15
B1	72	2.58	-3.17
B1	76	2.21	-3.77
B1	77	1.87	-4.77
B1	82	1.75	-5.96
B1	83	1.14	-6.71
B1	84	1.09	-6.18
B1	87b	0.52	-3.43
B2	1	2.34	-3.67
B2	3	1.89	-4.31
B2	6	2.36	-6.54
B2	7	2.46	-6.36
B2	8	2.65	-4.60
B2	9	2.58	-3.61
B2	10	2.66	-4.50
B2	19	2.51	-4.05
B2	22	2.05	-6.79
B2	23	1.89	-7.20
B2	24	2.53	-4.87
B2	25	2.17	-6.07
B2	26	2.28	-4.09
B2	27	2.25	-5.77
B2	28	1.85	-5.11
B2	29	1.62	-4.03
B2	31	1.12	-6.66
B2	32	1.25	-7.29
B2	36	1.40	-4.99
B2	38	1.68	-4.58
B2	64	1.96	-4.56
B2	66	1.48	-2.53
B2	68	1.71	-7.04
B2	11b	2.23	-3.02
B2	12b	1.75	-2.77
B2	30a	2.56	-6.05
B2	33b	2.02	-6.60
B2	34b	2.02	-6.61

	$\delta^{13}\text{C}_{\text{in}}$ (‰)
Mean	1.95
Standard Error	0.08
Median	1.99
Standard Deviation	0.51
Range	2.14
Minimum	0.52
Maximum	2.66
P05	1.11
P95	2.59
Count	38

# APPENDIX C

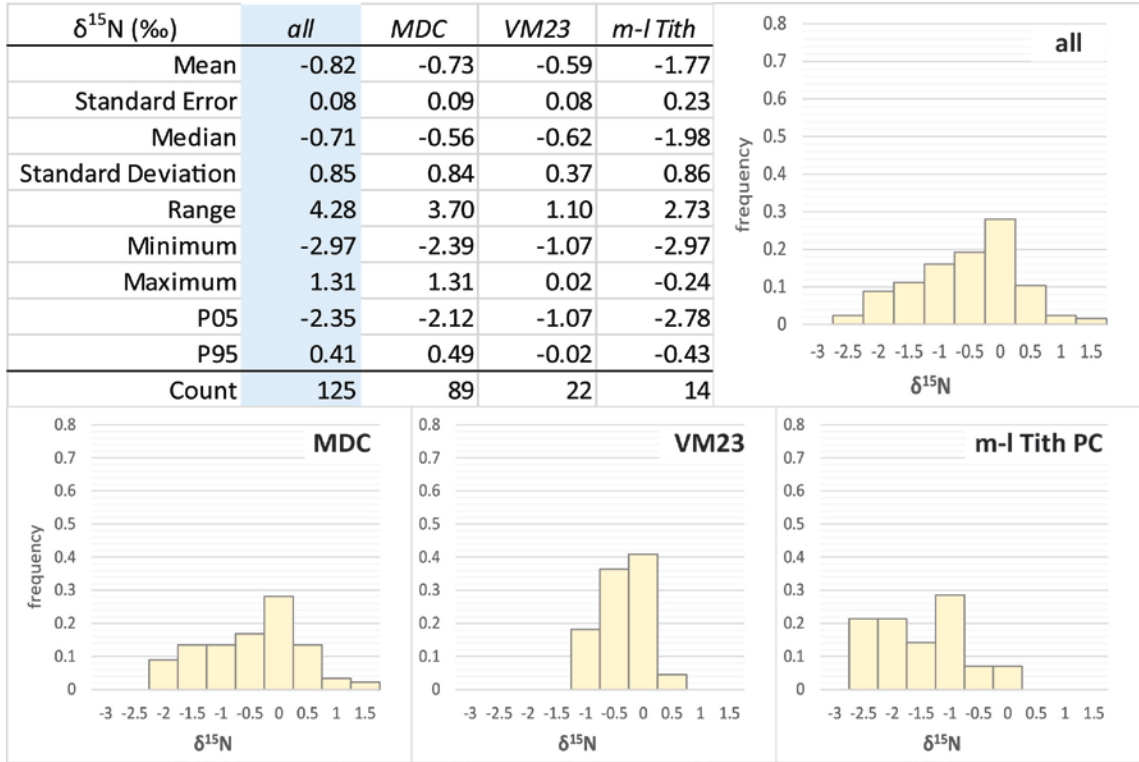
## GR correlation between El Trapial (Chevron) wells and PC section



Distinctive markers in red were used for the correlation between the PC reference section to the left and 3 wells from El Trapial field.

APPENDIX D

$\delta^{15}\text{N}$  data from the mid-late Tithonian intervals (MDC, VM23, PC)



Section	Sample	Depth	$\delta^{15}\text{N}$ (‰)
MDC1	MDC4-13	146.8	-0.02
MDC1	MDC4-12	145.8	-1.07
MDC1	MDC4-11	141.5	0.23
MDC1	MDC4-10	139.7	0.46
MDC1	P_139	137.9	-0.17
MDC1	MDC4-9	137.5	0.55
MDC1	P_141	137.3	0.09
MDC1	P_143	135	1.09
MDC1	MDC4-8	134.5	0.20
MDC1	P_145	134.2	0.11
MDC1	MDC4-6	132.2	-0.49
MDC1	MDC4-5	131	-0.19
MDC1	P_135	128.9	0.17
MDC1	P_137	128.1	-0.13
MDC1	MDC4-4	127	-0.31
MDC1	MDC4-3	126	-0.22
MDC1	MDC4-2	124.5	-0.25
MDC1	VM14-134	124.3	-0.27
MDC1	MDC5-7	124	-1.02
MDC1	P_130	124	-0.13
MDC1	P_133	123.6	-0.24
MDC1	VM14-133	123.4	-0.17
MDC1	VM14-132	122.7	-0.97
MDC1	MDC4-1	122.5	-0.71

Section	Sample	Depth	$\delta^{15}\text{N}$ (‰)
MDC1	VM14-131	122.25	0.61
MDC1	VM14-130	121.4	-0.74
MDC1	MDC5-6	121	-1.62
MDC1	VM14-129	120.6	0.52
MDC1	VM14-128	119.55	-0.81
MDC1	MDC5-5	119	-0.03
MDC1	VM14-127	118.7	-0.28
MDC1	VM14-126	117.7	0.05
MDC1	VM14-125	116.9	0.01
MDC1	VM14-124	116	-1.03
MDC1	VM14-135	115.9	0.42
MDC1	MDC5-4	115.8	-0.77
MDC1	VM14-123	114.5	-0.39
MDC1	VM14-122	113.3	-1.18
MDC1	VM14-121	112.5	-0.25
MDC1	VM14-119	110.6	-1.62
MDC1	VM14-137	110	-0.48
MDC1	VM14-118	109.5	0.10
MDC1	MDC5-2	109	0.08
MDC1	MDC5-1	108	-0.86
MDC1	VM14-115	106.5	-0.49
MDC1	MDC2-13	106	-0.02
MDC1	VM14-114	105.5	-0.94
MDC1	MDC2-12	105.3	1.31
MDC1	VM14-113	104.6	0.34
MDC1	MDC2-11	104.5	-0.36
MDC1	VM14-112	103.8	-0.83
MDC1	MDC2-10	103.5	-0.14
MDC1	VM14-111	103	-0.56
MDC1	MDC2-9	102.5	-0.03
MDC1	VM14-110	102.1	-0.71
MDC1	MDC2-8	102	-0.52
MDC1	MDC2-7	101.5	-1.09
MDC1	VM14-109	101.4	-1.47
MDC1	VM14-108	100.7	-1.55
MDC1	MDC2-6	100	-0.45
MDC1	VM14-107	99.75	-2.15
MDC1	MDC2-5	99.5	-0.44
MDC1	VM14-106	98.6	-2.01
MDC1	MDC2-4	98.5	-0.38
MDC1	VM14-105	97.4	-1.15
MDC1	VM14-104	96.6	-1.28
MDC1	VM14-103	95.9	-1.46
MDC1	VM14-102	94.7	-2.12
MDC1	MDC2-2	94.5	-2.39
MDC1	VM14-101	94.3	-2.10
MDC1	VM14-100	93.6	-2.20
MDC1	VM14-99	92.6	-1.84
MDC1	VM14-98	91.6	-1.48
MDC1	VM14-97	91.25	-1.97
MDC1	VM14-96	90.8	-2.12
MDC1	VM14-95	90.2	-2.38
MDC1	VM14-94	89.9	-1.76
MDC1	VM14-93	89.1	-1.50
MDC1	VM14-92	88.2	-1.87
MDC1	VM14-91	87.25	-1.80

Section	Sample	Depth	$\delta^{15}\text{N}$ (‰)
MDC1	VM14-90	86.45	-1.85
MDC1	VM14-89	85.55	-1.98
MDC1	VM14-87	84.6	-1.77
MDC1	MDC-GRL-1	84.3	-0.53
MDC1	VM14-86	83.25	-0.59
MDC1	VM14-85	82.25	-1.38
MDC1	VM14-84	81.5	-0.78
MDC1	VM14-83	80.7	-1.13
MDC1	VM14-82	79.95	-0.91
VM23	VM23-21.6	21.6	-0.83
VM23	VM23-20.5	20.5	-0.47
VM23	VM23-20	20	-0.11
VM23	VM23-19	19	-0.01
VM23	VM23-18.2	18.2	-0.17
VM23	VM23-17	17	-0.64
VM23	VM23-16	16	-0.45
VM23	VM23-14.8	14.8	-0.90
VM23	VM23-13.5	13.5	-0.61
VM23	VM23-12.5	12.5	-0.62
VM23	VM23-12	12	-1.03
VM23	VM23-10.9	10.9	-0.34
VM23	VM23-9.6	9.6	-0.08
VM23	VM23-8.5	8.5	0.02
VM23	VM23-7.6	7.6	-0.45
VM23	VM23-6.6	6.6	-0.93
VM23	VM23-5.6	5.6	-1.07
VM23	VM23-4.7	4.7	-1.07
VM23	VM23-4.5	4.5	-0.87
VM23	VM23-3.8	3.8	-0.97
VM23	VM23-2.1	2.1	-1.01
VM23	VM23-1.6	1.6	-0.28
m-l Tith	PC02-6.2	56.2	-1.99
m-l Tith	PC02-6	56	-2.48
m-l Tith	PC02-5	55	-2.25
m-l Tith	PC02-4	54	-2.67
m-l Tith	PC02-3	53	-2.97
m-l Tith	PC02-2	52	-2.41
m-l Tith	PC02-1	51	-1.96
m-l Tith	PC02-0	50	-2.64
m-l Tith	PC06-49	49	-1.17
m-l Tith	PC06-48.7	48.7	-1.29
m-l Tith	PC06-48	48	-1.07
m-l Tith	PC06-47	47	-0.24
m-l Tith	PC06-46	46	-1.14
m-l Tith	PC06-45	45	-0.53